University of Strathclyde

Department of Mechanical and Aerospace Engineering

The effect of acidity and salinity level in erosion-corrosion performance of metals

Georgios Karafyllias

A thesis submitted for the degree of Doctor of Philosophy

2017

Dedicated to my parents; Konstantinos and Stavroula, and my sister Maria for their continuous support and guidance.

Contents

Acknowledgments

First, I would like to thank my supervisors Dr. Alexander Galloway and Dr. Trevor Hodgkiess for their expert guidance and continuous support. During the last three years their inspired supervision has been invaluable. Without their support, I would not have been able to complete my Ph.D. thesis.

I would also like to express my sincere gratitude to Edward Humphries (R&D Director, Weir Minerals Australia), Alastair Pearson (Chief Metallurgist, Weir Engineering Services, Glasgow, UK) and Paul Abbott (Metallurgical Engineer, Weir Minerals North America, USA) for their insightful comments and excellent collaboration.

I thank my colleagues, Lampros-Gerasimos Giourntas, Frazer Brownlie, Evripidis Tsergas, Martin Yoon and Ioannis Violatos, for their help, friendship and all the fun we had, even when we were sleeplessly working to catch tight deadlines at the lab.

My sincere gratitude to James Kelly, who trained me in metallography laboratory and offered his wise advice in metallurgical topics; to Dr. Fiona Sillars for her advice and training in Scanning Electron Microscope investigations; and to Liza Hall who familiarised me with the surface topography equipment. Moreover, I would like to thank the technicians in the university's workshop, William Downie, Drew Irvine and Fuad Warsame.

Furthermore, I would like to thank my dear friends, Athanasios Anagnostakis, Fotis Mitsakis, Aldo Iannetti, Aleksandar Josifovic and Alejandro Lopez, who supported and made me enjoy life as a Ph.D. student.

Obviously, my special gratitude goes to my wonderful parents and sister who have always been on my side during these three years. I would not have been able to complete my Ph.D. project without them.

Abstract

The current study comprises an extended investigation of the effect of acidity and salinity levels on the erosion-corrosion behaviour of metallic materials used in the mining industry. In such environments, the level of both acidity and salinity significantly affects the alloys used for manufacturing either critical parts of pumps or pipelines that are subject to erosion-corrosion. The experimental approach consists of a detailed analysis with regards to the tested materials microstructure and their erosion-corrosion performance. In addition, the synergistic effects between erosion, sliding abrasion and corrosion were investigated by implementing electrochemical techniques. The post-test analysis enabled the evaluation of the materials behaviour in different hydrodynamic regions. The scope of the tested materials focused on white cast irons with either austenitic or martensitic matrix and various carbide volume fractions, whilst their erosion-corrosion performance was compared with commercial grades of stainless steel with austenitic and martensitic structure. The findings demonstrate that in neutral pH conditions and seawater the martensitic matrix and eutectic carbides are the optimum combination for the white cast irons, which are superior over the stainless steels. The increase of carbide volume fraction in conjunction with the presence of coarse/large carbides impair the erosion-corrosion performance of white cast irons. In acidic testing environment, the austenitic alloys exhibit substantially lower volume loss than the martensitic materials and this is associated with the enhanced corrosion resistance of austenitic structure. The current study extends to erosion-corrosion analysis in both neutral and very strong acidic conditions, in which two innovative alloys precipitated by σ-phase were investigated. The results illustrate that the controlled formation of σ-phase is beneficial in terms of erosion-corrosion. Furthermore, by increasing the salinity, the corrosion rates and the overall volume loss are higher on martensitic alloys with moderate corrosion resistance, whilst on austenitic or martensitic alloys with relatively good corrosion resistance the salinity has no effect.

List with abbreviations

WCI	white cast iron
SLEC	solid liquid erosion-corrosion
TML	total mass loss
TVL	total volume loss
DIZ	direct impinged zone
OA	outer area
VL$_{DIZ}$	volume loss in the direct impinged zone
VL$_{OA}$	volume loss in the outer area
CVF	carbide volume fraction
NbC	niobium carbides
CP	cathodic protection
SEM	scanning electron microscope
EDS	energy dispersive X-ray spectroscopy
EBSD	electron backscatter diffraction
CE	Carbon equivalent
HE	Hydrogen embrittlement

List with symbols

α, δ	ferrite
γ, γ₂	austenite, secondary austenite
σ	sigma phase
χ	chai phase
Al₂O₃	aluminium oxide
C	corrosion
Cr₂N	chromium nitride
E	potential
E_corr	corrosion potential
E₀	equilibrium potential
e	electrons
F	faraday constant
H_e	hardness of erodent
H_t	hardness of target material
H₂O	water
H₂	hydrogen
I	current
I_corr	corrosion current
i_corr	corrosion current density
-log [H⁺]	logarithmic concentration of hydrogens
M	mechanical damage
n	number of electrons
O₂	oxygen
(OH)⁻	hydroxide
Q	flow rate
R	radius
R_p	polarisation resistance
S	synergy
Sic, SiO₂	silicon carbide, silicon dioxide
V	velocity

Structure of the thesis

The structure this thesis consists of the introduction (chapter 1), which demonstrates general information about erosion-corrosion and the corresponding industries that this phenomenon occurs. Furthermore, in the introduction chapter, the rationale of the current thesis and its correlation with the industry is illustrated.

Chapter 2 involves the theory of wear (erosion/abrasion), corrosion and erosion-corrosion individually. In particular, the parameters that affect the erosion-corrosion phenomenon is demonstrated, whilst the corresponding literature review is quoted.

Since a wide range of materials has been investigated, an individual chapter presenting the literature review with respects to these materials is designated. Hence, chapter 3 demonstrates the background of the tested alloys in terms of metallurgy and erosion-corrosion performance in various testing conditions which some of them are similar with the environments used in the current project.

Chapter 4 illustrates the scientific approach of the project and providing details about the experimental protocol and the tools that were used in order to conduct the entire erosion-corrosion investigation.

Chapter 5 consists of the first experimental phase and involves the erosion-corrosion investigation of two white cast irons (WCI), one with austenitic matrix and the other with martensitic which are compared with two commercially available grades of stainless steels, one austenitic and one martensitic.

Commencing the investigation of the erosion-corrosion phenomenon in neutral and acidic conditions, the experimental work extends to more advanced WCIs in chapter 6. A WCI with large chromium carbides present and one experimental WCI reinforced with niobium carbides were entirely examined, whilst the results showed the correlation between the erosion-corrosion performance and the size/type of carbides (Cr or Nb).

Chapter 7 involves erosion-corrosion assessment in neutral and very strong acidic conditions on corrosion resistant alloys. In addition, two innovative proprietary alloys that contain σ-phase in their microstructure were included in this experimental phase, whilst according to the results, the presence of σ-phase was beneficial in erosion-corrosion. Also, the importance of Cr and Mo elements dispersion into the complex microstructure of the tested alloys was shown.

The last experimental phase is presented in chapter 8 and consists of erosion-corrosion investigation of WCIs and an austenitic stainless steel in different salinity levels. The importance of a certain level of corrosion resistance for optimum erosion-corrosion performance in high salinity and the existence of synergistic effects between erosion and corrosion in fresh water were two only of the important findings of this chapter.

Finally, in chapter 9, the ranking of materials in seawater/neutral conditions and the overall conclusions of the current Ph.D. thesis are presented. Among many conclusions, the vitality of low synergy for a given material/environment with respects to optimum erosion-corrosion performance was highlighted in the entire project. In addition, future research directions are included in the last part of the final chapter.

Chapter 1

Introduction

1.1 Introduction

Erosion-corrosion is a material deterioration phenomenon that occurs in various engineering systems that handle aggressive slurries. The selection of erosion–corrosion resistant materials and coatings is a challenge in many industries since the capabilities of the applied materials must be suitable for the operating conditions. The preferable alloys for erosive-corrosive environments should provide a balance between corrosion and wear resistance without impairing one or the other mechanism. For example, in the minerals and oil and gas industries, components that are usually subjected to erosion–corrosion are pumps (impellers, throat-bushes, wear rings liners), valves, seats and pipelines that handle slurries.

The importance of preventing damage to equipment due to erosion, corrosion and the combination of both factors in the Oil & Gas industry was emphasised by E.S. Venkatesh [1.1]. It is well known that erosion is mainly affected by the impinging velocity and the size/concentration of the solid particles [1.2–1.4]. On the other hand, corrosion is generally influenced by temperature, salinity level, pH and impinging velocity which impair the passivity of materials [1.5,1.6].

In mining operations, pumps and piping systems that transfer fluids are subjected to high rates of corrosive wear [1.7]. The wear rates are substantially influenced by the size of solid particles which have been reported to be between 0.04-10 mm [1.8]. The severity of corrosion can vary since the composition of the aqueous solutions from one mine to another is unique [1.9]. In some very aggressive environments, the pH level is very acidic (even down to 0–1) contributing, in conjunction with the high chloride levels which can vary between 0-10% NaCl, to significant material loss due to corrosion [1.10]. One example of low pH in water is the reaction of pyrite and other sulphide minerals with air, oxygen and water resulting in the formation of ferrous ions and sulphuric acid, well known as acid rock drainage [1.11].

Another industry in which erosion-corrosion is a concern is the Power Industry which includes nuclear reactors, wind turbines, coal and natural gas burners, hydro runners etc. In such examples, the corrosion mechanism is enhanced in applications where high temperatures occur, whilst erosion is affected by velocities or even the presence of solid particles (in case of hydro runners) [1.12,1.13].

The chemical industry often utilises very corrosive environments compared to other industrial sectors since the engineering components handle aggressive acids, such as phosphoric and sulphuric acid. In phosphoric acid plants, corrosion is additionally enhanced due to the presence of halogens and chlorides, whilst the operating temperature is usually around 100 °C [1.14]. Sulphuric acid plants are considered more corrosive on metals than those of phosphoric acid due to the nature of the operating chemical/temperature. The materials deterioration due to corrosive wear increases due to the presence of high fluid velocities and solid particles [1.15]. Moreover, another application that contains highly corrosive conditions, along with presence of erosion, is the flue gas desulphurisation [1.16,1.17].

The selection of materials for the above industries is a challenge, especially when cost effectiveness is taken into consideration. The main scope for material selection is the identification of the operating environment in which specific alloys will be able to optimise the service life of the engineering components. However, the performance of selected alloys is sometimes further complicated due to the interaction between erosion and corrosion, often referred to as synergy.

The current work consists of a comprehensive experimental approach based on erosion-corrosion tests, electrochemical monitoring and microscopy techniques, whilst the interactions between erosion and corrosion and how this affects the performance of alloys in aggressive environments are investigated. For this purpose, a wide range of corrosive wear resistant alloys, that are used for manufacturing pump components in the mining industry, have been tested in corrosive slurries at low pH values or different salinity levels. Consecutively, the focus on tested alloys comprises commercial/high alloyed stainless steels, a nickel-chromium alloy and a range of proprietary white cast irons (WCI).

The novelty of this study is portrayed in the fact that there is limited information in the literature with regards to the effect of low pH on erosion-corrosion and especially the effect of salinity on material performance under erosive-corrosive conditions. Also, the importance of the microstructure in materials ranking is also illustrated. Furthermore, the investigation of unique and innovative proprietary alloys adds a special value on the current thesis, whilst the findings contribute to the development of new innovative materials. The qualitative correlation between laboratory and industrial results provides a reliable materials database and hence, the research of the current work is implemented directly into the manufacturing process of engineering components. In addition, this study demonstrates the importance of a meticulous materials selection in engineering applications that the corrosive aggressiveness is varying.

1.2 References

[1.1] E.S. Venkatesh, Erosion Damage in Oil and Gas Wells, (1986).

[1.2] H.R. Copson, Effects of Velocity on Corrosion by Water, J. Ind. Eng. Chem. 44 (1952) 1745–1752.

[1.3] M. Divakar, V.K. Agarwal, S.N. Singh, Effect of the material surface hardness on the erosion of AISI 316, Wear. 259 (2005) 110–117.

[1.4] J.H. Tylczak, Erosion-corrosion of iron and nickel alloys at elevated temperature in a combustion gas environment, Wear. 302 (2013) 1633–1641.

[1.5] D. Brondel, R. Edwards, A. Hayman, D. Hill, T. Semerad, Corrosion in the Oil Industry, Oilf. Rev. (1994) 4–18.

[1.6] M.M. Stack, N. Pungwiwat, Erosion-corrosion mapping of Fe in aqueous slurries: Some views on a new rationale for defining the erosion-corrosion interaction, Wear. 256 (2004) 565–576.

[1.7] C.I. Walker, M. Hambe, Influence of particle shape on slurry wear of white iron, Wear. 332–333 (2014) 1–7.

[1.8] C.I. Walker, P. Robbie, Comparison of some laboratory wear tests and field

wear in slurry pumps, Wear. 302 (2013) 1026–1034.

[1.9] A.J. Mierzwa, Appendix T - Mining, 55 (2008).

[1.10] An internal communication with Edward Humphries, Director of R&D, Weir Minerals Sydney, Australia (2014).

[1.11] T.E. Shokes, G. Möller, Removal of disslolved heavy metals from acid rock drainage using iron metal, Environ. Sci. Technol. 33 (1999) 282–287.

[1.12] W.H. Ahmed, Flow Accelerated Corrosion in Nuclear Power Plants, Nucl. Power - Pract. Asp. (2012) 153–178.

[1.13] H. Turbine, C. Solutions, O. Metco, Solutions Flash Robust coating solutions for hydropower turbines extend operating life and maintain efficiency, (2014) 1–8.

[1.14] Nickel Development Institute, Corrosion resistance of nickel-containing alloy in phosphoric acid, CEB-4, (415)

[1.15] I. Forest, P.O.B. Suffern, The Corrosion Resistance of Nickel-Containing Alloys in Sulfuric Acid and Related Compounds, (1983).

[1.16] IEAGHG, Corrosion and Selection of Materials for Carbon Capture and Storage, (2010).

[1.17] R. Francis, G. Byrne, G. Warburton, S. Hebdon, Applications and experiences with superduplex stainless steel in wet FGD scrubber systems, Nace Int. Corros. 2016 Conf. Expo. 1998.

Chapter 2

Erosion-corrosion theory

2.1 Introduction

Erosion and corrosion are two different phenomena that can lead to material loss in many engineering systems. In cases when both mechanisms are present, the material deterioration is enhanced due to the interaction between erosion and corrosion, which is known as synergy. The theoretical background about these phenomena, as well as other degradation mechanisms and their complexities, are described in the current Chapter.

2.2 Wear

Wear is the general term for material removal due to a mechanical process which is one of the main reasons for failures in engineering components [2.1]. One type of wear mechanism is erosion which, in case of impinging flow and the presence of solid particles (e.g sand particles), involves solid impact on the target surface and material removal due to extrusion, mainly at high angles [2.2–2.5]. Other types of wear include two-body abrasion and three-body abrasion. Misra et al. demonstrated that the two-body abrasion is the material loss by fixed abrasive particles (i.e grinding process via abrasive papers on surface preparation) which are moving across the surface, whilst the three-body abrasion involves loose particles which are able to rotate while they attack the wearing surface [2.6]. In the same work [2.6], the similarities between low angle erosion and two-body abrasion, where cutting or scratching is the main mechanism (in both cases) for material removal, has been presented. Another study demonstrated the same interpretations for two-body abrasion and three-body abrasion [2.7]. On the other hand, erosion at high angles during impingement and three-body abrasion generate plastic deformation producing extruded material which is susceptible to removal by subsequent particles. Also, when there is a noticeable depth of wear on a surface, the terms "gouging wear" or "ploughing" are often used [2.8].

The interpretation of two-body and three-body abrasion has been stated slightly differently in the work of Gates [2.9]. According to his/her findings, the meaning of three-body abrasion appeared to involve a second metal as a counterface including abrasive particles. Hence, in the same work, the two-body abrasion can be defined as the interaction between two metal faces or one metal with abrasive particles. In general, considering either interpretations of two and three body abrasion, both of them can be defined as shown in Figure 2.1.
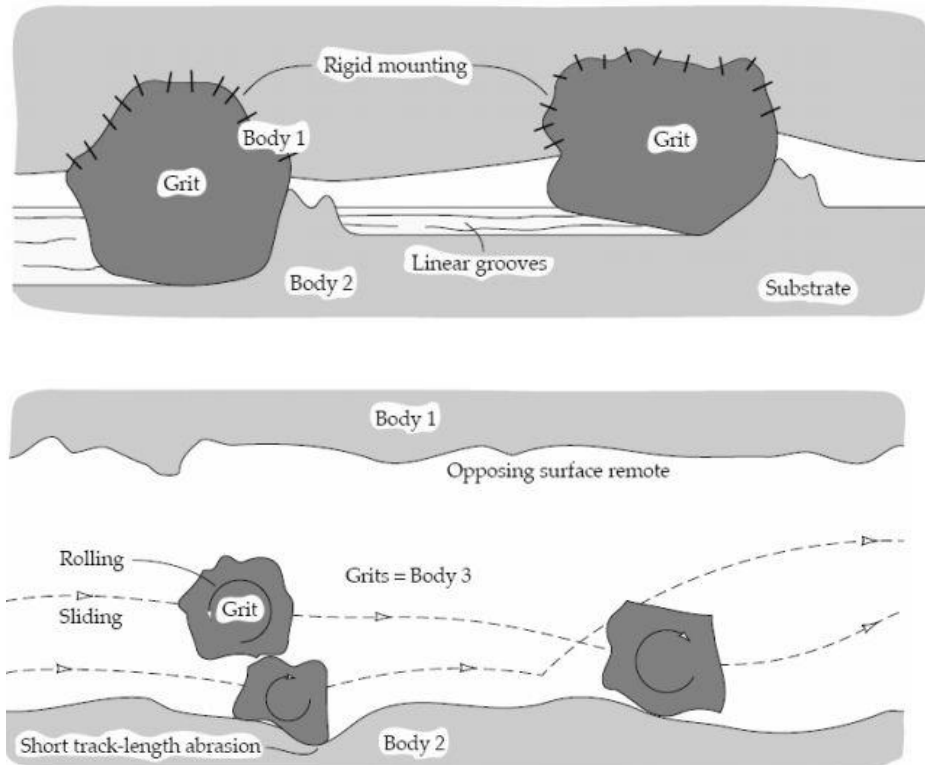
Figure 2.1: Representation of two body (top) and three body abrasion (bottom) [2.7].

In terms of initiation of the wear process, it has been shown that when a material is subjected to high velocities of aqueous solutions beyond its "specific threshold", material loss is caused by erosion whereas up to this specific threshold no erosion is observed [2.10]. The term "specific threshold" was introduced in this study [2.10], to define the initiation of erosion. However, it is generally accepted that the main parameter that increases the erosion rates is the presence of suspended solid particles in a flowing medium. Furthermore, the level of wear rate is dependent on the characteristics of the abrasive particles which are described as follows:

- Size

- Shape

- Sand concentration

- Hardness

Many researchers have demonstrated that, as the particle size becomes larger, there is a corresponding increase in the erosion rate [2.11–2.13]. However, Bahadur et al. reported that the erosion rates decreased with increasing the size of SiO_2 particles since the particles were circular, trend that was opposed to SiC and Al_2O_3 particles that had angular shape (than the SiO_2) [2.14]. The same authors [2.14] reported that the circular particles mostly caused ploughing on the metals, whilst the angular particles contributed to microcutting. Furthermore, it is generally accepted that particles with the same size but with more circular shape provide lower erosion rates since the wear/impact applied to the worn surface is lower than the corresponding with angular shape [2.13, 2.15].

The sand concentration is an important factor in determining the erosion rate. It has been shown that, by increasing the sand concentration, the erosion damage is enhanced [2.16]. A similar trend was presented elsewhere but it should be noted that, apart from higher sand concentration, the velocity was higher in the most aggressive conditions [2.17]. Xu et al. reported that the higher sand loading generated enhanced erosion-corrosion rates on UNS S32654 and UNS S31603 in slurry jet tests, whilst the electrochemical attack was increased too (higher current densities in higher sand loadings) [2.18]. Turenne et al. showed that in slurry jet tests with 17 m/s velocity and silica sand (200 – 300 μm diameter) in concentration between 1-20 wt%, the mass loss increased with increasing sand concentration [2.19]. However, the erosion efficiency in the same work (the ratio between wear and sand concentration) decreased from 1 to 13 wt% sand concentration and after 13% it remained constant. The explanation for this was that the rebounding particles act as a protective barrier on the surface and hence, the incident particles are unable to cause further damage.

The hardness of the solid particles (e.g sand particles) is a crucial parameter in terms of mechanical damage. It is well known that the ratio of hardness between the erodent (H_e) particles and the hardness of the target material (H_t) dictates the material's erosion

resistance, especially in relatively severe erosive conditions [2.20–2.22]; the higher the ratio, the higher erosion rates occur. On the other hand, when the material's hardness is higher than the corresponding hardness of the solid particles, high erosion resistance is provided.

Finally, the angle of attack is the last major parameter that affects the wear rates. According to the general notion with regards to angle of attack, the ductile materials demonstrate the highest erosive rates at low angle of attack ($15^o - 30^o$), whilst the brittle alloys possess the highest material loss at high angle of attack [2.23].

2.3 Pure electrochemical damage

2.3.1 Uniform corrosion

The corrosion phenomenon is defined as the electrochemical process between a metal and an aqueous solution and comprises two reactions: anodic and cathodic. The anodic reaction, or oxidation reaction, involves the dissolution of metal to metal ions and electrons and thus, can be described as follows [2.24]:

$$M \rightarrow M^{n+} + ne^-$$
Equation **2.1**

Where n is the number of electrons.

In contrast, the cathodic reaction, or the oxygen-reduction reaction, involves the consumption of electrons which are equal with the electrons from the anodic reaction. In the most natural waters (neutral pH value), the cathodic reaction can be described as follows [2.24]:

$$O_2 + 2H_2O + 4e^- \rightarrow 4(OH)^-$$
Equation **2.2**

The cathodic reaction is dependent on the environmental conditions. Thus, in acidic conditions it can be defined as [2.24]:

$$2H_2O + 2e^- \rightarrow 2(OH)^- + H_2 \quad \text{(water reduction)}$$
Equation **2.3**

$$2H^+ + 2e^- \rightarrow H_2 \quad \text{(in the absence of oxygen)}$$
Equation **2.4**

$$4H^+ + O_2 + 4e^- \rightarrow 2H_2O \qquad \text{(acidic water in the presence of oxygen)} \quad \textbf{\textit{Equation 2.5}}$$
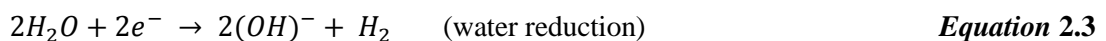
The charge being transferred at anodic and cathodic sites is obviously associated with the charge separation across the metal surface, known as the electrode potential. This electrode potential can be measured by connecting the metal with a high impedance voltmeter with a standard "reference electrode" (often saturated calomel electrode – SCE or Ag/AgCl). Once this electric field reaches a level such that no further metal dissolution is feasible (Equation 2.1), the condition is described as the "equilibrium condition" and the potential difference occurring across the metal's surface at this equilibrium condition is known as the "equilibrium electrode potential", E_0 [2.24].

Figure 2.2 illustrates the electrochemical process occurring on a metal in aqueous solution. The major outcome from this mechanism is the material loss of the metal due to corrosion. The corrosion rate is usually quantified as current density, i_{corr} (mA/cm^2), which is in fact the flowing current on the surface of the corroded metal. Thus, the metal loss due to corrosion is directly proportional to I_{corr} (via Faraday's Laws of electrolysis) [2.24].
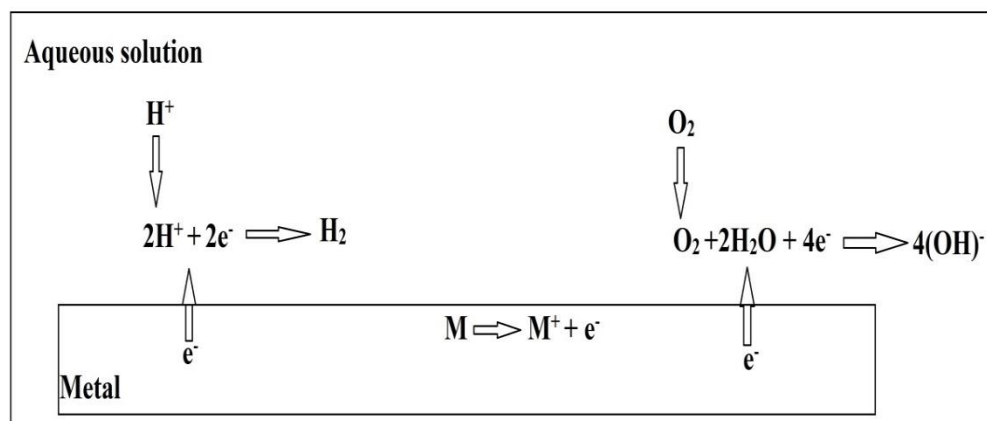
Figure 2.2: Representation of electrochemical mechanism of corrosion on metal in aqueous solution.

It should be noted that the I_{corr} cannot be measured directly since it is difficult to connect an ammeter in a micro electrical circuit and also, the anodic and cathodic reactions are carried out at different sites [2.24]. Electrochemical techniques have been

developed to identify the value of I_{corr} via extrapolation to the E_{corr} value which is the difference of electrode potential between a standard material (i.e reference electrode) and the potential of the working specimen. Hence, the I_{corr} is extrapolated to E_{corr} value since the working specimen corrodes in that electrode potential value (E_{corr}), as shown in Figure 2.3.
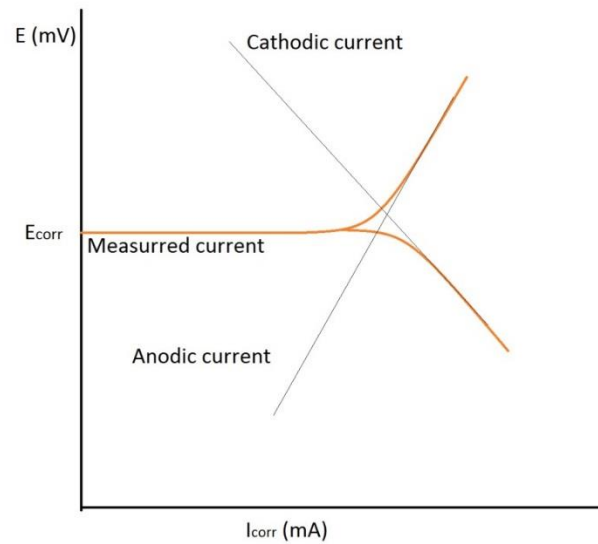
Figure 2.3: Polarisation plots produced during corrosion current monitoring.

Figure 2.4 demonstrates a typical electrochemical cell in which the working electrode (corroding metal) is measured against the reference electrode, whilst the auxiliary electrode transfers current from the potentiostat to the working electrode and thus, an open electrical circuit is formed [2.18, 2.24, 2.25]. The potential of the working electrode is shifted to more positive values than E_{corr} (anodic polarisation) or to more negative values than E_{corr} (cathodic polarisation). As the potential shifts to a more positive direction from E_0, the reaction is driven to the anodic direction (Eq. 2.3) and hence, the greater shift in potential from E_0, the faster will be the anodic reaction.
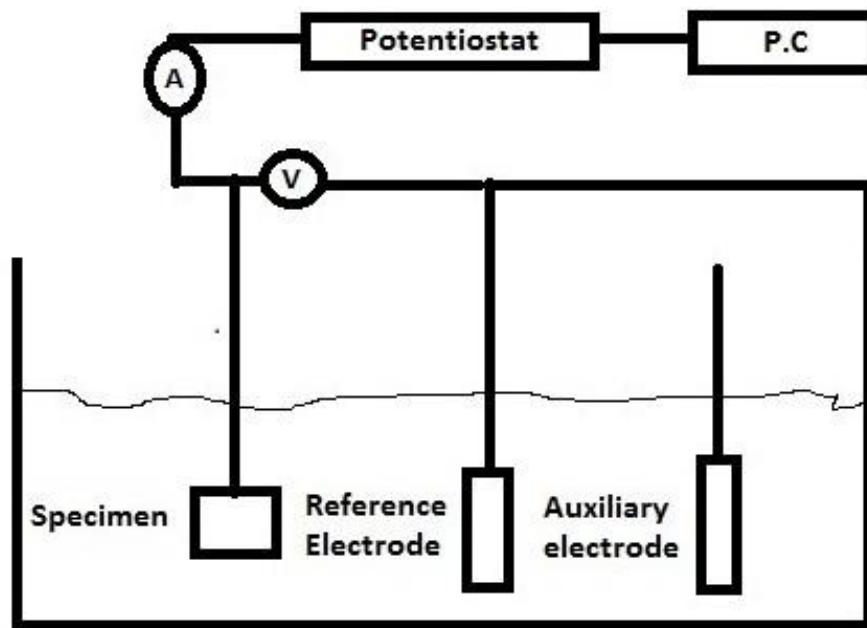
Figure 2.4: Representation of a typical electrochemical cell.

2.3.2 Factors affecting corrosion rates

The anodic reaction rate at any specific electrode potential is dependent on the phenomenon called polarisation, which controls the rate of the electrode reactions [2.25]. When a particular electrode reaction is severely polarised, as the potential is shifted to more positive than E_0 potentials, then a slow increase in the reaction rate occurs and subsequently, a low I_{corr} is observed [2.24].

At this stage, it is worth mentioning the phenomenon "concentration polarisation" which affects the reaction rates. During that phenomenon, the progress of a cathodic electrode reaction is restricted by the rate of supply of reactants. The concentration polarisation usually occurs in the cathodic reaction in either neutral/alkaline or acidic solutions. However, the phenomena related to increased corrosion rates due to concentration polarisation are varying in different levels of pH, as described below:

- In neutral or alkaline water, since the oxygen reduction cathodic reaction suffers from "concentration polarisation", any factor that stimulates the supply of dissolved oxygen to the corroded metal's surface will depolarise the

cathodic reaction resulting in higher corrosion rates, as shown in the example of Figure 2.5 [2.25].

- In acidic water, the cathodic reaction involves hydrogen production and therefore, the cathodic polarisation is less prominent due to the very small hydrogen ion diffusion at sufficient rates resulting to higher corrosion rates because of concentration polarisation (Figure 2.6) [2.25].
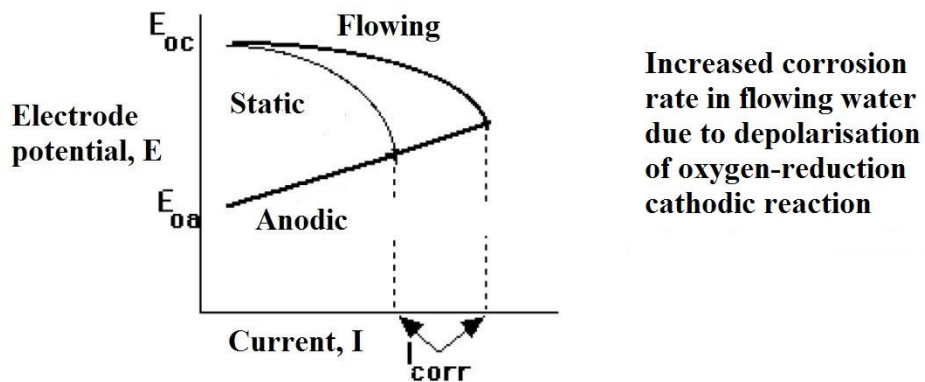
Figure 2.5: Dependence of corrosion rates on polarisation characteristics of the oxygen reduction cathodic reaction in neutral water.
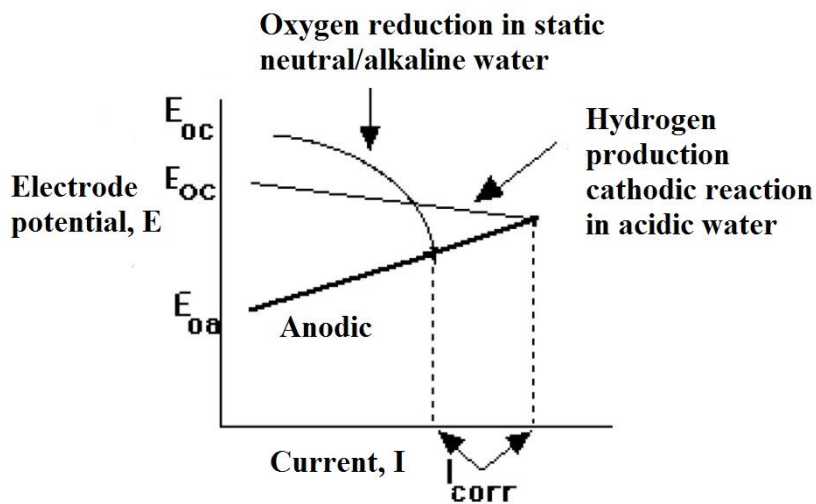
Figure 2.6: Dependence of corrosion rates on different on polarisation characteristics of hydrogen production and oxygen reduction cathodic reactions.

In general, the acidity of water is defined by the pH level which is the concentration of hydrogen ions expressed in the logarithmic scale, as shown in Equation 2.6. It is generally accepted that ten times more hydrogen ions are produced for every unit of pH below 7 (i.e from pH 5 to 4), which is the value of neutral water. The acidic water produces high corrosive rates on metals since it decreases the passivity and exposes the target surface to enhanced electrochemical reactions that are described above.

$$pH = -\log[H^+]$$ ***Equation* 2.6**

2.3.3 Localised corrosion

Anodic and cathodic reactions occur simultaneously on a corroded surface causing uniform corrosion. However, in many engineering systems the anodic and cathodic reactions are permanently separated in specific locations of the component's surface resulting localised corrosion with possible catastrophic consequences [2.25]. Localised corrosion consists of various forms, some of which are:

- Pitting corrosion
- Crevice corrosion
- Galvanic corrosion

When the corrosion protection breaks down locally, the corrosion is promoted at these local sites. Therefore, pits are developed at these sites and this term is well known as "pitting corrosion" [2.25]. On the other hand, "crevice corrosion" involves similar local attack due to corrosion but occurs usually in a sheltered location such as a gap of two bolted components [2.25].

Galvanic corrosion refers to the phenomenon that two components with different electrode potentials are connected electrochemically e.g with a wire via a weld or bolted together and exposed in an aqueous environment [2.25]. The component with the more negative electrode potential acts as an anode and the component with the more positive electrode potential act to some extent as a cathode [2.25]. Thus, the anode is corroded faster, whilst the cathode is "protected" from electrochemical attack [2.25].

2.3.4 Hydrogen embrittlement

The previously mentioned hydrogen production (Equation 2.6) occurs during the cathodic reaction in the electrochemical process. In cases that increased hydrogen ions are produced due to environmental conditions, potential absorption of hydrogen by a metal surface can be conducted resulting in a reduction of the metal's ductility and thereby brittle fracture, phenomenon known as hydrogen embrittlement (HE) [2.25, 2.26]. The hydrogen entry into a metal can be facilitated by insufficient control of cathodic reaction, which includes some operating conditions that generate hydrogen such as welding, electroplating, pickling and low pH solutions. Also, hydrogen embrittlement has been reported to be a severe issue for engineering components in cathodic protection applications in which high strength steels (around 700 MPa) or alloys possessing high hardness (>350HV) [2.27]. The absorption of hydrogen can cause engineering failures due to stress corrosion cracking which involves crack initiation and growth along the grains of metals. Further mechanisms of hydrogen embrittlement involve carbon content of materials and suggest that hydrogen diffuses along the grain boundaries and combines with the carbon to form methane gas. The methane gas is not mobile and collects in small voids along the grain boundaries where it builds up enormous pressures that initiate cracks [2.28].

2.3.5 Corrosion in engineering systems

In the field service, it is usually vital to quantify the material loss due to corrosion. Thus, the corrosion rates are converted to either mm/year or g (or mg) for a particular period of time. In the current Ph.D. thesis, the latter conversion was used by using Faraday's Law which is described as follows:

*C(mg) = I$_{corr}$ (mA) * 3600 (sec) * Mms (g/mole) / F (coulomb/mol) * n*   ***Equation 2.7***

Where, Mms is the molar mass, F is Faraday's constant equivalent to 96.485 C/mol, n is the number of electrons transferred in the anodic reaction and 3600 is the duration of the experiments in seconds.

An important feature in either field service or laboratory tests is whether the corrosive attack on the metal is constant for a period of time or not. For this purpose, the corrosion monitoring involves linear polarisation (or polarisation resistance) which

utilises the same experimental setup as shown in Figure 2.4 but the electrode potential is shifted from about -10 mV to +10 mV either side of E_{corr} for different periods of exposure time [2.25]. The method involves plotting potential versus current and calculating the gradient which is called the polarisation resistance, R_p which is inversely proportional to I_{corr}. In general, the consistency of R_p results indicate constant corrosion rate during the investigated period. Furthermore, the linear polarisation method consists of a semi quantitative method for corrosion evaluation since the higher R_p, the higher corrosion resistance is achieved.

2.3.6 Corrosion protection

In the past years, various methods have been developed for corrosion protection. Apart from materials selection that can withstand the electrochemical attack in specific environments, cathodic protection (CP) has widely been used in many industries [2.24].

CP application is achieved by implementing an "impressed current cathodic protection" (ICCP) which keeps the electrode potential to very negative values (usually) around -850 mV for steel where the anodic current densities are negligible and therefore, the corrosion is suppressed [2.25]. This method has been used in the current project for evaluation of pure mechanical damage (since corrosion and synergy are mitigated). Alternatively, another method of CP is the "sacrificial anode" in which zinc or aluminium is used as an anode providing very negative potential and hence, the working material is protected since it acts as a cathode [2.25].

2.4 Erosion-corrosion

Erosion-corrosion represents a complex phenomenon due to the involvement of different mechanisms; mechanical damage (erosion-abrasion), electrochemical damage (corrosion) and the interaction between the two phenomena. It is generally accepted [2.29, 2.30] that this material deterioration process can be explained by the following equation.

$$TML = E + C + \Delta Ec + \Delta Ce \qquad \qquad \textit{Equation } 2.8$$

where, TML is the total material loss, E is the mechanical damage, C is the material loss due to pure electrochemical reactions/corrosion, ΔEc is the enhanced erosion by the corrosion process, and ΔCe is the enhanced corrosion by the erosion processes.

However, since the corrosion tests in static water were not the focus of the author, a simplified version of Equation 2.8 is used, as follows:

$$TML = M + C + S$$ ***Equation* 2.9**

Where, TML is the total material loss, M is the mechanical damage, C is the corrosion that is occurring during erosion-corrosion conditions (C+ΔCe from Equation 2.8) and S is identical to ΔEc, the enhanced erosion by the corrosion process.

The importance of the synergistic effects has been emphasised by various researchers [2.31, 2.32]. Aribo et al. demonstrated the erosion-corrosion behaviour of an austenitic stainless steel and three different grades of duplex stainless steels in saline water (3.5% NaCl) by isolating the pure mechanical damage, corrosion and synergy (both ΔEc, ΔCe) through electrochemical techniques [2.33]. In their work [2.33], it was clearly shown that erosion and corrosion were enhanced as a result of the synergy and this is ignored from many researchers and engineers in industry due to lack of capabilities to determine the synergy. When a significant proportion of abrasive particles are present, it is well known that the erosion mechanism is dominant [2.17, 2.34]. The materials that are able to withstand the erosion-corrosion attack should provide resistance to each individual mechanism. An example of this was shown in the work of Giourntas et al. [2.31] who reported that the erosion-corrosion performance of medium carbon steel (UNS G10400) was poor compared to austenitic stainless steel (UNS S31600). This was mainly due to the vulnerability to corrosion in the case of UNS G10400, whilst the difference in erosion between the two materials was less significant [2.35].

2.5 References

[2.1] R. Malka, S. Nesic, D.A. Gulino, Erosion corrosion and synergystic effecrs in disturbed liquid-particle flow, Nace Expo. (2006) 22.

[2.2] M. Reyes, A. Neville, Mechanisms of erosion-corrosion on a cobalt-base alloy and stainless-steel UNS S17400 in aggressive slurries, J. Mater. Eng. Perform.

10 (2001) 723–730.

[2.3] D.H. Mesa, A. Toro, A. Sinatora, A.P. Tschiptschin, The effect of testing temperature on corrosion - erosion resistance of martensitic stainless steels, Wear. 255 (2003) 139–145.

[2.4] R.J.K. Wood, J.C. Walker, T.J. Harvey, S. Wang, S.S. Rajahram, Influence of microstructure on the erosion and erosion-corrosion characteristics of 316 stainless steel, Wear. 306 (2013) 254–262.

[2.5] T. Foley, A. Levy, The erosion of heat-treated steels, Wear. 91 (1983) 45–64.

[2.6] A. Misra, I. Finnie, Correlations between two-body and three-body abrasion and erosion of metals, Wear. 68 (1981) 33–39.

[2.7] I.K.Ř. Íková, B. Szewczyková, P. Blaškovitš, E. Hodúlová, E.L. Č, Study and Characteristic of Abrasive Wear Mechanisms, (2012) 1–9.

[2.8] C.I. Walker, P. Robbie, Comparison of some laboratory wear tests and field wear in slurry pumps, Wear. 302 (2013) 1026–1034.

[2.9] J.D. Gates, Two-body and three-body abrasion: A critical discussion, Wear. 214 (1998) 139–146.

[2.10] E.S. Venkatesh, Erosion Damage in Oil and Gas Wells, (1986).

[2.11] H.M. Clark, R.B. Hartwich, A re-examination of the "particle size effect" in slurry erosion, Wear. 248 (2001) 147–161.

[2.12] H.H. Tian, G.R. Addie, K. V. Pagalthivarthi, Determination of wear coefficients for erosive wear prediction through Coriolis wear testing, Wear. 259 (2005) 160–170.

[2.13] S.L. Palasamudram, S. Bahadur, Particle characterization for angularity and the effects of particle size and angularity on erosion in a fluidized bed environment, Wear. 203–204 (1997) 455–463.

[2.14] S. Bahadur, R. Badruddin, Erodent particle characterization and the effect of

particle size and shape on erosion, Wear. 138 (1990) 189–208.

[2.15] M. Vite-Torres, J.R. Laguna-Camacho, R.E. Baldenebro-Castillo, E.A. Gallardo-Hernández, E.E. Vera-Cárdenas, J. Vite-Torres, Study of solid particle erosion on AISI 420 stainless steel using angular silicon carbide and steel round grit particles, Wear. 301 (2013) 383–389.

[2.16] S.S. Rajahram, T.J. Harvey, R.J.K. Wood, Erosion-corrosion resistance of engineering materials in various test conditions, Wear. 267 (2009) 244–254.

[2.17] G. Karafyllias, L. Giourntas, T. Hodgkiess, A.M. Galloway, Relative performance of two cast irons and two stainless steels under erosion-corrosion conditions, Nace Int. Corros. 2016 Conf. Expo. (2016) 1–10.

[2.18] X. Hu, A. Neville, The electrochemical response of stainless steels in liquid-solid impingement, Wear. 258 (2005) 641–648.

[2.19] S. Turenne, M. Fiset, J. Masounave, The effect of sand concentration on the erosion of materials by a slurry jet, Wear. 133 (1989) 95–106.

[2.20] S.G. Sapate, A. V. Rama Rao, Effect of carbide volume fraction on erosive wear behaviour of hardfacing cast irons, Wear. 256 (2004) 774–786.

[2.21] S. Wada, Effects of Hardness and Fracture Toughness of Target Materials and Impact Particles on Erosion of Ceramic Materials, Key Eng. Mater. 71 (1992) 51–74.

[2.22] P.H. Shipway, I.M. Hutchings, The rôle of particle properties in the erosion of brittle materials, Wear. 193 (1996) 105–113.

[2.23] I. Finnie, Erosion of surfaces by solid particles, Wear. 3 (1960) 87–103.

[2.24] Anne Neville. An investigation of the corrosion behaviour of a range of engineering materials in marine environments. PhD thesis. Glasgow University (1995).

[2.25] H. Silman, Corrosion and Corrosion Control: An introduction to corrosion science and engineering, 2008.

[2.26] J. Alsarraf, Hydrogen Embrittlement Susceptibility of Super Duplex Stainless Steels, PhD Thesis. Cranfield University (2010).

[2.27] D.N. Veritas, Dnv-Rp-B401 Cathodic Protection Design, (2011).

[2.28] J. Cwiek, Hydrogen degradation of high-strength steels, J. Achiev. Mater. Manuf. Eng. 37 (2009) 193–212.

[2.29] V.A. De Souza, A. Neville, Corrosion and erosion damage mechanisms during erosion–corrosion of WC–Co–Cr cermet coatings, Wear. 255 (2003) 146–156.

[2.30] A. Neville, "Erosion-corrosion; Management of material damage", Corrosion Matters NACE Workshop, London, (2015).

[2.31] L. Giourntas, T. Hodgkiess, A. M. Galloway, Enhanced approach of assessing the corrosive wear of engineering materials under impingement, Wear. 338–339 (2015) 155–163.

[2.32] J.M. Perry, A. Neville, V.A. Wilson, T. Hodgkiess, Assessment of the corrosion rates and mechanisms of a WC-Co-Cr HVOF coating in static and liquid-solid impingement saline environments, Surf. Coatings Technol. 137 (2001) 43–51.

[2.33] S. Aribo, R. Barker, X. Hu, A. Neville, Erosion-corrosion behaviour of lean duplex stainless steels in 3.5% NaCl solution, Wear. 302 (2013) 1602–1608.

[2.34] A. Neville, T. Hodgkiess, Characterisation of high-grade alloy behaviour in severe erosion-corrosion conditions, Wear. 233–235 (1999) 596–607.

[2.35] L. Giourntas, T. Hodgkiess, A.M. Galloway, Comparative study of erosion–corrosion performance on a range of stainless steels, Wear. 332–333 (2015) 1051–1058.

Chapter 3

Erosion-corrosion performance review of evaluated materials

3.1 Introduction

This chapter comprises a literature review on the evaluated materials with regards to their microstructure and erosion-corrosion performance. As stated in chapter 1, the alloys used for manufacturing the wear parts of pumps in mining industries were investigated in the current study. The testing conditions were similar to which these materials are designated to operate in the field service (neutral/acidic pH, high/low salinity level), or even slightly more aggressive conditions in order to identify their behaviour beyond their capabilities. Furthermore, the wide range of tested alloys with different properties provided useful information about erosion-corrosion phenomena and demonstrated how the microstructure dictates the performance of materials under specific erosion-corrosion conditions. The material types included stainless steels, white cast irons (WCI) and a nickel-chromium alloy, whilst some of the proprietary alloys are considered innovative with respect to their unique microstructure which adds further value to research community.

3.2 Stainless steels

3.2.1 Austenitic – martensitic grades

A standard austenitic stainless steel (UNS S31600), which was used as a reference material and a martensitic stainless steel (UNS S42000) were assessed in neutral and acidic pH conditions. Stainless steels are ferrous alloys with a minimum Cr content of 11-12%. Different grades of stainless steels are characterised by their chemical composition, especially by Ni and Mo concentrations.

Stainless steels are widely used in many industries in which corrosion resistance is a requirement. Their corrosion resistance is the result of the passive oxide film, enriched with Cr, which is typically 1-3 nm thick and provides general passive behaviour in

many aqueous solutions [3.1]. The ability of stainless steels to remain passive in various environments is dependent on the Cr content and also on the presence of other elements such as Mo, W and N [3.2, 3.3]. Furthermore, when the passive film of stainless steels is attacked by an impinging velocity containing solid particles, depassivation and repassivation events occur. However, the corrosion rate is noticeably higher under flowing conditions than in static water, especially when the particles are present [3.1, 3.4]. It is well understood that, when the passive film is eliminated by either mechanical or electrochemical attack, the stainless steels are rapidly corroded [3.5].

Different grades of stainless steels provide a wide range of properties for many engineering environments. A typical martensitic grade contains typically 12-15 % Cr with relatively high C (0.14-0.64% wt) and is usually used in environments where erosion and/or abrasion resistance are necessary. The corrosion resistance of martensitic stainless steel is relatively moderate and it is the lowest among the stainless steels family [3.6].

Austenitic stainless steel contains a minimum 16% Cr and 6% Ni [3.7]. The Ni element is important because of its ability to stabilise the austenitic structure (along with Mn). This is achieved by expanding the temperature range for stable austenite by suppressing the α-γ transformation and raising the γ-δ transformation [3.8]. The austenitic alloys offer excellent corrosion resistance and very good ductility, especially when they are high alloyed with enhanced Cr, Ni and Mo, well known as the superaustenitic grades. On the other hand, the strength is lower than in the martensitic stainless steels and the erosion resistance is poorer compared to the stainless steels with a harder surface, such as the martensitic and duplex grades [3.9].

Several groups have investigated the erosion-corrosion performance austenitic and martensitic stainless steel in which the superaustenitic stainless steel (UNS S32654) was superior over austenitic stainless steel (UNS S31603) in 3.5% NaCl and neutral pH [3.10, 3.11]. Moreover, Wood et al. reported that the solid particle impact can create lip formation and a localised martensitic phase on UNS S31603 in fresh water, whilst in 3.5% NaCl solution the local martensitic phase was dissolved resulting in higher erosive rates for the alloy tested [3.12]. Atashin et al. showed, in an extensive

quantitative and qualitative study, how the environmental factors, especially the temperature, dictate the erosion-corrosion behaviour of UNS S31600 in marine environments and emphasise the differentiation in erosion, corrosion and synergy contributions to total material loss [3.13].

Comparing austenitic with martensitic grades, Lopez et al. demonstrated that, in strong acidic erosive-corrosive conditions (0.5 M H_2SO_4), the main mechanisms that contributed to total mass loss of austenitic UNS S30400 and martensitic UNS S42000 at various angles of attack under varying velocities were plastic strain and corrosion for the latter and former respectively [3.14]. In addition, it has been shown that the austenitic grades offer better corrosion resistance than the martensitic grades under erosive-corrosive conditions [3.15], but, in terms of wear resistance, the martensitic stainless steels are superior to austenitic stainless steels [3.16].

3.2.2 Duplex and Superduplex grades

A commercial superduplex stainless steel (UNS S32760) and a proprietary duplex stainless steel, containing a small quantity of σ phase were tested under aggressive erosion-corrosion conditions.

Duplex stainless steels are ferritic-austenitic alloys containing an approximate phase balance of 50% ferrite and 50% austenite. They provide superior corrosion and stress corrosion cracking resistance over the austenitic stainless steels, whilst improved erosion resistance is achieved too [3.17]. The superiority of duplex stainless steel (UNS S32205) over austenitic stainless steel (UNS S30400) under erosion-corrosion conditions in 3.5% NaCl has been demonstrated elsewhere [3.18, 3.19]. The advanced grades of duplex stainless steels that contain higher Cr, Ni, Mo and traces of N, known as superduplex, demonstrate enhanced erosion-corrosion and corrosion resistance over the standard duplex alloys [3.3] . At pH ranges between 5.5-7 and in either saline or no saline testing medium, previous studies have demonstrated that the erosion-corrosion and pure corrosion resistance of superduplex stainless steel was superior to the austenitic/martensitic stainless steels [3.15, 3.20, 3.21]. In terms of pure corrosion resistance, the excellent performance of superduplex stainless steels was reported by Neville and Hodgkiess [3.22], when it was compared with Inconel 625 and Stellite 6 in erosion-corrosion conditions (in saline water).

The excellent corrosion and erosion-corrosion resistance in acidic slurry applications of superduplex stainless steel has been emphasised elsewhere [3.23]. In the same study [3.23], laboratory tests and service experience illustrated the excellent performance at low pH (pH 3) erosive conditions as well as in many industries such as oil and gas, chemicals, fertiliser, mining extractions and flue gas desulphurisation. Also, superduplex stainless steel is successfully used in the hot concentrated sulphuric acid industry and, in some acid concentrations, has been found to be more corrosion resistant than high grade alloys such as UNS S31000, UNS N08020 and UNS S32750 [3.24].

In engineering applications where enhanced erosion is present, additional wear resistance along with corrosion resistance is necessary. In most cases, the increase in hardness via heat treatment of duplex stainless steel leads to the formation of intermetallic phases (χ, σ) and Cr carbides in the microstructure [3.25]. It has been reported that when N is present, the ferrite phase can transform to secondary phases, including chromium nitrides formation (Cr_2N), through the following eutectoid reaction [3.26]:

$$Ferrite \Rightarrow \chi + \sigma + Cr_2N \hspace{4cm} \textit{Equation 3.1}$$

In addition, the secondary austenite phase is often formed on the ferrite grain boundaries and is defined as γ_2 (δ ferrite $\rightarrow$ γ_2). Also, it has been reported that secondary austenite islands can be formed independently by diffusion at 800-950 $^{\circ}$C in the main austenitic structure toward the ferrite boundaries and contain higher Cr and Mo content than the γ_2 formed by the eutectoid reaction [3.27]. The χ phase forms earlier than the σ phase and it transforms into the σ phase after ageing. The growth of these χ and σ precipitates depletes Cr and Mo preferentially in ferrite over the austenite and this is due to the fact that ferrite contains more Cr than austenite and results in higher diffusion rates of Cr to the intermetallic phases. At 850 $^{\circ}$C, the σ phase can be formed by three mechanisms [3.28]:

- nucleation and growth from original ferrite
- eutectoid decomposition of ferrite (also forming secondary austenite)
- growth from austenite after total consumption of original ferrite.

Figure 3.1 demonstrates the phases in the microstructure of UNS S31803 duplex stainless steel during heat treatment for a given time duration and temperature in which the σ phase dissolution occurs at higher temperatures than 1000-1100 ℃ (depending on the specific alloy) [3.29, 3.30].
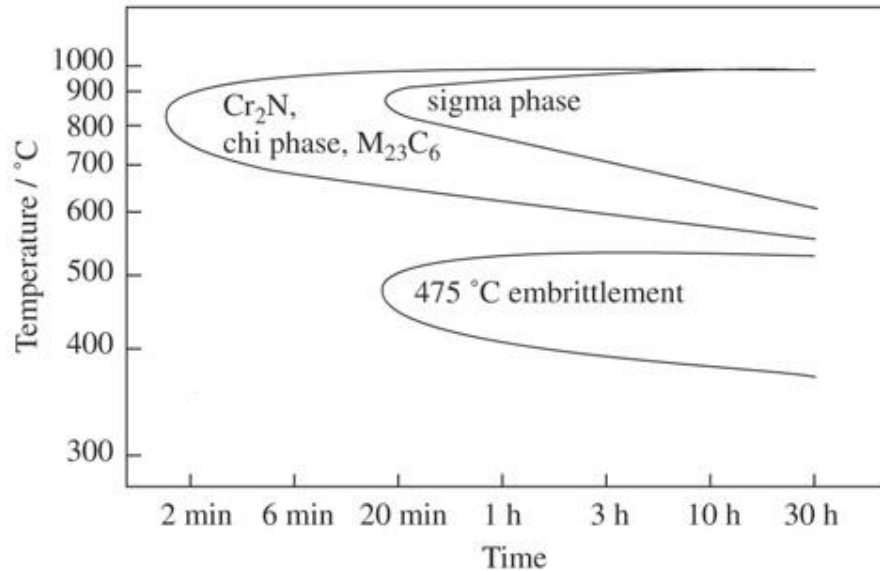

Figure 3.1: Precipitation diagram of UNS 31803 and phases formation in conjunction with time and temperature [3.30].

Chan et al. showed that σ phase reduces the impact toughness making the material more brittle suffering from phenomena such as hydrogen embrittlement, whilst the corrosion resistance is also impaired [3.26]. The negative effects of σ phase in corrosion resistance of duplex and superduplex stainless steels have been emphasised elsewhere [3.26, 3.31, 3.32]. Moreover, some researchers investigated the '475 embrittlement' (Figure 3.1) phenomenon on duplex stainless steel in which the α' prime phase is precipitated causing severe embrittlement and simultaneously, the mechanical and corrosion properties are impaired [3.33, 3.34]. Also, some researchers have reported on the rapid decrease in toughness on superduplex stainless steels containing intermetallic phases (σ, χ) [3.35–3.38]. In some innovative studies, micro-electrochemical techniques showed the vulnerability of intermetallic phases to corrosion [3.38, 3.39]. Furthermore, many researchers have reported the detrimental

effects of σ phase on pitting corrosion resistance [3.40, 3.41]. Finally, Paulraj et al. demonstrated in a recent extensive report all the above disadvantages of σ phase and also their overview analysed the effect of important chemical elements on the formation of intermetallic phases [3.42]. However, they did not report on the improved corrosive wear resistance on either duplex stainless steels or Ni-Cr alloys via the presence of controlled σ phase [3.43–3.45]. Thus, the challenge of investigating alloys in which σ phase increase the corrosive wear resistance was a motivation to include such alloys in the current Ph.D. programme.

3.3 High chromium white cast irons

Four commercially available WCIs and an experimental WCI with Nb carbides were tested in the current work under various erosion–corrosion conditions; the general description of the alloys is as follows:

- 27WCI - medium carbon, close to eutectic point
- 37WCI – low carbon, hypoeutectic
- 38WCI – high carbon, hypereutectic
- 30WCI – high carbon, hypereutectic
- 27WCINb – same as 27HWCI with additional Nb carbides

Further details about WCIs are demonstrated in the corresponding chapters.

3.3.1 Types of cast irons

Cast irons are primarily irons containing more than 2%C and generally high silicon concentrations (1-3%) since both elements improve the cast and age hardening properties (i.e the melting temperatures for molten iron are lower than the molten steel) [3.46]. Figure 3.2 demonstrates the approximate ranges of C and Si contents for steels and various cast irons. The upper dashed line corresponds to eutectic composition for Fe-C-Si alloys. In the absence of silicon, the eutectic composition is at 4.3% carbon, whilst as silicon is increased, the carbon eutectic is decreased. Since this is a linear relation it can be expressed simply by the Equation 3.2, known as carbon equivalent (CE) [3.47].
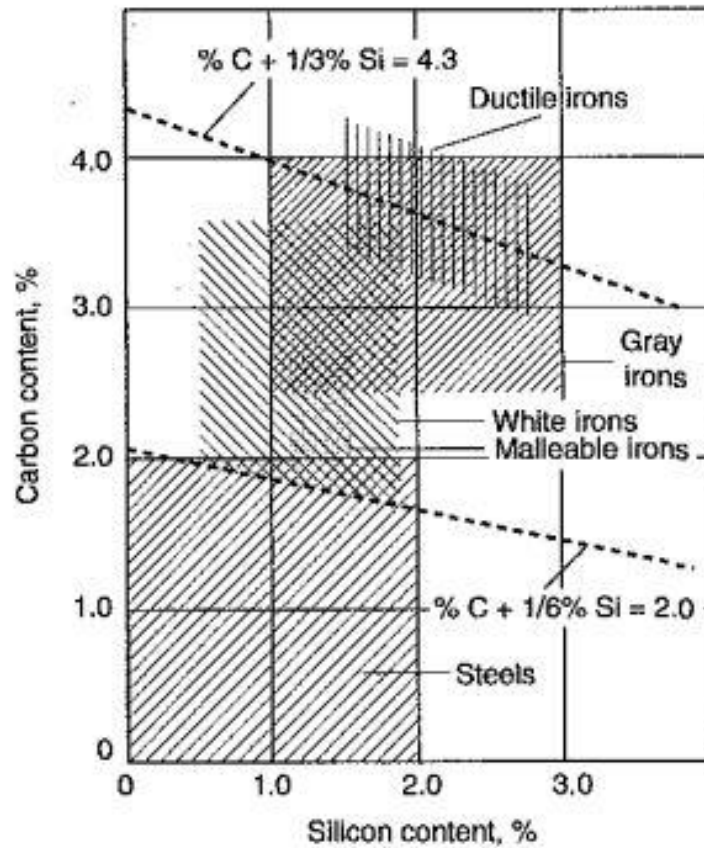
Figure 3.2: Approximate ranges of carbon and silicon for steels and various cast irons [3.47].

$$CE\ (\%wt) = C + \frac{Si}{3} \qquad\qquad\qquad\textit{Equation 3.2}$$

A low CE and high cooling rate promotes the formation of white cast iron, whilst a high CE with low cooling rate favours the formation of grey cast irons. During solidification, the major part of carbon precipitates in the form of cementite or graphite. After the completion of solidification process, the precipitated phase coexists with the austenitic matrix, which has CE concentration of about 2 wt% [3.47]. Further cooling leads to a decrease of carbon content of austenite due to the fact that more cementite or graphite precipitates from the solid solution. Also, in majority of cast irons, the austenite decomposes to pearlite at the eutectoid temperature [3.48].

In general, there are six generic types of cast irons, as summarised below [3.46]:

- Grey cast irons: The microstructure includes graphite flakes.

- Ductile cast iron: Refers to spheroidal graphite iron microstructure.

- Compacted graphite iron: The graphite occurs as blunt flakes which are interconnected within each cell. The graphite structure and the resulting properties are between the grey and ductile irons.

- Malleable iron: The major proportion of C is formed as irregularly nodules and graphite in the microstructure. This type of graphite is known as temper carbon since it is formed in the solid state during the heat treatment.

- White iron: The metal solidifies with C combined with iron as iron carbide. This type of cast iron is considered very brittle and it is free of graphite.

- High alloy irons: Commercial type which includes high alloy white irons, high alloy grey irons and high alloy ductile irons. They are used in special applications that extreme abrasion resistance is needed. These alloys are usually specified by their chemical composition.

3.3.2 White cast irons

Since the WCIs are the only type of cast irons that has been tested in the current project, an extensive literature review was carried out. In general, WCIs are mainly alloyed with chromium and carbon resulting in eutectic carbides formation during solidification and secondary carbides via heat treatment [3.49]. Wiengmoon showed that during heat treatment, the secondary carbides formed by destabilisation of austenite matrix of WCIs, do not nucleate and grow on the eutectic carbides but are precipitated within the matrix [3.50]. Furthermore, the WCIs are classified as hypoeutectic (<3%C), eutectic (around 3%C) and hypereutectic (>3%C) [3.51]. It has been shown that, with increasing carbon content (hypereutectic), large primary chromium carbides are formed increasing the carbide volume fraction (CVF), whilst the free Cr dissolved in the matrix is reduced thereby providing good wear resistance but poor corrosion resistance [3.49, 3.52]. On the other hand, hypoeutectic WCI's possess low CVF but the increase in dissolved Cr improves the corrosion resistance, whilst the wear resistance is reduced [3.49, 3.52]. Llewellyn et al. reported that hypereutectic WCIs were superior over eutectic and hypoeutectic alloys, with approximately the same %Cr in total, and also, superior over duplex and superduplex

stainless steels under Coriolis low angle erosion tests [3.49]. The superiority of hypereutectic WCIs compared to eutectic alloys, in terms of wear resistance, was also confirmed via field service reports and has been further demonstrated elsewhere [3.49, 3.53, 3.54]. However, WCI with a fine microstructure and fine distribution of Cr carbides showed improved wear resistance compared to materials with a coarse microstructure [3.49, 3.55, 3.56]. The importance of the fine microstructure was also reported by Chung et al. who showed that eutectic WCI with a finer structure than hypereutectic (with the same %Cr) performed better under erosion-corrosion conditions [3.51]. The superiority of a range of WCIs over UNS S31600 stainless steel under erosive-corrosive conditions in neutral pH conditions and saline water has been reported [3.57, 3.58].

Although the extent of published research on the erosion-corrosion behaviour of WCI's in low pH solutions is limited, Tang et al. investigated the erosion-corrosion performance of 45%Cr WCI with 1, 2, 3, 4, 5 and 6% carbon within a martensitic matrix at pH 7, 5 and 3. They reported that the 45%Cr with 4%C was the optimum alloy at all the pH levels [3.59]. Finally, Zhang et al. used an innovative approach that involved the study of interface galvanic effects during erosion-corrosion tests [3.60]. The erosion-corrosion tests at pH 1.5 displayed high calculated synergistic effects and substantial galvanic corrosion contributions which, however, were calculated from pure corrosion rates that had been measured in dynamic conditions but without the presence of solid particles. This experimental approach would inevitably yield low values of the corrosion component and high values of synergy respectively. Also, these experiments were conducted at a relatively low velocity of 5 m/s.

Many researchers in the past have investigated the improvement of wear resistance on WCI's maintaining or even improving the toughness via the refinement of Cr carbides by adding various elements, such as Ti, N, Mo, V, B, Nb, which are strong carbide formers and react spontaneously with the carbon [3.61–3.66]. Simultaneously, the hardness of the WCIs can be increased. It has been shown that Ti is an attractive element which in conjunction with the appropriate CVF (Cr carbides) and metallic matrix improves the wear resistance of WCIs, since hard Ti carbides are formed, without impairing the toughness [3.65, 3.66]. Ding et al. presented an important study

in which 0.2% N improved both wear resistance and toughness on a WCI with 2.2% C, 25% Cr and 0.8% Ti by forming Ti carbides and Ti nitrides on austenite-partially transformed to martensite [3.63]. In another study, involving pin on disk wear tests, cracks were observed in M_7C_3 carbides on hypoeutectic WCI but not in M_6C carbides that were produced by additions of Mo to the WCI. This might be expected to improve the toughness but can improve the toughness the toughness values were not quoted [3.64]. Also, it has been reported that additions of V improved both wear resistance and fracture toughness of the WCIs [3.65, 3.66].

3.3.3 Niobium white cast irons

With regards to NbC embedded in WCI's, it should be noted that there is limited literature. It has been reported that additions of Nb on WCIs consumes carbon since NbC are formed rapidly, whilst microstructure refinement occurs [3.68–3.70]. The same trend was also noticed in another study in which Nb was implemented in cast AISI H13 hot work tool steel [3.71]. Furthermore, Zhi et al. demonstrated that the formation of NbC decrease the volume fraction of primary M_7C_3 carbides on hypereutectic WCIs [3.72]. Filipovic et al. demonstrated the metallurgical investigation, including wear and toughness, of 2.9 %C white cast iron − austenitic matrix with three different additives: 1.5% Nb, 1.5% V and 1.5% Nb and 1.5% V. The results showed that the austenite was transformed partially to martensite, whilst the Charpy toughness and the abrasion resistance (dry-sand rubber wheel test) were increased in the alloy that Nb and V were added together. The resulting NbC concentrations were around 2% [3.73]. Similar trends in terms of wear resistance and toughness (similar amounts of Nb on WCI with austenite matrix) were noticed elsewhere [3.74]. Chung et al. demonstrated that the added Nb was more beneficial, in terms of high hardness and wear resistance, on a basic white cast iron (WCI − 25% Cr, 4% C) when the final alloy was in near-eutectic microstructure. The wear tests were performed on a pin-on-disk wear tester [3.75]. Chen et al. showed that 15% WCI (austenite matrix) with 1.47% Nb had the optimum wear resistance compared to 0.17%, 0.565, 0.86% Nb additions under wet rubber wheel tests. The benefits of 1.47% Nb on WCI (in the same work) were validated by field tests, which exhibited increase in the service life of impellers and liners by 67% and 47% respectively [3.76]. Finally,

Wang et al. reported that 6% Nb improves the abrasion resistance on 23Cr WCI, especially when 0.4% V and W are added [3.77].

3.4 Nickel-chromium alloys

A hardened nickel-chromium (Ni-Cr) alloy was tested under neutral and very strong acidic erosive-corrosive conditions, whilst it was also compared with other erosion-corrosion resistant materials.

The Ni-Cr alloys contain a fully austenitic matrix which provides optimum corrosion resistance in very corrosive environments which also include strong acids [3.78]. In addition, these materials are usually alloyed with elements that further enhance the corrosion resistance, such as Mo, Cu, W and N [3.79]. Moreover, Al-Malahy et al. demonstrated improvements in general corrosion and pitting corrosion of Hasteloy C-276 (UNS N10276) over ferritic UNS S43000, austenitic UNS S31603 and supeaustenitic UNS S31254 at different salinity levels of seawater [3.80].

In engineering applications where significant corrosive wear resistance is required, the Ni-Cr alloys are subjected to ageing in order to increase the strength, hardness and, subsequently, the wear resistance. A good example of a high strength Ni-Cr alloy with relatively good wear resistance is Inconel 625 which, in a past study, was slightly superior over superduplex stainless steel (UNS S32760) in saline water at 50 °C/pH 7 [3.22]. Another example of good erosion-corrosion resistance of Ni-Cr alloys in saline water and pH 7 is the superior performance of Inconel 718 coating on aluminium Al6061 substrate compared with the uncoated material in 3.5% NaCl slurry [3.81]. However, the Ni-Cr materials are prone to σ phase since they contain high Cr contents and hence, the disadvantages that mentioned above for σ phase in duplex stainless steel corresponds to such alloys too. On the other hand, Zheng et al. showed that Ni-Cr alloys with σ phase illustrated enhanced erosion-corrosion resistance in H_2SO_4 acidic slurries [3.43, 3.44].

3.5 Aspects of water constitution on erosion-corrosion

The objective of the current Ph.D. thesis was to investigate the effect low pH and salinity on erosion-corrosion performance of stainless steels - WCIs obtaining a closer

understanding about materials performance and mechanisms of deterioration. An extra motive for this work was the limited information existing in the literature with regards to the mentioned conditions and simultaneously, the great industrial interest for engineering applications that involve erosion-corrosion at low pH and different levels of chlorides.

3.5.1 Effect of pH on erosion-corrosion

Despite the fact that many studies have been carried out in acidic slurries investigating various alloys, only a few of them demonstrated the effect of low pH on erosion-corrosion phenomena on metals. Efremenko et al. demonstrated the performance of a range of alloys which includes stainless steels, carbon steels, Mn-based steels and WCIs in acidic, neutral and alkaline slurry [3.16]. Along with many concluding remarks in their work, the importance of the materials microstructure and chemical composition on erosion-corrosion resistance was emphasised. Also, according to the authors of the same work [3.16], the plastic deformation seemed to compensate the lack of corrosion resistance for low alloyed mixture of martensitic-austenitic and carbide-free structured materials which, in the majority of testing conditions, displayed sufficient overall performance. In another study, Naiheng et al. investigated the influence of Boron additions on 28%Cr WCI in corrosive wear resistance at pH 1, 3, 7 and 10 [3.82]. They found that 28%Cr without boron is favourable in pH<3 environments, whilst the 28%Cr with Boron is preferable in pH>3 testing medium. Tang et al. demonstrated the corrosive wear behaviour of 45%Cr WCIs alloyed with 1-6% carbon at pH 3-5-7 and they reported, unexpectedly, higher volume loss at pH 7 rather than in acidic mediums. [3.59]. According to the authors, the explanation for this erratic result was the fact that in neutral environment the tested alloys were passivated more efficiently than the acidic ones. Also, Yoganandh et al. displayed the erosion-corrosion performance of a Ni-Hard 4 WCI, 27%Cr WCI (austenitic matrix) and UNS J93370 (cast duplex stainless steel) at pH 3, 7 in various impinging velocities and angles of attack [3.83]. One of the concluding remarks in the latter study was that all tested materials exhibited higher volume loss at pH 3 in all velocities/angles of attack. Finally, the decrease of pH (from neutral to acidic) resulted in increasing of corrosion rates on various WCIs in static corrosion rates [3.84] and increasing mass loss rates under erosion-corrosion conditions with the presence of solid particles

[3.85]. Finally, the current author of this Ph.D. thesis presented that the acidic pH increased substantially the corrosion rates of medium carbon steel UNS G10400 and (much less) UNS S32760 compared to neutral pH under erosion-conditions, whilst the overall mass loss (due to erosion-corrosion) exhibited the same trend with the corrosion rates [3.86].

3.5.2 Effect of salinity on corrosion and erosion-corrosion

It should be emphasised that there is very limited literature about the effect of salinity on corrosion, especially on erosion-corrosion behaviour of various alloys, which was an extra motive for the current author to investigate this topic. For instance, the saline water (3.5% NaCl) is more corrosive than the fresh water for all materials; this is related with the increase of conductivity and the penetration of chlorides into the surfaces [3.87]. However, it has been suggested from some researchers that above a certain level of NaCl content the corrosion rate of metals is decreased in static water due to reduce of oxygen solubility [3.88–3.91]. Most of the researchers reported that above 3% NaCl the corrosion rates in static conditions are decreased on steels [3.87–3.89, 3.91] but Brondel et al. stated that the corresponding threshold is 5% NaCl [3.90]. Addis et al. demonstrated that the corrosion of mild carbon steel is reduced from 1% NaCl to 10% NaCl under flowing conditions [3.92]. In the same work [3.92], the erosion-corrosion rates on 1% wt and 2% wt sand additions at 1% NaCl were higher for 2% wt sand, whilst at 10% NaCl the erosion-corrosion rates were similar for the two different sand loadings. The latter, according to the authors, was due to the fact that at 1% NaCl the density and viscosity of the fluid was much lower than at higher salinity and hence, more entrained particles in the higher sand loading eroded the tested surface. It should be noted in the latter work [3.92], the authors measured the corrosion rates in testing medium without abrasive particles and with the presence of CO_2. Tian et al. presented that the measured corrosion and penetration rates on WCIs are decreased with increasing the NaCl concentration in static corrosion tests, especially at low concentration levels (in high concentration levels only minor changes occurred) [3.84]. This was explained by the ion crowding in the pits and crevices formed at carbide interfaces in the microstructure resulting in controlled corrosion reaction.

On the other hand, Al. Malahy et al. showed that UNS 31600 and UNS S43000

stainless steels experienced enhanced corrosion rates under severe flowing impingement (sand particles-free) and 5.5% NaCl compared to 3.5% NaCl solution [3.80]. In the same work, high grade alloys such as Titanium Grade 2 (UNS R50400), superaustenitic stainless steel (UNS S31254) and nickel based alloy (UNS N10276) demonstrated no effect between the two salinity levels. In another corrosive wear study without the presence of solid particles, Wu showed that the corrosion rates of UNS S30400 stainless steel had increasing trend from 0.035% to 0.35% and finally to 3.5% NaCl [3.93]. To that extent, Hasan claimed the same trend with the latter study for a steel pipe in distilled water, 0.1 N NaCl solution and seawater (flowing conditions without solid particles) [3.94]. Furthermore, the influence of chlorides ions (1.4 mol/l NaCl vs deionised water) on erosion rates of UNS S30400 were found to be detrimental only at 70º angle of attack but not at 30º [3.95]. Finally, the corrosion and pitting corrosion of UNS S30400 alloy were found to increase with the increase of NaCl content (fresh - no NaCl, 0.5%, 1.5%, 2.5%, 3.5% and 4.5% NaCl) at pH 2 [3.96].

3.6 References

[3.1] H.R. Copson, Effects of Velocity on Corrosion by Water, J. Ind. Eng. Chem. 44 (1952) 1745–1752.

[3.2] A.C. Lloyd, J.J. Noël, S. McIntyre, D.W. Shoesmith, Cr, Mo and W alloying additions in Ni and their effect on passivity, Electrochim. Acta. 49 (2004) 3015–3027.

[3.3] A. Neville, T. Hodgkiess, An assessment of the corrosion behaviour of high-grade alloys in seawater at elevated temperature and under a high velocity impinging flow, Corros. Sci. 38 (1996) 927–956.

[3.4] Z.B. Zheng, Y.G. Zheng, W.H. Sun, J.Q. Wang, Erosion-corrosion of HVOF-sprayed Fe-based amorphous metallic coating under impingement by a sand-containing NaCl solution, Corros. Sci. 76 (2013) 337–347.

[3.5] L. Bertolini, B. Elsener, P. Pedeferri, R. Polder, Corrosion of Steel in Concrete, 2004.

[3.6] J.F. Grubb, Martensitic Stainless Steels, Uhlig's Corros. Handb. (2000) 667–

676.

[3.7] A.M.L. Aalco, Stainless Steel Stainless Steel, Carbon N. Y. (2013) 304–306.

[3.8] M. Maalekian, Christian Doppler Laboratory for Early Stages of Precipitation The Effects of Alloying Elements on Steels (I), (2007).

[3.9] Outokumpu, High Performance Austenitic Stainless Steel, (2015) 1–12.

[3.10] X. Hu, A. Neville, An examination of the electrochemical characteristics of two stainless steels (UNS S32654 and UNS S31603) under liquid-solid impingement, Wear. 256 (2004) 537–544.

[3.11] X. Hu, A. Neville, The electrochemical response of stainless steels in liquid-solid impingement, Wear. 258 (2005) 641–648.

[3.12] R.J.K. Wood, J.C. Walker, T.J. Harvey, S. Wang, S.S. Rajahram, Influence of microstructure on the erosion and erosion-corrosion characteristics of 316 stainless steel, Wear. 306 (2013) 254–262.

[3.13] S. Atashin, M. Pakshir, A. Yazdani, Synergistic investigation into the marine parameters' effect on the corrosion rate of AISI 316 stainless steel, Mater. Des. 32 (2011) 1315–1324.

[3.14] D. López, J.P. Congote, J.R. Cano, A. Toro, A.P. Tschiptschin, Effect of particle velocity and impact angle on the corrosion-erosion of AISI 304 and AISI 420 stainless steels, Wear. 259 (2005) 118–124.

[3.15] L. Giourntas, T. Hodgkiess, A.M. Galloway, Comparative study of erosion–corrosion performance on a range of stainless steels, Wear. 332–333 (2015) 1051–1058.

[3.16] V.G. Efremenko, K. Shimizu, T. Noguchi, A. V. Efremenko, Y.G. Chabak, Impact-abrasive-corrosion wear of Fe-based alloys: Influence of microstructure and chemical composition upon wear resistance, Wear. 305 (2013) 155–165.

[3.17] Outokumpu, Duplex Stainless Steel, Data Sheet, Outokumpu (2013) 1–12.

[3.18] S. Aribo, R. Barker, X. Hu, A. Neville, Erosion-corrosion behaviour of lean duplex stainless steels in 3.5% NaCl solution, Wear. 302 (2013) 1602–1608.

[3.19] A. Neville, T. Hodgkiess, J.T. Dallas, A study of the erosion-corrosion behaviour of engineering steels for marine pumping applications, Wear. 186–187 (1995) 497–507.

[3.20] A. Neville, C. Wang, Erosion-corrosion of engineering steels-Can it be managed by use of chemicals?, Wear. 267 (2009) 2018–2026.

[3.21] H. Meng, X. Hu, A. Neville, A systematic erosion-corrosion study of two stainless steels in marine conditions via experimental design, Wear. 263 (2007) 355–362.

[3.22] A. Neville, T. Hodgkiess, Characterisation of high-grade alloy behaviour in severe erosion – corrosion conditions, Wear. 233–235 (1999) 596–607.

[3.23] A.R. Francis, G. Byrne, G.R.W.W. Materials, P. Works, N. Heath, Experiences with Zeron 100 ® superduplex stainless steel in the process industries, 40 (1999) 613–624.

[3.24] R. Francis, The performance of stainless steels in concentrated sulphuric acid, Stainess Steel World. (2009) 2–5.

[3.25] S.A. Vitek, J M, David, The Sigma Phase Transformation in Austenitic Stainless Steels, Weld. Res. Suppl. (Presented 65th Annu. AWS Conv. 1984). (1986) 106–s–111–s.

[3.26] K.W. Chan, S.C. Tjong, Effect of secondary phase precipitation on the corrosion behavior of duplex stainless steels, Materials (Basel). 7 (2014) 5268–5304.

[3.27] J.M. Pardal, S.S.M. Tavares, M.D.P.C. Fonseca, J.A. De Souza, L.M. Vieira, H.F.G. De Abreu, Deleterious phases precipitation on superduplex stainless steel UNS S32750: characterization by light optical and scanning electron microscopy, Mater. Res. 13 (2010) 401–407.

[3.28] R. Magnabosco, Kinetics of sigma phase formation in a Duplex Stainless Steel, Mater. Res. 12 (2009) 321–327.

[3.29] J.W. Elmer, T.A. Palmer, E.D. Specht, In situ observations of sigma phase dissolution in 2205 duplex stainless steel using synchrotron X-ray diffraction, Mater. Sci. Eng. A. 459 (2007) 151–155.

[3.30] I. Zucato, M.C. Moreira, I.F. Machado, S.M. Giampietri, Microstructural Characterization and the Effect of Phase Transformations on Toughness of the UNS S31803 Duplex Stainless Steel Aged Treated at 850 ° C, Mater. Res. 5 (2002) 385–389.

[3.31] J. Saithala, J. Clapp, J.D. Atkinson, H. Ubhi, S. Mahajanam, Effect of sigma phase on the environment assisted cracking of super duplex stainless steel in oil field environments, NACE Int. (2012) 1–12.

[3.32] D. Zou, Y. Han, W. Zhang, J. Yu, Sigma phase precipitation and properties of super-duplex stainless steel UNS S32750 aged at the nose temperature, J. Wuhan Univ. Technol. Mater. Sci. Ed. 26 (2011) 182–185.

[3.33] S.S.M. Tavares, R.F. de Noronha, M.R. da Silva, J.M. Neto, S. Pairis, 475 °C Embrittlement in a duplex stainless steel UNS S31803, Mater. Res. 4 (2001) 237–240.

[3.34] J.K. Sahu, U. Krupp, R.N. Ghosh, H.J. Christ, Effect of 475 ??C embrittlement on the mechanical properties of duplex stainless steel, Mater. Sci. Eng. A. 508 (2009) 1–14.

[3.35] I. Calliari, M. Breda, E. Ramous, K. Brunelli, M. Pizzo, C. Menapace, Impact Toughness of an Isothermally Treated Zeron®100 SDSS, J. Mater. Eng. Perform. 21 (2012) 2117–2123.

[3.36] S.S.M. Tavares, J.M. Pardal, J.L. Guerreiro, A.M. Gomes, M.R. da Silva, Magnetic detection of sigma phase in duplex stainless steel UNS S31803, J. Magn. Magn. Mater. 322 (2010) L29–L33.

[3.37] S. Topolska, Effect of microstructure on impact\ntoughness of duplex and

superduplex\nstainless steels, J. Achiev. Mater. Manuf. Enginering. 36 (2009) 143–149.

[3.38] M.A. Dominguez-Aguilar, R.C. Newman, Detection of deleterious phases in duplex stainless steel by weak galvanostatic polarization in alkaline solution, Corros. Sci. 48 (2006) 2560–2576.

[3.39] R.A. Perren, T. Suter, C. Solenthaler, G. Gullo, P.J. Uggowitzer, H. Böhni, M.O. Speidel, Corrosion resistance of super duplex stainless steels in chloride ion containing environments: Investigations by means of a new microelectrochemical method. II. Influence of precipitates, Corros. Sci. 43 (2001) 727–745.

[3.40] Z. Zhang, H. Zhao, H. Zhang, Z. Yu, J. Hu, L. He, J. Li, Effect of isothermal aging on the pitting corrosion resistance of UNS S82441 duplex stainless steel based on electrochemical detection, Corros. Sci. 93 (2015) 120–125.

[3.41] M.E. Wilms, V.J. Gadgil, J.M. Krougman, F.P. Ijsseling, Effect of ??-phase precipitation at 800 ??C on the corrosion resistance in sea-water of a high alloyed duplex stainless steel, Corros. Sci. 36 (1994) 871–881.

[3.42] P. Paulraj, R. Garg, Effect of Intermetallic Phases on Corrosion Behavior and Mechanical Properties of Duplex Stainless Steel and Super-Duplex Stainless Steel, Adv. Sci. Technol. Res. J. 9 (2015) 87–105.

[3.43] Y.G. Zheng, Z.M. Yao, W. Ke, Erosion-corrosion resistant alloy development for aggressive slurry flows, Mater. Lett. 46 (2000) 362–368.

[3.44] Y. Zheng, Z. Yao, X. Wei, W. Ke, The synergistic effect between erosion and corrosion in acidic slurry medium, Wear. 186–187 (1995) 555–561.

[3.45] X.-C. Lu, S. Li, X. Jiang, Effects of σ phase in stainless steels on corrosive wear behavior in sulfuric acid, Wear. 251 (2001) 1234–1238.

[3.46] C. Graphite, Understanding cast irons, Eng. Cast. Solut. 6 (2004) 28–29.

[3.47] D.M. Stefanescu, Classification and Basic Metallurgy of Cast Iron, ASM

Handb. Vol. 1 - Prop. Sel. Irons Steels High Perform. Alloy. (1990).

[3.48] ASM handbook, Cast Irons, Metall. Prop. Ductile Irons. 1 (1990) 54–79.

[3.49] R.J. Llewellyn, S.K. Yick, K.F. Dolman, Scouring erosion resistance of metallic materials used in slurry pump service, Wear. 256 (2004) 592–599.

[3.50] A. Wiengmoon, Carbides in high chromium cast irons, Naresuan Univ. Eng. J. 6 (2011) 64–70.

[3.51] R.J. Chung, X. Tang, D.Y. Li, B. Hinckley, K. Dolman, Abnormal erosion-slurry velocity relationship of high chromium cast iron with high carbon concentrations, Wear. 271 (2011) 1454–1461.

[3.52] B. Lu, J. Luo, S. Chiovelli, Corrosion and Wear Resistance of Chrome White Irons — A Correlation to Their Composition and Microstructure, 37 (2006).

[3.53] C.I. Walker, P. Robbie, Comparison of some laboratory wear tests and field wear in slurry pumps, Wear. 302 (2013) 1026–1034.

[3.54] Y. Xie, J. (Jimmy) Jiang, K.Y. Tufa, S. Yick, Wear resistance of materials used for slurry transport, Wear. 332–333 (2015) 1–7.

[3.55] Y.P. Wang, D.Y. Li, L. Parent, H. Tian, Improving the wear resistance of white cast iron using a new concept - High-entropy microstructure, Wear. 271 (2011) 1623–1628.

[3.56] Y.P. Wang, D.Y. Li, L. Parent, H. Tian, Performances of hybrid high-entropy high-Cr cast irons during sliding wear and air-jet solid-particle erosion, Wear. 301 (2013) 390–397.

[3.57] L.L. Parent, D.Y. Li, Wear of hydrotransport lines in Athabasca oil sands, Wear. 301 (2013) 477–482.

[3.58] M. Jones, R.J. Llewellyn, Erosion-corrosion assessment of materials for use in the resources industry, Wear. 267 (2009) 2003–2009.

[3.59] X.H. Tang, R. Chung, C.J. Pang, D.Y. Li, B. Hinckley, K. Dolman,

Microstructure of high (45wt.%) chromium cast irons and their resistances to wear and corrosion, Wear. 271 (2011) 1426–1431.

[3.60] A.F. Zhang, J.D. Xing, L. Fang, J.Y. Su, Inter-phase corrosion of chromium white cast irons in dynamic state, Wear. 257 (2004) 198–204.

[3.61] A. Bedolla-Jacuinde, R. Correa, I. Mejía, J.G. Quezada, W.M. Rainforth, The effect of titanium on the wear behaviour of a 16%Cr white cast iron under pure sliding, Wear. 263 (2007) 808–820.

[3.62] R.J. Chung, X. Tang, D.Y. Li, B. Hinckley, K. Dolman, Effects of titanium addition on microstructure and wear resistance of hypereutectic high chromium cast iron Fe-25wt.%Cr-4wt.%C, Wear. 267 (2009) 356–361.

[3.63] H. Ding, S. Liu, H. Zhang, J. Guo, Improving impact toughness of a high chromium cast iron regarding joint additive of nitrogen and titanium, Mater. Des. 90 (2016) 958–968.

[3.64] C. Scandian, C. Boher, J.D.B. de Mello, F. Rézaï-Aria, Effect of molybdenum and chromium contents in sliding wear of high-chromium white cast iron: The relationship between microstructure and wear, Wear. 267 (2009) 401–408.

[3.65] M. Radulovic, M. Fiset, K. Peev, M. Tomovic, The influence of vanadium on fracture toughness and abrasion resistance in high chromium white cast irons, J. Mater. Sci. 29 (1994) 5085–5094.

[3.66] M. Mohammadnezhad, V. Javaheri, M. Shamanian, M. Naseri, M. Bahrami, Effects of vanadium addition on microstructure, mechanical properties and wear resistance of Ni-Hard4 white cast iron, Mater. Des. 49 (2013) 888–893.

[3.67] A. Bedolla-Jacuinde, R. Correa, J.G. Quezada, C. Maldonado, Effect of titanium on the as-cast microstructure of a 16%chromium white iron, Mater. Sci. Eng. A. 398 (2005) 297–308.

[3.68] H. Berns, Comparison of wear resistant MMC and white cast iron, Wear. 254 (2003) 47–54.

[3.69] R. Kesri, M. Durand-Charre, Phase equilibria, solidification and solid-state transformations of white cast irons containing niobium, J. Mater. Sci. 22 (1987) 2959–2964.

[3.70] M. Youping, L. Xiulan, L. Yugao, Z. Shuyi, D. Xiaoming, Effect of Ti-V-Nb-Mo addition on microstructure of high chromium cast iron, China Foundry. 9 (2012) 148–153.

[3.71] S. Kheirandish, A. Noorian, Effect of Niobium on Microstructure of Cast AISI H13 Hot Work Tool Steel, J. Iron Steel Res. Int. 15 (2008) 61–66.

[3.72] X. Zhi, J. Xing, H. Fu, B. Xiao, Effect of niobium on the as-cast microstructure of hypereutectic high chromium cast iron, Mater. Lett. 62 (2008) 857–860.

[3.73] M. Filipović, Ž. Kamberović, M. Korać, Z. Andić, Wear resistance and dynamic fracture toughness of hypoeutectic high-chromium white cast iron alloyed with niobium and vanadium, Mater. Tehnol. 48 (2014) 343–348.

[3.74] M. Fiset, K. Peev, M. Radulovic, The influence of niobium on fracture toughness and abrasion resistance in high-chromium white cast irons, J. Mater. Sci. Lett. 12 (1993) 615–617.

[3.75] R.J. Chung, X. Tang, D.Y. Li, B. Hinckley, K. Dolman, Microstructure refinement of hypereutectic high Cr cast irons using hard carbide-forming elements for improved wear resistance, Wear. 301 (2013) 695–706.

[3.76] J. Lu, H. Lin, H. Chen, Effect of niobium on wear resistance of 15 % Cr white cast iron, Wear. 166 (1993) 197–201.

[3.77] Q. Wang, X. Li, Effects of Nb, V, and W on Microstructure and Abrasion Resistance of Fe-Cr-C Hardfacing Alloys, Weld. J. 89 (2010) 133–139.

[3.78] I. Forest, P.O.B. Suffern, The Corrosion Resistance of Nickel-Containing Alloys in Sulfuric Acid and Related Compounds, (1983).

[3.79] Nickel Development Institute, Corrosion resistance of nickel-containing alloys in phosphoric acid, Publication 415 (CEB-4)

[3.80] K.S.E. Al-Malahy, T. Hodgkiess, Comparative studies of the seawater corrosion behaviour of a range of materials, Desalination. 158 (2003) 35–42.

[3.81] C.S. Ramesh, S. Kumar, D.S. Devaraj, R. Keshavamurthy, Slurry Erosive Wear Behavior of Plasma Sprayed Inconel-718 Coatings on Al6061 Alloy, J. Miner. Mater. Charact. Eng. 10 (2011) 445–453.

[3.82] M.A. Naiheng, R. Qichang, Z. Qingde, Corrosion-abrasion wear resistance of 28%Cr white cast iron containing boron, Wear. 132 (1989) 347–359.

[3.83] J. Yoganandh, S. Natarajan, S.P. Kumaresh Babu, Erosive Wear Behavior of High-Alloy Cast Iron and Duplex Stainless Steel under Mining Conditions, J. Mater. Eng. Perform. 24 (2015) 3588–3598.

[3.84] P.A. Tian, Harry H. Taylor, Corrosion study on high alloyed white cast irons in acidic and chloride containing solutions, Nace Int. Corros. 2011 Conf. Expo. (2011) 1–14.

[3.85] H.H. Tian, G.R. Addie, R.J. Visintainer, Erosion–corrosion performance of high-Cr cast iron alloys in flowing liquid–solid slurries, Wear. 267 (2009) 2039–2047.

[3.86] G. Karafyllias, T. Hodgkiess, A. M Galloway, The Influence of Acidic Conditions in Erosion-Corrosion Behavior of Medium Carbon Steel (UNS G10400) and Superduplex Stainless Steel (UNS S32760), Dep. Def. -Allied Nations Tech. Corros. Conf. Pittsburgh. (2015).

[3.87] E.A.H. Al Zubaidy, F.S. Mohammad, G. Bassioni, Effect of pH, salinity and temperature on aluminum cookware leaching during food preparation, Int. J. Electrochem. Sci. 6 (2011) 6424–6441.

[3.88] H. Silman, Corrosion and Corrosion Control: An introduction to corrosion science and engineering, 2008.

[3.89] S.H. Mameng, A. Bergquist, E. Johansson, Corrosion of Stainless Steel in Sodium Chloride Brine Solutions, Corros. 2014. (2014) 1–12.

[3.90] D. Brondel, R. Edwards, A. Hayman, D. Hill, T. Semerad, Corrosion in the Oil Industry, Oilf. Rev. (1994) 4–18.

[3.91] K. Zakowski, M. Narozny, M. Szocinski, K. Darowicki, Influence of water salinity on corrosion risk - The case of the southern Baltic Sea coast, Environ. Monit. Assess. 186 (2014) 4871–4879.

[3.92] J. Addis, B. Brown, S. Nesic, M. Technology, Erosion-corrosion in disturbed liquid/particleflow Paper No. 08572, NACE Corros. 2008. (2008) 1–14.

[3.93] W. Chung-Wen, Corrosion-wear study of 304 stainless steel in various NaCl solutions, Wear. 162–164 (1993) 950–953.

[3.94] B.O. Hasan, Effect of Salt Content on The Corrosion Rate of Steel Pipe in Turbulently Flowing Solutions, 13 (2010) 66–74.

[3.95] H.E.H. Ernest, Mm Mm, 31 (1950) 1896–1949.

[3.96] M.D. Asaduzzaman, C. Mohammad, I. Mayeedul, Effects of concentration of sodium chloride solution on the pitting corrosion behavior of AISI 304L austenitic stainless steel, Chem. Ind. Chem. Eng. Q. 17 (2011) 477–483.

Chapter 4

Methods and procedures

4.1 Introduction

The current chapter describes the experimental approach of this Ph.D. project which is related to the evaluation of the tested alloys microstructure, the main experimental erosion-corrosion experiments and the post-test analysis. Apart from the implemented techniques, all the tools used in the entire experimental programme are described extensively.

4.2 Pre-test investigation

4.2.1 Supply of materials

The conventional materials (UNS S31600, UNS S42000 and UNS S32760) were supplied by commercial companies in wrought bars, which were then machined to produce the desired round shape for erosion-corrosion tests. The 27WCI and 37WCI were supplied as industrial frame plate liner inserts (Figures 4.1-4.2), while the rest of alloys were supplied in square cast blocks by the Weir Group PLC and therefore, they were cut via electro-discharge machine (EDM). The finished dimensions following the EDM process were (round shape) 38 mm diameter and 17 mm thickness for all materials, apart from 27WCINb alloy which was square with 25x25 mm size.

Figure 4.1: 27WCI frame plate liner insert (diameter 200 mm, thickness 30mm).

Figure 4.2: 37WCI frame plate liner insert (diameter 430 mm, thickness 35 mm).

4.2.2 Metallographic Preparation

The sample preparation consisted of cross sectioning by a Struers Discotom-2 abrasive cutting machine, hot mounting on a Struers Promtopress-10 mounting machine, grinding on a Struers Rotopol-21 using 220, 500, 800, 1200, 2000 and 2400 SiC grit papers, and diamond polishing followed by etching. The polishing procedure was carried out for 2 min on each 6 and 3 μm polishing pads, whilst different etching solutions were used for alloys with different metallic microstructure, as shown below:

- Austenitic/duplex based alloys: 10% Oxalic acid (electrolytic 1V) for 5 seconds.
- Martensitic based alloys: Kalling's reagent consisted of 2g cupric chloride, 40ml methanol, 40ml distilled water, 40ml hydrochloric acid.
- 37WCI special alloy for further metallurgical investigation: Tint etch 40% KOH (electrolytic 1V) for 10 seconds.

The samples designated for Electron Backscatter Diffraction (EBSD) investigation were polished down to 1 μm polishing pad (after the 6 and 3 μm diamond polishing steps) in colloidal silica solution with additions of hydrogen peroxide (4 min duration). No etching was conducted for the EBSD samples in order to identify the crystal structure clearly.

4.2.3 Material characterisation

4.2.3.1 Light and Scanning Electron Microscopy (SEM)

An Olympus GX51 light microscope was used for microstructural observations up to x500, whilst, for higher magnifications, a HITACHI S-3700 Scanning Electron Microscope (SEM) was used. The operation of SEM involves scanning the sample with a focused beam of electrons, which interacts with the atomic structure, producing various signals that correspond to information about the composition and topography of the scanned area. Furthermore, Energy-dispersive X-ray spectroscopy (EDS) was carried out via SEM in which the chemical composition of localised areas can be approximated. It is worth mentioning that measurements of elements with small atomic weight (i.e carbon) can be problematic through EDS since they can absorb entirely the X-ray resulting in electron's ejection from its orbital and therefore, the peaks may

change in different compounds. Also, elemental maps were used to evaluate the dispersion of chemical elements into the microstructure.

4.2.3.2 Electron Backscatter Diffraction (EBSD)

The Electron Backscatter Diffraction (EBSD) technique was used for identification of sigma phase since this was not feasible via EDS in case of type D1 alloy. The EBSD is an attachment of SEM in which electrons are diffracted to form a set of paired large-angle cones that correspond to each diffracting plane. Every plane contains specific crystal structure (i.e tetragonal), lattice parameters and Wyckoff positions which consist of a point belonging to a group of points for which site symmetry groups are conjugate subgroups of the space group.

4.2.3.3 Volume fraction measurements

The microscopic views obtained via light microscopy were analysed using Image J software for measuring volume fractions (i.e carbides). Every volume fraction was measured at least ten times. Since Image J measures a marked region, a standard scale was measured initially in order to calibrate the software. A typical error of individual measurements was found to be around $\pm$ 5%.

4.2.4 Hardness measurements

The bulk hardness (macrohardness) of the tested alloys was measured via a calibrated Vickers hardness machine with 5kgf load. The hardness of multi-phase microstructures was obtained through a Mitutoyo MVK-G1 microhardness machine and various force loads were used for different sizes of carbides; 50, 100 and 200 g. For all hardness values (either macro or micro), an average of 5 measurements was taken. The calibration of microhardness machine involved measurements on a standard sample with known hardness.

4.3 Erosion-corrosion experiments

4.3.1 Slurry jet apparatus

The experimental equipment comprised of a closed loop re-circulating rig (which is shown in Figure 4.8) which was used for solid/liquid erosion corrosion impingement (SLEC) at 90° angle. In general, the slurry jet apparatus is widely used for laboratory

erosion-corrosion tests [4.1–4.4]. The rig recirculates an aqueous solution through a 4mm diameter nozzle with the aid of a pump and an assembly of piping. Silica sand with 420-500 μm average size (which was measured through standard sieves with sizes 710, 600, 500, 420, 355 μm), and angular shape was used, as demonstrated in Table 4.1 and Figure 4.3 respectively. The acidic environment was accomplished by adding controlled amounts of hydrochloric acid (HCl), dropping the pH from 7 to the desirable level and confirmed with the aid of a pH meter. The experiments that were designated to investigate the effect of pH on SLEC used a saline level of 3.5% NaCl in all pH levels. On the other hand, in cases where the salinity was examined, the pH was maintained at neutral level, whilst different additions of NaCl (0.05%, 3.5%, 10%) adjusted the salinity level. All SLEC experiments were carried out for 1 hour and the temperature was maintained at 40±1 °C as measured by a commercial thermometer, whilst a fresh solution was used after each experiment. The testing temperature was established by the fact that at 40 °C the operation of the pump was maintaining a constant temperature, whilst at lower temperatures a larger temperature range was noticed due to interactions with the atmosphere and hence this could potentially increase corrosion rates during the 1h of each test.

Prior to slurry jet testing, each specimen was ground with 220, 500, 800 and 1200 SiC grit papers. Therefore, they were submerged in the aqueous solution with a fixed distance of 5 mm between the nozzle and the specimen surface, as shown in Figure 4.4. The comparison between the two different testing coupons shape/size was achieved by testing square samples of UNS S31600. The tested square (25x25 mm) samples of UNS S31600 displayed the same volume loss with the round 38 mm diameter samples of the same material. Accurate measurements of material loss from the tested specimens were obtained using a Sartorius mass balance with 0.0001 g accuracy after being washed with methanol and dried with a commercial drier. The tested coupons were washed with water-methanol and dried with air drier. Specimens that exhibited corrosion product after tests (martensitic based alloys) were immersed for 4 seconds in an inhibited acid solution (Clarke's solution) in order to remove the corrosion product to obtain an accurate measurement of the mass loss. At least two replicates for each material were carried out for erosion-corrosion and pure erosion or corrosion. UNS S31600 stainless steel was used as a standard comparator material,

samples of which were tested frequently in order to ensure that the testing conditions were remaining constant throughout the experimental programme.

Table 4.1: Sand size distribution.

Sieve size (µm)	Sand mass percentage (%)
710	0.9
600	10.4
500	<u>39.7</u>
420	22.7
355	16.2

Figure 4.3: Microscopic view of the angular shape of silica sand.
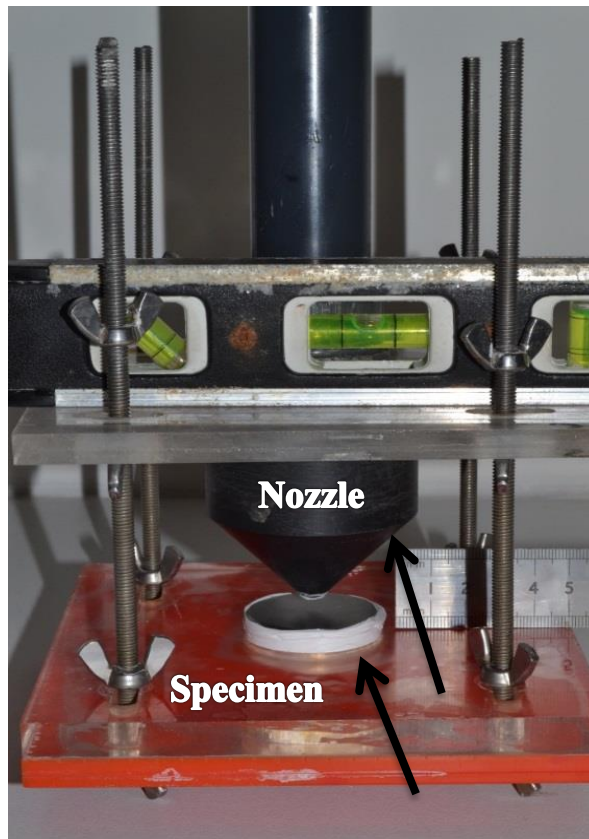
Figure 4.4: Testing holder setup.

4.3.2 Flow velocity/sand concentration measurements

Both flow velocity and sand concentration were measured by placing a plastic hose under the nozzle for 30 seconds in submerged condition (as in SLEC tests) but without the testing coupon placed. The flowing water was collected in 10L beaker in which the solid particles were accumulated in a 180 μm sieving filter. Therefore, the sieving filter was remaining in a furnace for more than 2h at 220 °C to ensure that the solid particles would be completely dry before they were weighted in mass balance with accuracy of 0.0001 g.

The jet velocity, which was measured several times during each experimental phase to ensure that it remains constant, was calculated by the following equation:

V = Q/30 x πR²   ***Equation 4.1***

Where, V is the velocity, Q is the flowing rate per 30 seconds and R is the nozzle radius.

The jet velocity for the entire experimental programme was 20-21 m/s.

4.3.3 Segmentation of the tested samples

The segmentation of the specimens was conducted in order to determine the corrosion rates under the jet and in the turbulent area adjacent to it. Through a Maxiem 1515 water jet machine, a 38 mm diameter coupon was segmented in two different specimens; one with 0.2 cm^2 which corresponds to the direct impinged zone (DIZ) and one with 11.0 cm^2 which corresponds to the outer area (OA). The two sections of the segmented sample were spot welded with two electrical wires to form electrodes. Therefore, the small coupon was inserted into the remained specimen surrounded by a heat shrink (0.8 mm diameter) in order to insulate electrically the two different regions. The two different sections of the sample were encapsulated in 40 mm cold mounting moulds. A typical representation of the segmentation process is shown in Figure 4.5, whilst in Figures 4.6-4.7 the final view of a segmented specimen is presented. Giourntas et al. demonstrated the segmentation process in a past study [4.5].
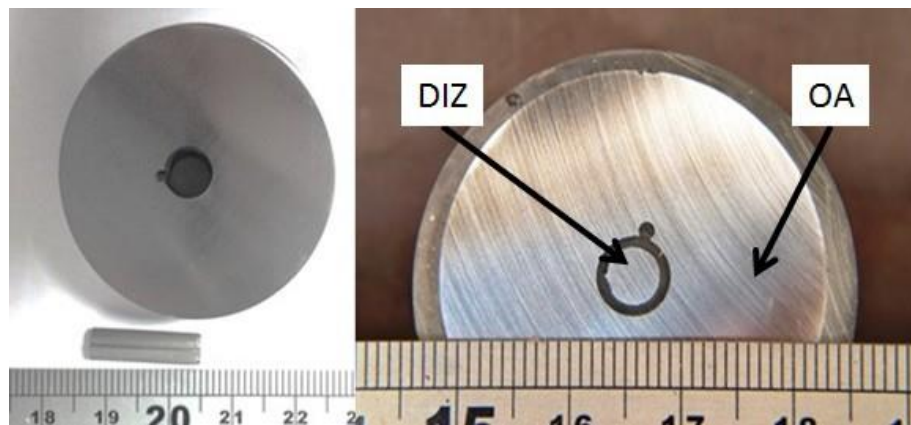
Figure 4.5: A typical representation of segmented sample (left) and encapsulated segmented on the right [4.6]

Figure 4.6: Representation of segmented specimen (front side).

Figure 4.7: Representation of segmented specimen (rear side).

4.3.4 Electrochemical tests

Further analysis was conducted on the deterioration of materials under study for a given environment. Taking into consideration that different mechanisms, such as mechanical damage, corrosion and synergy, are occurring on the specimen's surface during the erosion-corrosion tests, electrochemical monitoring was applied. The typical representation of the electrochemistry set up is illustrated in Figure 4.8. Cathodic protection (CP), anodic-cathodic polarisation sweep and linear polarisation

tests were carried out during SLEC tests. The reference electrode was silver/silver chloride (Ag/AgCl) and the auxiliary electrode was platinum.
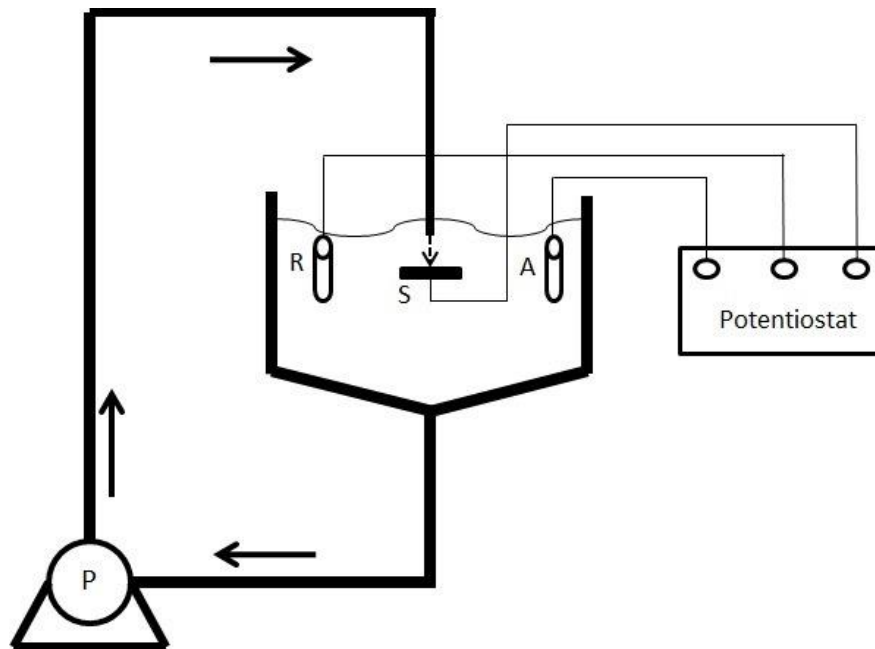
Figure 4.8: Schematic diagram of solid/liquid jet impingement circulating rig showing electrochemical monitoring equipment (A-Auxiliary Electrode, R-Reference Electrode, S-Specimen (Working Electrode)).

4.3.4.1 Cathodic protection

By applying impressed current cathodic protection (CP), the specimen was protected from corrosion and, as a result, the only phenomenon which occurred during CP tests was mechanical damage - erosion (E) in direct impinged zone (DIZ) and sliding abrasion in the outer area zone (OA). During the CP tests, the electrode potential was kept at -0.85 V (Ag/AgCl) at which the residual anodic current densities were estimated to be less than 0.0004 mA/cm^2 for a given material/environment. However, -0.75 V potential was implemented in UNS S32760 alloy providing improved corrosion and synergy protection than at -0.85 V (lower volume loss) indicating possible involvement of hydrogen embrittlement (HE) in CP tests at -0.85 V. Some past studies reported the vulnerability of UNS S32760 to HE during CP applications

at -0.85 V potenial [4.7–4.9]. All CP tests were performed at pH 7 and 3.5% NaCl in SLEC tests.

4.3.4.2 Anodic-cathodic polarisations

Anodic polarisation scans were conducted for all test materials in all tested environments which led to corrosion rates estimation. More specifically, all tested materials were subjected to impingement for 5 min prior to polarisation in order to stabilise the free corrosion potential E_{corr}. The electrochemical equipment was a GILL AC unit and utilised a standard three-electrode cell. The working electrode (test piece) was shifted from 20 mV more negative to E_{corr}, to more positive potentials at a sweep rate of 14 mV/min (widely used in cyclic polarisation monitoring) for a sufficient potential range (about 300 mV) to facilitate corrosion current determination though Tafel extrapolation. Tafel extrapolation was used to generate the corrosion currents and involves plotting a straight line running through the average of the fluctuations in the monitored current. The mass loss due to corrosion is obtained by Faraday's Law, as described below:

C (mg) = I_{corr} (mA)*3600 (sec)* Molar mass (g/mole)/ F (coulomb/mol)*n   **Equation 4.2**

Where, F is Faraday's constant equivalent to 96.485 C/mol, n is the number of electrons transferred in the anodic reaction and 3600 is the duration of the experiments in seconds.

Therefore, the mass loss was converted to volume loss via material's density. It is well known that electrochemistry and Tafel extrapolation is widely used by many researchers to estimate the level of corrosive attack [4.10–4.12]. Furthermore, McCafferty validated the results obtained from electrochemical tests by comparing them with the results from independent chemical methods (i.e weight loss measurements, measurement of the depth of penetration due to uniform corrosion etc.) [4.13].

Cathodic polarisation scans was included to support the estimations of corrosion rates and also, the comparison of cathodic reaction rates at different pH levels. The setup

was the same as with the anodic polarisation, but the working electrode was shifted from 20 mV more positive to E_{corr} to more negative potentials (up to -900 mV).

4.3.4.3 Linear polarisation

Linear polarisation monitoring was performed in order to confirm that corrosion was occurring at a constant rate during 1h SLEC experiments. The technique involved sweeping the specimen electrode potential from about -20 mV to +20 mV either side of E_{corr}. Thus, the scans were conducted after 5, 20 and 35 min from the beginning of each experiment. The method involved plotting potential versus current and calculating the gradient, called the polarisation resistance, R_p, which is inversely proportional to the corrosion current, I_{corr}. In general, a constant value of R_p indicates a constant corrosion rate during the erosion-corrosion experiment. In addition, higher R_p, means better corrosion resistance.

4.4 Post-test analysis

The post-test analysis included surface profiling and volume loss measurements of the wear scar depth in the DIZ via a 3D Alicona Infinite Focus G5 machine. The surface profiling involved measurement of the wear scar depth under the perpendicular jet which was caused after the SLEC tests. Figure 4.9 demonstrates a typical representation of surface profiling. It should be noted that due to the nozzle design and testing conditions (i.e hydrodynamics, duration etc.), the shape of the wear scar was "U" shape indicating that the stagnation point is less prominent than in cases where the wear scars possess "W" shape. The volumetric analysis provided information about the volume loss in the two hydrodynamic regions of the testing specimens; in the DIZ (where the wear scar is located) and in the OA. In the DIZ, the volume loss is measured directly through the 3D optical machine, whilst this volume loss is subtracted from the total volume loss obtained by the SLEC/CP tests (Equation 4.3). This method provides information about materials behaviour under rapid erosive-corrosive rates (DIZ) and under abrasive-corrosive rates with less aggressiveness since the solid particles lose kinetic energy after the first impact in the DIZ area. The volumetric analysis has also been explained in a past study [4.5]. Figure 4.10 illustrates a typical volume loss measurement of the wear scar.
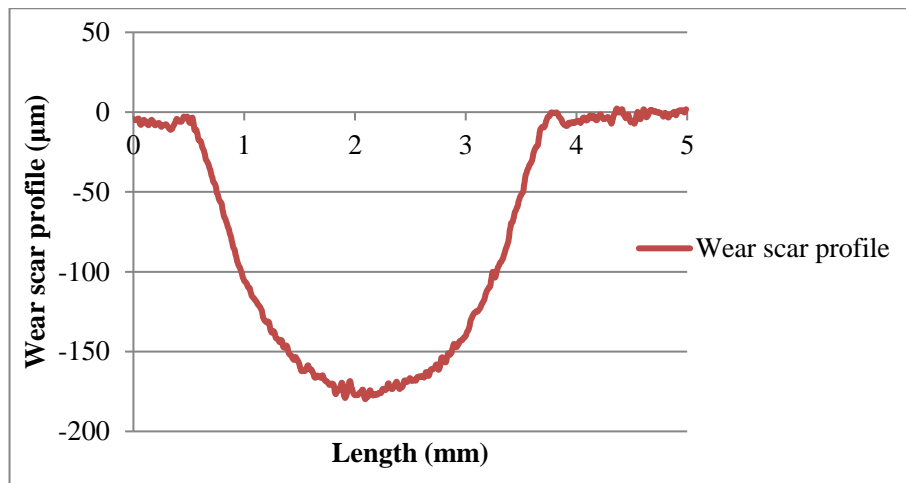
Figure 4.9: Typical 2D representation of wear scar profile.

$$VL_{OA} = TVL - VL_{DIZ} \qquad\qquad\qquad\qquad \textbf{\textit{Equation 4.3}}$$

Where, VL_{OA} is the volume loss in the OA, TVL is the total volume loss and VL_{DIZ} is the volume loss in the DIZ.
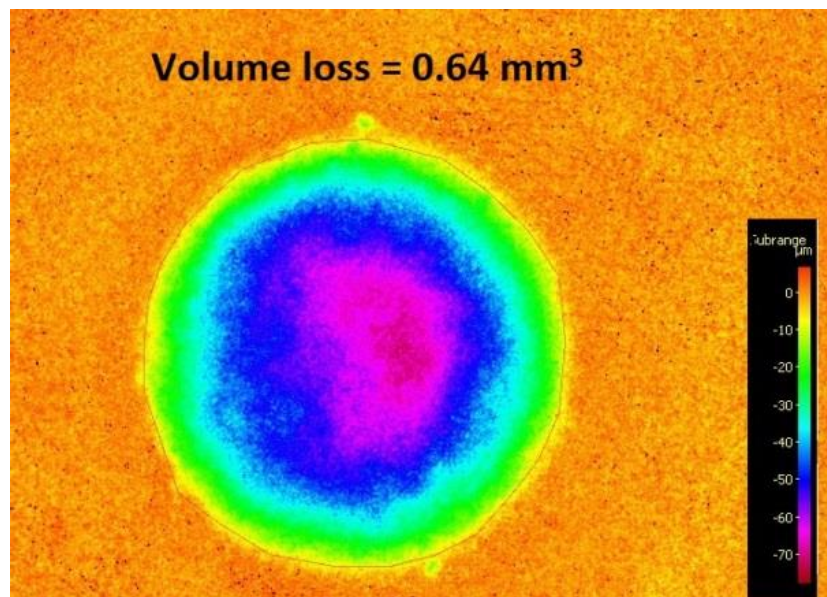
Figure 4.10: Typical representation of DIZ volume loss.

Through the above assessment, the volume loss of materials under study due to erosion, corrosion and synergy in the DIZ and OA regions were identified.

Also, apart from micro/macro evaluation of tested coupons, the post-test analysis includes the investigation of increased volume loss in the DIZ under acidic conditions for WCIs. Thus, testing samples were cross sectioned through the wear scar and polished in order to provide additional information about the wear scars of WCIs in both neutral and acidic environments.

4.5 References

[4.1]   Y. Xie, J. (Jimmy) Jiang, K.Y. Tufa, S. Yick, Wear resistance of materials used for slurry transport, Wear. 332–333 (2015) 1–7.

[4.2]   G.T. Burstein, K. Sasaki, Effect of impact angle on the slurry erosion-corrosion of 304L stainless steel, Wear. 240 (2000) 80–94.

[4.3]   A. Neville, T. Hodgkiess, Characterisation of high-grade alloy behaviour in severe erosion − corrosion conditions, Wear. 233–235 (1999) 596–607.

[4.4]   S. Aribo, R. Barker, X. Hu, A. Neville, Erosion-corrosion behaviour of lean duplex stainless steels in 3.5% NaCl solution, Wear. 302 (2013) 1602–1608.

[4.5]   L. Giourntas, T. Hodgkiess, A. M. Galloway, Enhanced approach of assessing the corrosive wear of engineering materials under impingement, Wear. 338–339 (2015) 155–163.

[4.6]   L.G.Giourntas, Investigation of erosion-corrosion behaviour of pump materials, PhD thesis. University of Strathclyde (2016).

[4.7]   D.N. Veritas, Dnv-Rp-B401 Cathodic Protection Design, (2011).

[4.8]   A.M. Elhoud, N.C. Renton, W.F. Deans, Hydrogen embrittlement of super duplex stainless steel in acid solution, Int. J. Hydrogen Energy. 35 (2010) 6455–6464.

[4.9]   T. Zakroczymski, A. Glowacka, W. Swiatnicki, Effect of hydrogen concentration on the embrittlement of a duplex stainless steel, Corros. Sci. 47

(2005) 1403–1414.

[4.10] V.A.D. Souza, A. Neville, Corrosion and synergy in a WC-Co-Cr HVOF thermal spray coating - Understanding their role in erosion-corrosion degradation, Wear. 259 (2005) 171–180.

[4.11] T. Hodgkiess, A. Neville, S. Shrestha, Electrochemical and mechanical interactions during erosion-corrosion of a high-velocity oxy-fuel coating and a stainless steel, Wear. 233–235 (1999) 623–634.

[4.12] L. Giourntas, T. Hodgkiess, A.M. Galloway, Comparative study of erosion–corrosion performance on a range of stainless steels, Wear. 332–333 (2015) 1051–1058.

[4.13] E. McCafferty, Validation of corrosion rates measured by the Tafel extrapolation method, Corros. Sci. 47 (2005) 3202–3215.

Chapter 5

The effect of low pH on erosion-corrosion resistance of white cast irons and stainless steels

5.1 Introduction

The current chapter presents the erosion-corrosion behaviour of an austenitic and martensitic stainless steel and two white cast irons (WCI), one with austenitic metallic matrix and one with martensitic matrix. The main aspect was to investigate the importance of the microstructure in erosion-corrosion performance in environments where the corrosion is enhanced (from neutral to acidic water). Prior to the main experiments, a preliminary investigation on UNS S31600 and UNS S42000 under different velocities and sand concentrations in neutral water was conducted. After the evaluation of the preliminary tests, the testing conditions for the main experimental work were selected.

5.2 Materials and methods

5.2.1 Materials

As indicated above, the alloys under investigation were:

- Austenitic stainless steel UNS S31600
- Martensitic stainless steel UNS S42000
- A WCI of nominal eutectic structure and martensitic matrix (27WCI)
- A hypoeutectic WCI with austenitic matrix (37WCI)

Both WCIs are designated for wear parts of pumps, such as impellers, frame plate liner inserts, wear rings etc. The 27WCI is used in environments in which wear resistance is necessary in the range of 5-14 pH, whilst the 37WCI alloy is implemented in high corrosive environments in the range of 1-14 pH [5.1]. Both alloys were manufactured by the conventional sand casting method.

Figures 5.1-5.2 show the microstructure of austenitic UNS S31600, which exhibited the expected equiaxied grain structure and the martensitic structure of UNS S42000. As demonstrated in Figure 5.3, the microstructure of 27WCI includes eutectic M_7C_3 carbides rich in Cr (light colour) in a hardened matrix of martensite, which also contains some secondary carbides - rich in Cr (dark colour). The 37WCI consists of austenite dendrites (light colour) and small eutectic carbides rich in Cr (blue) in an austenitic matrix, as presented in Figure 5.4.
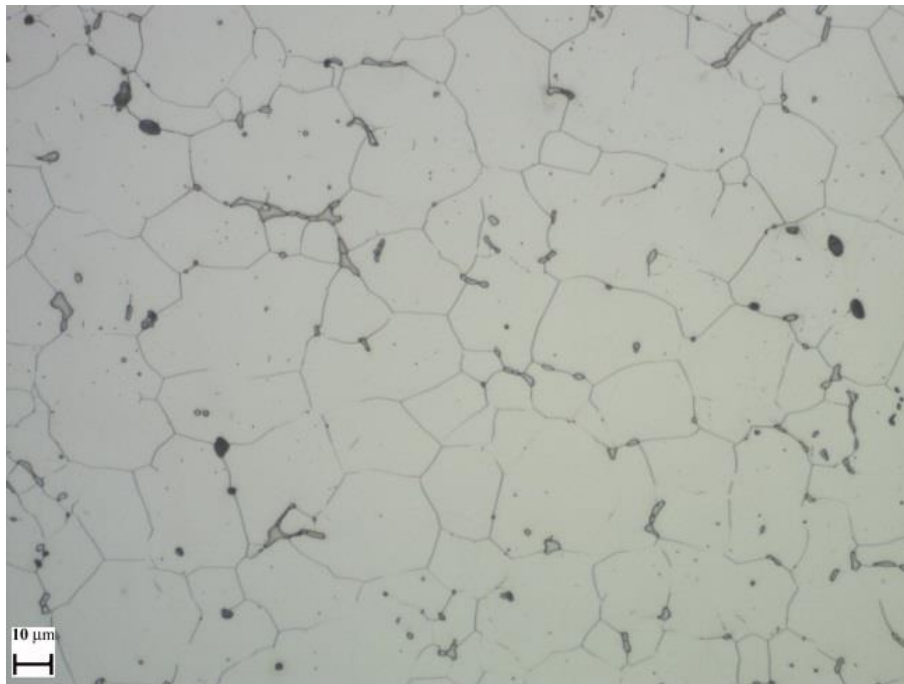
Figure 5.1: Microstructure of UNS S31600 [etched].

Figure 5.2: Microstructure of UNS S42000 [etched].
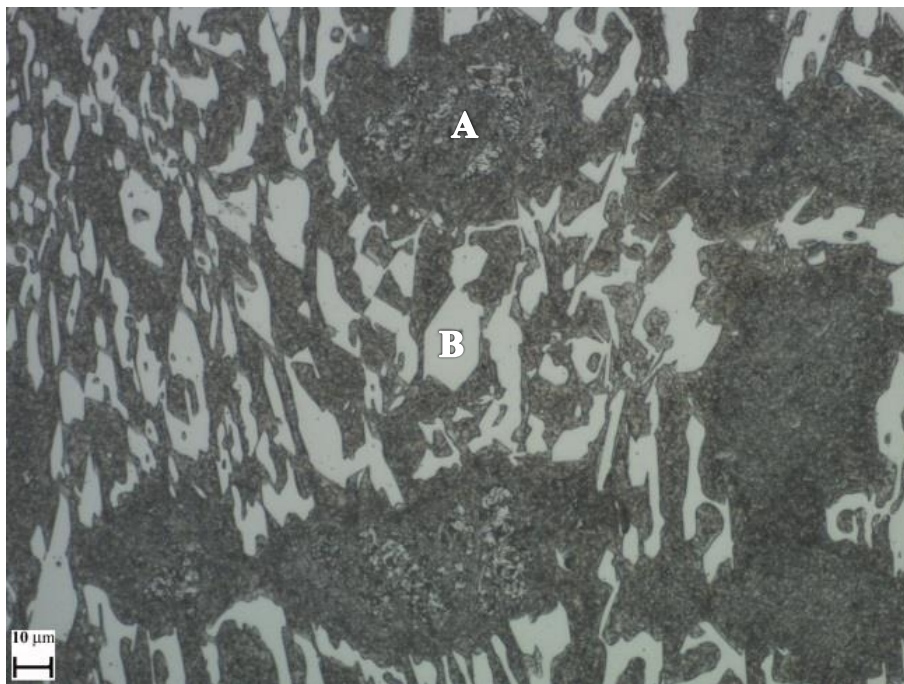
Figure 5.3: Microstructure of 27WCI (A-matrix and secondary carbides, B-eutectic Cr carbides) [etched].
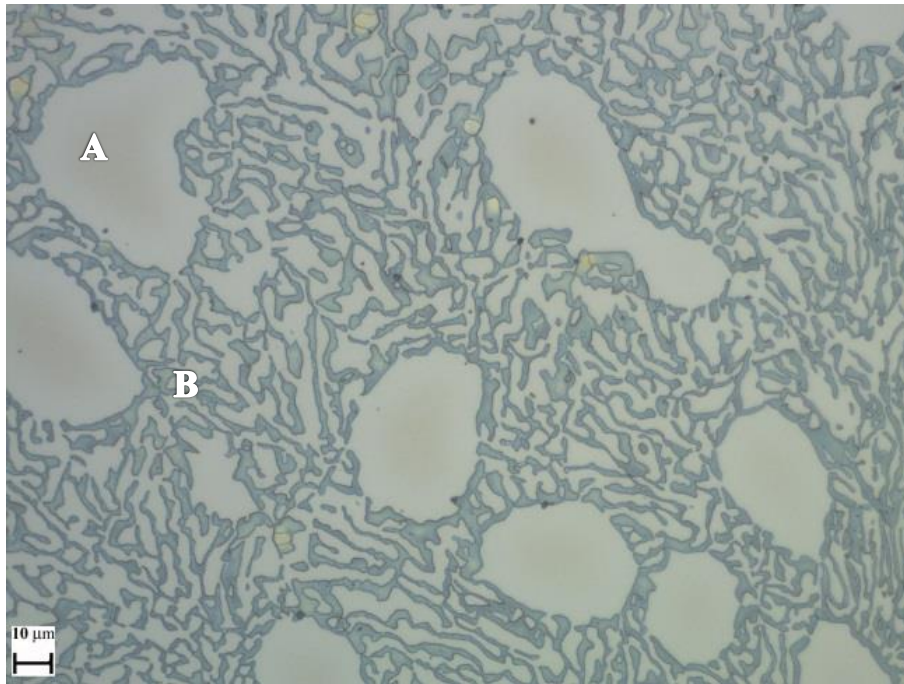
Figure 5.4: Microstructure of 37WCI (A-matrix, B-small eutectic Cr carbides and austenitic dendrites) [etched].

The nominal Cr and C contents of the experimental materials are given in Table 5.1 along with the densities and their bulk hardness values. Furthermore, the microhardness values of the metallic matrices and Cr carbides of WCIs are demonstrated in Table 5.2. However, the hardness of Cr carbides in the 37WCI could not be measured due to the small size of the particles. In addition, the wide range of hardness in the eutectic structure of 37WCI was the result of the fine structure; some indentations contained larger areas of austenite matrix (lower hardness) and others included larger areas of Cr carbides (higher hardness).

Table 5.1: Nominal specifications of tested materials.

Material	Nominal composition (%)	Measured bulk hardness (HV$_5$)	Densities (g/cm^3)
UNS S31600	17Cr , 0.04C, 2.5Mo, 12Ni, 0.4Si, 0.05N, 1Mn, 0.025P, 0.015S, Fe bal.	175±10	8.00
UNS S42000	13Cr, 0.08C, 0.5Si, 0.5Mn, 0.02P, 0.015S, Fe bal.	280±5	7.74
27WCI	27Cr – 2.8C	705±25	7.53
37WCI	37Cr – 1.5C	360±10	7.65

Table 5.2: Average microhardness measurements for WCI alloys.

Materials	Matrix+secondary carbides (HV$_{0.2}$)	Matrix+eutectic carbides (HV$_{0.1}$)	Eutectic carbides (HV$_{0.05}$)
27WCI	610±30	740±30	1102±80
37WCI	270±5	330 - 440	-

Furthermore, chemical analysis involving Energy Dispersive Spectroscopy (EDS) determination on the Scanning Electron Microscope (SEM) was used in order to obtain an indication of the Cr content in different phases in the microstructure of WCIs.

Figures 5.5-5.6 and Tables 5.3-5.4 demonstrate the Cr content of the two WCIs as measured via EDS technique. *Other elements are present such as Si, Mo, Ni but the demonstration of their contents is constrained by the sponsor and this is the case for all proprietary alloys investigated in the entire thesis*. Also, the carbides volume fractions (CVF) of 27WCI and 37WCI are presented in Table 5.5, as measured directly through Image J software.
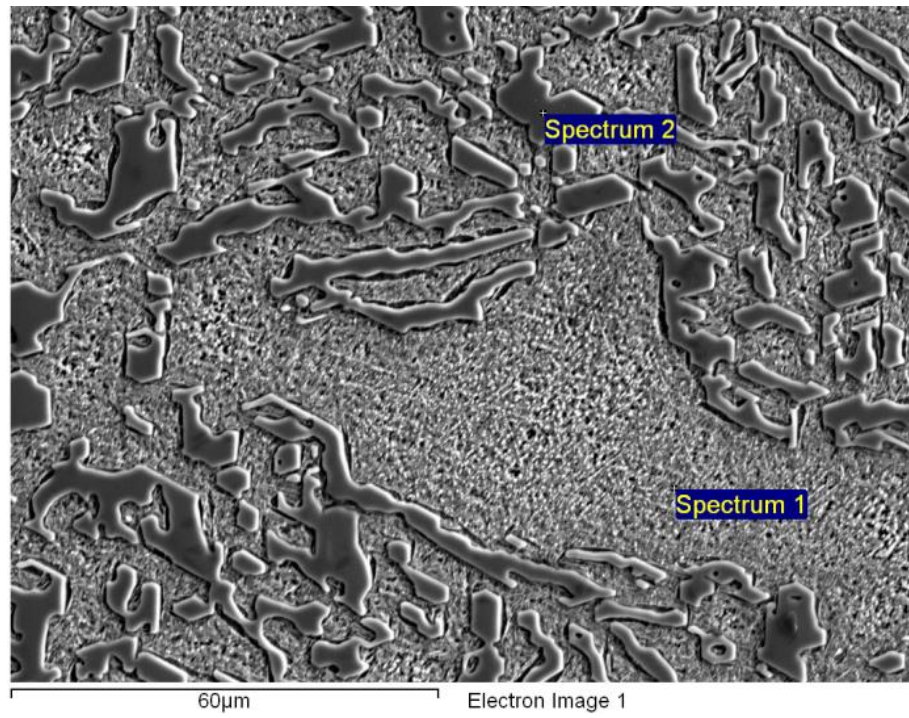
Figure 5.5: SEM image of 27WCI [etched].

Table 5.3: Cr content on 27WCI.

Spectrums	Cr (wt %)
Spectrum 1	14.9
Spectrum 2	67.4
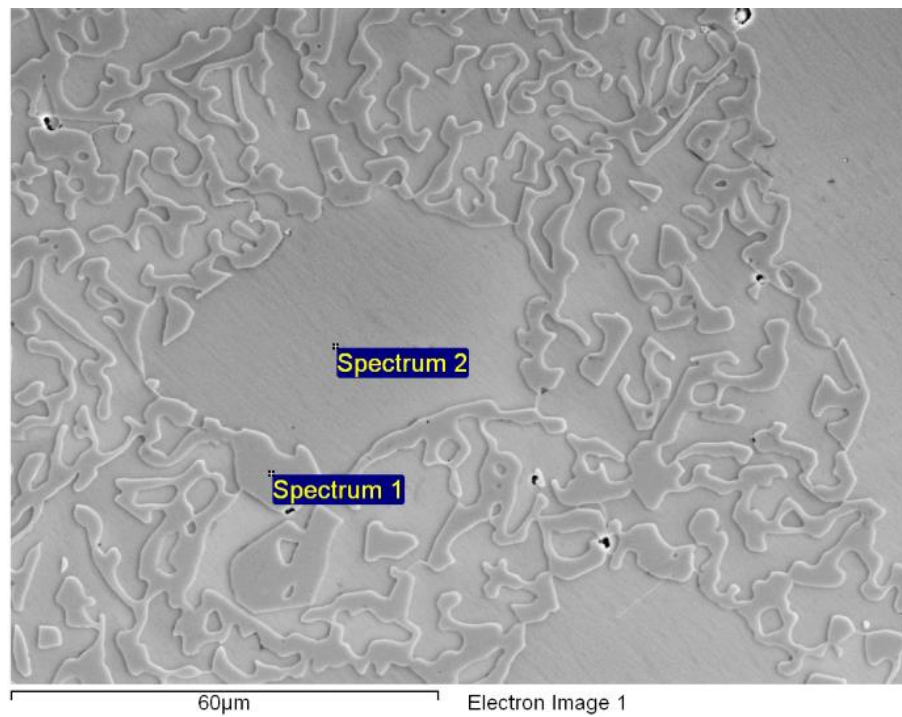
Figure 5.6: SEM image of 37WCI [etched].

Table 5.4: Cr content on 37WCI.

Spectrums	Cr (wt %)
Spectrum 1	70.7
Spectrum 2	27.7

Table 5.5: CVF measurements of WCIs.

Material	CVF (vol %)
27WCI	26
37WCI	17

5.2.2 Testing conditions - methods

The testing regimes in the current chapter contained 3.5% NaCl at pH 7 and pH 3. The velocity at the exit of nozzle was measured at 21 m/s, whilst the sand concentration was 0.5±0.05 g/l. The erosion-corrosion assessment consists of:

- Erosion-corrosion experiments at pH 7 and pH 3 including 3.5% NaCl in both cases and cathodic protection (CP) application.
- Anodic-cathodic polarisations in both flowing and static conditions.
- Linear polarisations.
- Post-test analysis (as has been presented in previous chapter).
- Crack investigations on the 27WCI and 37WCI.

5.3 Results

5.3.1 Volume loss

5.3.1.1 Preliminary tests on US S31600 – UNS S42000

Preliminary tests on UNS S31600 and UNS S42000 under different velocities and sand concentrations were conducted at pH 7 in order to investigate the similarities of these experimental testing conditions to the results that are generated in the field. The motivation for these preliminary tests was the work of Walker et al. in which they showed the complexities of correlating the field results with laboratory tests [5.2]. In their various testing apparatus, WCIs were investigated with both round and sharp solid particles. According to their findings [5.2], inconsistencies in material ranking and wear mechanisms was observed between field trials and laboratory tests, thus emphasising the importance of conducting the experimental tests with as close a match as possible to the operational conditions in the field.

Since erosion was the dominant mechanism in erosion–corrosion tests in the present work (Table 5.8), an attempt to establish results more relevant to the mining industry and field tests was made. It is expected that the martensitic structure provides significant benefits against the austenitic structure in terms of erosion-corrosion, especially in fresh water industrial applications [5.3]. However, in saline environments this difference is expected to diminish due to superior corrosion resistance of austenitic structure. The two different testing conditions were selected for erosion-corrosion tests in neutral conditions:

- Less severe - 18 m/s velocity and 0.2 g/l sand concentration (angular sand – 500 μm mean size)

- More severe - 21 m/s velocity and 0.5 g/l sand concentration (angular sand – 500 μm mean size) which therefore was selected to be the setup for this experimental phase.

Figure 5.7 shows the volume loss of both stainless steels in the two different testing regimes. In less severe conditions, the UNS S31600 showed better erosion-corrosion performance than UNS S42000, whilst in more aggressive conditions the UNS S42000 was slightly superior over UNS S31600 in terms of average volume loss. This occurred because in less severe conditions, the erosion mechanism was not sufficient to emerge the poor erosion/abrasion resistance of UNS S31600 and hence, in conjunction with its the performance in terms of corrosion and synergistic effects, the austenitic stainless steel was superior over UNS S42000 in these conditions. Thus, it was evident how complicated is the erosion-corrosion phenomenon in lab conditions.
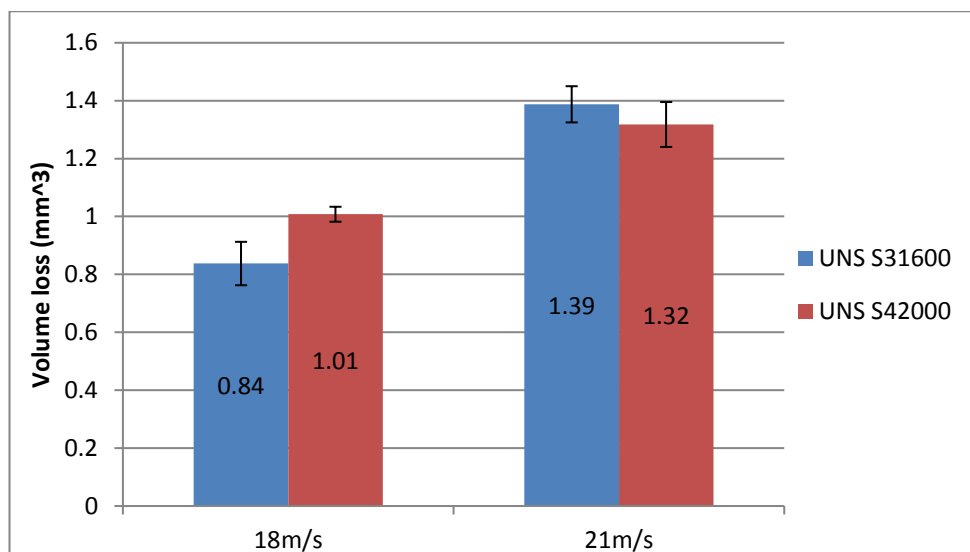
Figure 5.7: Average volume loss of UNS S31600 and UNS S42000 under different erosive-corrosive testing conditions in 3.5% NaCl and neutral water.

Moreover, in order to obtain a better understanding between the erosion-corrosion phenomena, the post-test analysis was carried out for these initial experiments. Figures 5.8-5.9 present the volumetric analysis of tested specimens showing the total volume

loss (TVL) breakdown in the different hydrodynamic regions; volume loss in the direct impinged zone (VL$_{DIZ}$) and volume loss in the outer area (VL$_{OA}$). It was evident that in the DIZ, UNS S31600 was superior to UNS S42000 in less severe conditions, whilst in the more severe setup the two alloys had similar performance. It can be concluded that in more severe conditions, a balance between erosion and ductility in the DIZ is required, whilst, in less severe conditions, high the ductility is more crucial than the erosion resistance under the perpendicular jet.

Both corrosion and synergy were not quantified for both experimental conditions but it can be reasonably expected that their contributions are not expected to be major since the erosion is the dominant mechanism (it is obvious from the results later in this chapter).

Thus, the more aggressive environment was selected in order to provide results more relevant to mining operations. It should be noted that the lab tests presented in this thesis provide a qualitative comparison to the field tests, not quantitatively since the field service is more complicated than the laboratory conditions. It is well understood that in mining operations at neutral pH and any level of chlorides, the erosion-corrosion performance of WCIs is far superior to stainless steels [5.1].
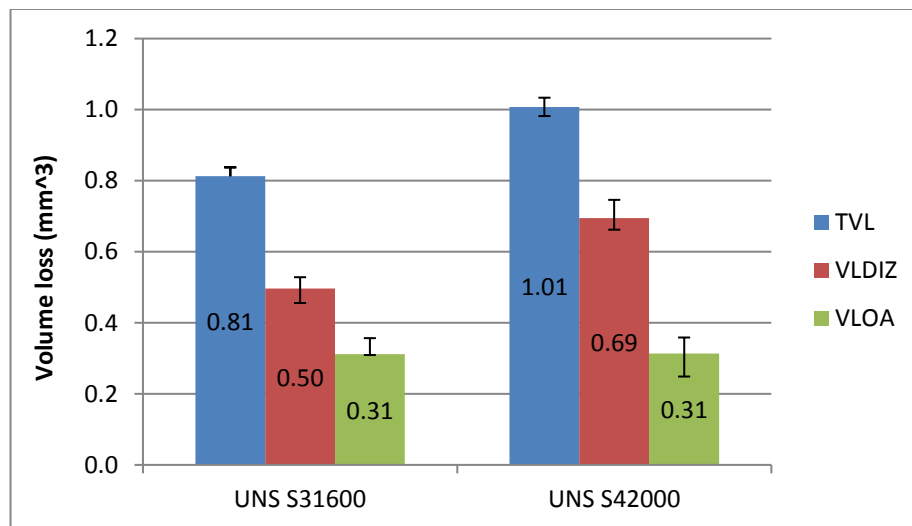
Figure 5.8: Breakdown of average volume loss in less severe conditions.
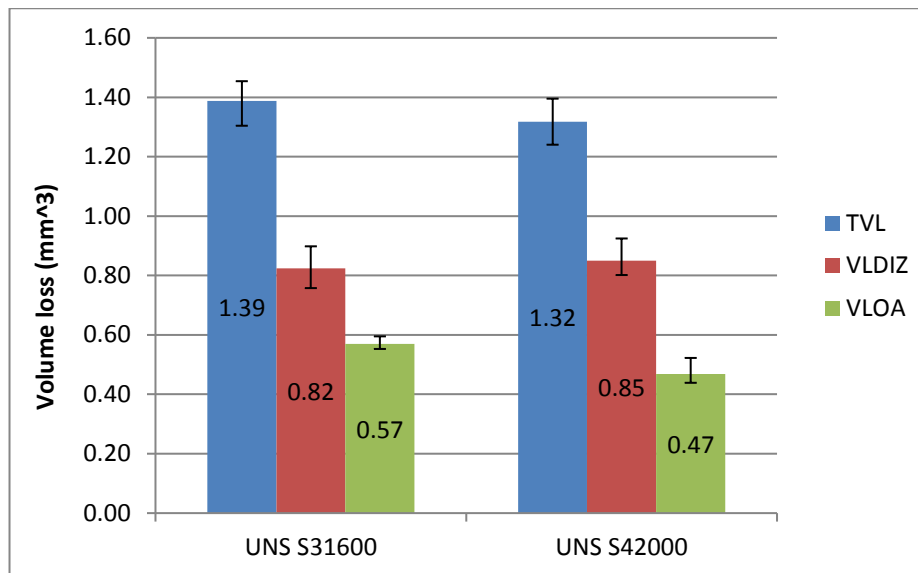
Figure 5.9: Breakdown of average volume loss in more severe conditions.

5.3.1.2 Comparison of stainless steels - WCIs

The average volume loss under solid-liquid erosion-corrosion (SLEC) conditions at both pH levels and CP conditions are presented in Figure 5.10. In the neutral environment, the 27WCI showed the lowest volume loss followed by the 37WCI. The UNS S42000 was slightly superior to UNS S31600 in terms of average volume loss but both stainless steels depicted higher volume loss than WCIs. The effect of acidic conditions, compared to pH 7, was to produce substantial increases in material loss in the martensitic alloys but little, or only-modest, effects on the austenitic alloys. Hence, in acidic conditions, the austenitic alloys (UNS S31600 and 37WCI) exhibited superiority over the martensitic-structured coupons. The 27WCI displayed lower volume loss than UNS S42000, whilst UNS S31600 and 37WCI exhibited similar performance considering the error bars, but the UNS S31600 showed slightly lower average volume loss. The application of CP (pH 7) yielded modest reductions in material loss for all alloys. The 27WCI alloy exhibited the lowest volume loss, whilst the UNS S42000 and 37WCI showed similar wear performance, followed by UNS S31600 which displayed the highest volume loss.
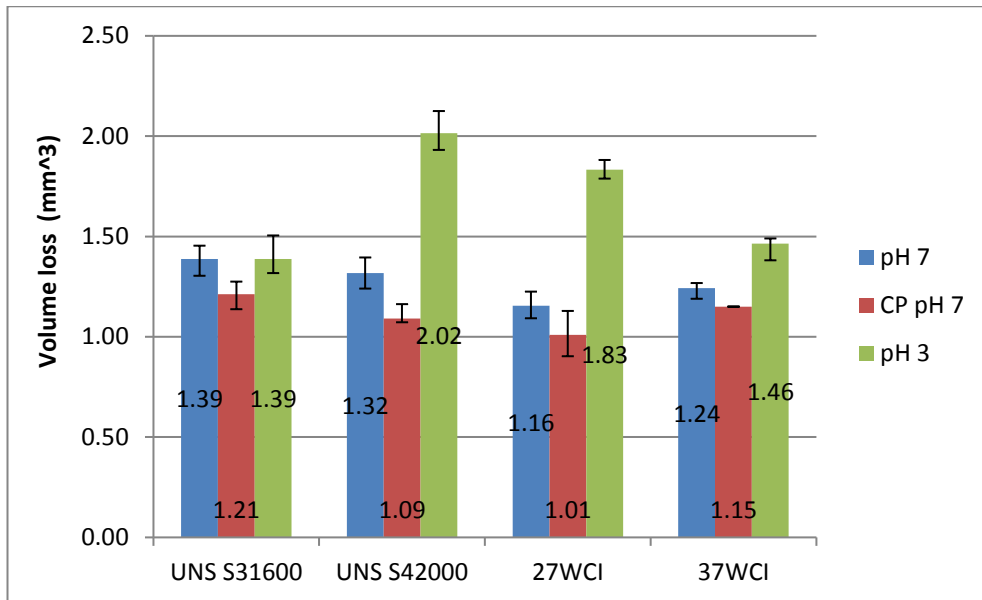
Figure 5.10: Average volume loss of materials under SLEC conditions at pH 7, CP pH 7 and pH 3.

5.3.2 Electrochemical tests

5.3.2.1 Anodic polarisation scans

Figure 5.11 exhibits the, in-situ, anodic polarisation scans of the materials under study in neutral and acidic environments during SLEC tests. The rapid fluctuations in current are indicative of repetitive de-passivation and re-passivation events. Table 5.4 shows the i_{corr} (corrosion rate) values and the relevant volume loss for the tested alloys at pH 7 and pH 3. The corrosion rates of the austenitic-structured alloys were considerably lower than those of the alloys with the martensitic structure at pH 7 and especially in acidic conditions. The UNS S42000 depicted lower corrosion rates than 27WCI in both environments. It is worth mentioning that the corrosion rate of UNS S42000 at pH 3 was evaluated from a cathodic polarisation scan, as presented in section 5.3.2.3, since it was not feasible to be determined from the anodic polarisation curve. The corrosion rates for all the other materials, in anodic and cathodic scans, were in good agreement. An interesting feature was that the anodic current density of 27WCI at -850 mV in acidic conditions was 0.009 mA/cm^2 which corresponds to 0.013 mm^3 volume loss due to pure corrosion. Thus, it can be concluded that CP at pH 3 would not suppress completely the corrosion and probably the synergy for martensitic-structured alloys.
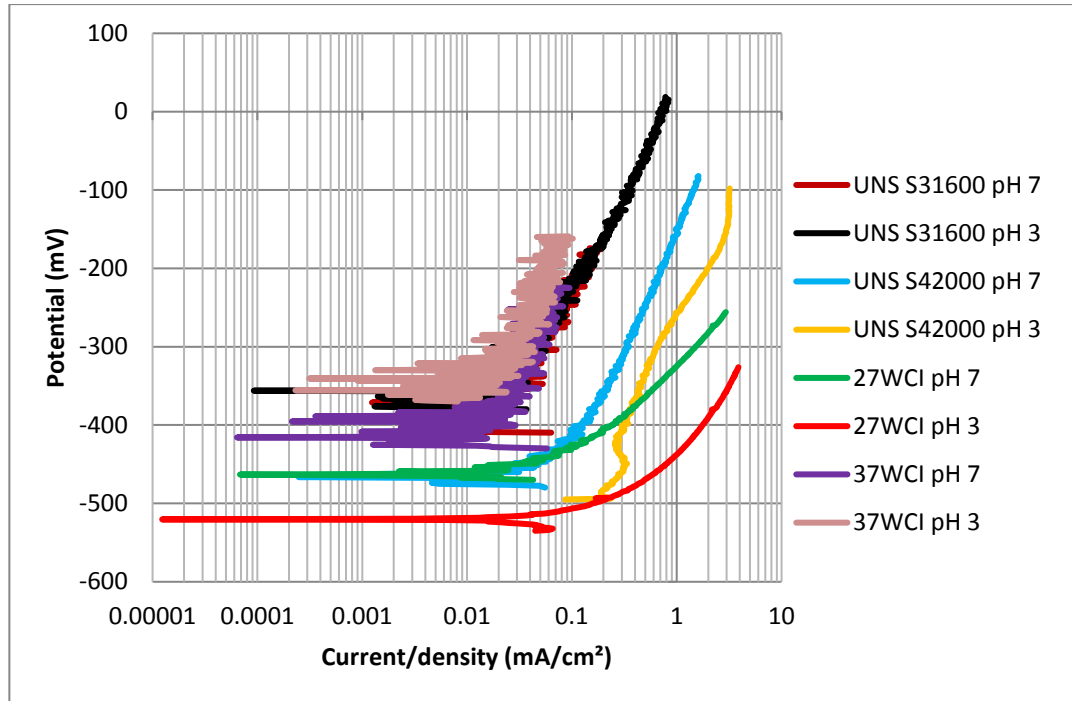
Figure 5.11: Anodic polarisation curves of materials in SLEC conditions at both pH levels.

Table 5.6: Corrosion rates and volume loss of materials under study in neutral and acidic environment.

Material	i_{corr}(mA/cm^2) pH 7	i_{corr}(mA/cm^2) pH 3	Volume loss (mm^3) pH 7	Volume loss (mm^3) pH 3
UNS S31600	0.015	0.017	0.021	0.023
UNS S42000	0.061	0.200	0.093	0.301
27WCI	0.088	0.308	0.132	0.462
37WCI	0.013	0.015	0.019	0.022

5.3.2.2 Linear polarisation monitoring

Linear polarisation tests were conducted in 1h SLEC tests, whilst a typical representation of UNS S31600 at pH 7 is shown in Figure 5.12. Figures 5.25-5.31 in the Appendix of this chapter show the linear polarisation curves for all material at both pH values. A noticeable feature was that the UNS S31600-37WCI alloys exhibited

rapid oscillations indicative of intermittent passive behaviour, whilst the UNS S4200-27WCI alloys displayed active corrosion behaviour. All calculated R_p values are presented in Table 5.7. The main finding is that, for each material and environment, the corrosion rates were essentially unchanged during the 1h experiment. In general, comparisons of R_p values are qualitatively in accord with the comparisons obtained from I_{corr} measurements, i.e much lower corrosion rates (higher R_p) for the austenitic alloys compared to the materials with martensitic structure.
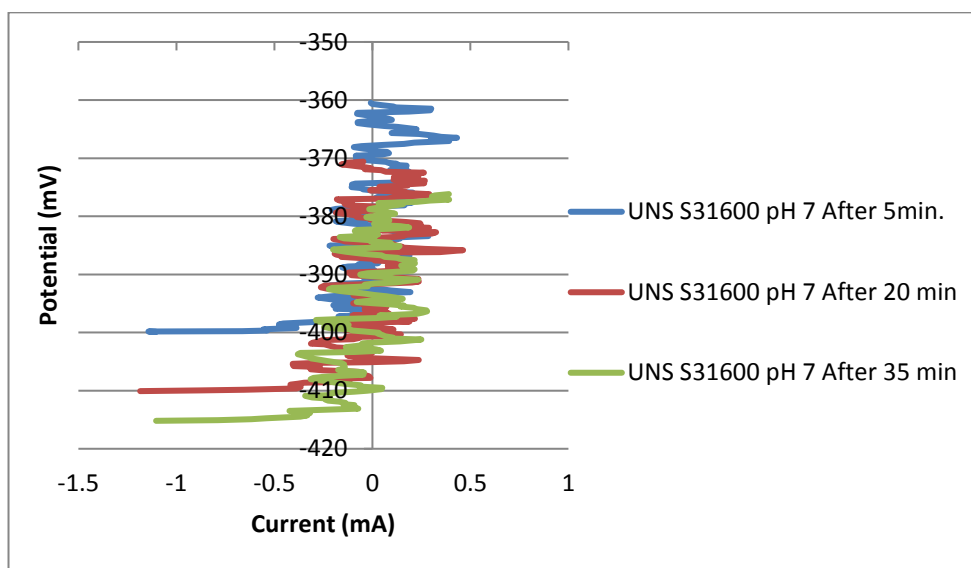
Figure 5.12: Linear polarisation for UNS S31600 at pH 7.

Table 5.7: R_p results for linear polarisations of materials under study at pH 7 and pH 3.

Material	R_p after 5 min (Ohms)	R_p after 20 min (Ohms)	R_p after 35 min (Ohms)
UNS S31600 pH 7	233	233	233
UNS S42000 pH 7	133	Not determined	123
27WCI pH 7	40	42	40
37WCI pH 7	280	280	280
UNS S31600 pH 3	160	160	160
UNS S42000 pH 3	15	15	15
27WCI pH 3	15	14	15
37WCI pH 3	200	200	200

5.3.2.3 Cathodic polarisations

Figure 5.13a shows the full cathodic polarisation plots for the four materials in both environments. Figure 5.13b represents an attempt to emphasise the large differences in the cathodic reaction rates at electrode potential negative to E_{corr} and there is a distinct separation between the currents (cathodic reaction rates) at the two different pH levels. As was expected, the cathodic reaction rate was substantially higher in the acidic solution and hence enhanced hydrogen production occurs.
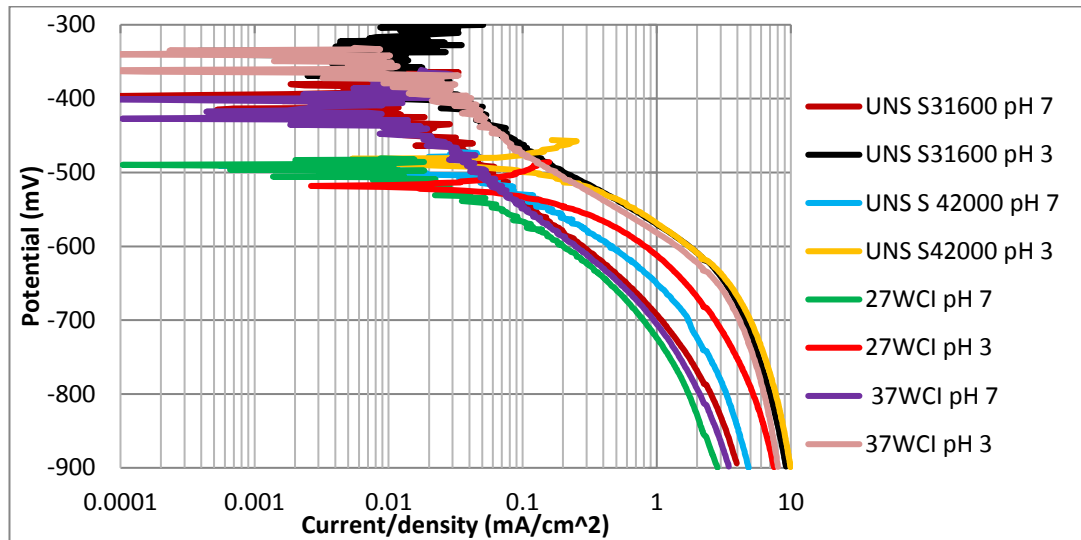
Figure 5.13a: Cathodic polarisation curves in SLEC conditions for materials under study at both pH levels.
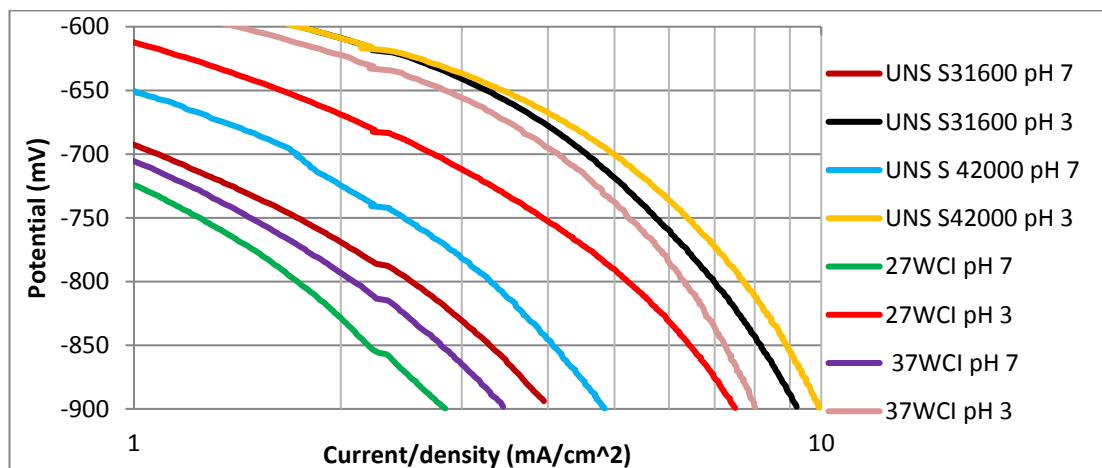
Figure 5.13b: Magnified view of the relevant part of Figure 5.20a.

5.3.3 Contribution to the erosion-corrosion mechanisms with respect to TVL

Tables 5.8-5.9 present the overall volume loss and the volume loss produced by each deterioration mechanism individually at both pH values along with the corresponding proportions. An important feature is that at neutral pH, the mechanical damage was the dominant mechanism for all the tested alloys. On the other hand, in acidic conditions, the two martensitic-structured materials displayed increased proportions of corrosion and synergy, whilst the 37WCI also, showed increased synergy. The UNS S31600 had the same proportions in both corrosive environments.

Table 5.8: Volume loss produced by different mechanisms for materials under study at pH 7.

Material	Total volume loss (mm³)	Erosion + Sliding abrasion (mm³/proportion %)	Corrosion (mm/proportion %)	Synergy (mm³/proportion %)
UNS S31600	1.39	1.21/87	0.021/2	0.159/11
UNS S42000	1.32	1.09/82	0.093/7	0.137/11
27WCI	1.16	1.01/87	0.132/11	0.018/2
37WCI	1.24	1.15/93	0.019/1	0.071/6

Table 5.9: Volume loss produced by different mechanisms for materials under study at pH 3.

Material	Total volume loss (mm³)	*Erosion + Sliding abrasion (mm³/proportion %)	Corrosion (mm³/proportion %)	Synergy (mm³/proportion %)
UNS S31600	1.39	1.21/87	0.023/2	0.159/11
UNS S42000	2.02	1.09/54	0.301/15	0.629/31
27WCI	1.83	1.01/55	0.462/25	0.358/20
37WCI	1.46	1.15/78	0.022/2	0.288/20

5.3.4 Post-test analysis

5.3.4.1 Surface profiling

Figure 5.14 presents the average wear scar depths of materials under study in neutral, CP and acidic conditions. The 27WCI alloy possessed the lowest wear scar in all environments, whilst the 37WCI was the second best alloy in neutral and CP conditions. At pH 3, the two stainless steels displayed similar wear scar depths with the 37WCI alloy. In general, as it will be shown further below, there was no correlation between the wear scar depths and volume loss in the DIZ since in some cases the wear scar exhibited different shape. A typical example of the latter is shown in Figure 5.15 in which the wear profile of 37WCI in CP tests is maintained in relatively high values for longer distance than UNS S42000 in the same environment.
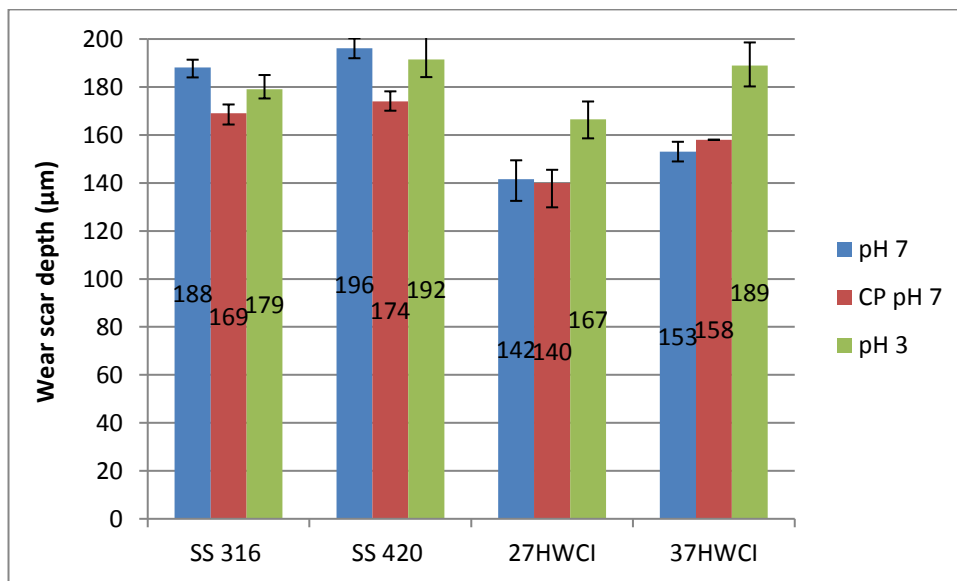
Figure 5.14: Average wear scar depths for materials under study in all testing environments.
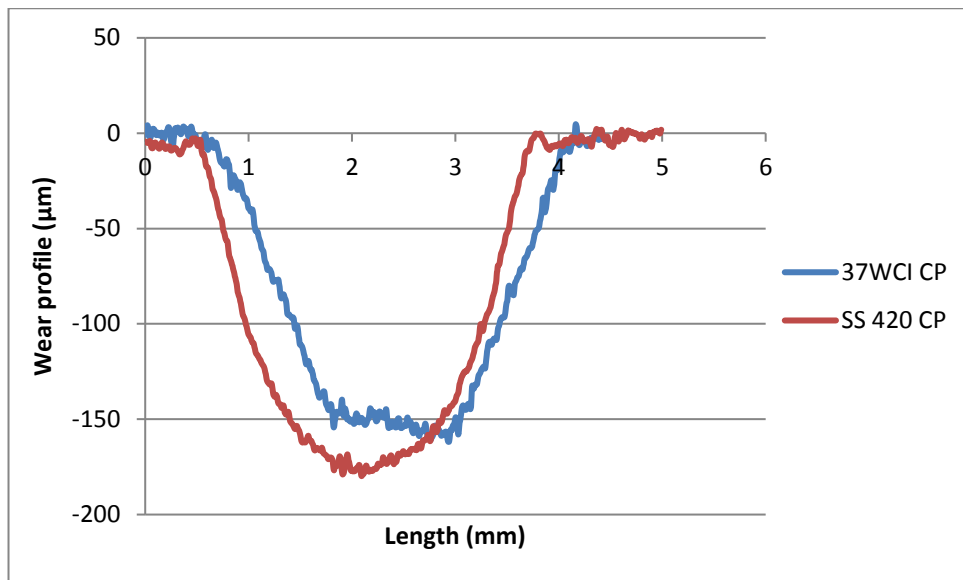
Figure 5.15: Wear scar profiles for 37WCI and UNS S42000 in CP environment.

5.3.4.2 Volumetric analysis

Figures 5.16-5.18 illustrate the average volume loss of the materials for the DIZ and the OA region at both pH values and under CP conditions.

In neutral conditions, 27WCI showed lower volume loss in the DIZ than the other materials which displayed similar performance. In the OA region, UNS S31600 showed higher volume loss than the other three alloys.

Under acidic conditions, the susceptibility of martensitic-structured alloys to corrosion was confirmed by the results in the OA zone, in which the austenitic structured alloys displayed lower volume loss. In the DIZ at the pH 3, 37WCI exhibited higher volume loss than the rest of the materials which showed similar material loss.

In CP conditions, the 37WCI alloy displayed higher volume loss in the DIZ than the rest of materials which were similar in behaviour. In the OA, the same trend with the FEC results at pH 7 was observed, with the UNS S31600 demonstrating the worst performance in sliding abrasion.
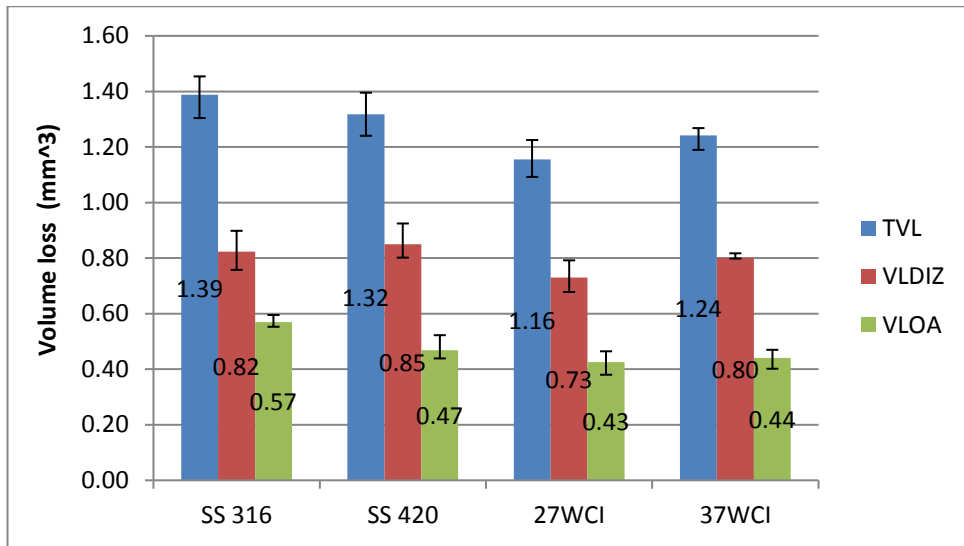
Figure 5.16: Breakdown of average volume loss for materials under study at pH 7.
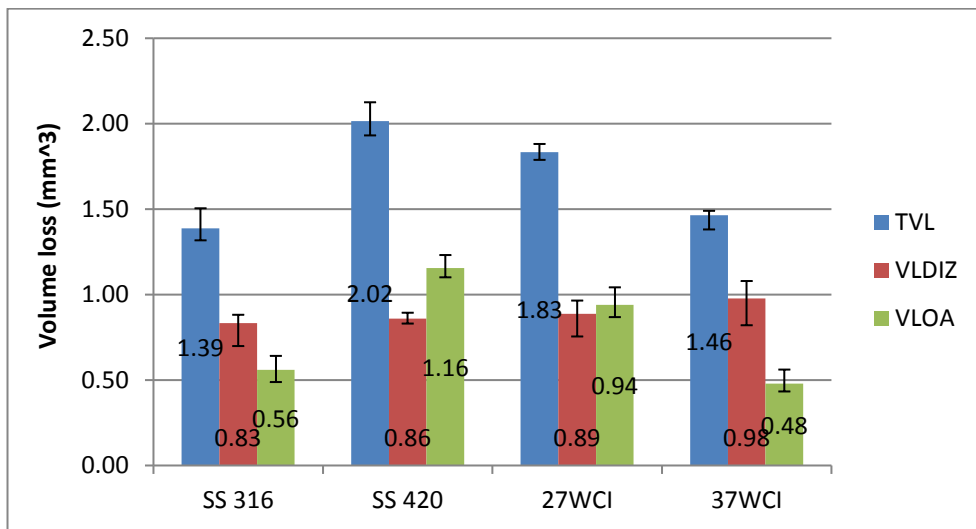
Figure 5.17 Breakdown of average volume loss for materials under study at pH 3.
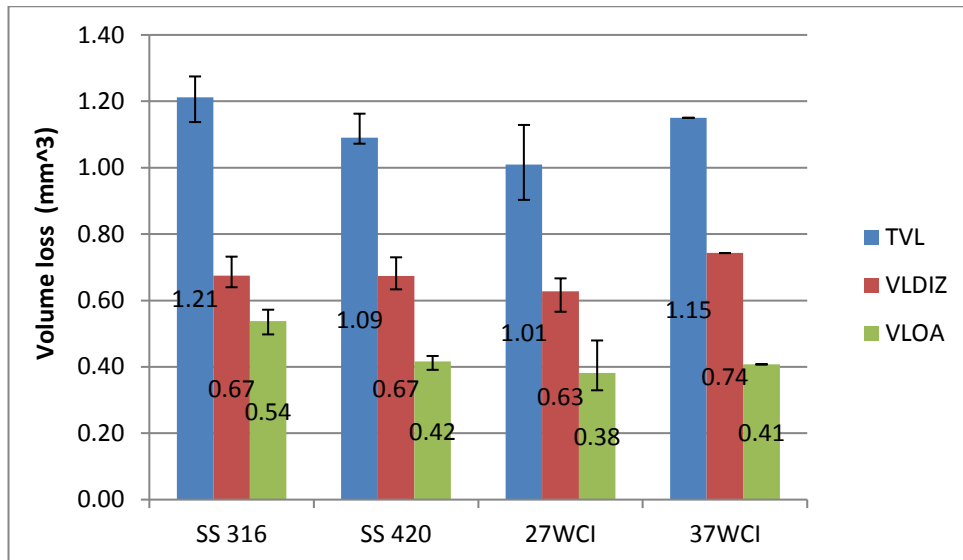
Figure 5.18: Breakdown of average volume loss for materials under study in CP environment at pH 7.

5.3.4.3 Microscopic post-test evaluation

Figure 5.19 demonstrates the microscopy of UNS S31600 under study at in acidic environment. It was noticeable that abrasive markings have been identified outside of the wear scar after 1h SLEC test and which was a common phenomenon for all materials, as shown in the Appendix of this chapter in Figures 5.32-5.36. It was evident that the UNS S42000 and 27WCI displayed, in relation with the erosion-corrosion results, high level of corrosion products while UNS S31600 and 37WCI showed no difference between the two environments. It should be noted that 27WCI showed some corrosion attack even in neutral conditions as a result of possible galvanic interactions between the matrix and the Cr carbides.

Figure 5.19: UNS S31600 OA at pH 3 after 1h SLEC test – abrasive markings (arrow).

5.3.4.4 Examination of cracks on WCIs

As shown in Figures 5.16-5.17, the WCIs displayed higher volume loss in the DIZ at pH 3 than at pH 7. Thus, further investigation of the DIZ region of WCIs was carried out. As demonstrated in Figures 5.20-5.23, more cracks were observed on Cr carbides at pH 3 than in the case of neutral pH for both WCIs. It should be noted that no surface cracking was observed in the OA thereby demonstrating the observed cracks were not produced from the cross section operations (Figure 5.24).
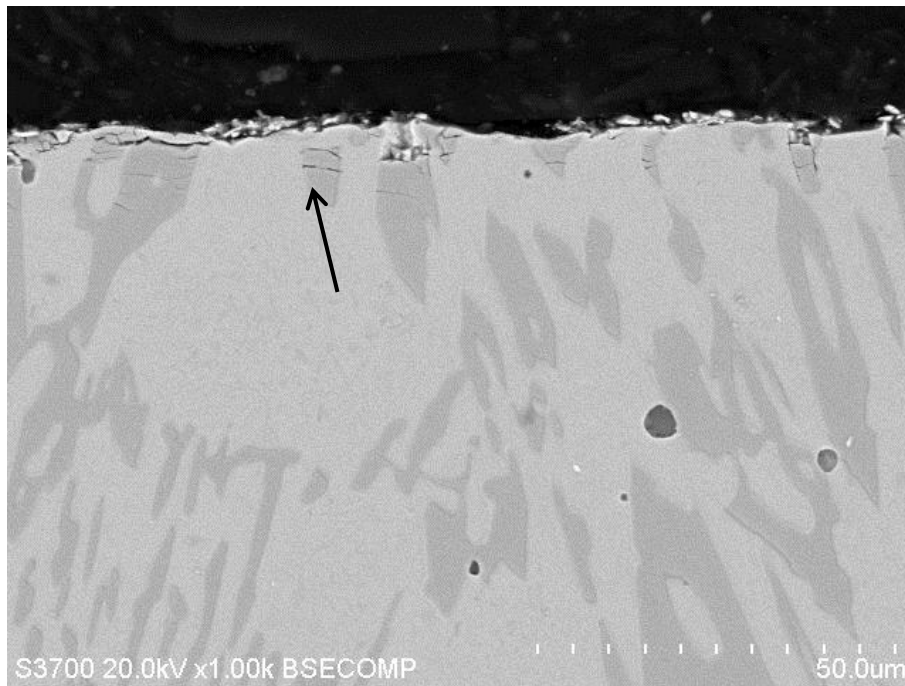
Figure 5.20: Cracks on cross sectioned wear scar of 27WCI after 1h SLEC test at pH 7 [etched].
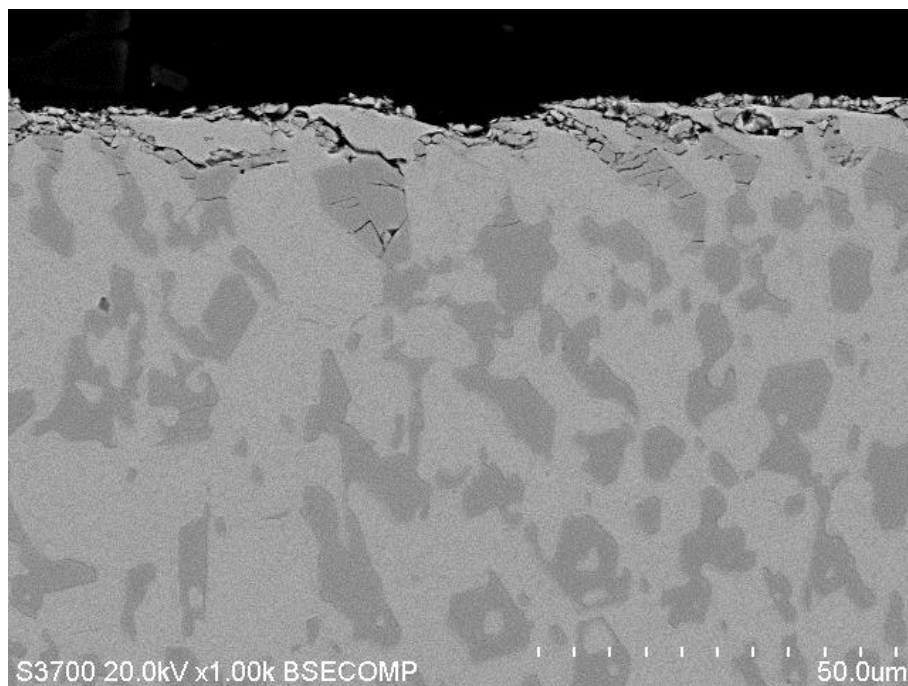
Figure 5.21: Cracks on cross sectioned wear scar of 27WCI after 1h SLEC at pH 3 [etched].
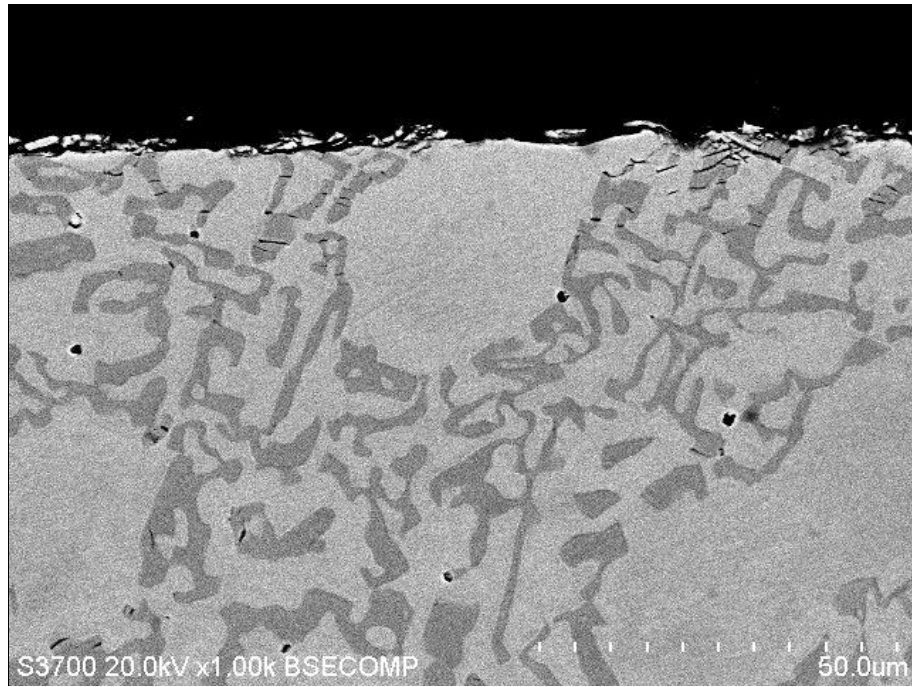
Figure 5.22: Cracks on cross sectioned wear scar of 37WCI after 1h SLEC at pH 7 [etched].
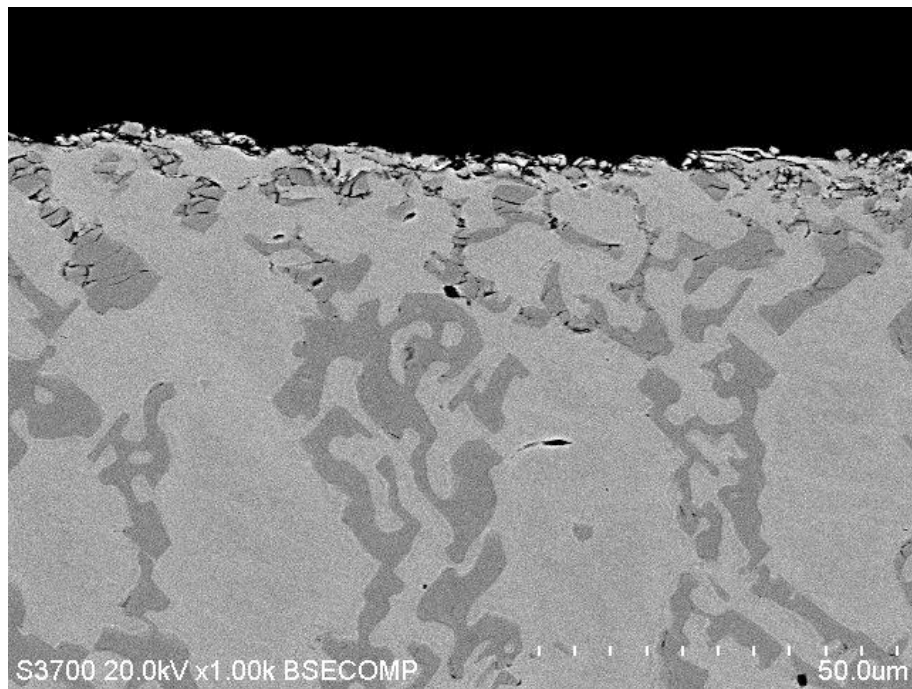
Figure 5.23: Cracks on cross sectioned wear scar of 37WCI after 1h SLEC at pH 3 [etched].
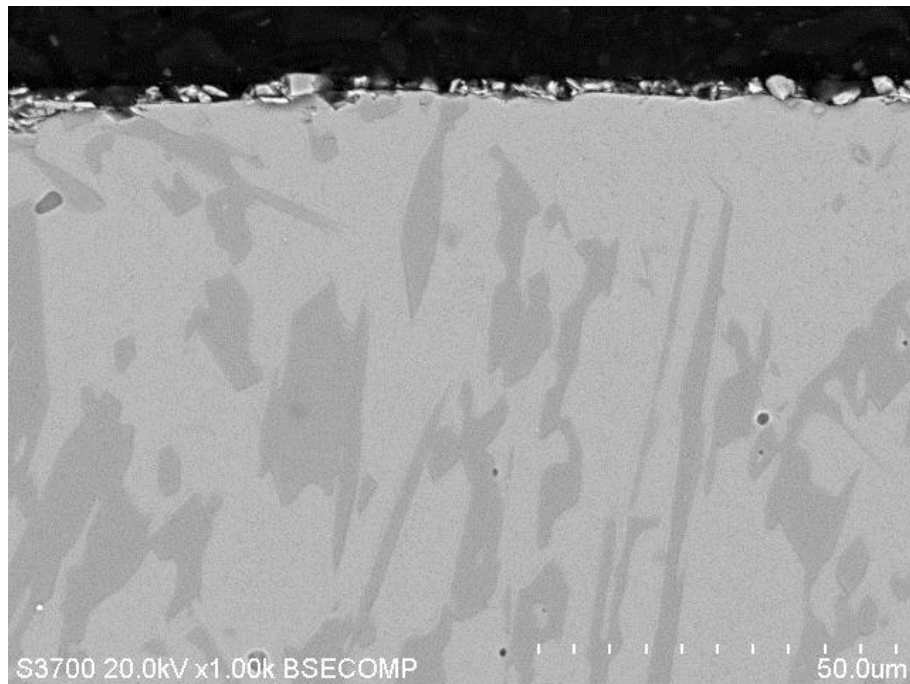
Figure 5.24: No cracks observed in the OA of 27WCI after 1h SLEC at pH 7 [etched].

5.4 Discussion

5.4.1 Erosion-corrosion in neutral conditions

The erosion-corrosion mechanisms were obtained from volume loss under SLEC conditions (Table 5.8). In terms of overall volume loss, the two WCI alloys were superior to the two stainless steels due to their microstructure which is a mixture of metallic matrix and eutectic Cr carbides. This is in good agreement with the literature [5.4, 5.5]. The 27WCI was the optimum material (highest hardness and about 25% CVF) followed by 37WCI (17% CVF), despite the fact that, in terms of corrosion, it exhibited the highest corrosion rate. The UNS S42000 showed slightly lower volume loss than the UNS S31600 displaying the same trend as the cast irons in terms of influence of metallurgical structure (martensitic superior to austenitic). Moreover, the austenitic-structured alloys demonstrated lower corrosion attack than the martensitic-structured materials. The 37WCI illustrated similar corrosion resistance to that of UNS S31600, whilst the UNS S42000 experienced a lower corrosion rate than the 27WCI despite the lower nominal Cr (13% against 15% in the matrix of 27WCI). It is well known that the WCIs experience galvanic corrosion due to the different corrosion

potentials between the carbides and the ferrous matrix [5.6]. Thus, it can be argued that the galvanic interactions were more evident in the case of 27WCI rather than 37WCI due to higher CVF (26% against 17%) and especially the poorer corrosion resistance which is related with the lower Cr dissolved in the matrix (15% against 28%).

In terms of enhanced erosion due to corrosion (synergy), the WCIs showed lower synergy than the stainless steels. Generally, the interaction between erosion and corrosion is rather peculiar. Thus, for a given material/environment the analysis of the synergy on the tested materials must be conducted individually. According to the result, the following statements can be claimed (with regards to the synergy):

- UNS S31600 showed the highest synergy due to poor erosion resistance despite its very good corrosion resistance.
- UNS S42000 exhibited slightly lower synergy than UNS S31600 but much higher than the two WCIs. A possible explanation for that is the fact that there was no balance between erosion and corrosion resistance and an important factor for that was the relatively high corrosion rates.
- The 27WCI showed negligible synergy despite the fact that it showed the highest corrosion rates. However, its erosion resistance masked the corrosion attack resulting in very low synergy.
- The 37WCI displayed negligible synergy which can be associated with the relatively good erosion resistance since the corrosion rates were similar as in case of UNS S31600 (which possessed higher synergy than 37WCI).

As a general observation, for the tested alloys and under the current testing conditions, the synergy was enhanced for materials with lower hardness.

From pure erosion point of view (CP results), hardness cannot be directly linked to erosion resistance for comparing alloys with entirely different structure (i.e comparison of UNS S42000 and 37WCI) but for the same structured alloys or the same family group (i.e WCIs or stainless steels) the higher hardness provided enhanced erosion resistance.

Some researchers have reported that, at perpendicular incidence, the Cr carbides are fractured leading to high wear rates of the matrix [5.7, 5.8]. In the present work, similar observations in terms of Cr carbides fracture in the WCIs were made (Figures 5.20-5.23). The fact that the volume loss in the DIZ was lower in the case of 27WCI than the other materials was associated with the erosion resistance of the metallic matrix and eutectic Cr carbides. Also, the 37WCI showed cracks even though is less brittle than 27WCI (less CVF, lower hardness and austenitic matrix), indicating that the austenitic matrix 37WCI undergoes plastic deformation which resulted in microcracking and carbide detachment, an observation that has been reported in a past study [5.9]. Comparing the types of stainless steel, their performance in the DIZ was similar since the benefits from the erosion resistance of UNS S42000 were masked by its brittleness under the perpendicular jet. In the OA, all materials showed similar behaviour apart from UNS S31600, which experienced the highest volume loss due to its low hardness and poor sliding abrasion resistance.

5.4.2 Erosion-corrosion in acidic conditions

Under these severe corrosive conditions, the two austenitic-structured materials illustrated superiority to the two martensitic-structured alloys since the former alloys provided greater corrosion resistance. It was evident that the corrosion and synergy were crucial mechanisms in this environment and the austenitic alloys with higher Cr (in the matrix for 37WCI), displayed similar corrosion rates as those at neutral pH. On the other hand, the effect of reducing the pH from 7 to 3 produced a substantial increase in corrosion rate for martensitic structured alloy. The importance of a high level of Cr in the metallic matrix for WCI in terms of corrosion resistance, has been reported in many studies [5.4, 5.10–5.12]. In addition, 37WCI exhibited slightly higher average volume loss than UNS S31600 but its performance was affected by enhanced erosion due to corrosion which resulted in higher volume loss compared neutral conditions. On the other hand, the UNS S31600 displayed the same material loss at both pH levels.

On the other hand, despite the fact that the 27WCI displayed enhanced cracks on the Cr carbides at pH 3 than at pH 7 (Figures 5.20-5.21), it demonstrated better overall performance than UNS S42000. The explanation for that was the superiority of the

27WCI over the UNS S42000 in mechanical damage and synergy which masked the poorer corrosion resistance. Unlike in neutral conditions, the synergistic effects on all tested alloys was affected by the corrosion rates or possibly HE involvement and not by the hardness.

The value of carrying out the post-test analysis was evident in Figure 5.17 which shows that the higher total erosion-corrosion resistance of the austenitic structured alloys was associated with the behaviour in the OA rather than in the DIZ. Hence, it can be concluded that the when high impact loads and erosion are present, the corrosion mechanism is suppressed, whilst when the mechanical damage is reduced (OA compared to the DIZ) the corrosion at low pH becomes aggressive on less corrosion resistant alloys such as martensitic-structured materials.

The results of UNS S42000 and UNS S31600 in the current study do not agree with the findings of Lopez et al. work in which UNS S42000 was superior over UNS S30400 in strong acidic slurry tests (submerged technique) at 30° and 90° angle of attack and various velocities [5.13]. However, the authors of this work [5.13] used circular and relatively small (200-300 μm) SiO_2 abrasive particles, and the maximum velocity was 8.5 m/s. All their experimental parameters resulted in 0.006 mA/cm^2 maximum corrosion rate (as measured) on UNS S42000 which was 33 times lower than the corresponding maximum corrosion rate in the current study despite the fact that the pH was 0.3. Thus, it can be concluded how the testing conditions can affect the materials performance, especially those with moderate corrosion resistance such as the martensitic structured alloy. A similar trend was reported elsewhere (UNS S42000 superior to UNS S30400) [5.14] but comparisons with the current study cannot be made since the two experimental apparatus are entirely different (laboratory mill circuit).

From the current work, the enhanced cracks of Cr carbides on WCIs in the DIZ in acidic conditions, which yielded increased volume loss than at pH 7, can only partially be explained via the experimental techniques used in the current study. For 27WCI case, it can be reasonably assumed that the increased corrosion resulted in higher synergy and hence, the Cr carbides underwent an increased erosion-corrosion damage. In case of 37WCI, the corrosion rates were similar to pH 7 and hence the increased

synergy in the DIZ (comparison of Figures 5.16-5.17) is unlikely to be produced from the corrosion mechanism. A possible reason for that could be the involvement of HE which is attributed to the fact that 10000 more hydrogen ions are produced at pH 3 than at pH 7 and therefore, HE could potentially occur on a vulnerable material. Such a phenomenon was previously reported by D N Veritas [5.15]. Other past studies [5.16-5.18] have described the involvement of HE in engineering CP applications or in acidic water and also, the material groups that are susceptible to that phenomenon. Steels with yield strength about 700 MPa and hardness of 350 HV are vulnerable to HE [5.15].

The following outcomes from their work [5.16-5.18] are as follows:

- the hydrogen production in acidic conditions was found to promote abrasive wear damage [5.16].
- the postulated mechanisms of HE, one of which involves the role of alloy carbon content and suggests that hydrogen diffuses along the grain boundaries and combines with the carbon to form methane gas. The methane gas is not mobile and collects in small voids along the grain boundaries where it builds up enormous pressures that initiate cracks [5.17]. Thus, since the WCI alloys contain relatively much more carbon than stainless steels, they are possibly susceptible to HE phenomenon under the perpendicular jet in the present work.
- the role of chromium on HE in Ni-Cr-Fe alloys and the findings from this study showed that alloys with higher Cr content were more susceptible to HE [5.18]. This supported the general notion that the mechanism of low temperature (25°C) stress corrosion cracking, in hydrogenated water, is hydrogen embrittlement.

5.6 Conclusions

1) At pH 7, the WCIs displayed superiority over the stainless steels. The 27WCI alloy demonstrated the optimum performance, followed by 37WCI, UNS S42000 and UNS S31600. The better performance of the 27WCI is attributed to enhanced resistance in both the DIZ and OA.

2) In acidic conditions, the austenitic-structured materials (UNS S31600 and 37WCI) showed superiority over the martensitic-structured alloys due to their enhanced corrosion resistance that is associated with the higher Cr dissolved in the matrix. The two austenitic-structured alloys exhibited similar volume loss, while the 27WCI was superior to UNS S42000.

3) The benefit of the austenitic alloys occurs in the OA (abrasion zone) where corrosion is important since the erosion rates are decreased compared with the DIZ. In the DIZ, where erosion rates are maximised, there was scarcely any discrimination between the four materials. Thus, the post-test analysis represents a powerful demonstration of the crucial importance of this analysis technique in differentiating between different wear zones.

4) In neutral conditions, the UNS S31600 was the most vulnerable to erosion-corrosion damage in the OA and this is attributed to its low hardness. However, at pH 3, the UNS S31600 possessed the highest resistance to damage in the OA indicating that high hardness is not necessarily correlated with high erosion resistance in severe corrosive environments.

5) Minor advantages of applying CP at pH 7 were observed. This is validated by the volume loss for all materials under study being lower in CP applications than in free erosion–corrosion conditions, showing the successful isolation of mechanical damage during CP tests.

6) The high hardness provides benefits in overall erosion-corrosion performance at pH 7 since it minimises the enhanced erosion due to corrosion (Tables 5.1, 5.8).

5.7 References

[5.1] An internal communication with Edward Humphries, Director of R&D, Weir Minerals Sydney, Australia, (2015).

[5.2] C.I. Walker, P. Robbie, Comparison of some laboratory wear tests and field wear in slurry pumps, Wear. 302 (2013) 1026–1034.

[5.3] An internal communication with Gerry Russel, Vice President of Engineering

& Field Service,Weir American Hydro, York, Pennsylvania, USA, (2015).

[5.4] M. Jones, R.J. Llewellyn, Erosion-corrosion assessment of materials for use in the resources industry, Wear. 267 (2009) 2003–2009.

[5.5] L.L. Parent, D.Y. Li, Wear of hydrotransport lines in Athabasca oil sands, Wear. 301 (2013) 477–482.

[5.6] X.H. Tang, R. Chung, C.J. Pang, D.Y. Li, B. Hinckley, K. Dolman, Microstructure of high (45wt.%) chromium cast irons and their resistances to wear and corrosion, Wear. 271 (2011) 1426–1431.

[5.7] M.A. Al-Bukhaiti, S.M. Ahmed, F.M.F. Badran, K.M. Emara, Effect of impingement angle on slurry erosion behaviour and mechanisms of 1017 steel and high-chromium white cast iron, Wear. 262 (2007) 1187–1198.

[5.8] A.N.J. Stevenson, I.M. Hutchings, Wear of hardfacing white cast irons by solid particle erosion, Wear. 186-187 (1995) 150–158.

[5.9] J.J. Coronado, A. Sinatora, Abrasive wear study of white cast iron with different solidification rates, Wear. 267 (2009) 2116–2121.

[5.10] R.J. Llewellyn, S.K. Yick, K.F. Dolman, Scouring erosion resistance of metallic materials used in slurry pump service, Wear. 256 (2004) 592–599.

[5.11] R.J. Chung, X. Tang, D.Y. Li, B. Hinckley, K. Dolman, Abnormal erosion-slurry velocity relationship of high chromium cast iron with high carbon concentrations, Wear. 271 (2011) 1454–1461.

[5.12] Y.P. Wang, D.Y. Li, L. Parent, H. Tian, Improving the wear resistance of white cast iron using a new concept - High-entropy microstructure, Wear. 271 (2011) 1623–1628.

[5.13] D. López, J.P. Congote, J.R. Cano, A. Toro, A.P. Tschiptschin, Effect of particle velocity and impact angle on the corrosion-erosion of AISI 304 and AISI 420 stainless steels, Wear. 259 (2005) 118–124.

[5.14] V.G. Efremenko, K. Shimizu, T. Noguchi, A. V. Efremenko, Y.G. Chabak, Impact-abrasive-corrosion wear of Fe-based alloys: Influence of microstructure and chemical composition upon wear resistance, Wear. 305 (2013) 155–165.

[5.15] D.N. Veritas, Dnv-Rp-B401 Cathodic Protection Design, (2011).

[5.16] T.C. Zhang, X.X. Jiang, S.Z. Li, Hydrogen-Induced Embrittlement Wear of a High-Strength, Low-Alloy Steel in an Acidic Environment, Corros. 53 (1997) 200–205.

[5.17] J. Cwiek, Hydrogen degradation of high-strength steels, J. Achiev. Mater. Manuf. Eng. 37 (2009) 193–212.

[5.18] D. Symons, Hydrogen embrittlement of Ni-Cr-Fe alloys, Metall. Mater. Trans. A. 28 (1997) 655–663.

5.8 Appendix
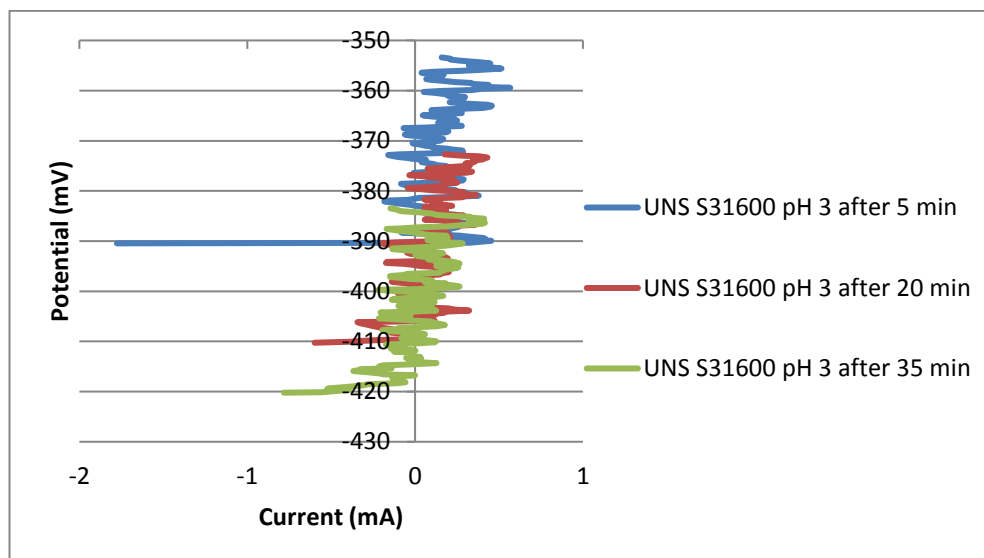
Figure 5.25: Linear polarisation for UNS S31600 at pH 3.
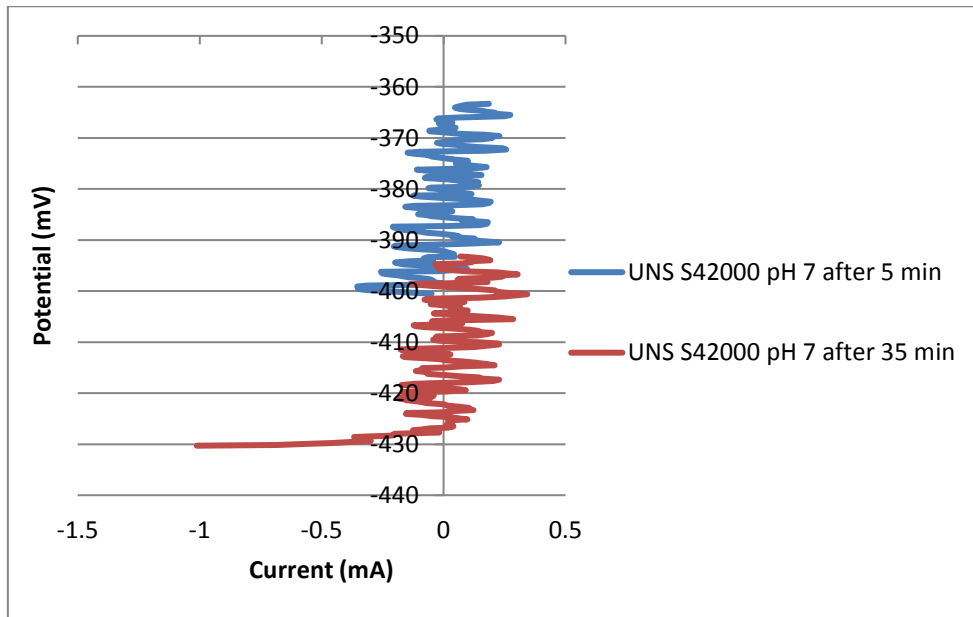
Figure 5.26: Linear polarisation for UNS S42000 at pH 7.
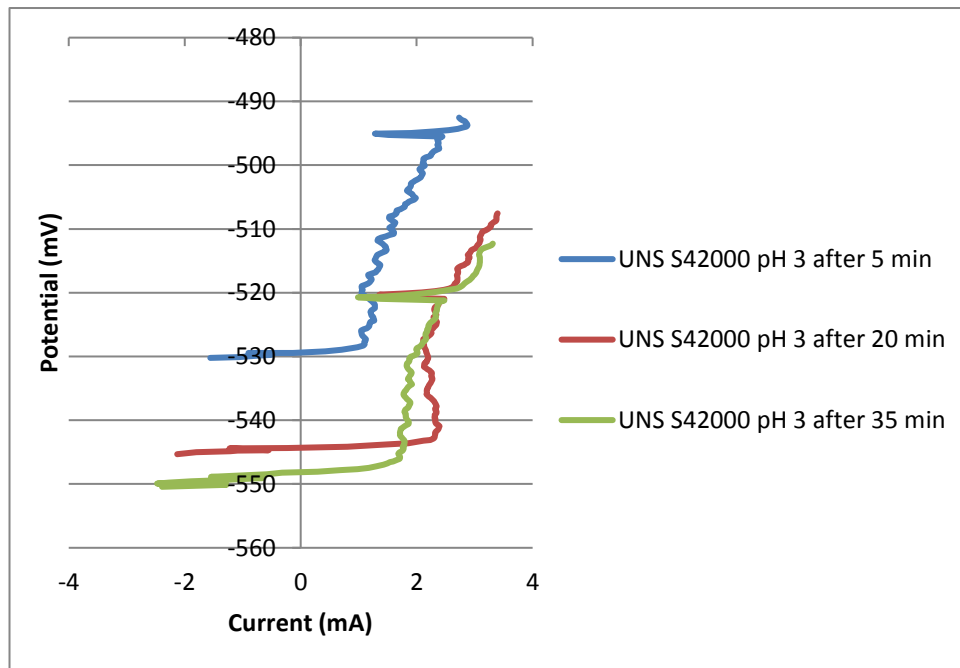
Figure 5.27: Linear polarisation for UNS S42000 at pH 3.
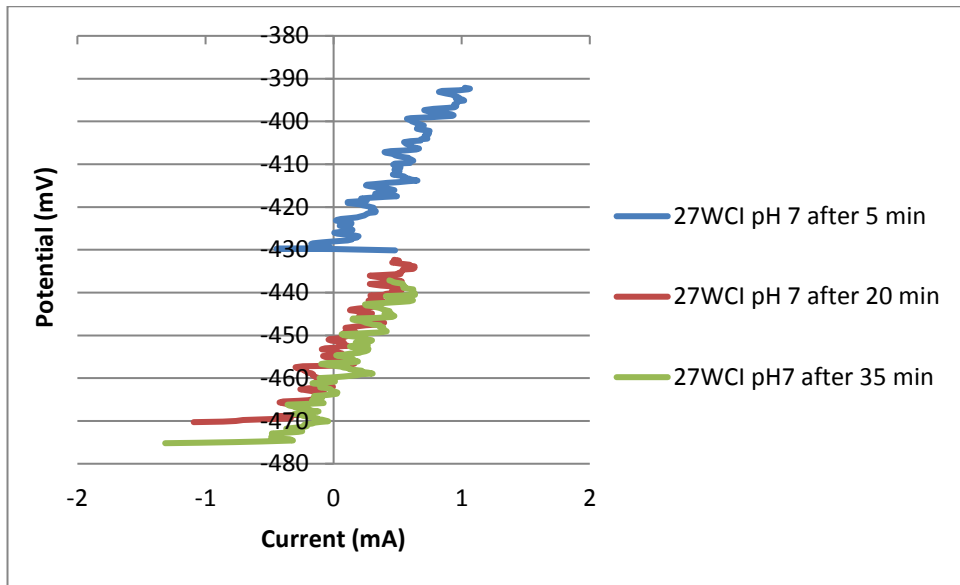
Figure 5.28: Linear polarisation for 27WCI at pH 7.
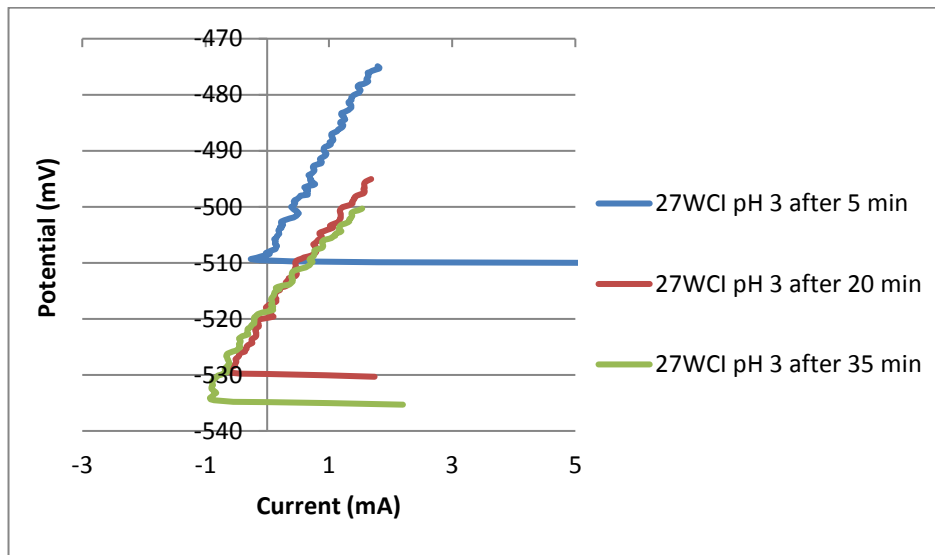
Figure 5.29: Linear polarisation for 27WCI at pH 3.
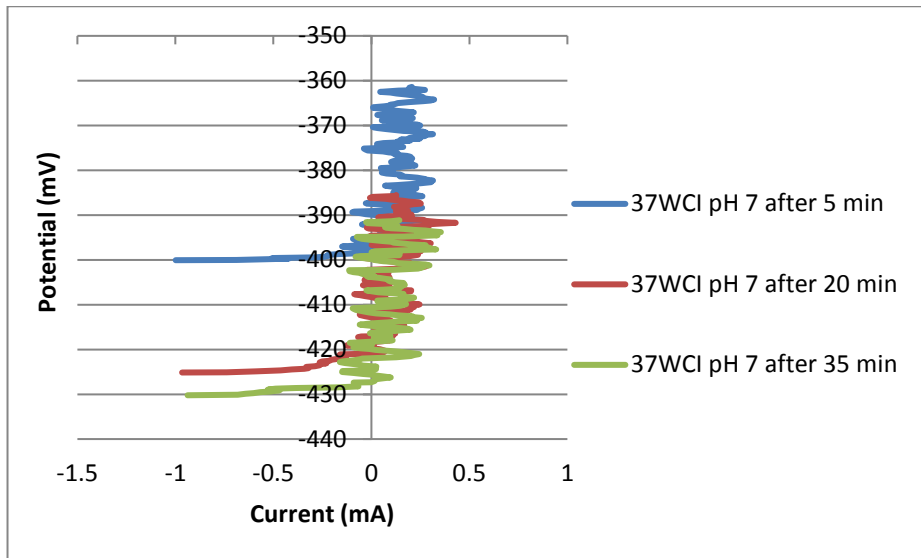
Figure 5.30: Linear polarisation for 37WCI at pH 7.
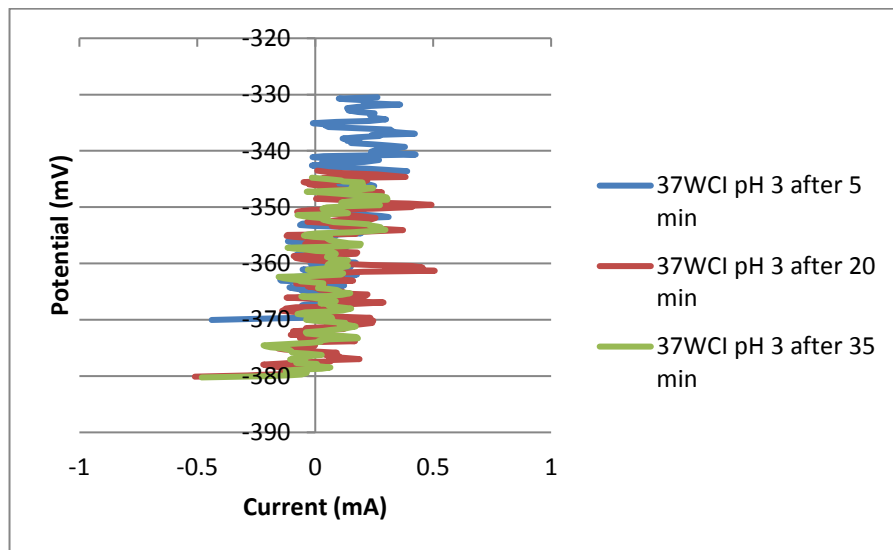
Figure 5.31: Linear polarisation for 37WCI at pH 3.

Figure 5.32: UNS S42000 OA at pH 7 after 1h SLEC test.
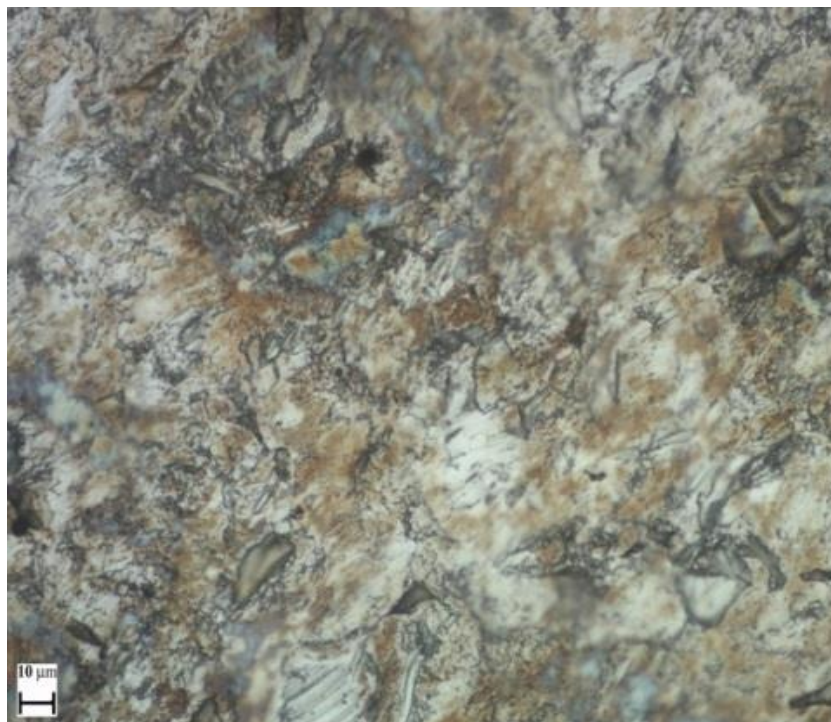
Figure 5.33: UNS S42000 OA at pH 3 after 1h SLEC test.
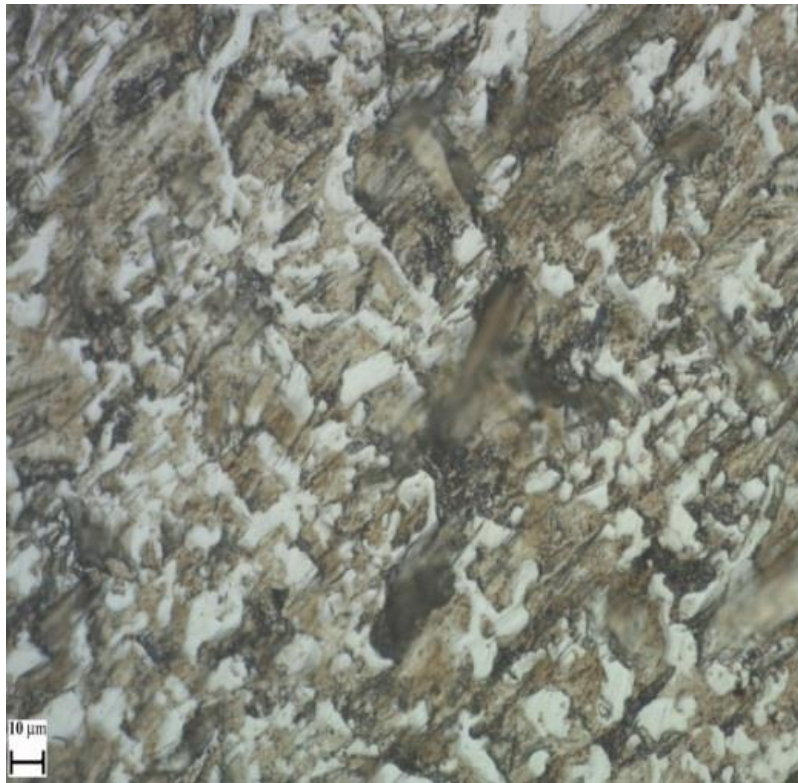
Figure 5.34: 27WCI OA at pH 7 after 1h SLEC test.
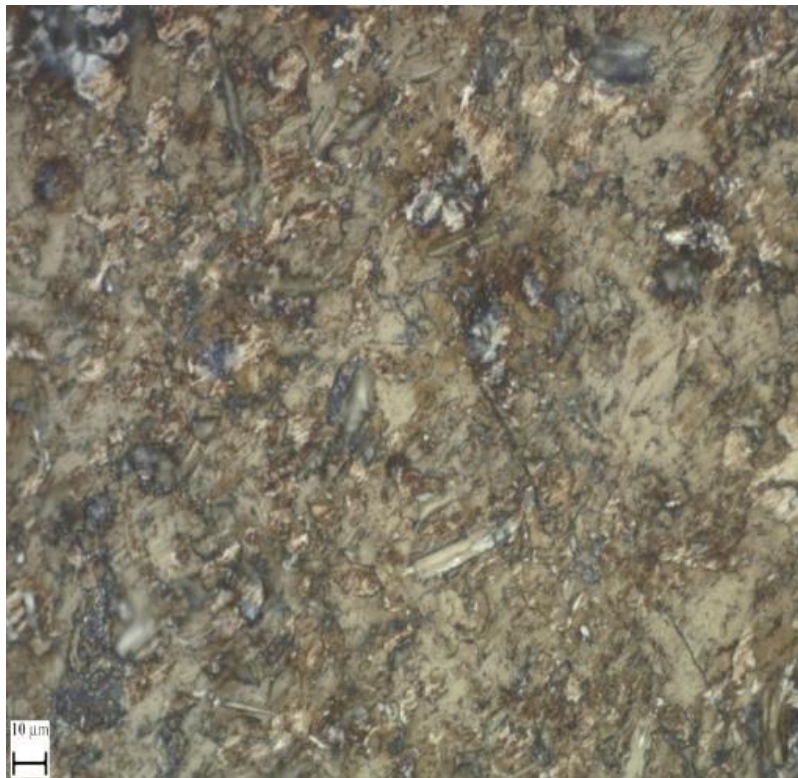
Figure 5.35: 27WCI OA at pH 3 after 1h SLEC test.
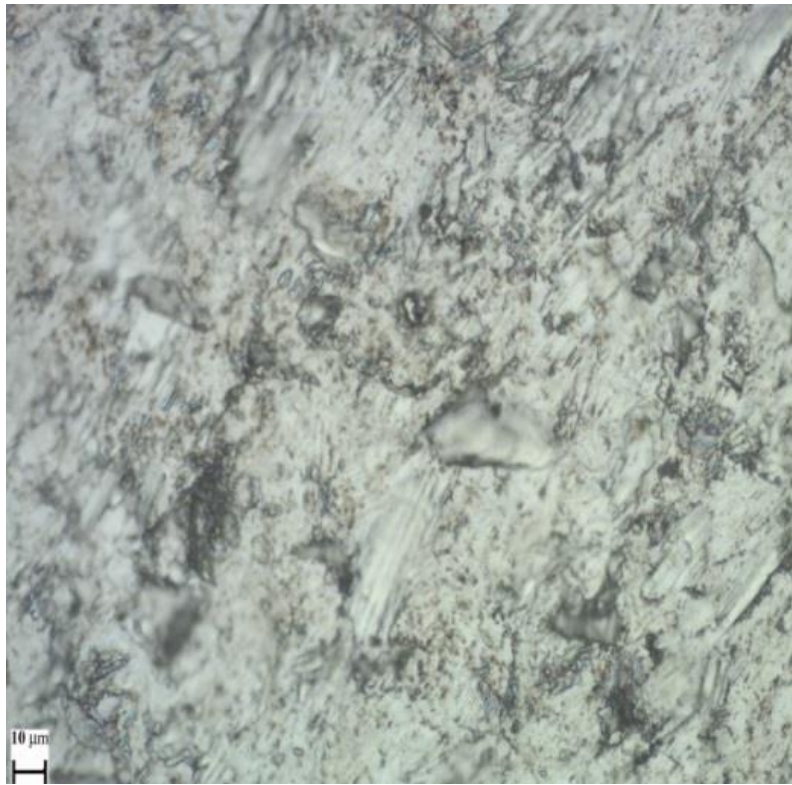
Figure 5.36: 37WCI OA at pH 3 after 1h SLEC test.

Chapter 6

Erosion-corrosion assessment of advanced white cast irons in neutral and acidic conditions

6.1 Introduction

As a continuation of the work presented in chapter 5, two advanced white cast irons (WCI) were evaluated in the erosion-corrosion programme at pH 7 and pH 3; a hypereutectic WCI with 38% Cr (38WCI) and an experimental WCI with Nb carbides (NbC) which basically is the 27WCI alloy, tested in the previous chapter, reinforced with NbC (27WCINb). Thus, it was decided the new two alloys to be compared with the 27WCI. The UNS S31600 was not entirely tested in this chapter since it was used as a reference material. Both of the new alloys were supplied by the Weir Group PLC.

6.2 Materials and experimental conditions

6.2.1 Materials

38WCI is a 38% Cr/4% C hypereutectic WCI made by the sand casting method. This alloy is used in mining applications in which high erosion/abrasion conditions are present in corrosive environments that contain chlorides or low pH (down to 4). Figure 6.1 shows the microstructure of 38WCI which consists of large primary carbides, eutectic (small) carbides − light colour (37% volume fraction in total − as measured via Image J) and secondary carbides in a martensite retained austenite structure - dark colour (67% in total). The primary carbides were eutectic carbides were found to be approximately 15% and 22% respectively, as measured by Image J software.
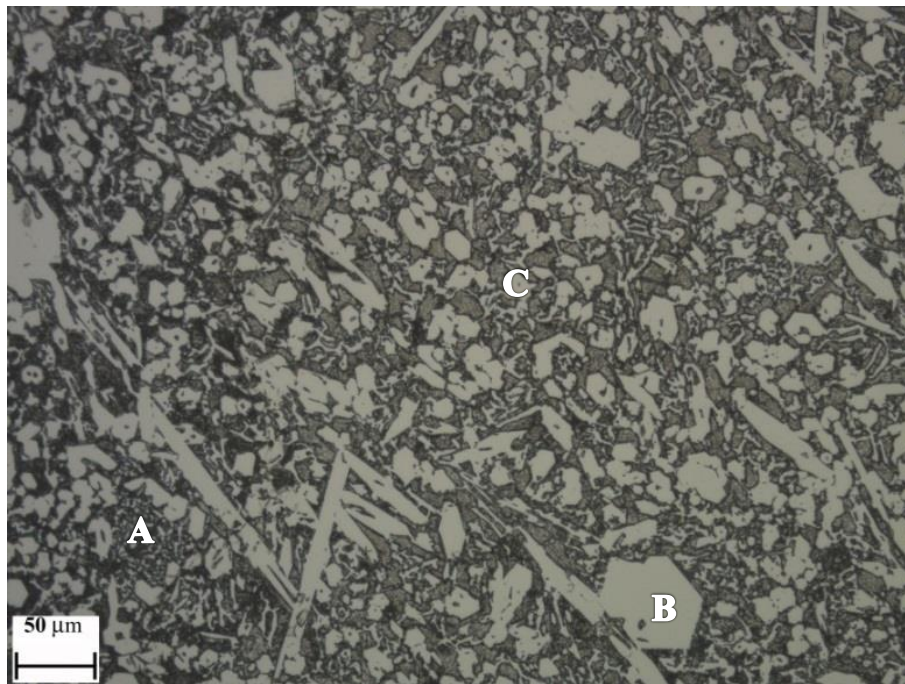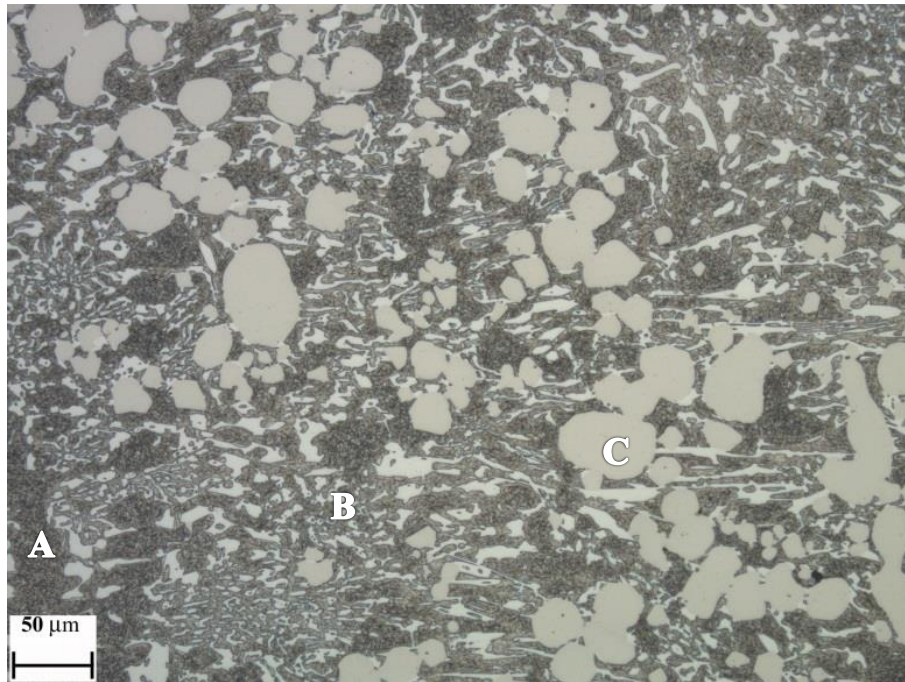
Figure 6.1: Microstructure of 38WCI (A-matrix and secondary carbides, B-primary Cr carbides, C-eutectic Cr carbides) [etched].

Figure 6.2 and Table 6.1 demonstrate the Cr content of 38WCI via the EDS technique. Spectrums 1 & 3 represent the Cr carbides, spectrum 5 a mix of eutectic structure – Cr carbides and martensitic matrix, whilst Spectrums 2, 4, 6 and 7 show the martensitic matrix. The observed Cr content in the matrix was around 20 wt% which is in line with the specifications of the alloy.
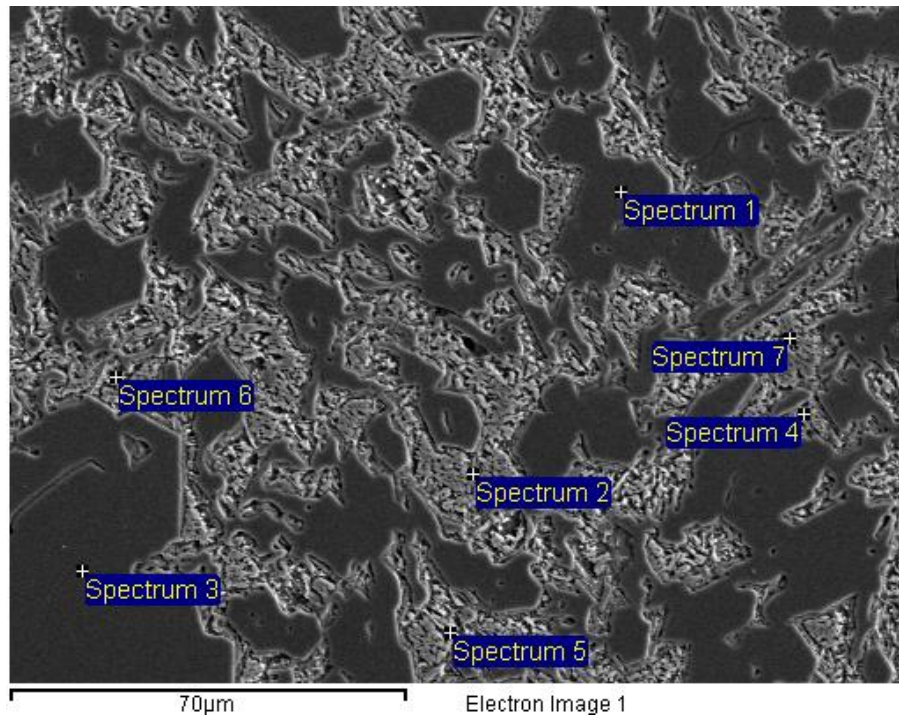
Figure 6.2: Chemical spot analysis on 38WCI via SEM [etched].

Table 6.1: Cr content of Figure 6.2.

Spectra	1	2	3	4	5	6	7
Cr (wt%)	73.8	17.3	76.2	18.5	35.8	25.4	20.8

The 27WCINb advanced white cast iron is an experimental alloy that contains reinforced NbC carbides in the 27WCI material, whilst the NbC are uniformly dispersed in the microstructure by using the centrifugal casting method. During the fabrication process, Fe-Nb (around 18 wt%) and additional carbon are added to a pre-melt mixture in order to form the final microstructure. The additional carbon is implemented in order to promote the NbC formation, whilst the final carbon level would be the same as in case of 27WCI alloy (2.8 %). The microstructure of 27WCINb comprises 70% eutectic matrix − dark colour (combination of martensite retained austenite and secondary Cr carbides), 20% NbC (light round particles) and 10% eutectic Cr carbides, as displayed in Figure 6.3 (all values were obtained via Image J).

Figure 6.3: Microstructure of 27WCINb ((A-matrix and secondary carbides, B-eutectic Cr carbides, C-Nb carbides) [etched].

Figure 6.4 and Table 6.2 illustrate Cr and Nb content of 27WCINb via SEM. Spectrum 1 represents the NbC and spectra 2-3 show the martensitic matrix and Cr carbides respectively. An interesting observation was that the NbC possess high Nb content (98%), whilst the level of Cr in Cr carbides is about 68%, trend that has been noted in a past study [6.1].
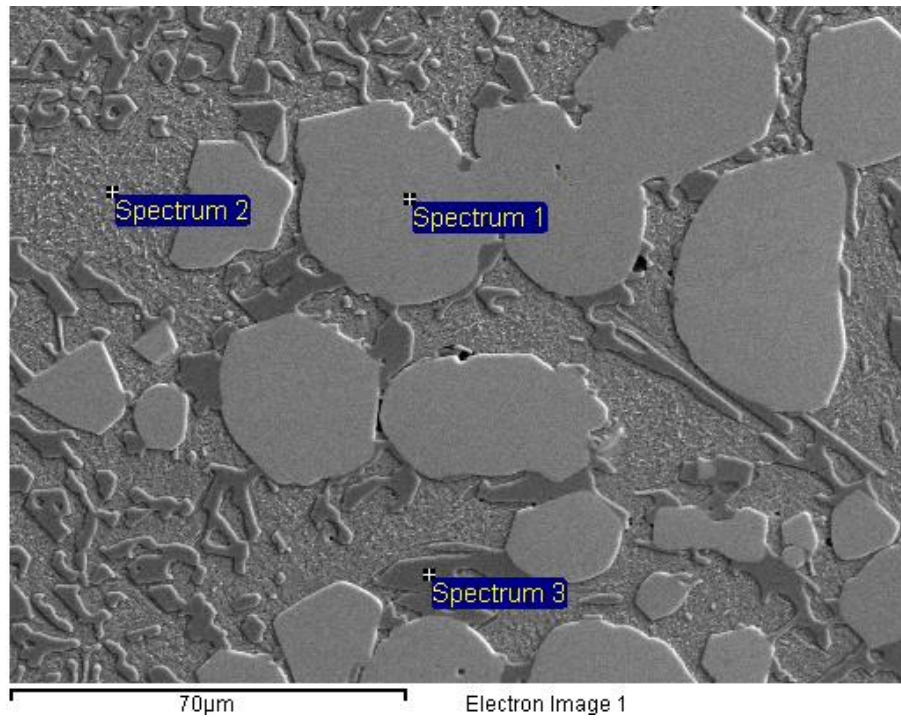
Figure 6.4: Chemical spot analysis on 27WCINb via SEM [etched].

Table 6.2: Cr and Nb analysis of Figure 6.4.

Spectra	1	2	3
Cr%	0.5	13.9	67.9
Nb%	98.1	0.0	0.4

Table 6.3 presents the bulk hardness and the hardness on the individual phases of WCIs (microhardness) in the microstructure as an average of ten measurements of each alloy/phases.

Table 6.3: Hardness of tested alloys and constituent phases.

Material	Bulk hardness (HV$_5$)	Matrix+secondary carbides (HV$_{0.2}$)	Matrix+eutectic carbides (HV$_{0.1}$)	Eutectic carbides (HV$_{0.05}$)	Primary carbides (HV$_{0.05}$)
UNS S31600	175±10	-	-	-	-
27WCI	705±25	610±30	740±30	1102±80	-
38WCI	690±10	650±40	845±20	1220±80	1585±50
27WCINb	690±10	605±40	750±25	1035±80	2000±100

All the above data with regards to 38WCI and 27WCINb alloys validated the specifications provided by the Weir Group PLC.

6.2.2 Testing conditions - methods

The solid-liquid erosion-corrosion (SLEC) conditions in the current chapter contained 3.5% NaCl at pH 7 and pH 3. The velocity at the exit of nozzle was measured at 20 m/s, whilst the sand concentration was 0.75±0.05 g/l. The erosion-corrosion assessment consists of:

- volume loss measurements after 1h SLEC tests
- Cathodic protection (CP) application
- anodic-cathodic polarisations in SLEC and static conditions
- Linear polarisations
- anodic polarisations on segmented specimens
- Post-test analysis
- Crack investigations on the 38WCI and 27WCINb.

6.3 Results

6.3.1 Volume loss

As observed in Figure 6.5, 27WCI demonstrated superiority over the rest of materials at pH 7. The 38WCI alloy was slightly inferior to 27WCI, followed by UNS S31600, whilst 27WCINb exhibited significantly high volume loss.

In CP conditions, 38WCI and 27WCI demonstrated the lowest volume loss followed by UNS S31600 and 27WCINb. It should be noted that the difference in volume loss between 27WCINb and 27WCI-38WCI was lower than in SLEC. A general observation for all materials under study was that the material loss in CP conditions were lower than SLEC indicating the benefits associated with the suppression of corrosion and synergy.

In acidic conditions, as expected, all WCIs were subject to higher volume loss than UNS S31600 due to the martensitic matrix which is vulnerable to corrosion. As it has been illustrated in the previous chapter, the UNS S31600 volume loss showed no difference between pH 7 and pH 3. 27WCI and 38WCI showed equal performance, whilst the volume loss of 27WCINb was 65% higher than the other two WCIs.
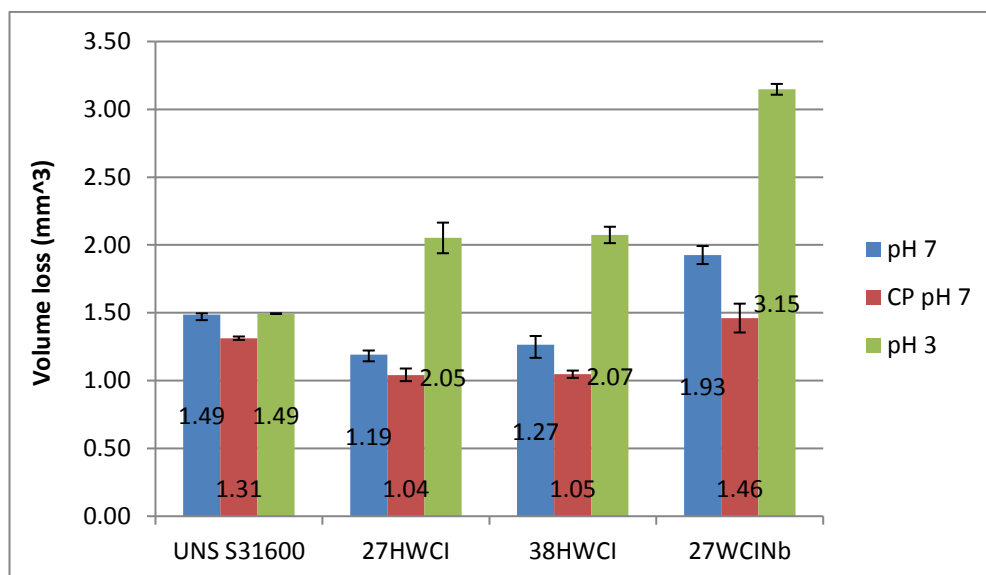
Figure 6.5: Average volume loss of materials under SLEC conditions at pH 7, CP pH 7 and pH. 3.

6.3.2 Electrochemical tests

6.3.2.1 Anodic-Cathodic polarisations

Figure 6.6 illustrates the dynamic anodic polarisation scans in both neutral and acidic testing regimes. Table 6.4 demonstrates the i_{corr} values and the volume loss due to

corrosion for all materials in both environments. In general, the i_{corr} values obtained from either anodic or cathodic plots were in good agreement. However, it was decided to take into consideration the anodic polarisation plots for i_{corr} and volume loss (due to corrosion) estimations in order to be comparable with the anodic polarisation tests on segmented samples (no cathodic polarisations were obtained on segmented samples). As was expected, UNS S31600 depicted the lowest corrosion rate due to its austenitic structure. 38WCI showed the lowest corrosion rate from the WCIs, especially in acidic conditions. Its performance was two times better than 27WCI at pH 7, whilst at pH 3 it was 4 times better. 27WCI exhibited 5 times lower corrosion rates than 27WCINb in the neutral environment indicating the same trend with the volume loss, as presented in the previous section. However, in acidic conditions, 27WCI was superior over 27WCINb but their difference was not great as at pH 7. The latter material exhibited only a minor increase in corrosion rates from neutral to acidic environment.
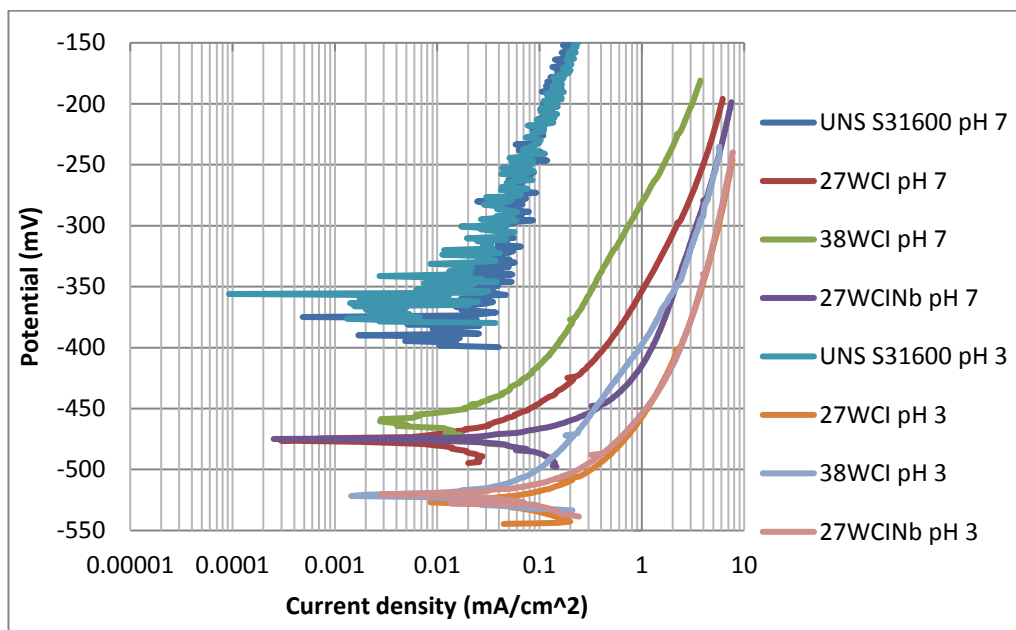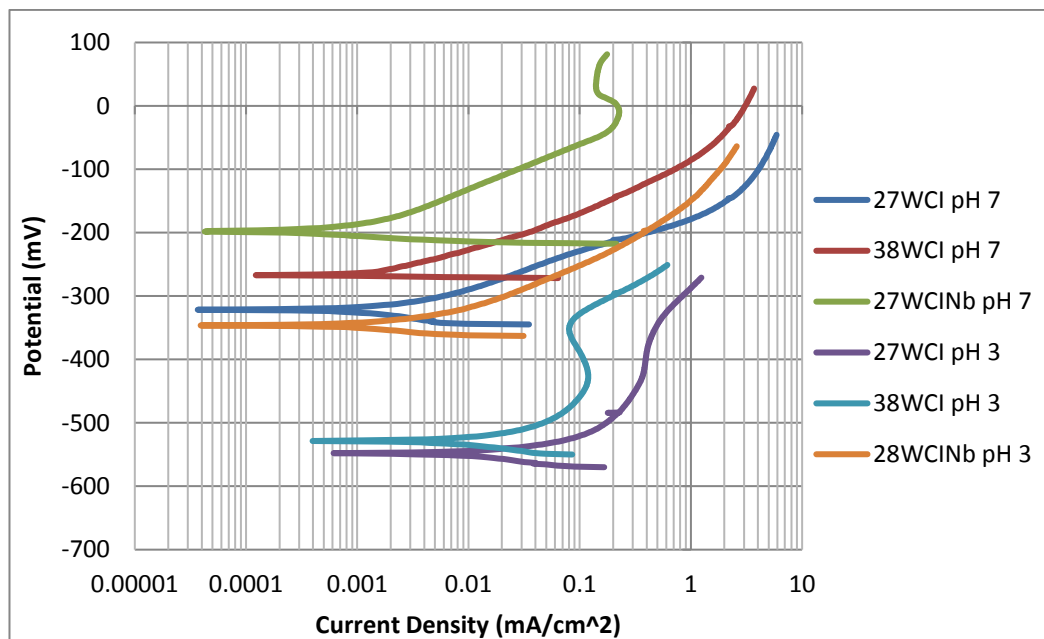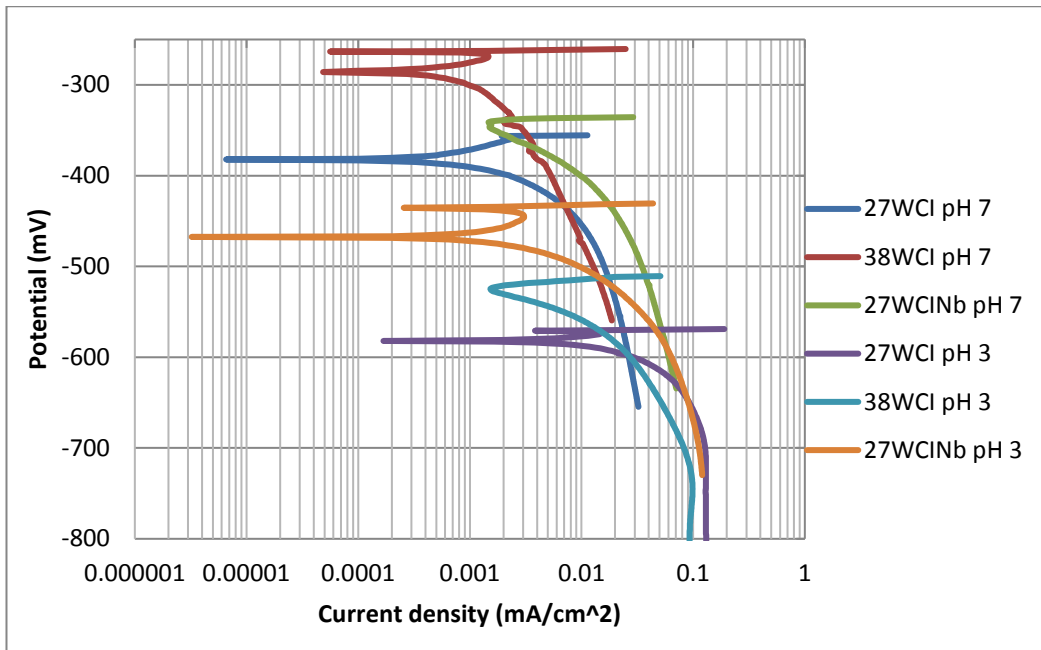

Figure 6.6: Anodic polarisation scans of materials in SLEC conditions at pH 7 and pH 3.

Table 6.4: Anodic polarisation data for materials under study at pH 7 and pH 3.

Material	i_{corr} - Current density pH 7/pH 3 (mA/cm^2)	Volume loss pH 7/pH 3 (mm^3)
UNS S31600	0.015/0.017	0.021/0.023
27WCI	0.11/0.42	0.16/0.62
38WCI	0.05/0.11	0.08/0.13
27WCINb	0.5/0.6	0.45/0.49

Figure 6.7 illustrates the cathodic polarization plots for materials under study at both pH values. It was evident that the cathodic reaction rates were 2-3 times greater in acidic conditions rather than neutral and hence, the hydrogen evolution that occurs at pH 3 was substantially higher.
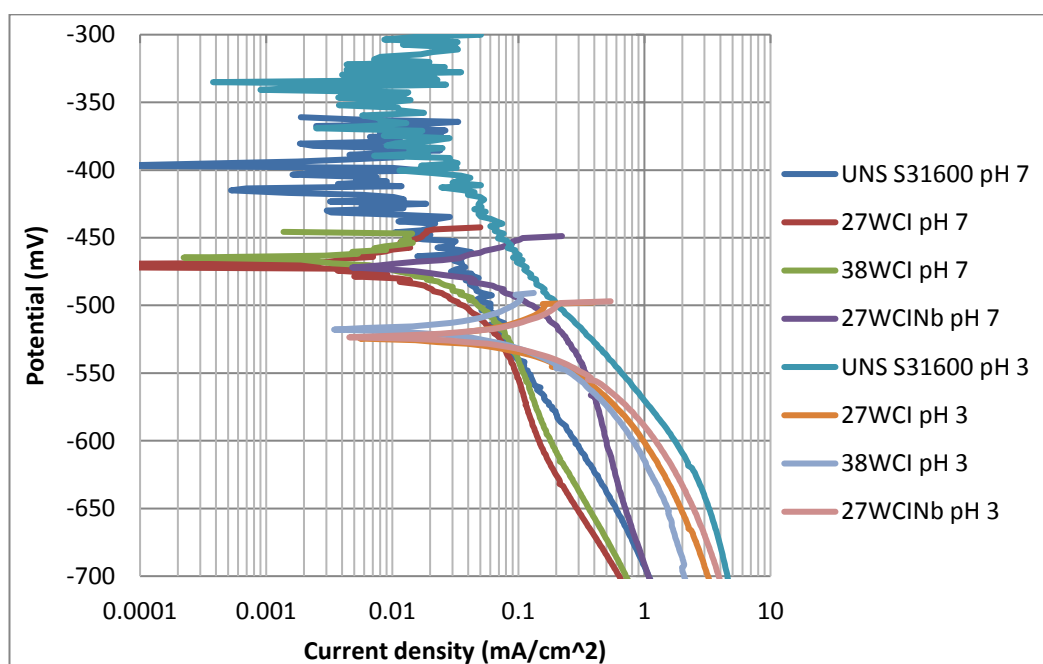
Figure 6.7: Cathodic polarisation scans of materials in SLEC conditions at pH 7 and pH 3.

In order to investigate further the unexpected minor increase of 27WCINb corrosion rate from pH 7 to acidic water, electrochemical tests were performed on WCIs in the same environments but under static conditions (not on UNS S31600). Figures 6.8-6.9

present the anodic and cathodic polarisation scans respectively in static conditions at both pH values. It should be noted that, as a matter of consistency, the i_{corr} values for all materials in both neutral and acidic conditions were obtained via cathodic polarisation scans (Figure 6.9) since it was unfeasible to use Tafel extrapolation on anodic scans for 27WCI and 38WCI at pH 3. As shown in Table 6.5, in neutral environment, the 38WCI was (as expected) the superior alloy followed by 27WCI and 27WCINb which both showed very similar corrosion rates, a trend that was the opposite to that observed in dynamic corrosion measurements.

In acidic conditions, 38WCI was slightly better than 27WCINb and both displayed significantly lower corrosion rates than 27WCI. The latter is an important observation which is discussed in the Discussion section of this chapter.

Figure 6.8: Anodic polarisation scans of materials in static conditions at pH 7 and pH 3.

Figure 6.9: Cathodic polarisation scans of materials in static conditions at pH 7 and pH 3.

Table 6.5: Cathodic polarisation data for materials at both pH levels in static conditions.

Material	i_{corr} - Current density pH 7/pH 3 (mA/cm2)	Volume loss pH 7/pH 3 (mm3)
27WCI	0.007/0.11	0.011/0.170
38WCI	0.0016/0.012	0.002/0.017
27WCINb	0.008/0.02	0.006/0.031

6.3.2.2 Anodic polarisation scans on segmented specimens

In this section, the corrosion rates of the direct impinged zone (DIZ) and the outer area (OA) for all WCIs under erosion-corrosion conditions are presented (Figures 6.10-6.12). As shown in Table 6.6, the DIZ region for all tested materials in both environments experienced significantly higher corrosion rates than the OA zone. However, since the surface area of DIZ is much smaller than the OA, the volume loss due to corrosion are substantially lower. Also, Table 6.6 shows the volume loss due to corrosion in DIZ-OA regions.

In neutral conditions, 38WCI possessed the lowest corrosion rate in the DIZ but in the OA it was slightly better than the 27WCI, whilst the 27WCINb alloy displayed the highest corrosion rates in both regions, following the same trend as in the full specimen's electrochemical tests.

At pH 3, all WCIs showed the same corrosive behaviour in both regions as with the full specimens and hence, the 38WCI was the optimum alloy followed by 27WCI and 27WCINb.
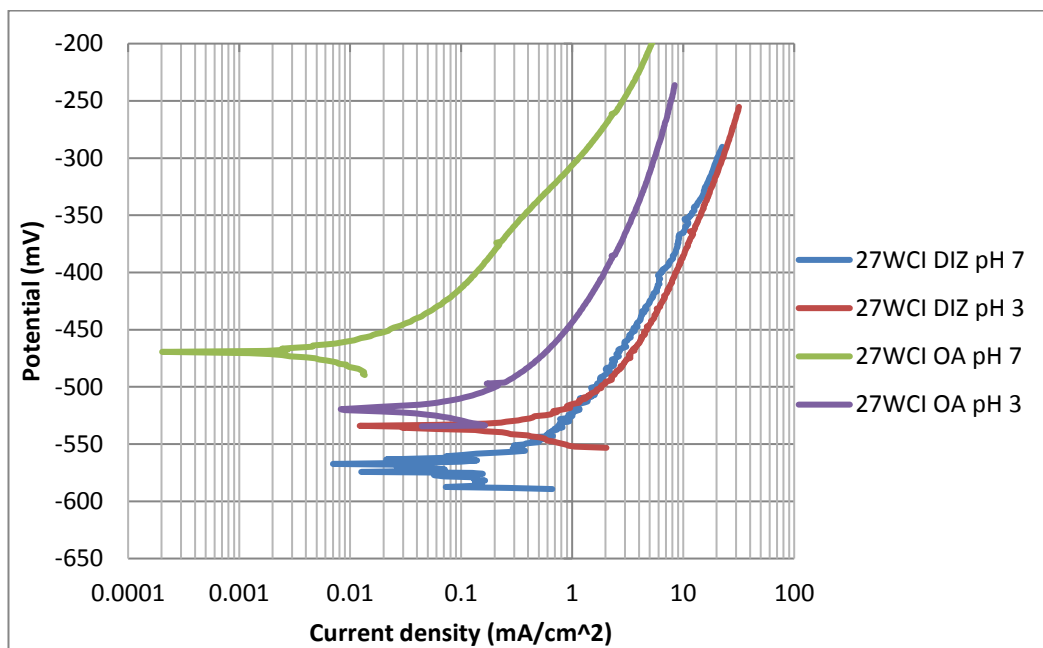
Figure 6.10: Anodic polarization curves for 27WCI DIZ-OA at both pH levels.
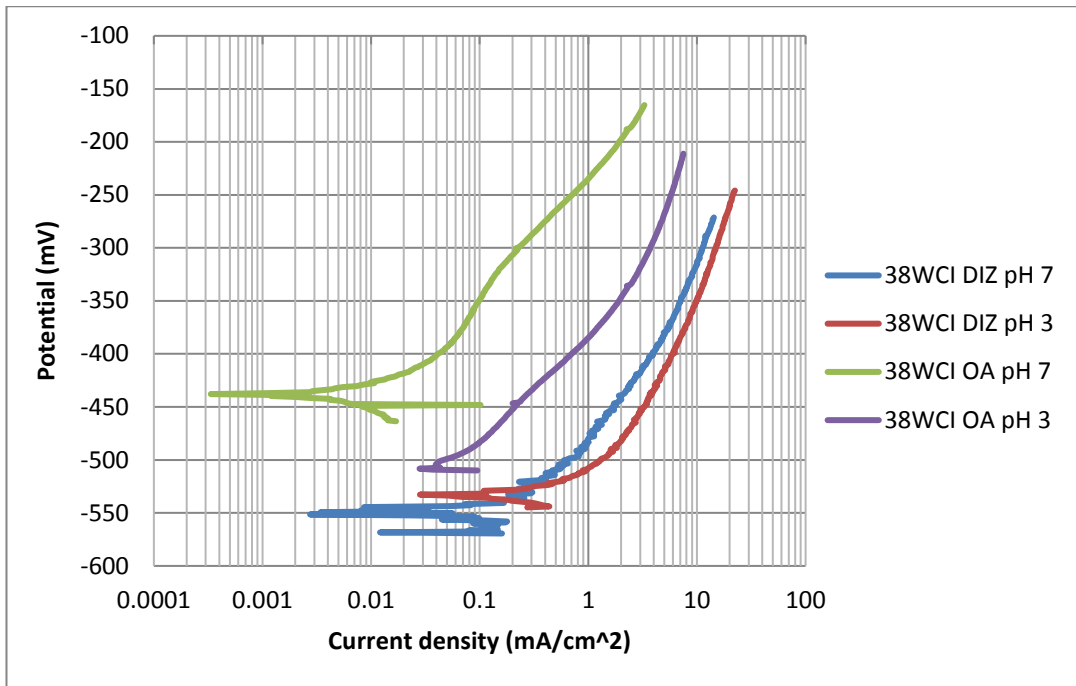
Figure 6.11: Anodic polarization curves for 38WCI DIZ-OA at both pH levels.
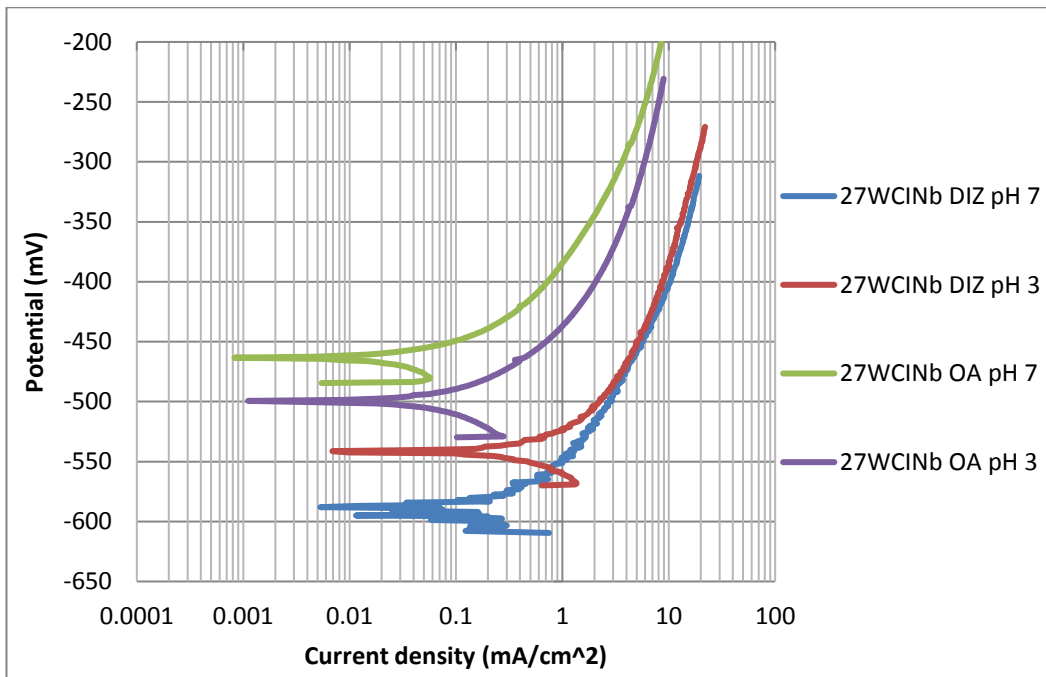
Figure 6.12: Anodic polarization curves for 27WCINb DIZ-OA at both pH levels.

Table 6.6: Anodic polarisation data for materials under study in DIZ-OA regions at both pH levels.

Material	i_{corr} DIZ/OA pH 7 (mA/cm^2)	i_{corr} DIZ/OA pH 3 (mA/cm^2)	Volume loss DIZ/OA pH 7 (mm^3)	Volume loss DIZ/OA pH 3 (mm^3)
27WCI	0.65/0.03	1.7/0.35	0.02/0.04	0.04/0.51
38WCI	0.4/0.023	1.1/0.09	0.01/0.03	0.03/0.13
27WCINb	0.8/0.35	2.0/0.6	0.02/0.31	0.06/0.44

6.3.2.3 Linear polarisation scans

Further consideration about the corrosion rates of materials under study was carried out. Figure 6.13 is a typical representation of linear polarisation curve and corresponds to 27WCI at pH 7, whilst the Figures 6.28-6.32 in the Appendix of this chapter illustrate the linear polarisation curves for all materials in neutral and acidic conditions. The R_p values obtained by 6.13, 6.28-6.32 Figures are presented in Table 6.7 from which the following features were observed:

- Lower Rp values (high corrosion rates) at pH 3 than in neutral conditions.
- Generally similar materials ranking as from the i_{corr} values from the full anodic polarisation curves.
- For a given material/pH value, R_p values are generally similar over the experimental exposure time. This is indicative of a broadly constant corrosion rate with time.
- The 27WCINb alloy showed similar R_p values at both pH levels depicting the same trend with the i_{corr} values obtained from anodic polarisation curves.
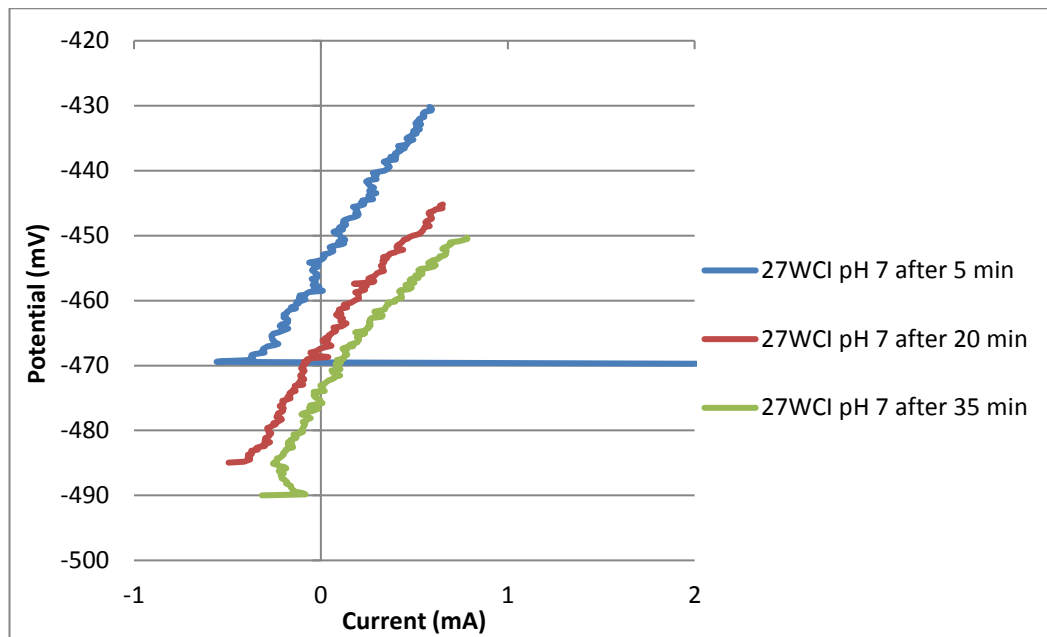
Figure 6.13: Linear polarisation scans for 27WCI at pH 7.

Table 6.7: Linear polarisation data for materials under study at both pH levels.

Material	R_p Ohms after 5 min	R_p Ohms after 20 min	R_p Ohms after 35 min
27WCI pH 7	38	36	37
27WCI pH 3	12	11	9
38WCI pH 7	71	69	60
38WCI pH 3	25	27	18
27WCINb pH 7	23	17	14
27WCINb pH 3	18	14	14

6.4 Post-test analysis

6.4.1 Surface profiling

Figure 6.14 demonstrates the average wear scars for the materials under study in neutral, acidic and CP conditions. In neutral conditions, 27WCI depicted the lowest wear scar depth, followed by UNS S31600 and 38WCI, which exhibited similar

performance. On the other hand, the 27WCINb displayed a significant deep wear scar. In CP conditions, 27WCI, UNS S31600 and 38WCI showed similar wear scar depths, followed by 27WCINb. Finally, in the acidic environment, 27WCI illustrated again the lowest wear scar depth. UNS S31600 was slightly better than the 38WCI, whilst 27WCINb showed a substantially deeper wear scar compared with the rest of the alloys.
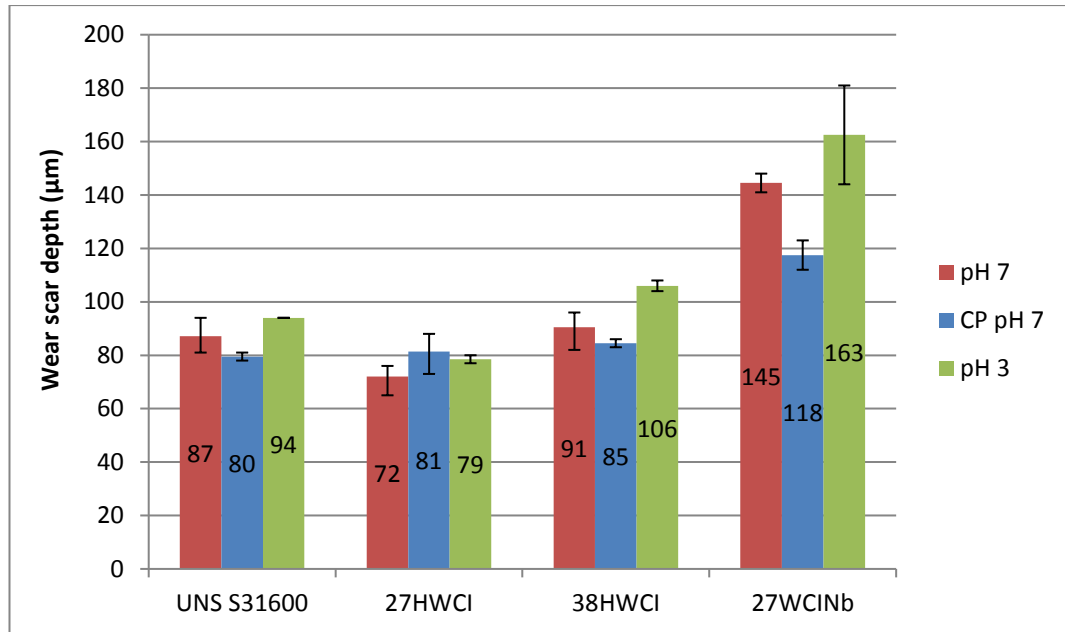
Figure 6.14: Average wear scar depths for materials under study in neutral, acidic and CP conditions.

6.4.2 Volumetric analysis

Figure 6.15 demonstrates the breakdown of the total volume loss (TVL) to volume loss in the DIZ (VL_{DIZ}) and volume loss in the OA (VL_{OA}) for all tested materials in neutral conditions. In the DIZ, 27WCI showed marginally the lowest volume loss, followed by UNS S31600 and 38WCI. The 27WCINb alloy depicted extremely high volume loss which is in line with the deep wear scar resulting in high TVL. In the OA zone, 38WCI illustrated the optimum erosion-corrosion performance, followed by 27WCI. 27WCINb and UNS S31600 exhibited similar volume loss considering the corresponding error bars.
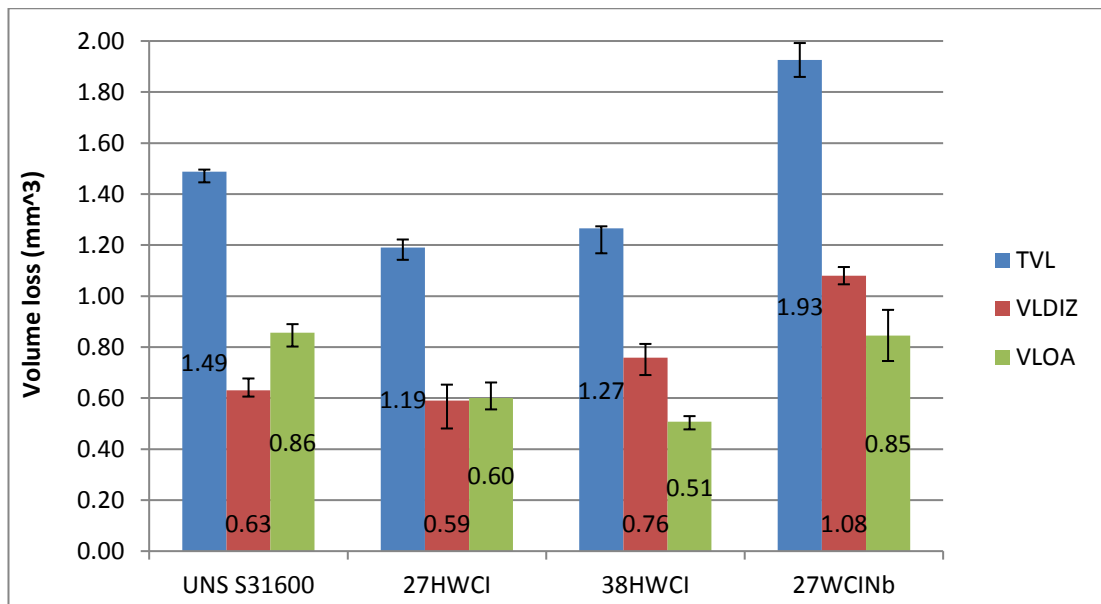
Figure 6.15: Breakdown of average volume loss for materials under study at pH 7.

Figure 6.16 presents the breakdown of volume loss for all materials under acidic conditions. In the DIZ, 27WCI and UNS S31600 depicted similar performance, whilst 38WCI showed higher volume loss but much lower than 27WCINb. In the OA, UNS S31600 displayed the lowest material loss due to superior corrosion resistance, followed by 38WCI. The 27WWCI alloy was the third material in ranking while once again the 27WCINb illustrated the highest abrasion-corrosion rates. An important feature was the higher volume loss in DIZ for all WCIs in the acidic environment compared with neutral pH, whilst that was not the case for UNS S31600.
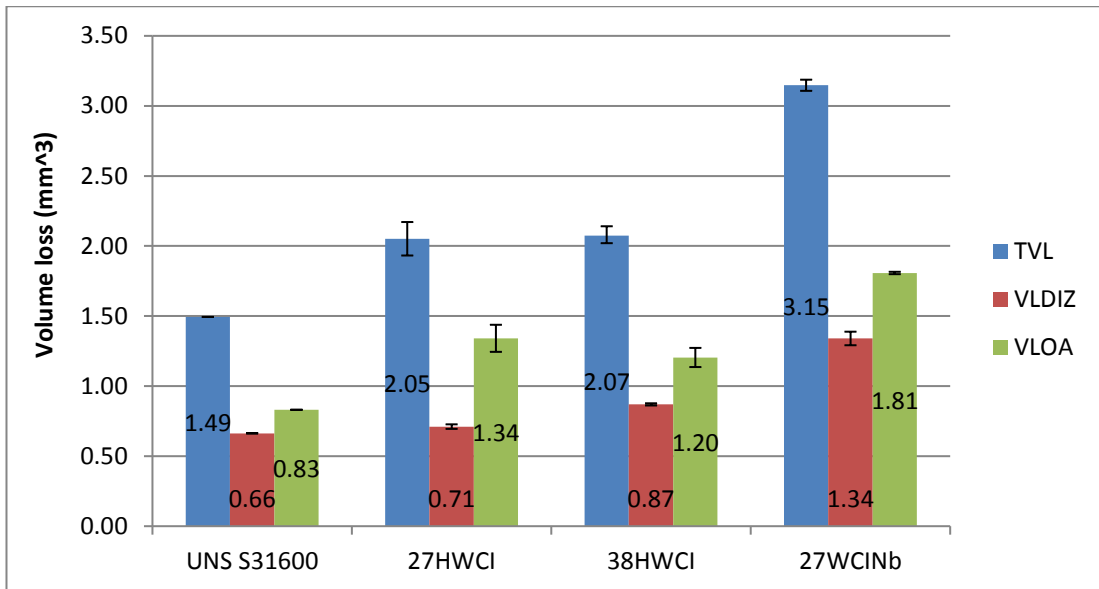
Figure 6.16: Breakdown of average volume loss for materials under study at pH 3.

Figure 6.17 presents the breakdown of volume loss during the CP tests and it is related to the erosion (DIZ) and sliding abrasion (OA) mechanisms. In the DIZ, all materials apart from 27WCINb, which displayed significant material loss, showed equal erosion resistance. In the OA, 27WCI and 38WCI depicted the best sliding abrasion resistance, followed by 27WCINb. As expected, the UNS S31600 performance was poor due to its low hardness.
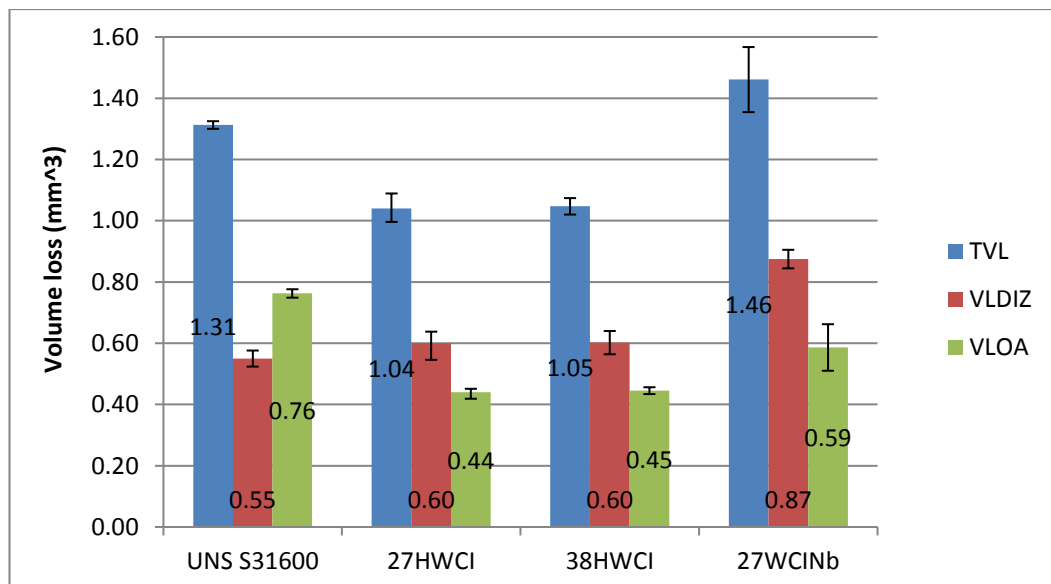
Figure 6.17: Breakdown of volume average loss for materials under study in CP conditions.

6.4.3 Examination of cracks on 38WCI and 27WCINb

As shown in the previous section, the WCIs displayed higher volume loss in the DIZ region during the acidic tests rather than in neutral pH conditions which also was associated with deeper wear scar. The technique that was demonstrated in the previous chapter was carried out for 38WCI and 27WCINb (not for the 27WCI since its cracks were displayed previously). Figures 6.18-6.23 illustrate the cross sectioned of both DIZ/OA regions for materials under study in both environments. The importance of this technique in cracks investigation is portrayed in Figure 6.24 in which the top surface of 27WCINb at pH 7 is illustrated; it was evident that due to very rough surface, no conclusions can be made in terms of crack initiation.

The evaluation of Figures 6.18-6.23 concludes the following:

- Both WCIs showed cracks in the DIZ and spalling on the carbides (Cr/Nb) in both environments.
- The enhanced cracks resulted in increased VL_{DIZ} for a given material/environment. Thus, the more cracks, the higher VL_{DIZ}.
- Few cracks (but less than in the DIZ) in the OA even at pH 7.
- The fact that all WCIs displayed more cracks in the acidic environment was the result of increased corrosion and synergy.
- 38WCI exhibited less cracks than 27WCINb due to the smaller carbides size.
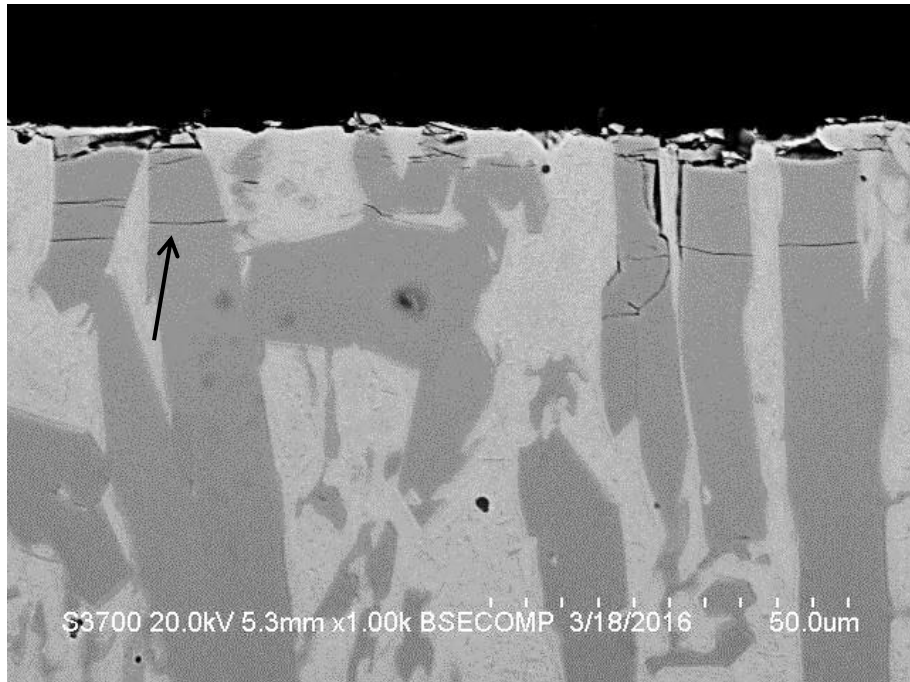
Figure 6.18: Cracks observed in the DIZ of 38WCI at pH 7 [etched].
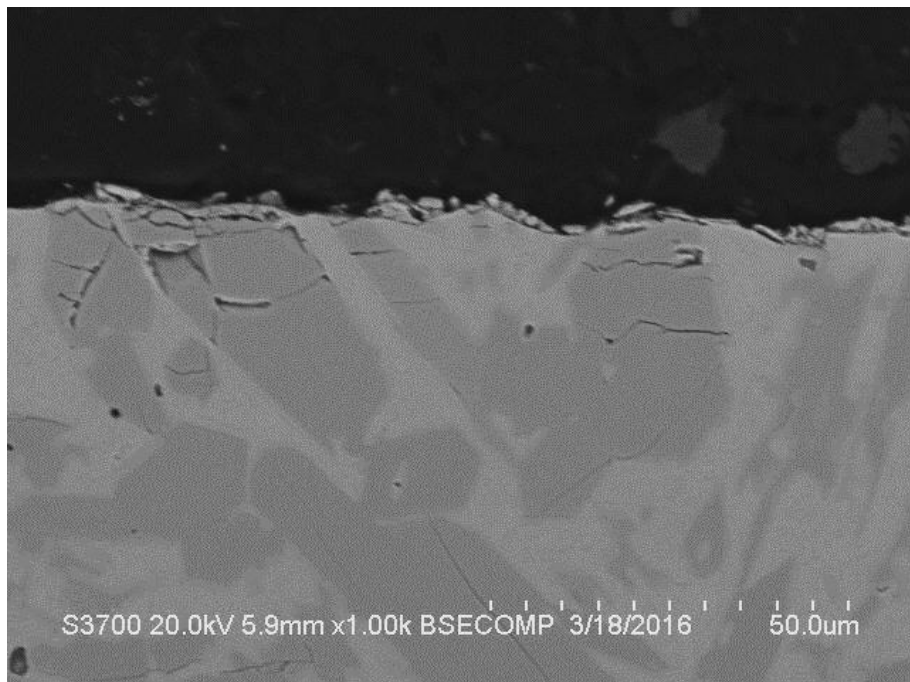
Figure 6.19: Cracks observed in the DIZ of 38WCI at pH 3 [etched].
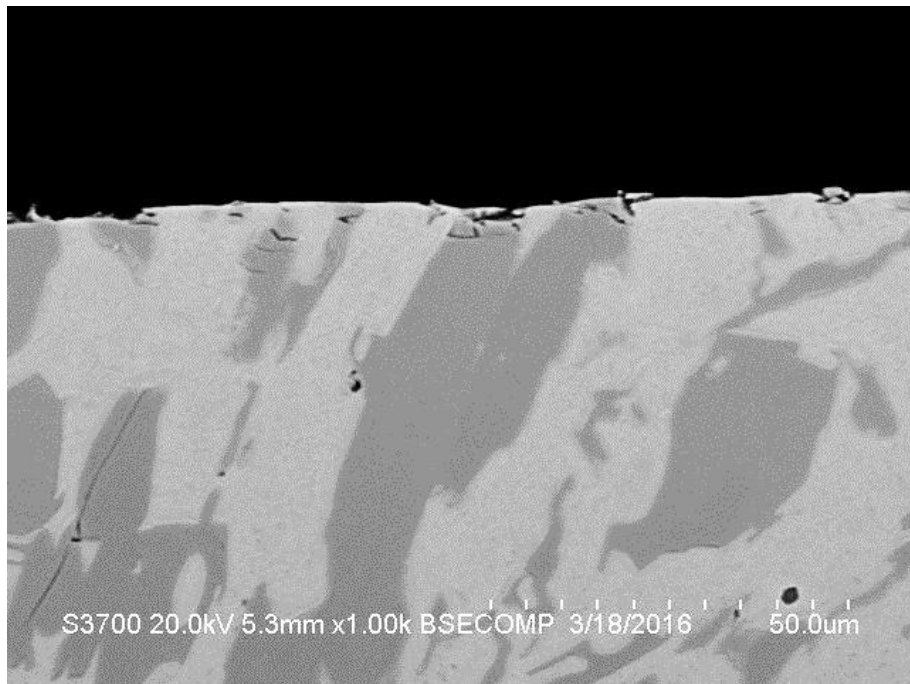
Figure 6.20: Cracks observed in the OA of 38WCI at pH 7 [etched].
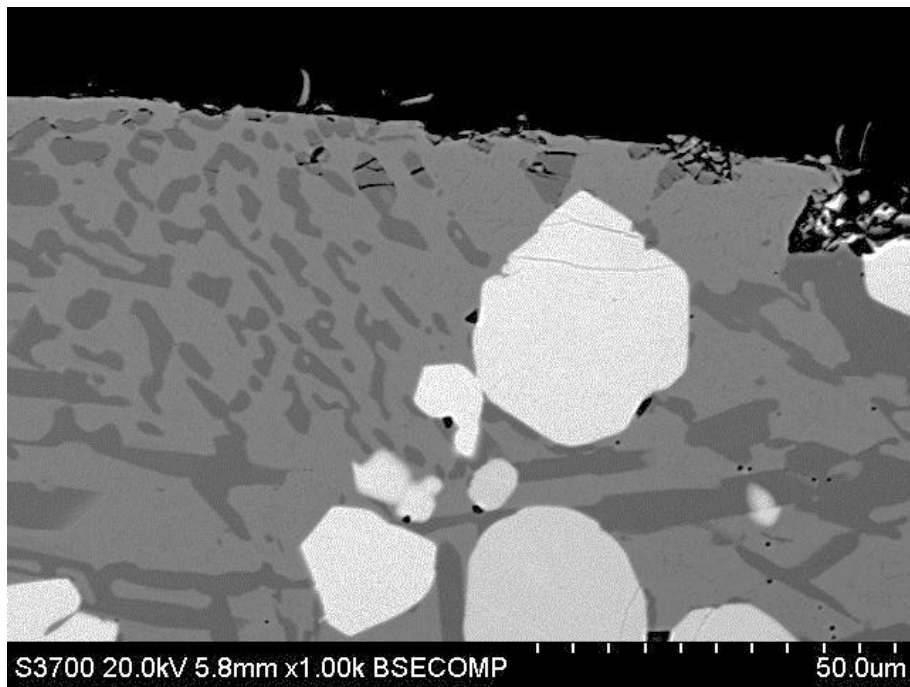
Figure 6.21: Cracks observed in the DIZ of 27WCINb at pH 7 [etched].
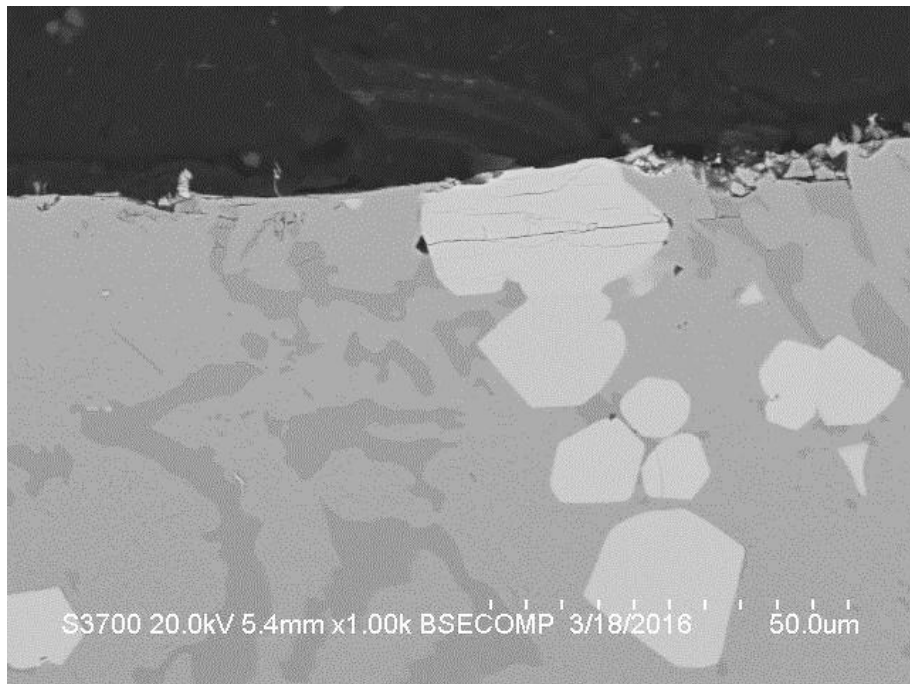
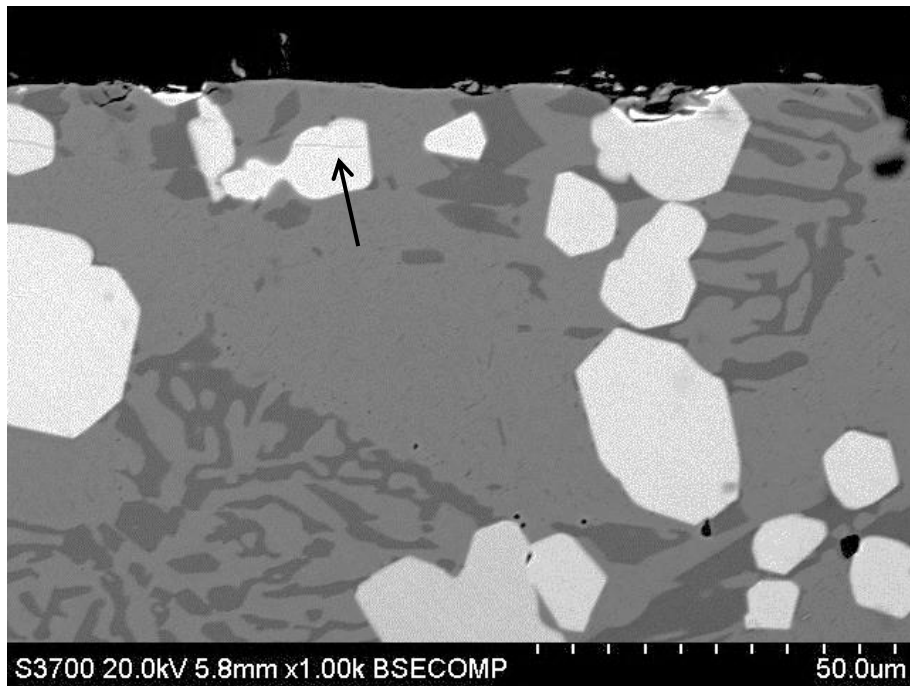Figure 6.22: Cracks observed in the DIZ of 27WCINb at pH 3 [etched].

Figure 6.23: Few cracks observed in the OA of 27WCINb at pH 7 [etched].
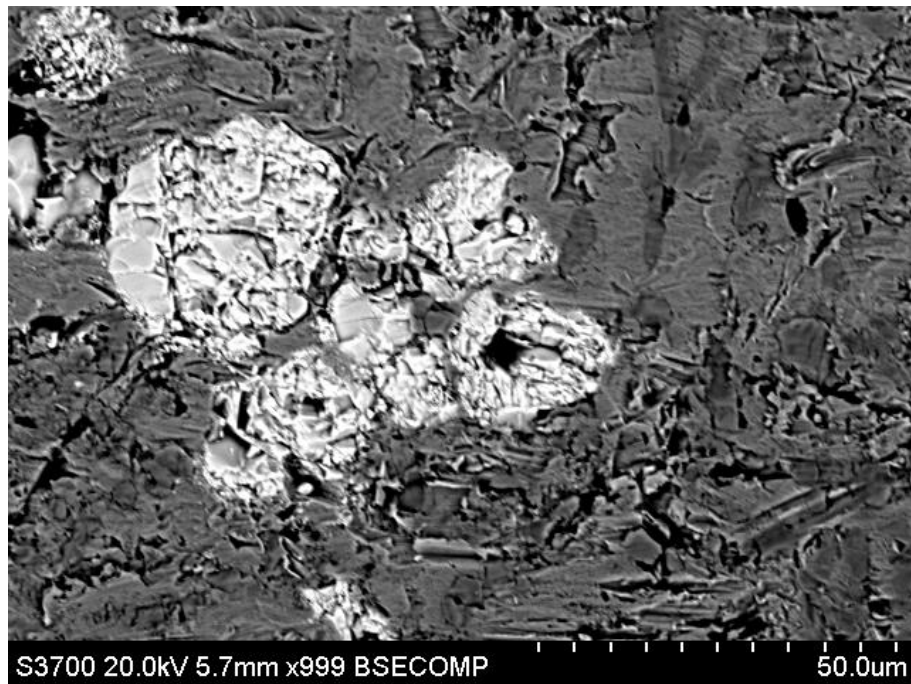
Figure 6.24: Top surface of 27WCINb at pH 7.

6.4.5 Summary of results

Table 6.8 shows the proportion of each degradation mechanism for materials under study at both pH values. In neutral conditions, the mechanical damage was dominant for all materials, especially for 27WCI and 38WCI. The 27WCINb exhibited proportionally high volume loss due to corrosion (23%).

On the other hand, in the acidic environment, only 50% of the total volume loss of all alloys was due to mechanical damage. In terms of the remaining 50%, 27WCI showed similar proportions of corrosion and synergy, whilst 38WCI and 27WCINb showed higher proportions of synergy than of corrosion.

Table 6.8: Proportion of degradation mechanisms at both pH levels.

Material	Erosion + sliding abrasion pH 7/ pH 3 (%)	Corrosion pH 7/pH 3 (%)	Synergy pH 7/pH 3 (%)
UNS S31600	88/88	1/1	11/11
27WCI	87/50	13/30	0/20
38WCI	83/50	6/7	11/43
27WCINb	76/47	23/16	1/37

Figures 6.25-6.26 and Tables 6.9-6.10 demonstrate the volume loss of each mechanism in the DIZ and OA for tested materials at both pH values, where the terms CP, C and S refer to Cathodic Protection, Corrosion and Synergy respectively. It should be noted that the synergy in both DIZ/OA zones was calculated via the subtraction of CP and corrosion values from the total volume loss for the individual region.
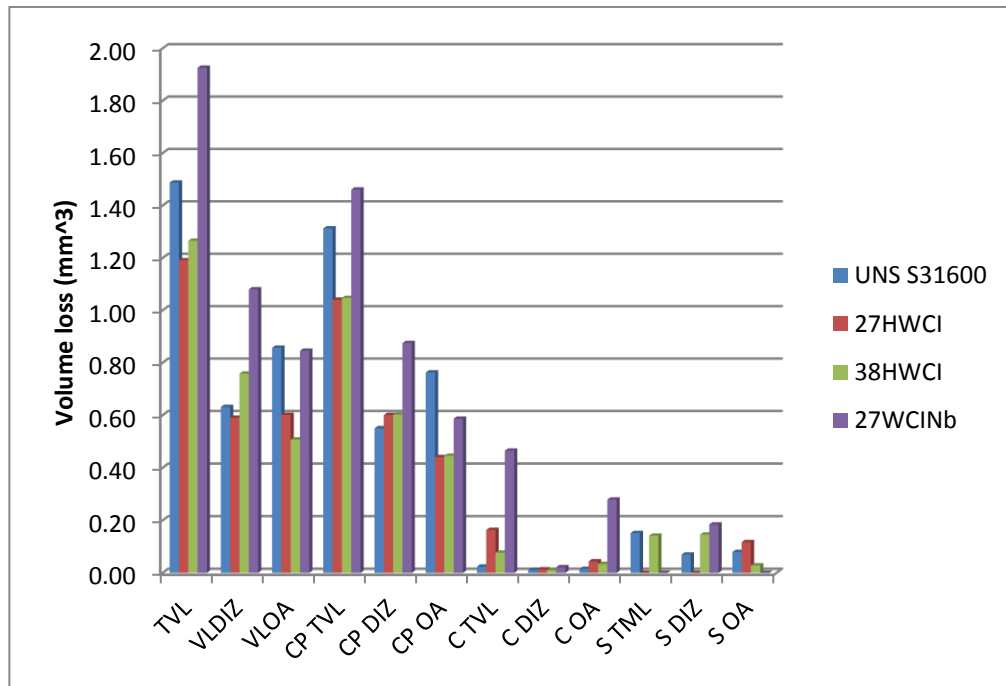
Figure 6.25: Summary of average volume loss breakdown of materials at pH 7.

Table 6.9: Summary of average volume loss at pH 7 (mm^3).

Material	TVL	VL DIZ	VL OA	CP TVL	CP DIZ	CP OA	C TVL	C DIZ	C OA	S TVL	S DIZ	S OA
UNS S31600	1.49	0.63	0.86	1.31	0.55	0.76	0.02	-	-	0.15	-	-
27WCI	1.19	0.59	0.60	1.04	0.60	0.44	0.16	0.01	0.04	0.00	0.02	0.12
38WCI	1.27	0.76	0.51	1.05	0.60	0.45	0.08	0.01	0.03	0.14	0.15	0.03
27WCINb	1.93	1.08	0.85	1.46	0.87	0.59	0.46	0.02	0.28	0.00	0.18	0.02
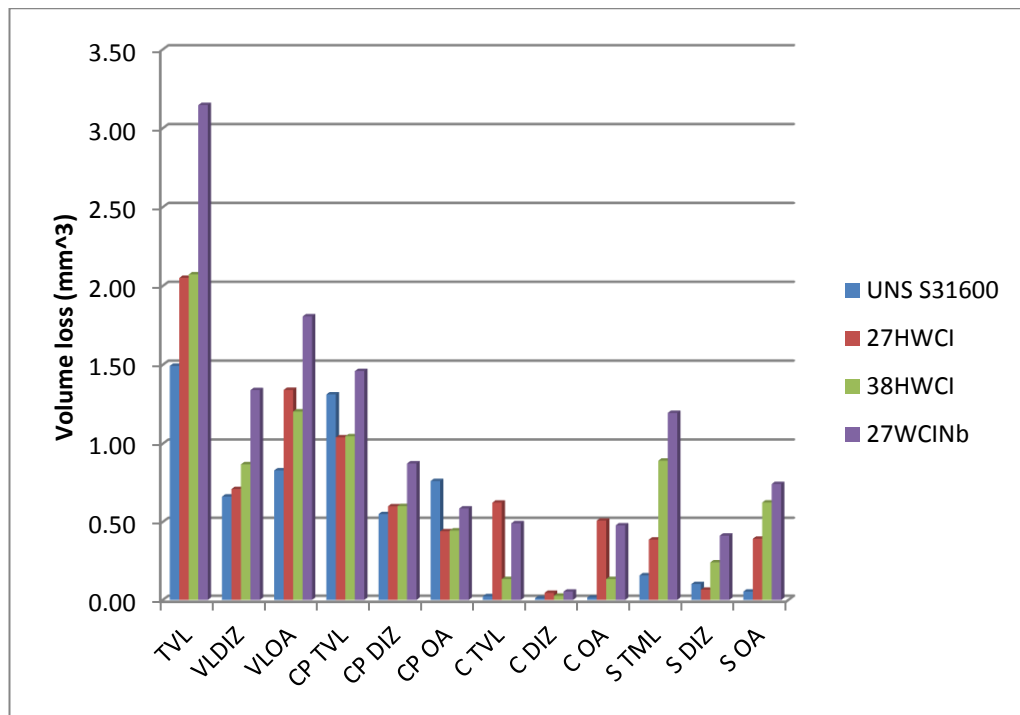
Figure 6.26: Summary of average volume loss breakdown of materials at pH 3.

Table 6.10: Summary of average volume loss at pH 3 (mm^3).

Material	TVL	VL DIZ	VL OA	CP TVL	CP DIZ	CP OA	C TVL	C DIZ	C OA	S TVL	S DIZ	S OA
UNS S31600	1.49	0.63	0.86	1.31	0.55	0.76	0.02	-	-	0.15	-	-
27WCI	2.05	0.71	1.34	1.04	0.60	0.44	0.62	0.05	0.51	0.39	0.07	0.39
38WCI	2.07	0.87	1.20	1.05	0.60	0.45	0.13	0.03	0.13	0.89	0.24	0.63
27WCINb	3.15	1.34	1.81	1.46	0.87	0.59	0.49	0.05	0.48	1.20	0.41	0.74

6.5 Discussion

6.5.1 Erosion-corrosion in neutral conditions

For ease of understanding of the erosion-corrosion phenomena the discussion will report on each material individually. It is worth mentioning that all findings for each material obtained by SLEC tests at both pH values are in good agreement with the field service [6.2].

27WCI: Since more advanced WCIs were compared with the basic 27WCI, more detailed investigation than the one presented in the previous chapter can be obtained. As presented in Results section, 27WCI showed superior erosion-corrosion performance compared to the rest of the materials. It was observed that the microstructure of this alloy lacks primary M_7C_3 and hence, the eutectic carbides provide improved erosion resistance, a trend that has been reported in past studies [6.3–6.5]. In particular, Llewellyn et al. presented the erosion performance of two different versions of 27% Cr WCI (one with primary Cr carbides and the other with absence of primary Cr carbides – this alloy is the 27WCI tested in this project) in a low angle Coriolis erosion tester [6.3]. The results displayed in their work showed superiority (2.5 times) of the alloy with transformed hypoeutectic microstructure in which no primary M_7C_3 were detected [6.3]. Also, the performance of this particular 27WCI was superior over a hypereutectic and just inferior to the hypereutectic with the highest carbide volume fraction (CVF) [6.3].

The main reason for the very good erosion-corrosion behaviour of 27WCI was its performance in the DIZ. Despite the brittle nature of this alloy, the volume loss in the DIZ was slightly lower than UNS S31600 indicating good balance between the brittleness and ductility which is associated with the eutectic carbides and CVF level. This notion was confirmed by the minimum cracks of 27WCI in the wear scar depth, compared with the rest of the WCIs, as it has been displayed in the previous chapter. In the OA, it was inferior only to 38WCI as a result of the higher corrosion resistance of the latter alloy.

In terms of pure mechanical damage (CP tests), the 27WCI showed equal performance in both DIZ and OA regions with the 38WCI indicating that the there are no benefits in erosion/abrasion resistance in cases of higher CVF when primary carbides are present (38WCI alloy). In an unpublished work, Walker reported that in Coriolis erosion tester, the size and shape of sand particles is a crucial factor for materials performance [6.6]. In his study, the 27WCI showed similar performance with a hypereutectic 35Cr iron in Coriolis tester (in fresh water) under 0.35 medium coarse sand tests, while in tests with finer sand particles the hypereutectic alloy was 40%

better than the standard 27WCI alloy. Thus, the results in the current Ph.D. thesis support the findings in Walker's work.

The corrosion resistance of 27WCI alloy was superior only over 27WCINb. An interesting feature was the increased corrosion rates of 27WCI in these testing conditions compared with the corrosion rates in the previous chapter (0.11 as opposed to 0.088 at pH 7 and 0.42 as opposed to 0.31 at pH 3/all numbers in mA/cm^2). Thus, the higher sand concentration (0.75 as opposed to 0.5 g/l) led to higher erosive and corrosive rates in the current conditions. Consecutively, it can be reasonably concluded that there is a linear relationship between corrosion resistance and erosion resistance in alloys with relatively moderate corrosion resistance (i.e martensitic structured). Finally, no synergy was observed in neutral conditions, as has been reported in the previous chapter.

38WCI: The overall erosion-corrosion performance was slightly lower than that of 27WCI. According to the volumetric analysis, 60% of the total volume was in the DIZ indicating vulnerability to perpendicular erosion and synergy. Also, the amount of cracks on Cr carbides in the DIZ validated the volume loss in this hydrodynamic area. Thus, the higher CVF resulted in higher volume loss in normal incidence, finding that has been reported in a past studies [6.7–6.9]. Moreover, apart from the high CVF, the vulnerability of Cr carbides to cracking was due to the fact that 15% (out of 37%) were coarse primary Cr carbides, as shown in Figure 6.18.

On the other hand, the performance of 38WCI in the OA zone was substantially superior over the rest of the materials since all mechanisms of degradation possessed very low rates. In comparison with 27WCI, the corrosion resistance of 38WCI was crucial factor for its better performance, despite the fact cracks were observed in the OA (Figure 6.20). It is believed that the significant cracks in this region are associated with the 500 μm mean size and the coarse shape of the silica sand. In past studies (including lab and field tests) the hypereutectic WCIs were superior over eutectic at low angle of attack under tests with 300 μm size sand, whilst the shape was either round or coarse [6.10, 6.11]. However, Chung et al. showed that in erosion-corrosion tests with "near rounded" sand and average 600 μm sand in tap water, the hypereutectic

WCIs were inferior to eutectic ones indicating that the size is probably more crucial factor than the shape for WCIs erosion-corrosion performance [6.12].

From pure erosion point of view (CP tests), a noticeable feature was that the 38WCI showed equal volume loss with 27WCI in the DIZ region indicating the contribution of corrosion and synergy into the volume loss in this zone (Table 6.9).

In terms of corrosion, 38WCI was superior over the rest of WCIs, particularly in the OA, due to its higher Cr content dissolved in the matrix. An important feature was that 38WCI exhibited 3 times higher corrosion rates than UNS S31600 despite the fact that the Cr in the matrix is slightly higher than the nominal Cr in UNS S31600 (20% against 17%). This is an indication that the austenitic matrix is more corrosion resistant than the martensitic matrix due to the presence of Ni and Mo elements, regardless the Cr level.

27WCINb: The niobium WCI was subject to much interest due to the unique microstructure – NbC+27WCI. The erosion-corrosion experiments displayed significantly high volume loss compared to the rest of the WCIs and even to UNS S31600. As shown in Figure 6.21, the NbC are fractured due to high impact loads under the perpendicular jet and in combination with their relatively large size (compared with the eutectic Cr carbides), resulted in less support to the matrix and eventually, higher volume loss in the DIZ.

Furthermore, even in the OA region the material loss was substantially high compared to the rest of the WCIs due to high corrosion rates and few cracks (Figure 6.23). An interesting observation shown in Figure 6.23 was the fact that cracks were found on NbC (but less compared with the DIZ) but not on the Cr carbides. The latter finding is an indication about the brittleness of NbC which under the current conditions it was detrimental for the overall material's performance. It should be noted that cracking of NbC was not evident in past studies in either high or low angle of attack [6.1, 6.13–6.15]. However, the white cast irons with NbC that have been tested in past studies [6.1, 6.13–6.15] possessed lower CVF level (max. around 10%) and smaller particle size of 27WCINb, whilst the preferable matrix for the most studies was austenitic [6.1,

6.13, 6.15]. Nevertheless, in the study of Lu et al. [6.15] the martensitic matrix provided optimum abrasion resistance,

Apart from SLEC tests, even in CP conditions the 27WCINb possessed moderate erosion/abrasion performance. This is associated with the angular sand particles used in the current work which caused cracks on relatively large NbC in conjunction with their high hardness [6.2]. On the other hand, it has been reported that the round NbC increase the abrasion resistance (since NbC possess 2000-2200 HV hardness) and maintain or even increase the toughness since the round carbides absorb less impact loads than the coarse [6.16]. Thus, it can be concluded that the CVF of NbC, their size and the testing conditions (i.e angle of attack, type/size/shape/ of sand particles) are important factors that affect the erosion-corrosion performance of the WCIs containing NbC.

The electrochemical tests on 27WCINb showed 5 times higher corrosion rates than the 27WCI, despite the fact that the Cr in the matrix was practically the same. On the other hand, the static anodic polarisation scans displayed similar corrosion resistance between 27WCINb and 27WCI indicating that in erosive-corrosive conditions the corrosion behaviour of 27WCINb is affected negatively by the poor erosion resistance. This is directly linked with the observation about the corrosion behaviour of 27WCI in different sand loadings (comparison of corrosion rates in chapter 5-6) and hence, the relationship between the erosion resistance and corrosion resistance on martensitic structured alloys is validated. It is worth mentioned that there is no information from the literature regarding electrochemical investigation for WCIs with NbC. Moreover, the synergy of 27WCINb were negligible, as demonstrated in Table 6.9.

6.5.2 Erosion-corrosion in acidic conditions

All WCIs experienced higher volume loss than UNS S31600 largely in account of the higher corrosion rates of their martensitic structure compared to austenitic UNS S31600.

27WCI: In acidic conditions, the 27WCI alloy displayed significant high volume loss compared with its performance at pH 7, but it was equal to 38WCI in this acidic

environment. The deterioration due to electrochemical reactions was almost 4 times more severe than in neutral environment and simultaneously, the synergistic effects were enhanced. It is worth noting that the corrosion and the synergy were the 50% of the TVL.

According to the volumetric analysis, the volume loss in the OA was 65% of the TVL. Also, in both DIZ/OA, the synergy was increased due to enhanced corrosion rates in these regions trend that was observed also for 38WCI and 27WCINb. An indication of the poor corrosion performance of 27WCI at pH 3 was that in the static corrosion tests, the current density was 15 times higher than in neutral pH. Thus, it can be concluded that the martensitic matrix with 15% Cr is unsuitable at this level of pH and chlorides even in static water.

38WCI: The hypereutectic alloy exhibited equal volume loss to 27WCI under acidic conditions despite its better corrosion resistance. More specifically, the corrosion rates of 38WCI were just 2 times higher than in neutral pH but almost 5 times lower than the corresponding of 27WCI. Thus, the additional 5% of Cr dissolved in the matrix compared to 27WCI was beneficial improving the significantly the corrosion resistance in acidic tests. An important feature was that the corrosion rates in dynamic conditions were 7.5 times higher than in static conditions (the corresponding value was 15 times for 27WCI).

However, the synergy on 38WCI was more than 2 times higher than 27WCI (in both DIZ and OA) contributing to the great overall volume loss and masking its enhanced corrosion resistance compared with 27WCI. One possible explanation for the high synergy of 38WCI is that since enhanced corrosion rates were present (pH 3 compared to pH 7), the synergy can be increased in a more complex microstructure which includes metallic matrix, eutectic and primary Cr carbides whereas, in a less complex microstructure (27WCI) this effect is less prominent.

In terms of comparison between the high Cr matrix of 38WCI and the UNS S31600, it should be noted the austenitic UNS S31600 alloy exhibited 6 times lower i_{corr} than 38WCI indicating that the less corrosion resistant alloy (38WCI-martenitic matrix) is attacked severely at low pH compared to pH 7.

27WCINb: In acidic conditions, the 27WCINb alloy displayed again the highest volume loss and the difference with the rest of the materials was greater than at pH 7 as a result of the significant enhanced erosion due to corrosion (synergy). Despite the fact that the corrosion rates in acidic conditions were similar as at pH 7 (three replicates were conducted for anodic polarisations at both pH levels), the i_{corr} values on the individual regions (DIZ/OA) were higher at pH 3 than at pH 7. This can be potentially interpreted as follows:

- In neutral conditions, the sum of volume loss due to corrosion in both DIZ/OA (C_{DIZ}/C_{OA}) was less than the C_{TVL} of the whole specimen, trend that was noticed on 27WCI and 38WCI alloys too. This indicates that between DIZ and OA zones there are galvanic effects since they possess different E_{corr}. On the other hand, for all tested WCIs in acidic conditions, the sum of both C_{DIZ}/C_{OA} was very similar with the C_{TVL} and it can be reasonably assumed that the severe corrosive attack in acidic water masked and basically "substituted" the galvanic effects between DIZ/OA and hence the corrosion rates locally in these regions were increased from pH 7 to pH 3.

Thus, the increase of corrosion rates in the DIZ/OA zones individually was the reason for the increased synergy on 27WCINb alloy in both regions. As shown in Figure 6.27, the increased synergy (compared with the corresponding at pH 7) caused cracks on NbC and even on Cr carbides in the OA contributing to high volume loss.

Compared to the 27WCI and 38WCI, the 27WCINb was the only alloy that depicted similar overall (on the whole specimen) corrosion rates at both pH levels, despite that in acidic medium was again the worst material since its corrosion performance was deteriorated by the poor erosion/abrasion resistance (as mentioned previously). This unique corrosion behaviour of 27WCINb in acids is an evident that the NbC provide support to the metallic matrix which can withstand the corrosive attack better than in case of 27WCI whereas the metallic matrix is supported only from Cr carbides (same Cr level in the matrix for both alloys). Also, the anodic scans in static conditions displayed only 2.5 higher corrosion rates than at pH 7, whilst the corresponding number for 27WCI and 38WCI was 15 and 7.5 respectively. The latter finding makes the Nb element promising for developing a WCI with controlled NbC volume fraction

area which could be used in chemical industry in cases that erosion/abrasion resistance is required.
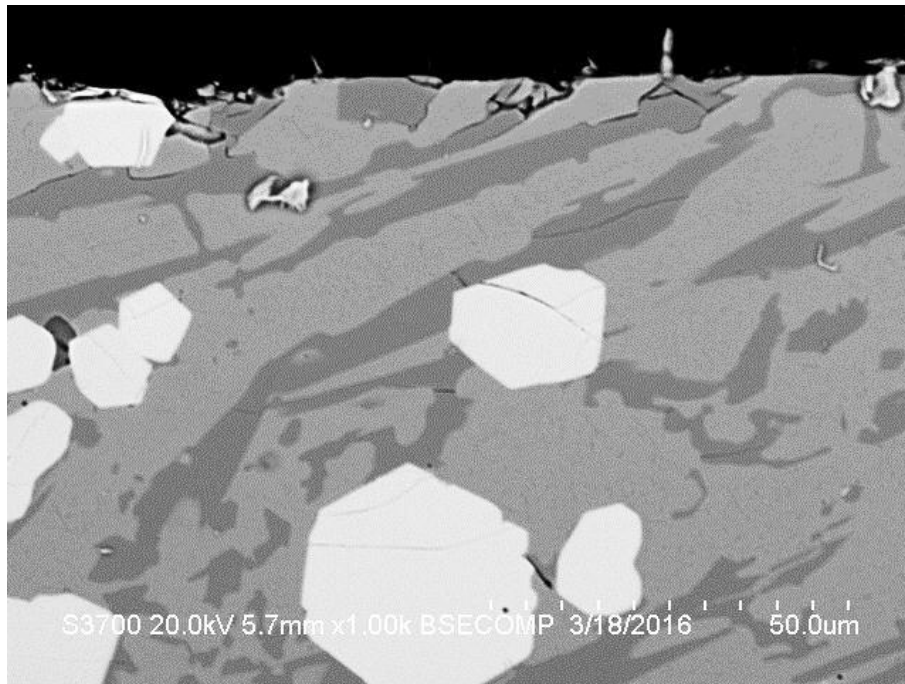
Figure 6.27: Cracks on NbC and Cr carbides of 27WCINb in the OA zone at pH 3 [etched].

6.6 Conclusions

1. In corrosive wear conditions, it was observed that the 38WCI alloy was no better (overall) than the competitive material 27WCI at both pH levels. However, the detailed assessment demonstrated that, at both pH levels, the volume loss in the DIZ was higher for 38WCI but in the OA the volume loss was lower than 27WCI. This implies that 38WCI is superior in sliding abrasion-corrosion to 27WCI but worse under direct impingement.

2. However, upon applications on CP, no differences were noticed between the 2WCI and 38WCI alloys in both DIZ and OA. This implies the relative performances of these alloys in different hydrodynamic regions are dependent on the severity of the corrosive environment.

3. The primary Cr carbides and higher CVF are detrimental on erosion-corrosion performance.

4. The 27WCINb exhibited the worse overall erosion-corrosion performance at both pH levels. At pH 7 this relatively poor behaviour was seen in both DIZ-OA due to severe cracks of NbC, in the DIZ particularly. At pH 3, cracks were observed in both DIZ/OA regions.

5. In acidic conditions, all WCIs displayed higher volume loss than UNS S31600 due to their poor corrosion resistance.

6. The synergy was a crucial factor for materials performance for a given environment.

7. Comparing the corrosion performance of 27WCI and 27WCINb at pH 7, it can be concluded that the corrosion performance is greatly affected by the erosion resistance.

8. In acidic conditions, the increase of overall corrosion rate (full specimen) was negligible on 27WCINb, whilst a substantial increase was noticed in cases of 27WCI and 38WCI.

9. The corrosion measurements on segmented samples contributed to an important in-depth erosion-corrosion investigation that evaluates completely the performance of alloys with complex microstructures.

6.7 References

[6.1] R.J. Chung, X. Tang, D.Y. Li, B. Hinckley, K. Dolman, Microstructure refinement of hypereutectic high Cr cast irons using hard carbide-forming elements for improved wear resistance, Wear. 301 (2013) 695–706.

[6.2] An internal communication with Edward Humphries, Director of R&D, Weir Minerals Sydney, Australia, (2016).

[6.3] R.J. Llewellyn, S.K. Yick, K.F. Dolman, Scouring erosion resistance of metallic materials used in slurry pump service, Wear. 256 (2004) 592–599.

[6.4] Y.P. Wang, D.Y. Li, L. Parent, H. Tian, Improving the wear resistance of white cast iron using a new concept - High-entropy microstructure, Wear. 271 (2011) 1623–1628.

[6.5]   Y.P. Wang, D.Y. Li, L. Parent, H. Tian, Performances of hybrid high-entropy high-Cr cast irons during sliding wear and air-jet solid-particle erosion, Wear. 301 (2013) 390–397.

[6.6]   Walker, Influence of particle size and shape on slurry erosion wear of different white irons, unpublished work.

[6.7]   M.A. Al-Bukhaiti, S.M. Ahmed, F.M.F. Badran, K.M. Emara, Effect of impingement angle on slurry erosion behaviour and mechanisms of 1017 steel and high-chromium white cast iron, Wear. 262 (2007) 1187–1198.

[6.8]   S.G. Sapate, A. V. Ramarao, Erosive wear behaviour of weld hardfacing high chromium cast irons: Effect of erodent particles, Tribol. Int. 39 (2006) 206–212.

[6.9]   S.G. Sapate, A. V. Rama Rao, Effect of carbide volume fraction on erosive wear behaviour of hardfacing cast irons, Wear. 256 (2004) 774–786.

[6.10] C.I. Walker, P. Robbie, Comparison of some laboratory wear tests and field wear in slurry pumps, Wear. 302 (2013) 1026–1034.

[6.11] Y. Xie, J. (Jimmy) Jiang, K.Y. Tufa, S. Yick, Wear resistance of materials used for slurry transport, Wear. 332-333 (2015) 1–7.

[6.12] R.J. Chung, X. Tang, D.Y. Li, B. Hinckley, K. Dolman, Abnormal erosion-slurry velocity relationship of high chromium cast iron with high carbon concentrations, Wear. 271 (2011) 1454–1461.

[6.13] M. Filipović, Ž. Kamberović, M. Korać, Z. Andić, Wear resistance and dynamic fracture toughness of hypoeutectic high-chromium white cast iron alloyed with niobium and vanadium, Mater. Tehnol. 48 (2014) 343–348.

[6.14] M. Fiset, K. Peev, M. Radulovic, The influence of niobium on fracture toughness and abrasion resistance in high-chromium white cast irons, J. Mater. Sci. Lett. 12 (1993) 615–617.

[6.15] J. Lu, H. Lin, H. Chen, Effect of niobium on wear resistance of 15 % Cr white cast iron, Wear. 166 (1993) 197–201.

[6.16] R. Chung, Comprehensive study of the abrasive wear and slurry erosion behaviour of an expanded system of high chromium cast iron and microstructural modification for enhanced wear resistance, Ph.D. Thesis, University of Alberta, Canada (2011).

6.8 Appendix
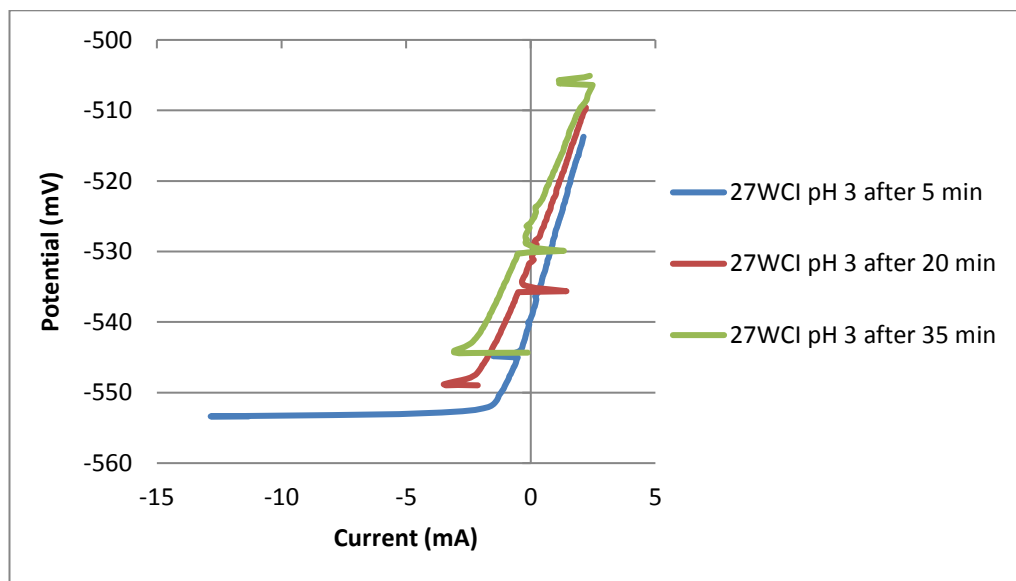
Figure 6.28: Linear polarisation scans for 27WCI at pH 4.
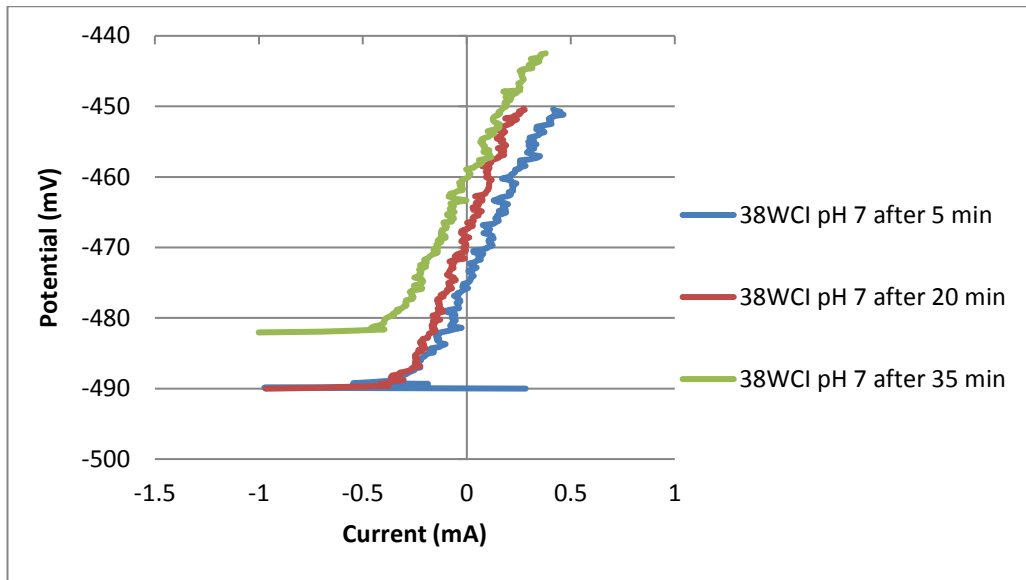
Figure 6.29: Linear polarisation scans for 38WCI at pH 7.
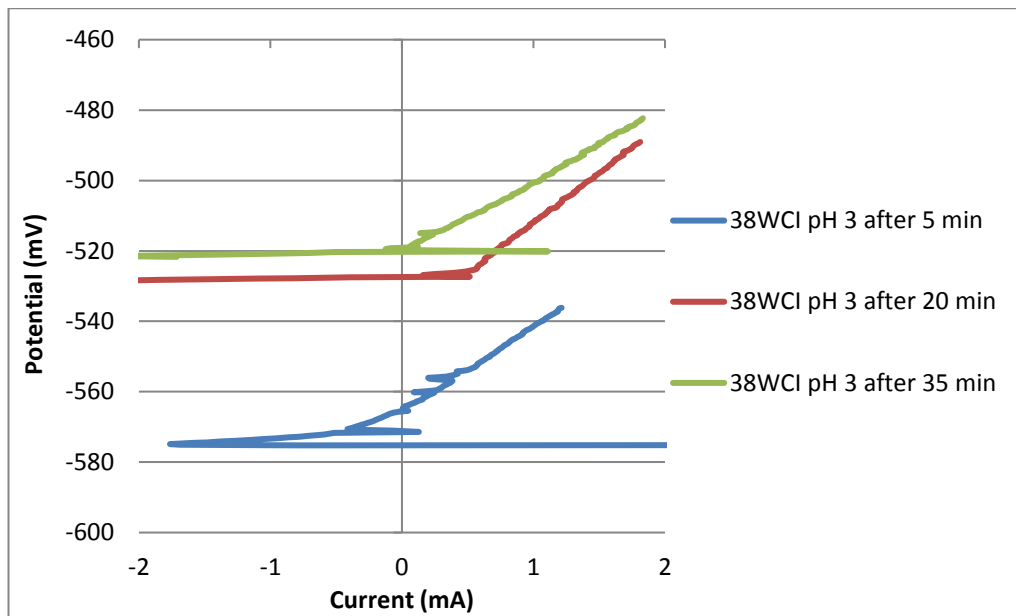
Figure 6.30: Linear polarisation scans for 38WCI at pH 3.
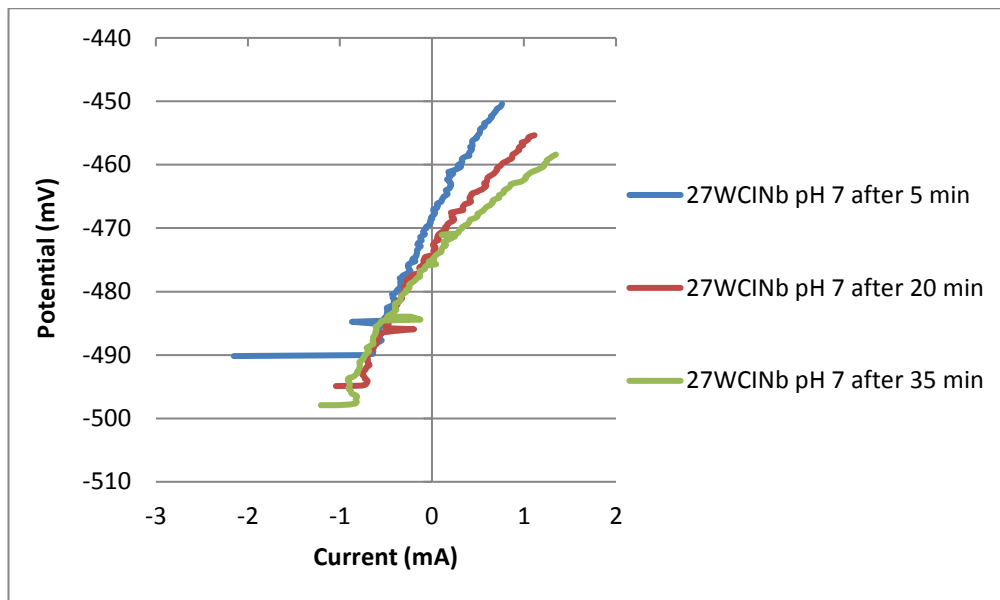
Figure 6.31: Linear polarisation scans for 27WCINb at pH 7.
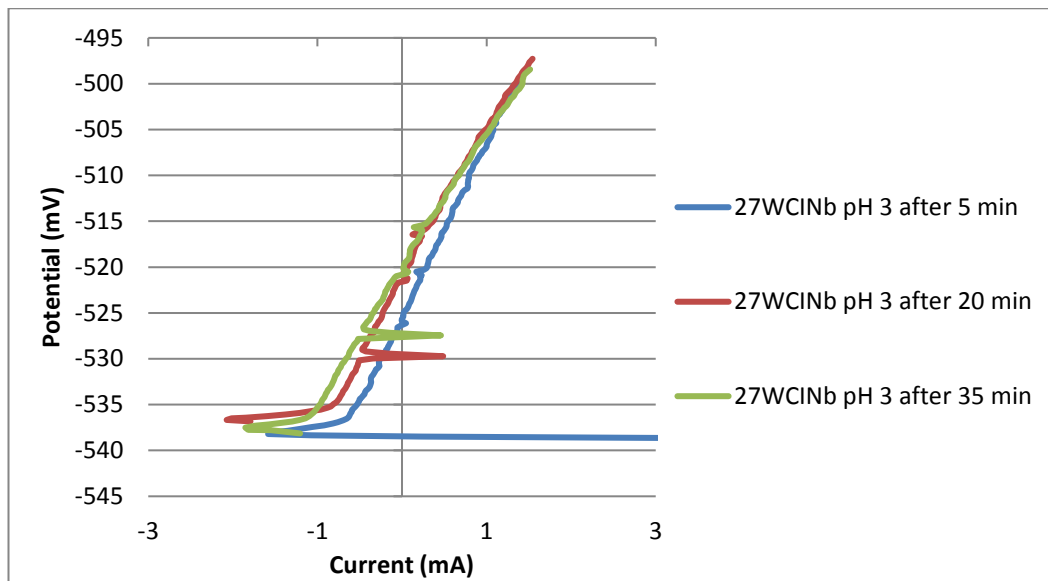
Figure 6.32: Linear polarisation scans for 27WCINb at pH 3.

Chapter 7

Erosion-corrosion in neutral and strong acids

7.1 Introduction

As a continuation of the erosion-corrosion investigation at low pH, erosion-corrosion experiments in neutral and strong acidic environment were conducted. For instance, the pH level was decreased to pH 0 whilst the 3.5% NaCl level was maintained. Consequently, the scope of materials under study for this chapter was differentiated due to corrosive aggressiveness and hence, alloys that resists to acids and erosion were selected. The wide range of alloys tested in the current experimental phase provided a better understanding about the interaction between corrosion and mechanical wear under neutral and especially acidic pH. The industrial link between this work and industry is in aggressive mining and chemical industry operations in which the pH level is very low.

7.2 Materials and methods

7.2.1 Materials

The following list of alloys were evaluated:

- UNS S31600 – reference material.
- UNS S32760 – austenitic-ferritic stainless steel.
- 37WCI – the material presented in chapter 5.
- Type N1 alloy – A proprietary Ni-Cr alloy in the age hardened condition.
- Type D1 alloy – A proprietary duplex stainless steel in the age hardened condition.

7.2.1.1 UNS S32760

Apart from UNS S31600, a wrought version of a commercial UNS S32760 grade with almost 50-50 ratio of austenitic/ferritic was tested. Table 7.1 displays the nominal chemical composition of UNS S32760:

Table 7.1: Nominal chemical composition (wt %) of UNS S32760.

C	Cr	Cu	Mo	Mn	Ni	P	S	Si	W	N	Fe
0.03 max	25.0	0.75	3.5	1.0 max.	7.0	0.03 max	0.01 max.	1.0 max	0.75	0.25	61.7

Figure 7.1 shows the microstructure of UNS S32760 in which ferritic (dark colour) and austenitic (light colour) are appeared.
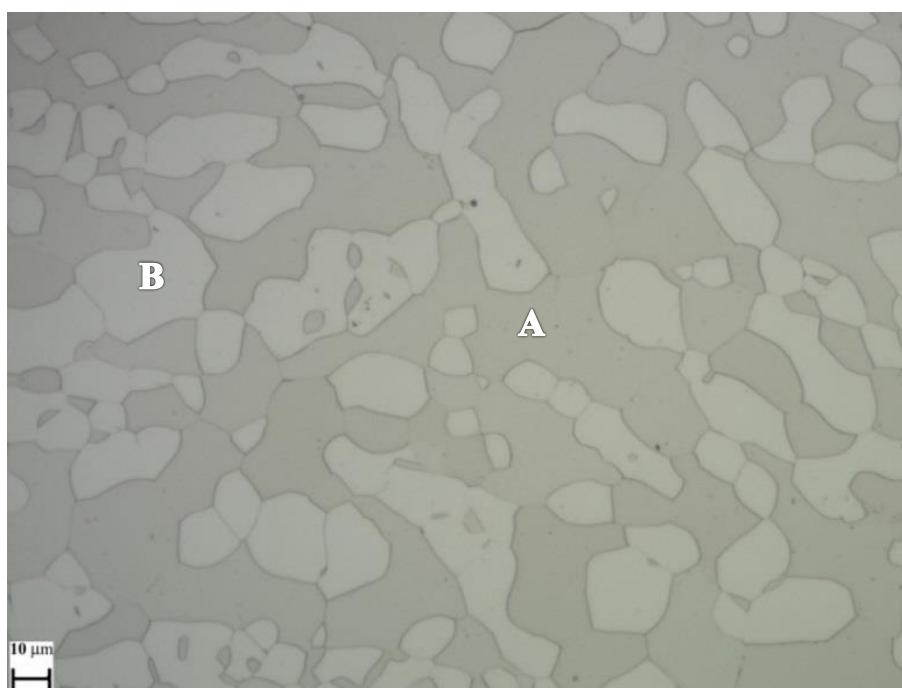
Figure 7.1: A-Ferrite matrix and B-austenite grains of UNS S32760 [etched].

7.2.1.2 Alloy 37WCI

As has been shown in chapter 5, the 37WCI alloy consists of austenitic dendrites in small eutectic carbides rich in Cr. The corrosion resistance of this material is a consequence of the high Cr contents which is dissolved in the metallic matrix (around

28% as measured). Despite the fact that 37WCI is used in acidic environments in which the minimum pH value is 1, its erosion-corrosion performance was investigated beyond the limits of the alloy (pH 0). In order to evaluate the correlation between the microstructure of 37WCI and its erosion-corrosion performance in very aggressive fluids, a more detailed investigation of the microstructure was carried out. Hence, a 37WCI sample was prepared for metallography, whilst for etchant solution potassium hydroxide (KOH) and 1V electrolytic was used. As shown in Figure 7.2, the eutectic structure appeared to have different colours (light blue, light brown and dark brown) indicating that different phases in the eutectic structure occur since they reacted with the KHO etchant.
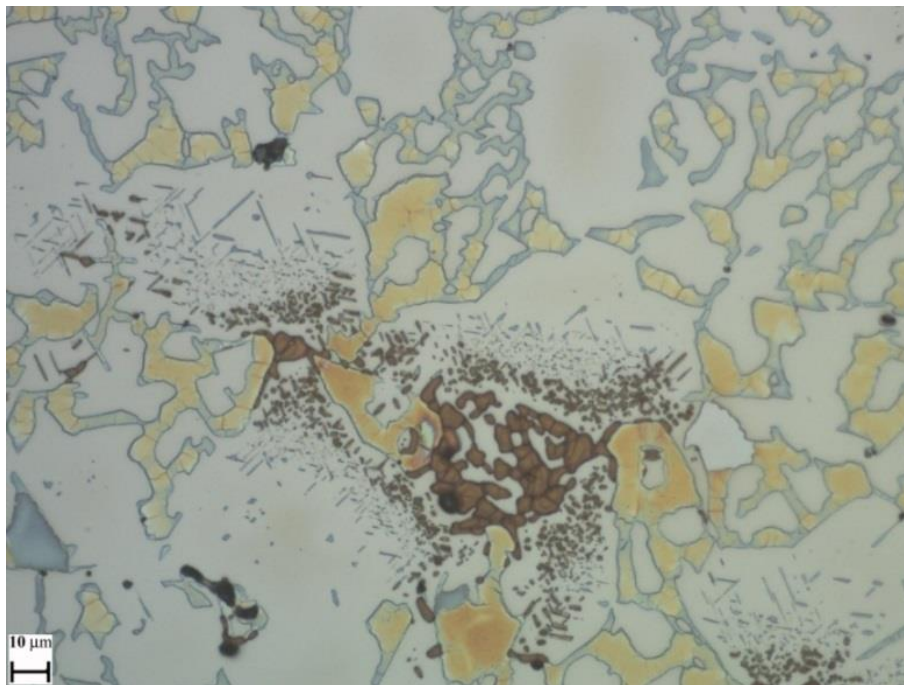
Figure 7.2: Microstructure of 37WCI with KHO etchant.

Therefore, an EDS elemental map was conducted in order to identify the main elemental dispersion within the eutectic structure. Figure 7.3 is the actual SEM image analysed in elemental maps – Cr (Figure 7.4) and Mo (Figure 7.5). The Cr carbides are identified in the red regions of Figure 7.4, whilst in some parts the Cr content was relatively low (10-16% - black spots). Also, as shown in Figure 7.5, a "sub-phase" rich in Mo (25-60% Mo) was observed. It is believed that the local areas in this "sub-phase"

that contain almost 60% Mo are Mo_2C carbides which were expected to be found, according to information obtained by the Weir Group PLC.
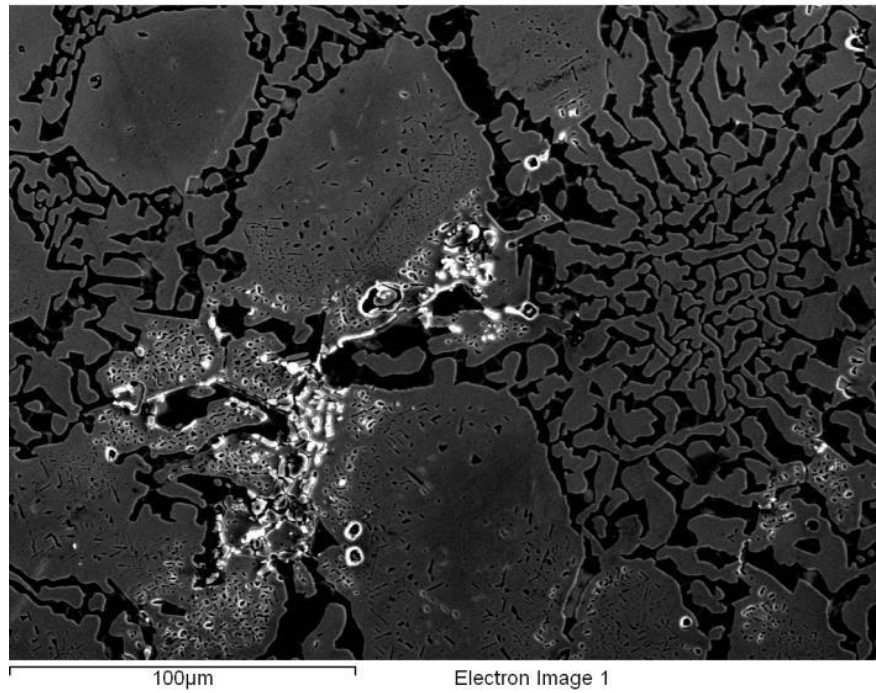
Figure 7.3: Microstructure of 37WCI with KHO etchant on SEM.
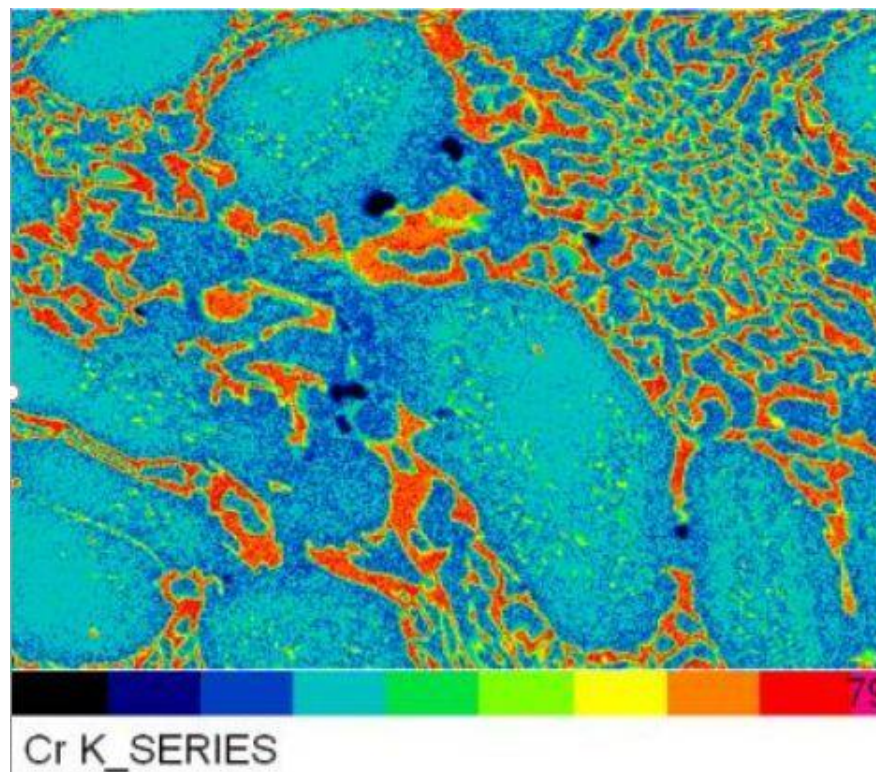
Figure 7.4: Chromium map of Figure 7.3 on 37WCI.
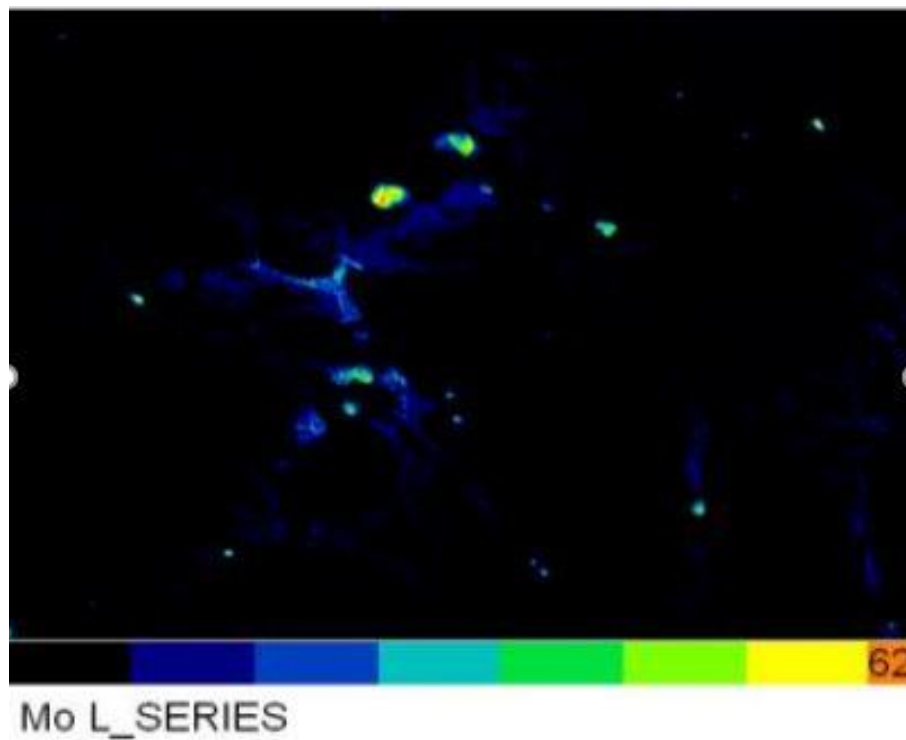
Figure 7.5: Molybdenum map of Figure 7.3 on 37WCI.

7.2.1.3 Type N1 alloy

The type N1 alloy is a centrifugally cast Ni-Cr (31% Cr, 3.5% Mo, Ni bal.) alloy, which contains austenitic matrix and blocky σ-phase due to ageing process. This material, supplied by the Weir Group PLC, is utilised in corrosive wear applications, especially in acidic environments but without the presence of chlorides. The components usually made from type N1 alloy are impellers, liners, wear rings and valves/valve seats. This alloy was tested in environments that contain chlorides in order to identify if the high strength and erosion/corrosion resistance would outweigh concerns on corrosion resistance due to presence of σ-phase. Figure 7.6 and Table 7.2 show the spot chemical analysis of type N1 alloy in which spectrum 1 corresponds to the blocky σ-phase that contains the highest Cr level in the entire microstructure of this alloy and relatively high Mo content, especially compared to the nominal value. Some past studies have demonstrated the same trend in EDS analysis with respects to correlation between Cr and Mo contents with σ-phase [7.1, 7.2]. Spectrum 2 is an independent phase enriched in Mo, which in fact, is embedded to the blocky σ-phase. Spectrum 3 demonstrates the austenitic nickel-base matrix, which contains elements

in solid solution, such as boron and cobalt. Spectrum 4 exhibits the chemical analysis on the interface between the σ and the austenitic matrix, which was very similar with the nominal Cr – Mo level of this alloy.
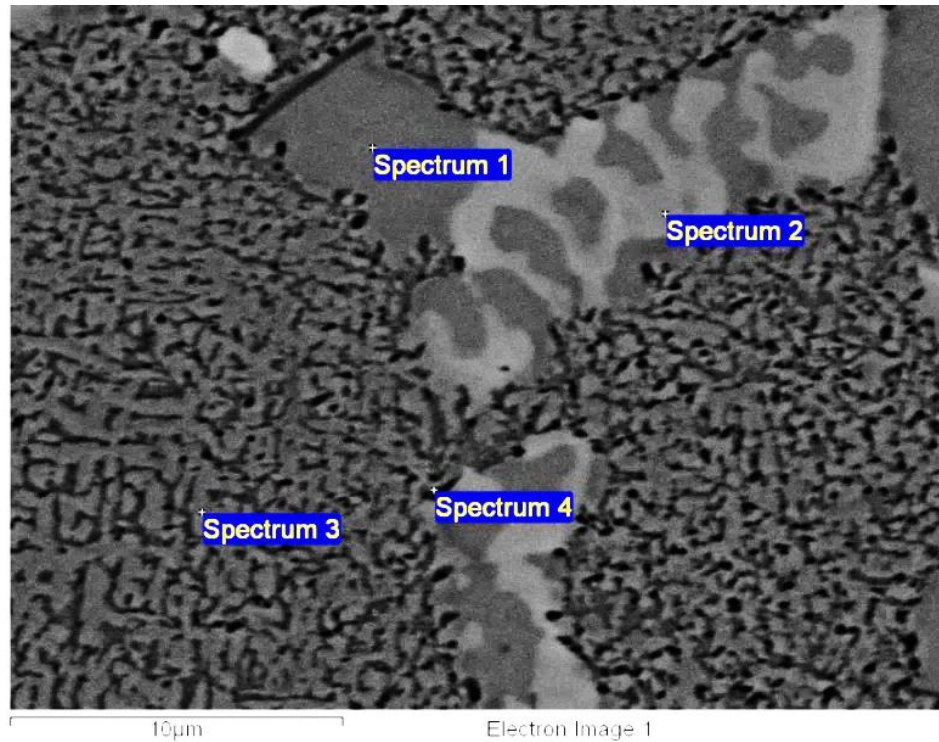
Figure 7.6: Spot chemical analysis on type N1 alloy [etched].

Table 7.2: Spot analysis of Figure 7.6.

Spectra	Cr%	Mo%
Spectrum 1	43.23	10.14
Spectrum 2	30.96	19.22
Spectrum 3	35.22	4.39
Spectrum 4	31.55	3.42

Further investigation of the complex microstructure of type N1 alloy was conducted via elemental maps, as displayed in Figures 7.7-7.10. A noticeable feature in Figure 7.7 (which was used for elemental maps) was the fine Widmastatten microstructure.

The Cr content (Figure 7.8) was up to almost 45% into the blocky σ, whilst in other regions was approximately 20%, much lower than the nominal level (31%). As presented in Figure 7.9, the Mo concentrations was at high levels (around 25 - 30%) in the Widmanstatten morphology confirming the spot chemical analysis presented in Table 7.2. Less Mo content was appeared in blocky σ-phase and especially in the austenitic matrix. The variations of Cr and Mo level were associated with the ageing process/σ-phase formation, as expected [3–5]. Finally, high concentrations of Ni (40 - 48 %) was observed in the austenitic matrix (as expected – Figure 7.10), whilst in the blocky σ-phase the Ni level was reduced down to 16 – 24 % approximately.
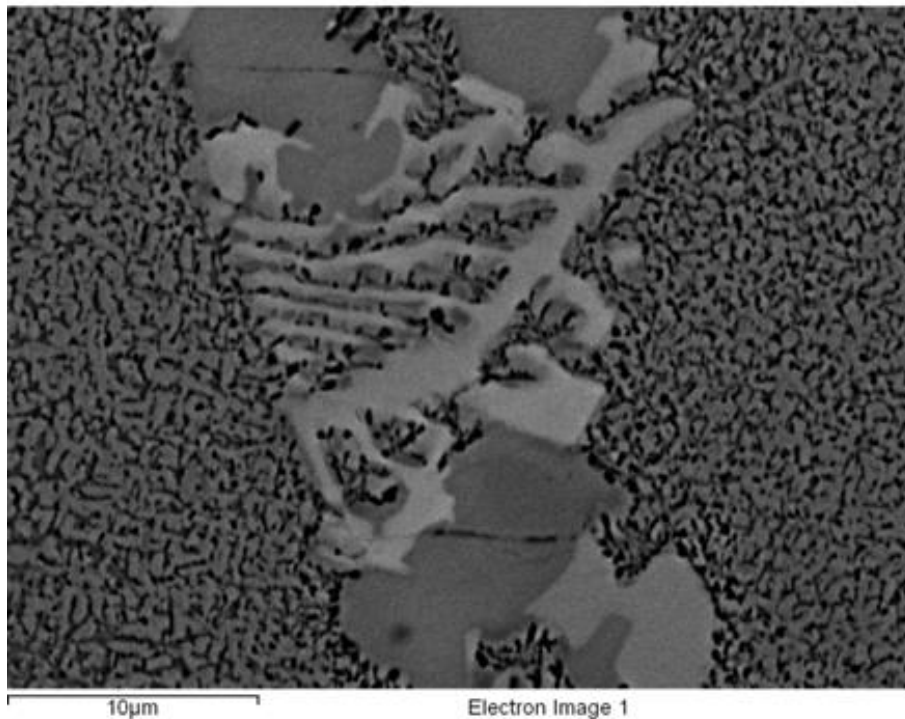
Figure 7.7: Widmastatten microstructure of type N1 alloy [etched].
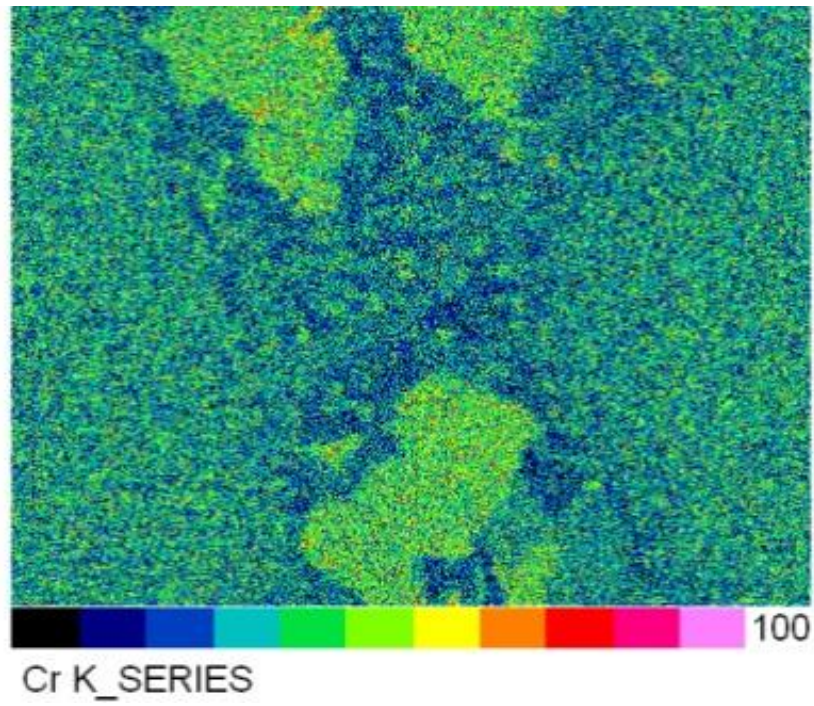
Figure 7.8: Chromium map of Figure 7.7 on type N1 alloy.
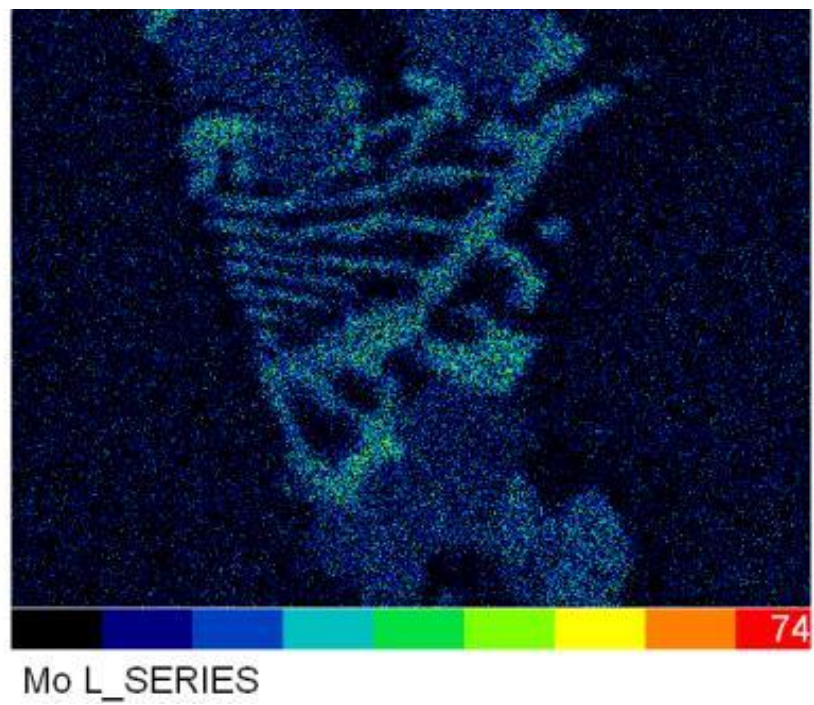
Figure 7.9: Molybdenum map of Figure 7.7 on type N1 alloy.
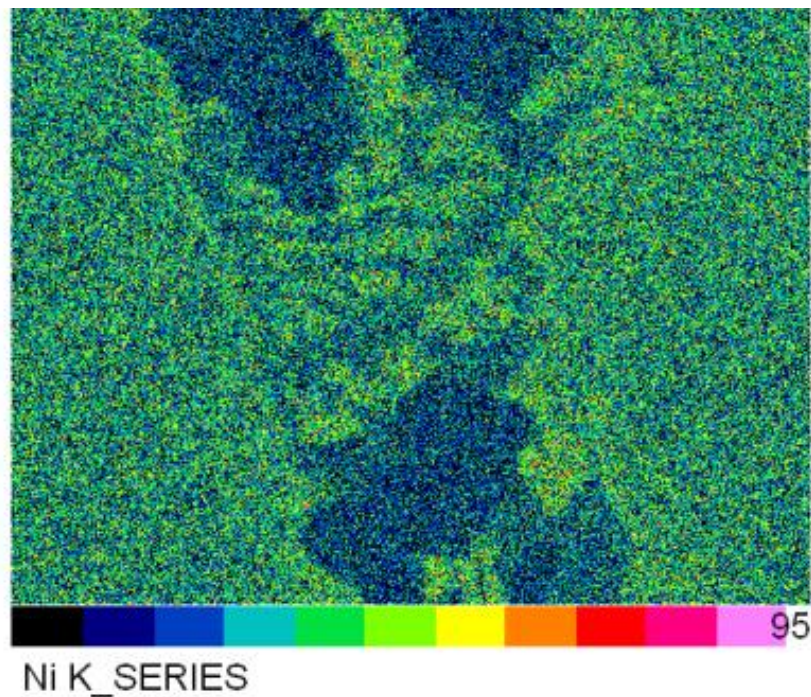
Figure 7.10: Nickel map of Figure 7.7 on type N1 alloy.

7.2.1.4 Type D1 Alloy

Type D1 alloy is a centrifugally cast aged 28% Cr duplex stainless steel precipitated by σ-phase supplied by The Weir Group PLC and is used in acidic slurries in absence of chlorides. Components made from type D1 alloy are, as in case of type N1 alloy, impellers, liners, valves/valve seats. Its microstructure is shown in Figure 7.11 in which the light colour presents the austenite and the dark colour is transformed ferrite (to σ-phase as discussed below).

The EDS analysis is demonstrated in Figure 7.12 and Table 7.3. Spectrums 2 and 5 represent the Cr carbides formed through the ageing process, whilst Spectrum 1 shows the austenite structure. Spectrums 3 and 4 describe the Cr content on the transformed ferrite and γ_2 islands respectively that were formed after ageing. However, due to very small size of γ_2 islands there is uncertainty if the Cr analysis corresponds to secondary austenite structure or to σ-phase.
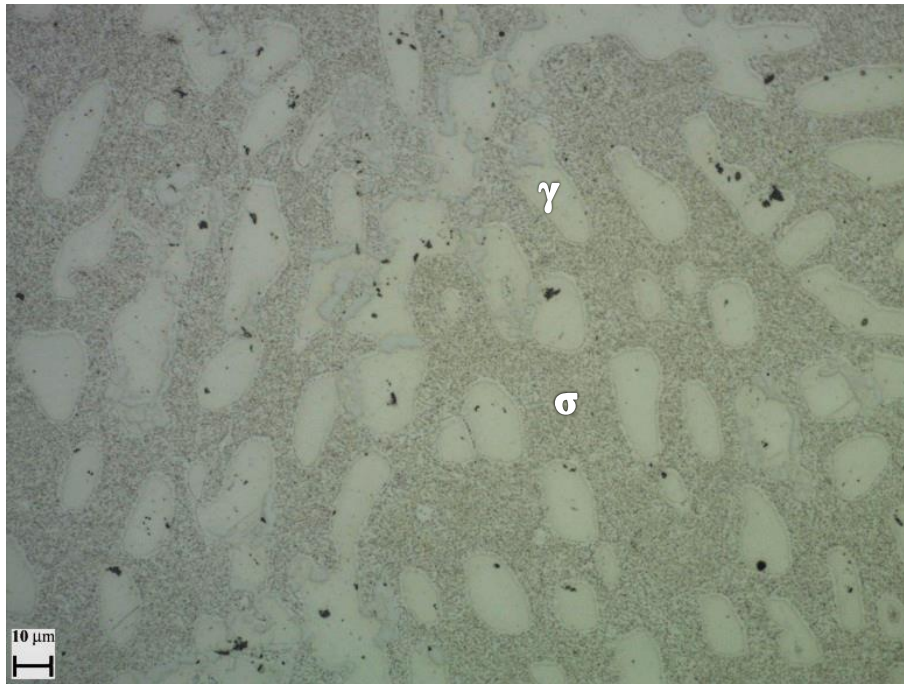
Figure 7.11: Microstructure of type D1 alloy [etched].
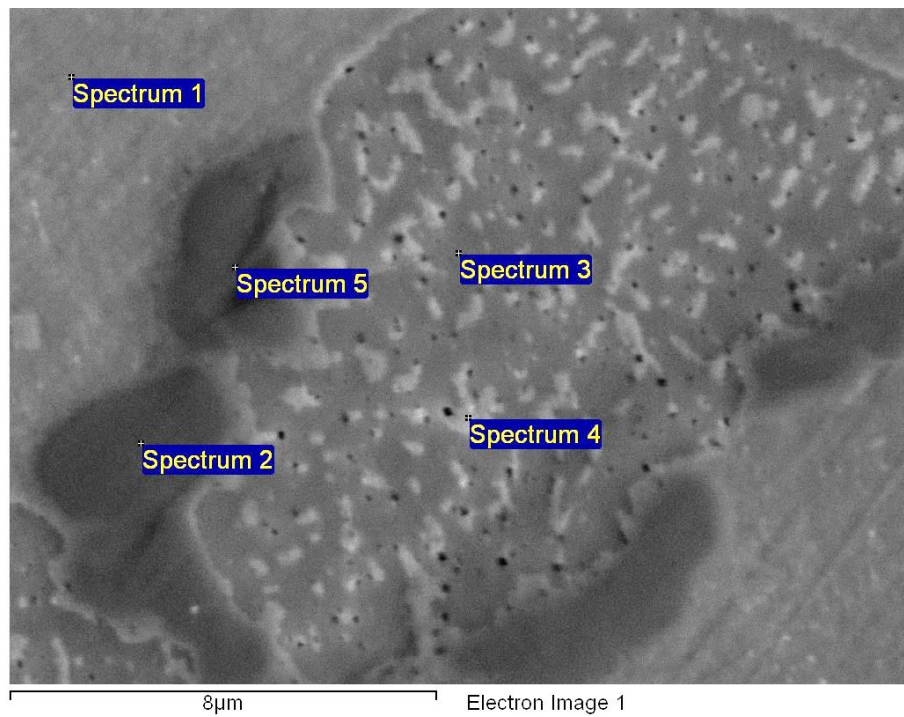
Figure 7.12: Spot chemical analysis of type D1 alloy [etched].

Table 7.3: Spot analysis of Figure 7.12.

Spectra	Cr%
Spectrum 1	22.8
Spectrum 2	71.9
Spectrum 3	32.0
Spectrum 4	29.9
Spectrum 5	72.3

Figures 7.13-7.15 show the elemental maps of type D1 alloy. According to Figure 7.14, the Cr level showed a descending trend into the following phases of alloy's complex microstructure:

- Cr carbides,
- σ-phase,
- γ_2 islands (embedded into the σ-phase and possess slightly lower Cr),
- austenite

It was also evident that the Cr dispersion of type D1 alloy was more uniform in the individual phases than in cases of 37WCI and type N1 alloy.

The Mo content was uniformly dispersed into the individual phases, especially in the σ-phase where it is well known that the Mo is increased [7.1, 7.6]. Also, χ-phase was absent on type D1 alloy since it was transformed to σ-phase (χ is formed in the first stages of ageing) [7.1, 7.4, 7.7].
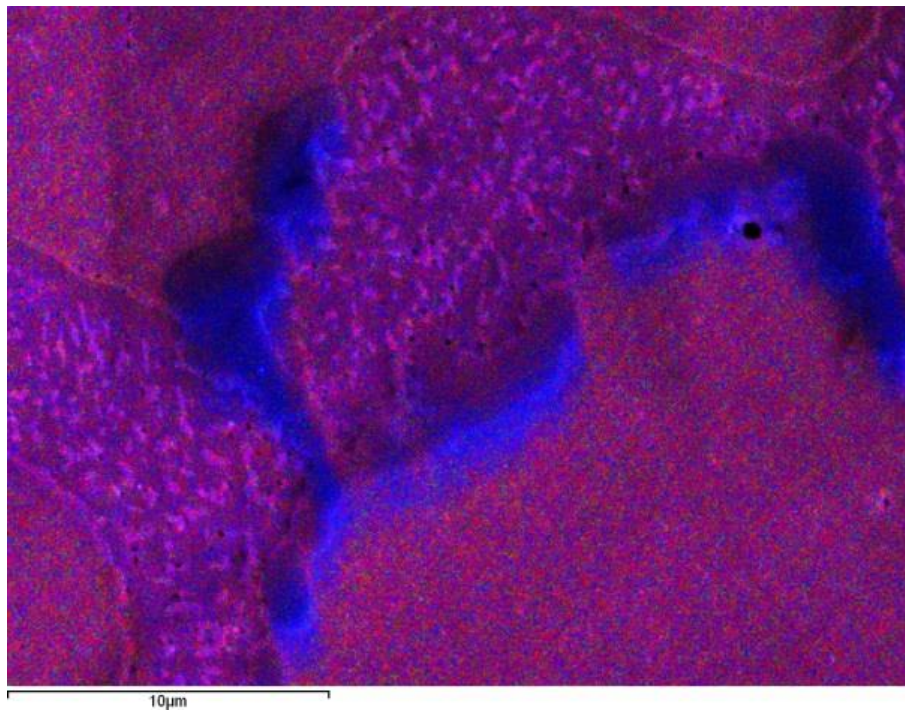
Figure 7.13: SEM view of type D1 alloy microstructure used for elemental maps [etched].

Cr K_SERIES
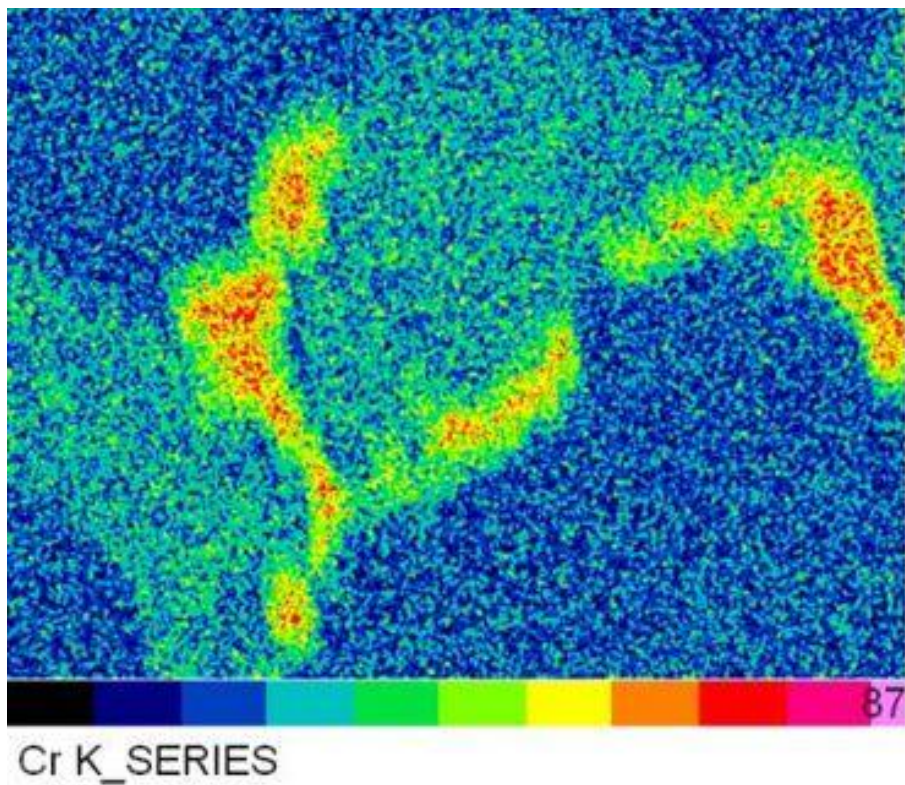
Figure 7.14: Chromium map of Figure 7.13 on type D1 alloy.

Mo L_SERIES
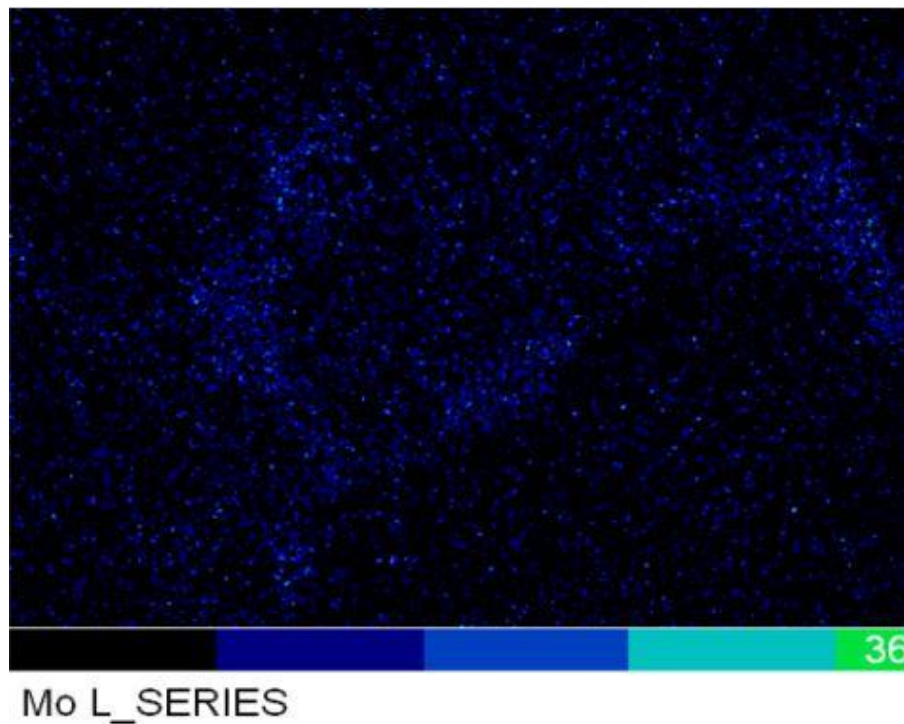
Figure 7.15: Molybdenum map of Figure 7.13 on type D1 alloy.

In order to understand the correlation between the σ-phase and the ferrite on type D1 alloy, the Electron Backscatter Diffraction (EBSD) technique was carried out. Also, as a matter of comparison, EBSD scanning was conducted for UNS S32760 too. The results of Figure 7.16 displayed the expected 50-50 ratio between ferrite and austenite on UNS S32760, as obtained directly through EBSD:

- Red: FCC (austenite): 50-52 %
- Blue: BCC (ferrite): 48-50%
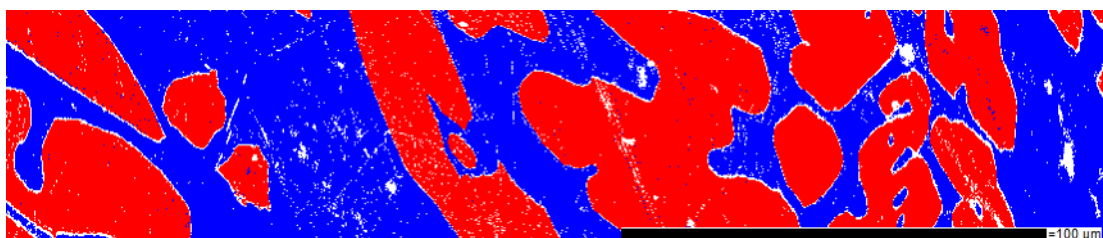
Figure 7.16: EBSD map for UNS S32760.

Subsequently, the results of EBSD map (Figure 7.17) for type D1 alloy are the following:

- Red: FCC (austenite): 50-55%
- Blue: BCC (ferrite): 5%
- Green: Sigma phase: 35-40%
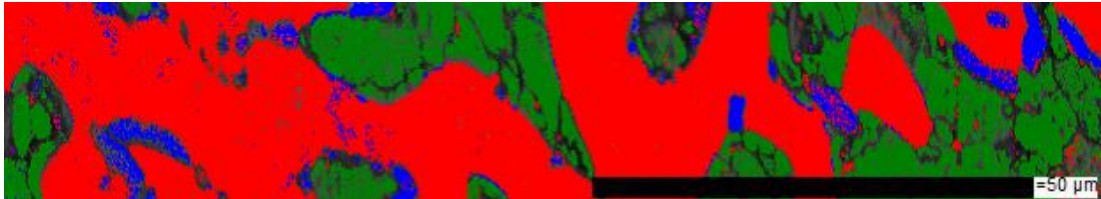
Figure 7.17: EBSD map for type D1 alloy.

Table 7.4 demonstrates the hardness values of all tested materials, as measured on Vickers macrohardness machine. Also, microhardness measurements were obtained for type D1 alloy in order to investigate the variation of hardness due to the presence of Cr carbides, as presented in Table 7.5.

Table 7.4: Macrohardness values of materials under study.

Material	Hardness (HV_5)
UNS S31600	172±10
UNS S32760	255±10
37WCI	365±10
N1	465±10
D1	445±5

Table 7.5: Microhardness values of different phases in type D1 alloy microstructure.

Material	Austenite ($HV_{0.2}$)	Sigma+ferrite ($HV_{0.2}$)	Sigma+Carbides ($HV_{0.1}$)
D1	295±5	467±15	775±20

7.2.2 Testing conditions - methods

The erosion-corrosion solid-liquid impingement (SLEC) conditions comprised aqueous solution of 3.5% NaCl at pH 7 and pH 0. The velocity at the exit of nozzle was 20 m/s, whilst the sand concentration was 0.80±0.05 g/l. The erosion-corrosion assessment consists of:

- volume loss measurements after 1h erosion-corrosion tests
- Cathodic protection (CP) application (at pH 7)
- anodic-cathodic polarisations in flowing conditions
- Linear polarisations and anodic polarisations on segmented specimens
- Post-test analysis
- Crack investigation on the 37WCI

7.3 Results

7.3.1 Volume loss

Figure 7.18 illustrates the volume loss of the materials under study. At pH 7, the performance of tested alloys was discriminated into three groups; type N1 and D1 alloys were the optimum, followed by 37WCI and UNS S32760, whilst UNS S31600 was the worst alloy.

In CP conditions, type D1 and N1 alloys were again superior to the other alloys, whilst minor differences were observed between UNS S32760, UNS S31600 and 37WCI. It should be noted that the applied potential for CP tests on UNS S32760 was -0.75 V instead of -0.85 V. The reason for that was the lower volume loss at -0.75 V than at -0.85 V, as shown in Table 7.6. The anodic current density at this electrode potential was estimated to be lower than 0.0007 mA/cm^2 indicating that the corrosive attack was negligible.

At pH 0, the best erosion-corrosion performance was noted by the type D1 alloy, followed by UNS S32760. The type N1 alloy showed lower volume loss than 37WCI, whilst UNS S31600 experienced much higher volume loss than all tested alloys due to vulnerability to corrosion, as described in the following sections. A noticeable feature was that two of two type D1 alloy specimens showed lower hardness (360 HV) in the

centre – direct impinged zone (DIZ), while the overall hardness was 445 HV. However, 5-10 mm next to this ''soft'' point, the hardness was 445 HV. All the other specimens of the type D1 alloy possessed uniform hardness of about 445 HV. One of these (with lower hardness in the centre) samples was tested in erosion corrosion conditions at pH 0 conditions and displayed higher volume loss (1.57 mm^3) than the other two replicates, but this result is not included in Figure 7.18.
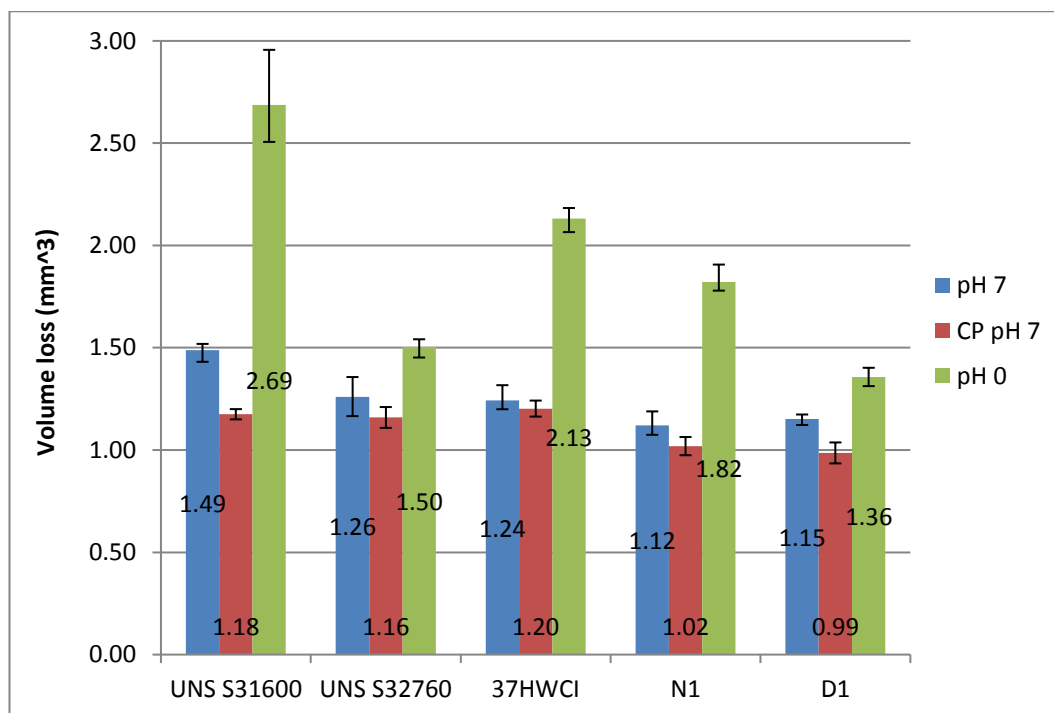

Figure 7.18: Average volume loss of materials in all testing environments under SLEC conditions.

Table 7.6: CP results for UNS S32760 at different electrode potentials.

Material	Volume loss (mm^3) -750 mV	Volume loss (mm^3) - 850 mV
UNS S32760	1.11, 1.21	1.30

7.3.2 Electrochemical tests

7.3.2.1 Anodic-cathodic polarisations

<u>Neutral conditions</u>

Figures 7.19-7.20 show the anodic and cathodic polarisation plots for materials under study at pH 7 respectively. The rapid fluctuations are indicative of periodic de-passivation and re-passivation events. Table 7.7 displays the i_{corr} and the volume loss due to corrosion for all tested alloys at pH 7. It should be noted that the i_{corr} values were similar either obtained either by anodic or cathodic polarisation scans. As a matter of preciseness, the i_{corr} values presented in Table 7.7 are the average values of anodic-cathodic plots. The type N1, D1 alloys and UNS S32760 exhibited more than two times better corrosion resistance than UNS S31600, whilst 37WCI showed intermediate performance. However, in neutral conditions, all materials displayed excellent corrosion performance and the proportions of corrosion to the total volume loss were almost negligible.
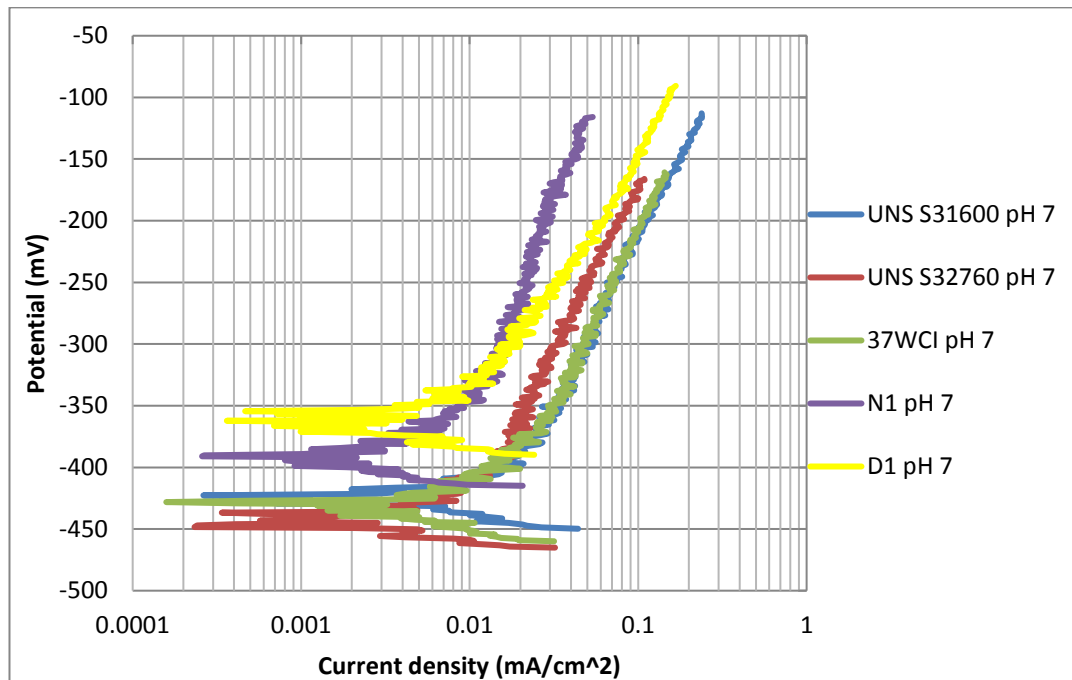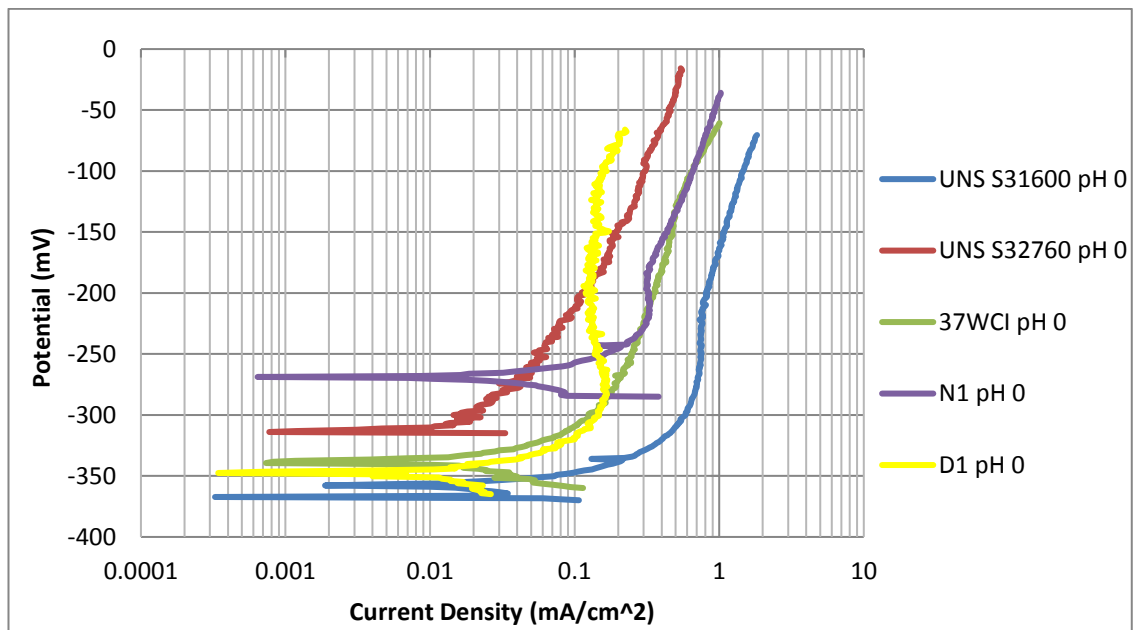

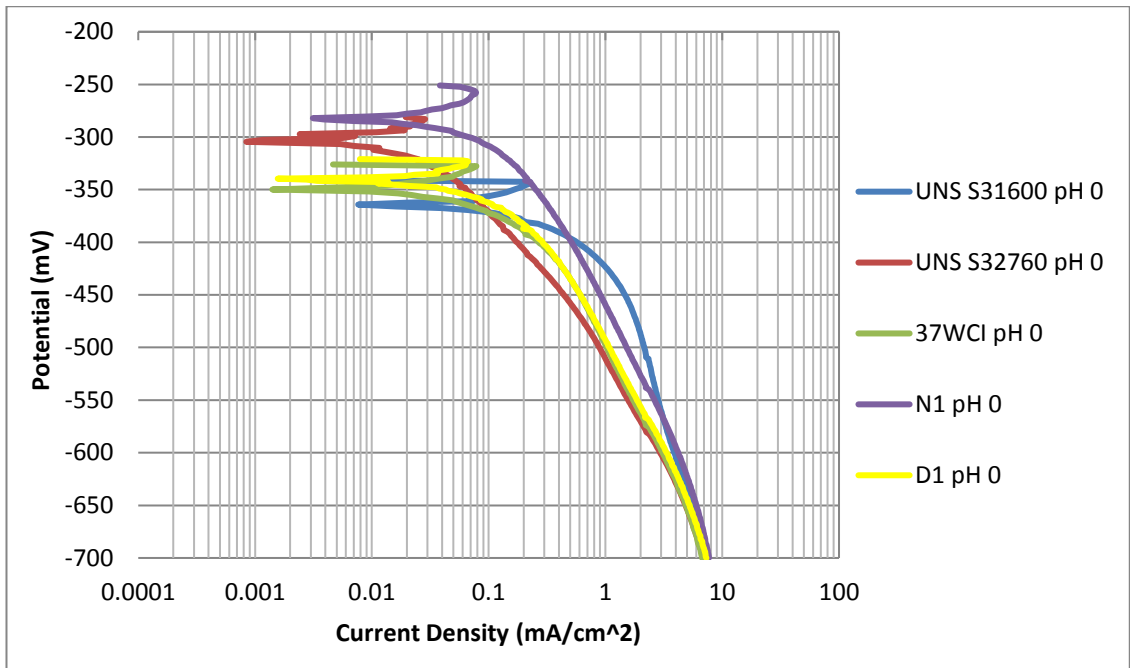Figure 7.19: Anodic polarisation plots for materials in SLEC conditions at pH 7.
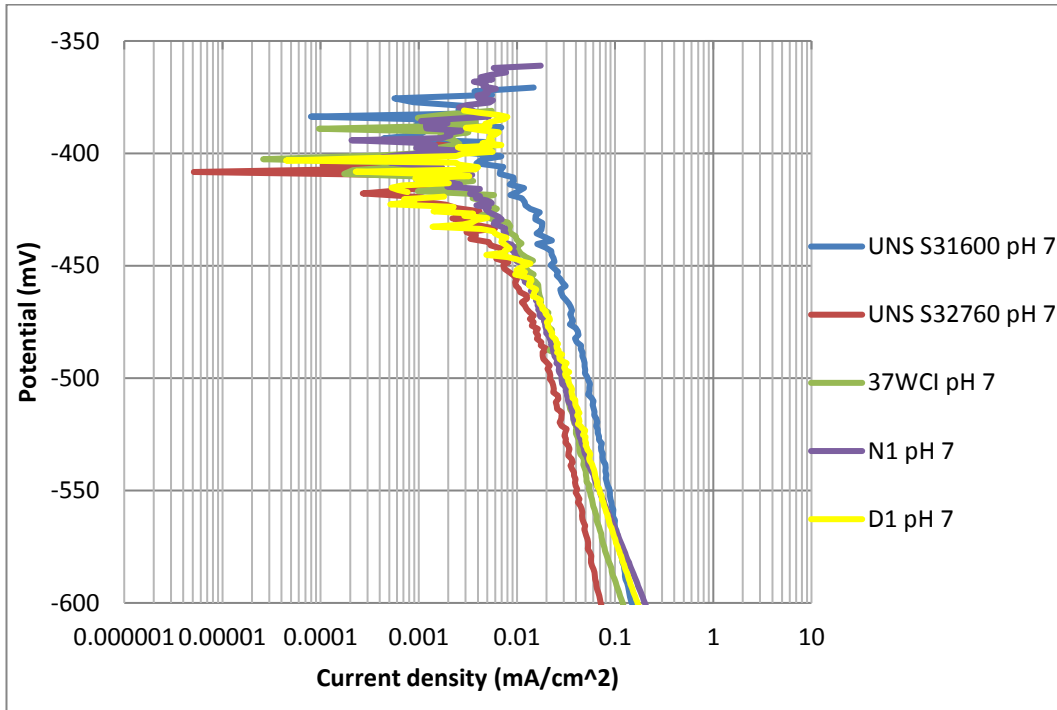
Figure 7.20: Cathodic polarisation plots for materials SLEC conditions at pH 7.

Table 7.7: Corrosion rates and volume loss of materials under study at pH 7.

Material	i_{corr} (mA/cm^2)	Volume loss (mm^3)
UNS S31600	0.017	0.024
UNS S32760	0.007	0.010
37WCI	0.011	0.015
N1	0.005	0.008
D1	0.006	0.009

Acidic conditions

Figures 7.21-7.22 demonstrate the anodic and cathodic polarisation plots respectively in acidic conditions. The first observation was that all materials experienced less oscillations compared to neutral conditions indicating that the passive film of all tested alloys was severely attacked by the HCl. Another interesting feature was that three

alloys (UNS S31600, type N1 and D1 alloys) showed a constant current region commencing about 50-90 mV more positive to E_{corr}. In this region, the electrochemical behaviour of these alloys cannot be considered as passive because of the rapid increase of current density at more positive electrode potentials to the E_{corr} (until the initiation of the region where the current is constant). Nevertheless, this constant feature made estimation of i_{corr} by the Tafel extrapolation method impossible. Thus, the corrosion rates were measured for all materials through the cathodic polarisation curves and the results are shown in Table 7.8, along with the corresponding volume loss. UNS S32760 displayed the lowest corrosion rates, whilst type D1 alloy, 37WCI and type N1 alloy had similar corrosion performance. Finally, the UNS S31600 showed significantly high corrosion rates which were aligned with high volume loss in erosion-corrosion conditions (Figure 7.18).

Figure 7.21: Anodic polarisation plots for materials in SLEC conditions at pH 0.

Figure 7.22: Cathodic polarisation plots for materials in SLEC conditions at pH 0.

Table 7.8: Corrosion rates and volume loss of materials under study at pH 0.

Material	i_{corr} (mA/cm^2)	Volume loss (mm^3)
UNS S31600	0.770	1.09
UNS S32760	0.070	0.10
37WCI	0.149	0.22
N1	0.141	0.23
D1	0.149	0.20

7.3.2.2 Anodic-cathodic polarisations on segmented samples

Figures 7.23-7.24 show the anodic and cathodic polarisation scans on segmented samples of UNS S31600 in SLEC conditions, whilst Figures 7.37-7.44 in the Appendix refer to the remaining materials. The alloys, in which Tafel extrapolation was not feasible in anodic polarisations of whole specimens at pH 0, depicted the same trend in the same environment in the outer area (OA). Thus, as a matter of consistency, cathodic polarisation scans were conducted in both DIZ-OA for all materials in acidic

conditions. The corrosion rates of all tested materials at both pH levels are demonstrated in Table 7.9. A number of observations can be summarised as follows:

- For a given alloy/environment, the corrosion rate in the DIZ was much higher than the OA region. Nevertheless, the volume loss was due to corrosion was larger in the OA due to larger tested surface area (11 cm^2 against 0.2 cm^2 for the DIZ)

- In neutral conditions, a clear superiority of type D1 and N1 alloys was noticed over the other alloys in the DIZ. The 37WCI and UNS S32760 experienced similar corrosion rates in this region followed by UNS S31600. In the OA, all tested materials displayed similar rates, whilst UNS S31600 possessed higher corrosion rates.

- In acidic conditions and the DIZ region, the type D1, N1 alloys and 37WCI were showed slightly lower corrosion rates than UNS S32760, whilst UNS S31600 again was the worst alloy. In the OA, the type D1 alloy, 37WCI and UNS S32760 were superior to the type N1 alloy. The UNS S31600 experienced very high corrosion rates, as expected (considering the performance of the whole specimen at pH 0).
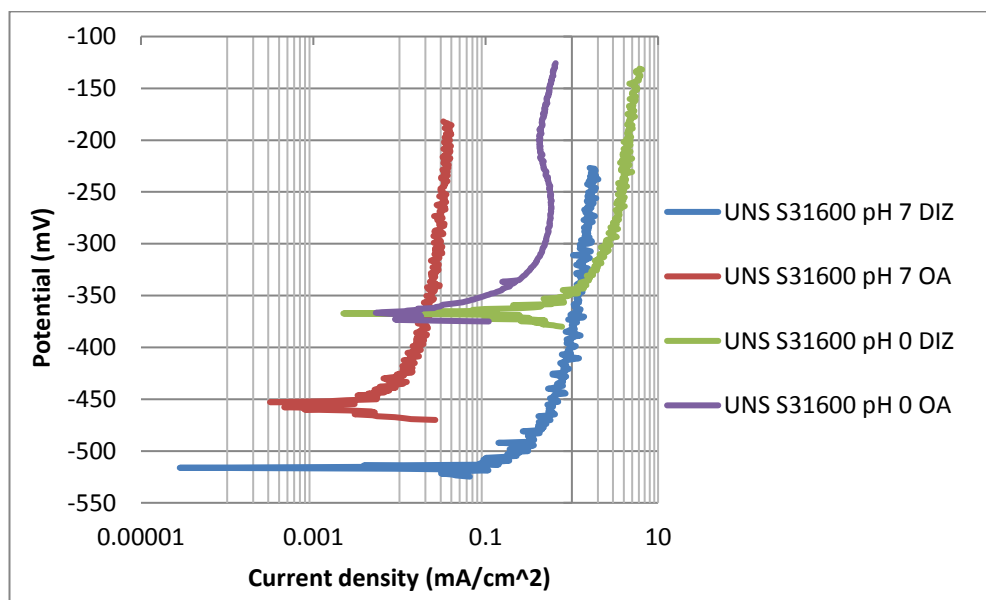
Figure 7.23: Anodic polarisation plots for UNS S31600 in the DIZ-OA regions at both pH levels.
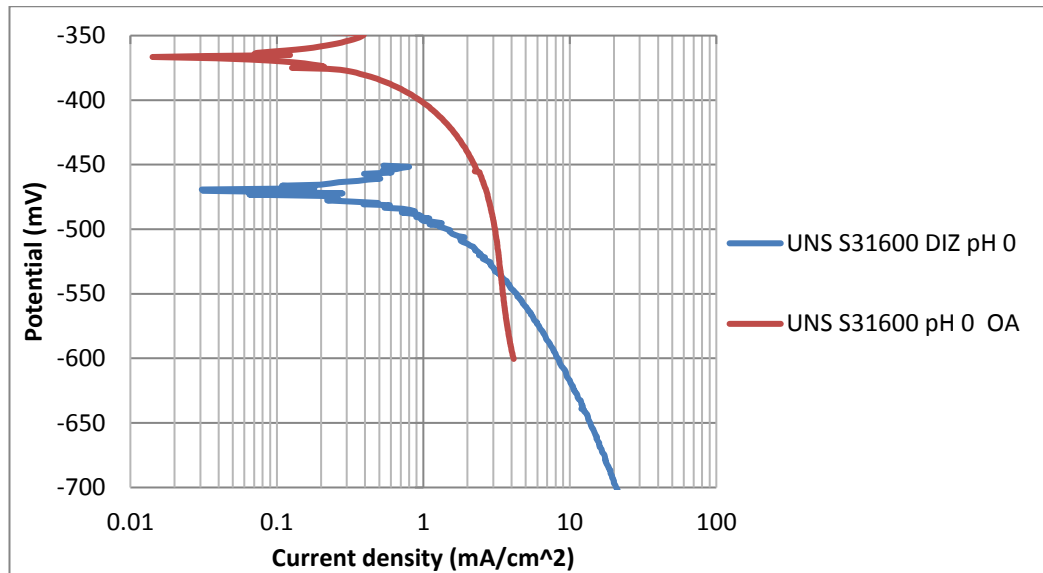
Figure 7.24: Cathodic polarisation plots for UNS S31600 in the DIZ-OA regions at pH 0.

Table 7.9: Corrosion rates in the DIZ-OA regions for materials under study at both pH levels.

Material	i_{corr} DIZ pH 7/pH 0 (mA/cm²)	Volume loss DIZ pH 7/pH 0 (mm³)	i_{corr} OA pH 7/pH 0 (mA/cm²)	Volume loss OA pH 7/pH 0 (mm³)
UNS S31600	0.550/1.9	0.011/0.050	0.01/0.80	0.015/1.08
UNS S32760	0.225/1.0	0.006/0.025	0.006/0.06	0.008/0.09
37WCI	0.200/0.85	0.007/0.026	0.005/0.06	0.007/0.10
N1	0.015/0.75	0.004/0.025	0.003/0.10	0.008/0.14
D1	0.005/0.80	0.0001/0.026	0.005/0.07	0.005/0.10

7.3.2.3 Linear polarisation scans

Figure 7.25 shows the linear polarisation plots for UNS S31600 at pH 7 and 7.45-7.53 for all materials at both pH levels (Appendix), whilst Table 7.10 presents the R_p values. The following observations were noticed:

- Lower Rp values (high corrosion rates) at pH 0 than in neutral conditions.
- Especially low Rp for UNS S31600 at pH 0.
- General similar materials ranking as from the i_{corr} values from the full anodic/cathodic polarisation curves.
- For a given material/pH value, Rp values are generally similar over the experimental exposure time. This is indicative of a broadly constant corrosion rate with time.
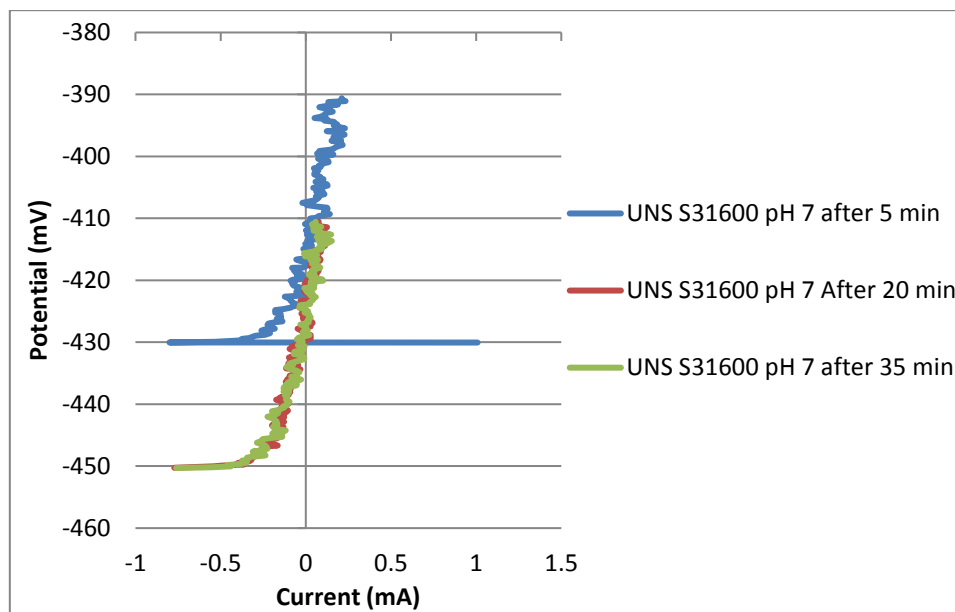
Figure 7.25: Linear polarisation plots for UNS S31600 in neutral conditions.

7.10: Linear polarisation data at both pH values.

Material	R_p Ohms after 5 min	R_p Ohms after 20 min	R_p Ohms after 35 min
UNS S31600 pH 7	120	120	120
UNS S31600 pH 0	5	9	9
UNS S32760 pH 7	300	300	283
UNS S32760 pH 0	133	125	125
37WCI pH 7	165	176	176
37WCI pH 0	30	26	30
N1 pH 7	300	285	285
N1 pH 0	28	27	18
D1 pH 7	285	280	300
D1 pH 0	44	38	40

7.4 Post-test analysis

7.4.1 Surface profiling

Figure 7.26 demonstrates the wear scar depths of materials tested at both pH levels and under CP conditions. In neutral environment, the type D1 and N1 alloys showed the lowest wear scars followed by UNS S32760, whilst 37WCI and UNS S31600 exhibited similar performance.

In CP application, greater reduction on wear scar depths was observed in the UNS S31600 and UNS S32760 indicating contribution of corrosion process even at pH 7, whilst the 37WCI, type N1 and D1 alloys displayed similar wear scars with and without the CP application.

In acidic conditions, all materials showed deepest wear scars, apart from type D1 alloy and this was the reason for its superiority compared to the rest of alloys. Type N1 alloy was ranked as second, followed by UNS S32760 and UNS S31600. The 37WCI showed significant deep wear scar and this trend is discussed below.
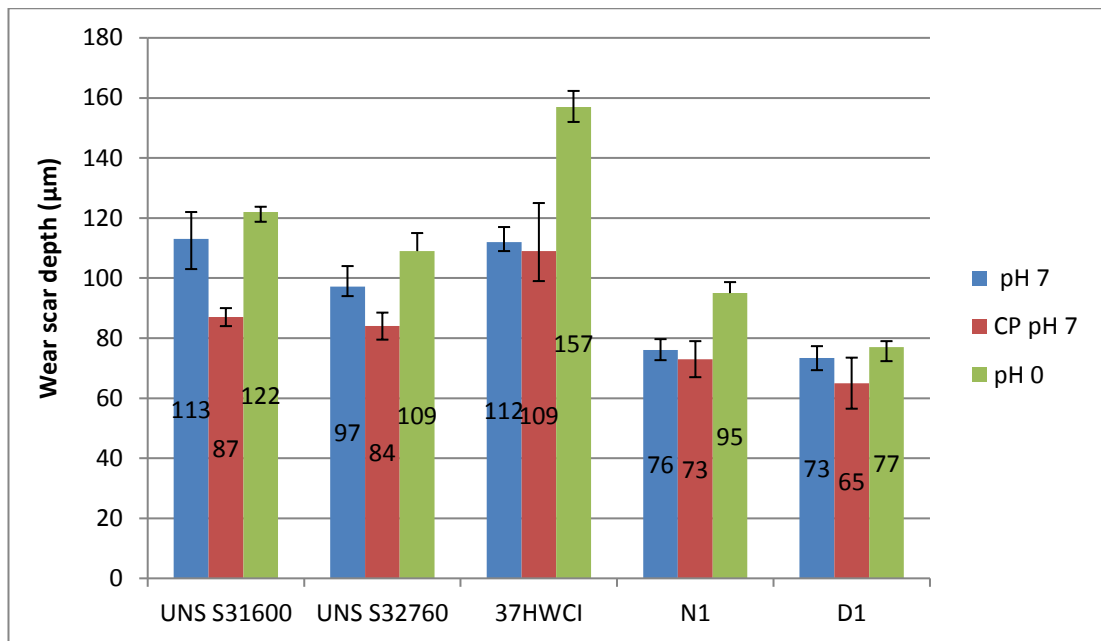
Figure 7.26: Average wear scar depths for materials under study at both pH levels.

7.4.2 Volumetric analysis

Figures 7.27-7.29 present the breakdown of total volume loss (TVL) into the DIZ/OA zones (VL_{DIZ}/VL_{OA}) for all materials under neutral, CP and acidic conditions. At neutral pH, the type D1 and N1 alloys showed the best erosion-corrosion behaviour in the DIZ and the UNS S32760 was ranked as third in this testing region. UNS S31600 and 37WCI possessed the highest volume loss in the DIZ. On the other hand, in the OA region, the 37WCI displayed the lowest average volume loss, followed by type N1, D1 alloys and UNS S32760. The UNS S31600, as expected, experienced the highest volume loss in the OA due to its low hardness.

In CP conditions, the type D1, N1 alloys and UNS S31600 showed similar erosion resistance in the DIZ, whilst UNS S32760 was slightly inferior and 37WCI experienced the highest volume loss. In the OA, the type D1, N1 alloys and 37WCI were the optimum alloys followed by UNS S32760 and UNS S31600.

At pH 0/DIZ, three groups of materials were observed in terms of their performance; type D1 alloy showed a remarkable erosion-corrosion resistance and its volume loss was similar with the corresponding at pH 7 and this was the reason for its superiority

to the other alloys. The second group consists of UNS S32760, type N1 alloy and UNS S31600 with minor differences in their performance (UNS S32760>type N1 alloy>UNS S31600). 37WCI depicted substantial volume loss in the DIZ, which is in good line with the wear scar measurement presented in Figure 7.26. In the OA zone, the type D1 alloy and UNS S32760 showed the lowest volume loss. The 37WCI was slightly better than type N1 alloy, whilst UNS S31600 possessed substantial volume loss due to poor corrosion resistance in the current testing regime.
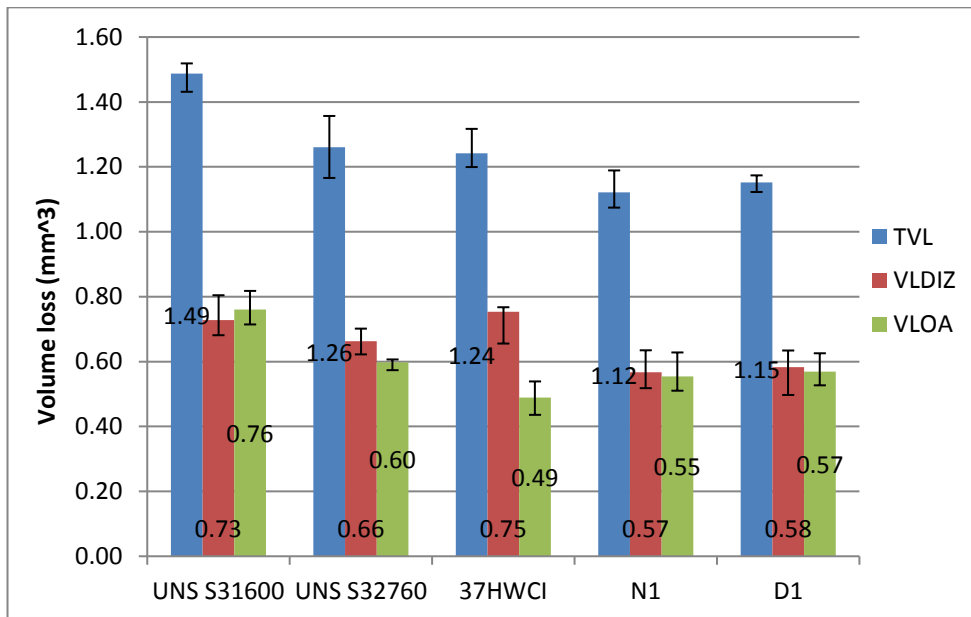
Figure 7.27: Breakdown of volume loss for materials under study at pH 7.
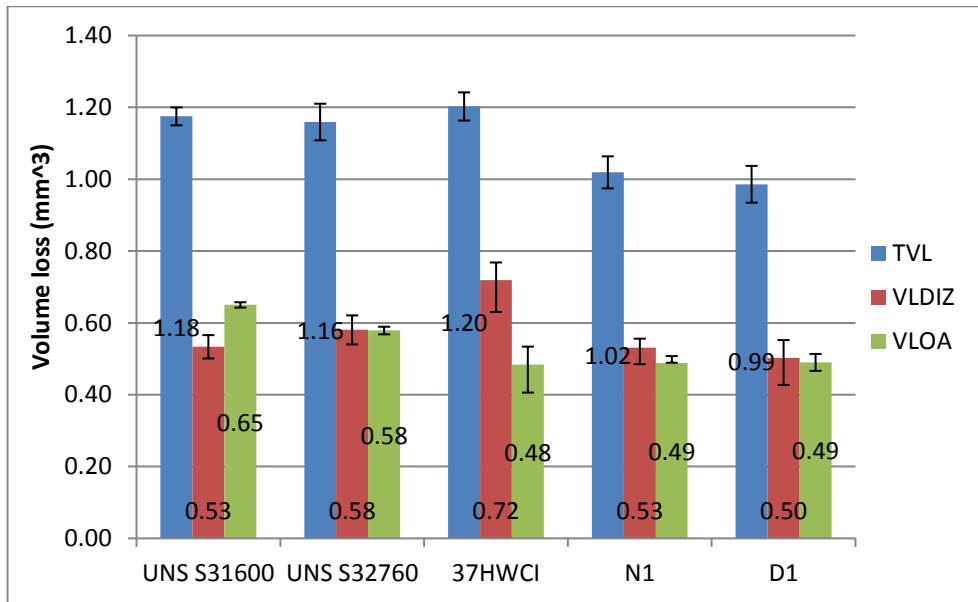
Figure 7.28: Breakdown of average volume loss for materials under study in CP conditions at pH 7.
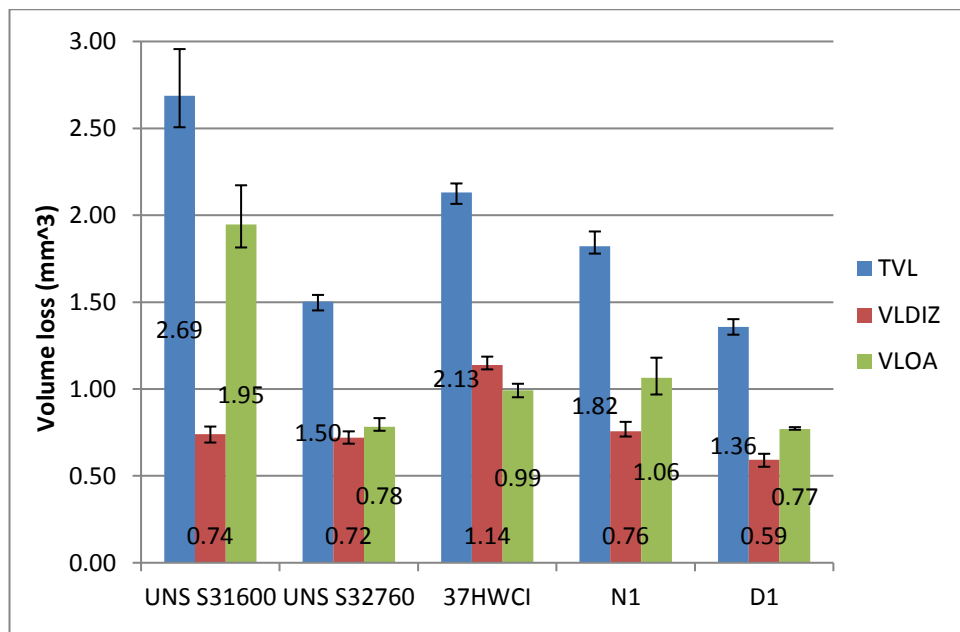
Figure 7.29: Breakdown of average volume loss for materials under study at pH 0.

7.4.3 Examination of cracks on 37WCI

As it has been stated in previous chapters, all the WCIs tested showed higher volume loss in acidic conditions rather in neutral under the perpendicular jet. In the current tests, the 37WCI experienced very high volume loss in the DIZ at pH 0 which affected inevitably its overall performance. Thus, crack investigation in neutral and acidic conditions was carried out. As shown in Figures 7.30-7.31, more severe cracks were observed in acidic conditions.

In Figure 7.32, in another area of DIZ, a significant crack at pH 0 is presented (at higher magnification so the length of the crack can be estimated). Thus, it was evident that the poor performance of 37WCI in the DIZ at pH 0 was associated with the presence of severe cracks. In the OA, no cracks were observed in neutral conditions, whilst at pH 0 a few cracks were noticed (Figures 7.33-7.34).
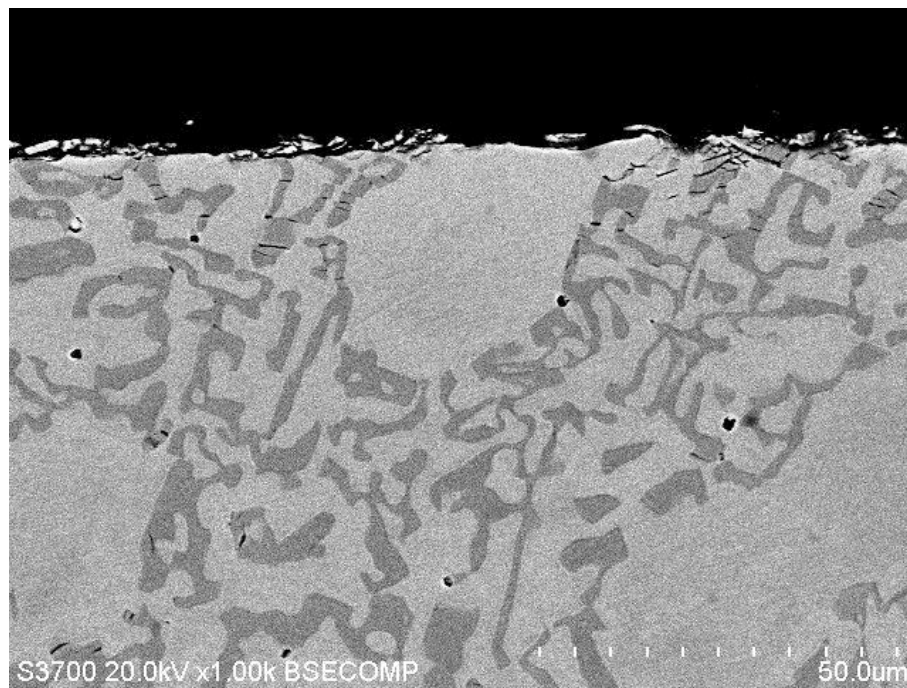
Figure 7.30: Cracks on Cr carbides of 37WCI in the DIZ at pH 7 and SLEC conditions [etched].
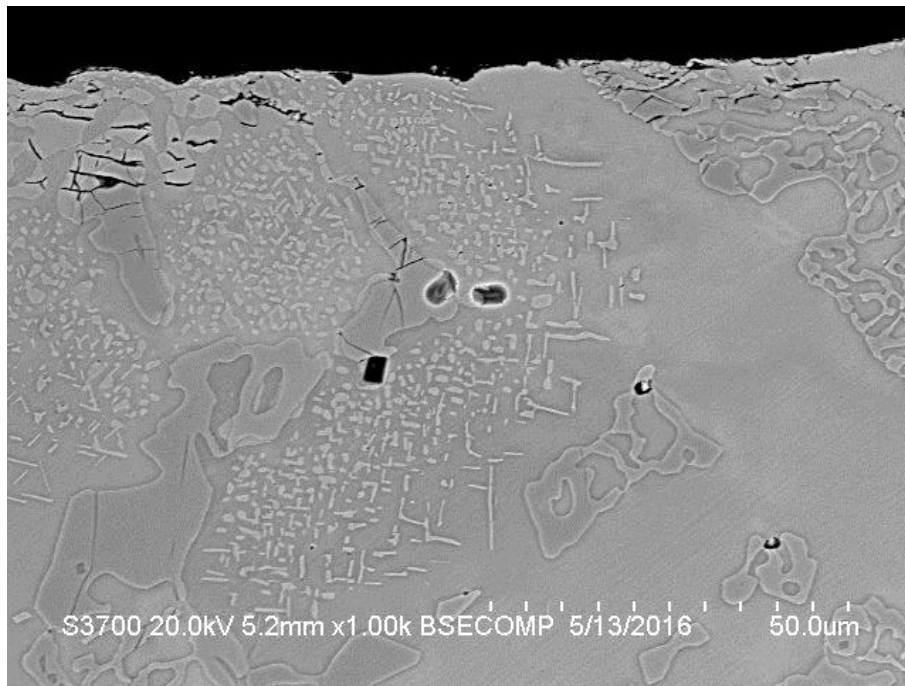
Figure 7.31: Enhanced cracks on Cr carbides of 37WCI in the DIZ at pH 0 [etched].
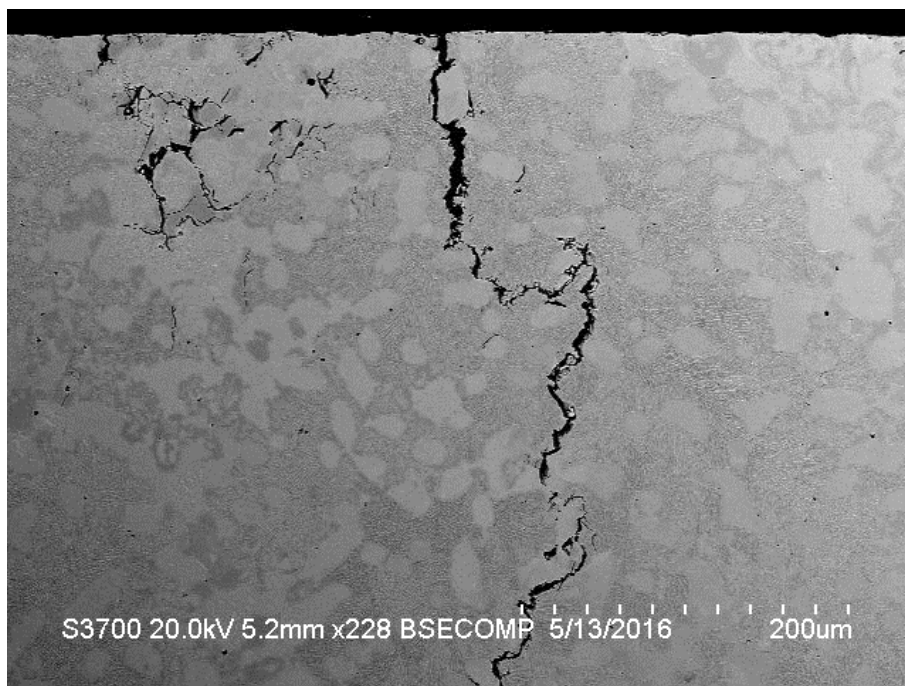
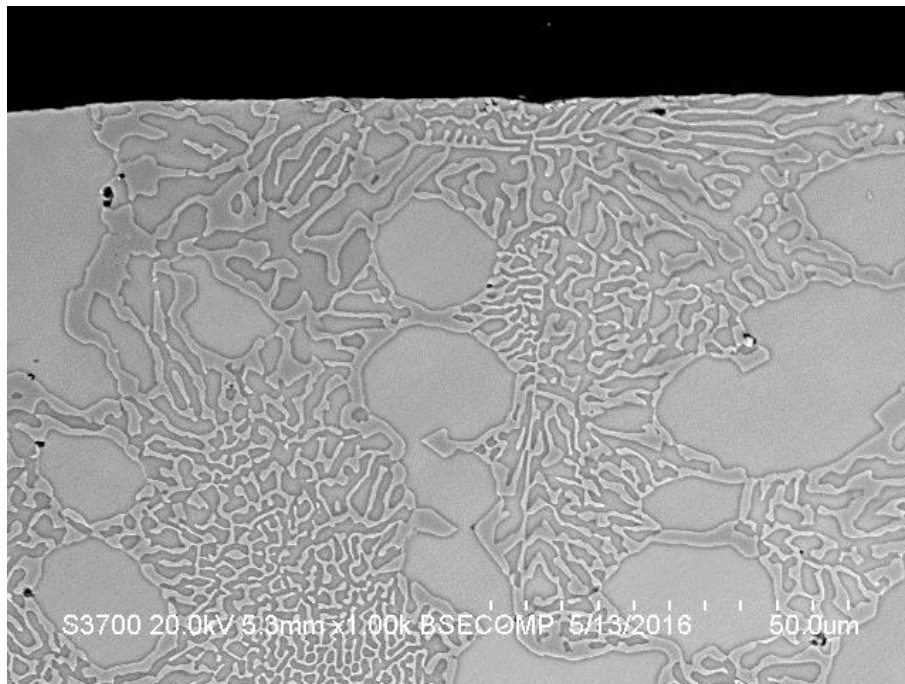Figure 7.32: Significant crack on 37WCI in the DIZ at pH 0 [etched].

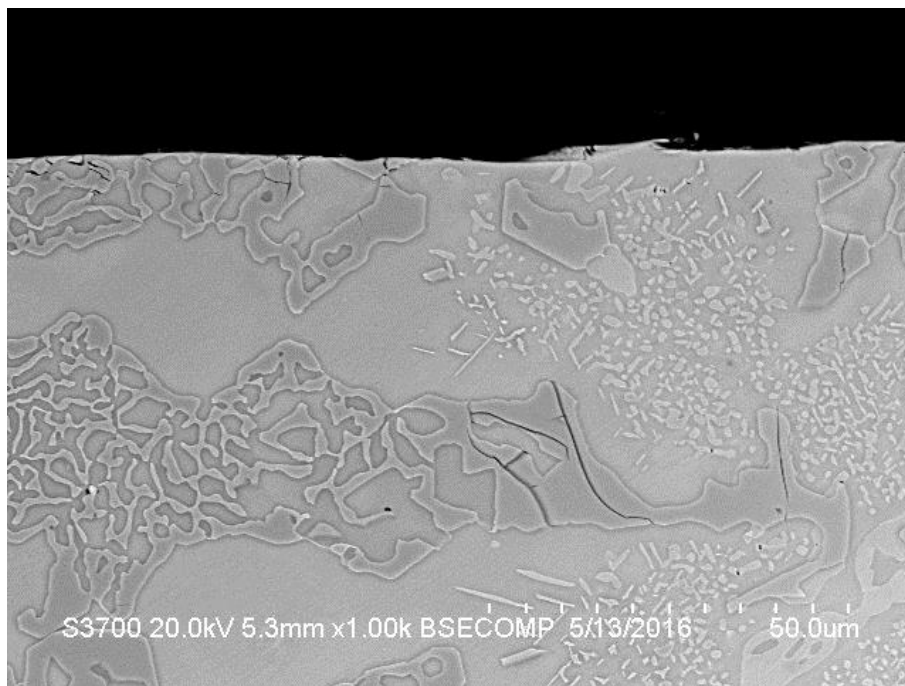Figure 7.33: No crack in 37WCI in the OA at pH 7 [etched].

Figure 7.34: Cracks on 37WCI in the OA at pH 0 [etched].

7.4.4 Summary of results

Table 7.12 presents the proportion of each degradation mechanism to the total volume loss at both pH levels for materials under study. The main features of this data are discussed in the next section but it is useful to note, at this point, the low corrosion rates at pH 7. On the other hand, a detailed illustration of the average volume loss due to the individual mechanisms in the DIZ/OA under neutral and acidic conditions is displayed in Figure 7.35/Table 7.13 and Figure 7.36/Table 7.14 respectively. The terms CP, C and S refer to Cathodic Protection, Corrosion and Synergy respectively. The discussion in the following section is based on the results presented on Tables 7.13-7.14.

Table 7.12: Proportions of degradation mechanisms at both pH levels.

Material	*Erosion + Sliding abrasion pH 7/pH 0 %	Corrosion pH 7/pH 0 %	Synergy pH 7/ pH 0 %
UNS S31600	80/44	2/41	18/15
UNS S32760	92/77	1/6	7/17
37WCI	97/57	2/10	1/33
D1	85/72	1/15	14/13
N1	92/57	1/13	7/30

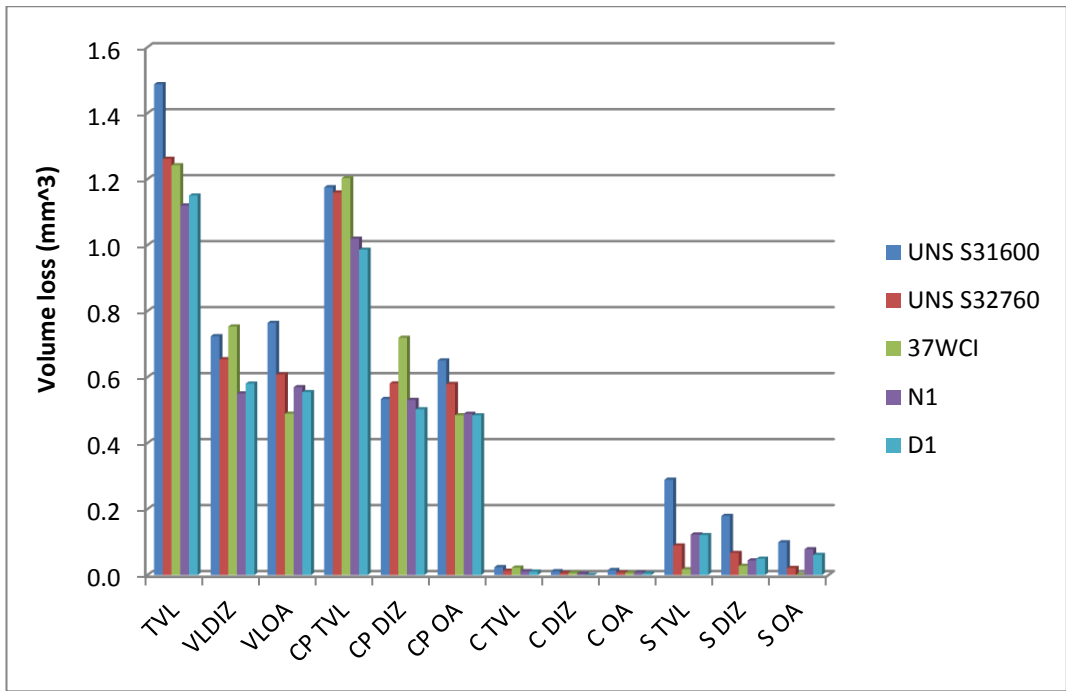*The CP results at pH 0 were obtained from pH 7 environment

Figure 7.35: Summary of average volume loss breakdown of materials at pH 7.

Table 7.13: Summary of average volume loss at pH 7 (mm^3).

Material	TVL	VL DIZ	VL OA	CP TVL	CP DIZ	CP OA	C TVL	C DIZ	*C OA	*S TVL	S DIZ	S OA
UNS S31600	1.49	0.73	0.76	1.18	0.53	0.65	0.02	0.011	0.01	0.29	0.18	0.10
UNS S32760	1.26	0.65	0.61	1.16	0.58	0.58	0.01	0.006	0.01	0.09	0.07	0.02
37WCI	1.24	0.75	0.49	1.20	0.72	0.48	0.01	0.007	0.01	0.02	0.03	0.00
N1	1.12	0.55	0.57	1.02	0.53	0.49	0.007	0.004	0.01	0.1	0.04	0.08
D1	1.15	0.58	0.55	0.99	0.50	0.49	0.01	0.000	0.01	0.15	0.05	0.06

*Some negligible values are rounded up
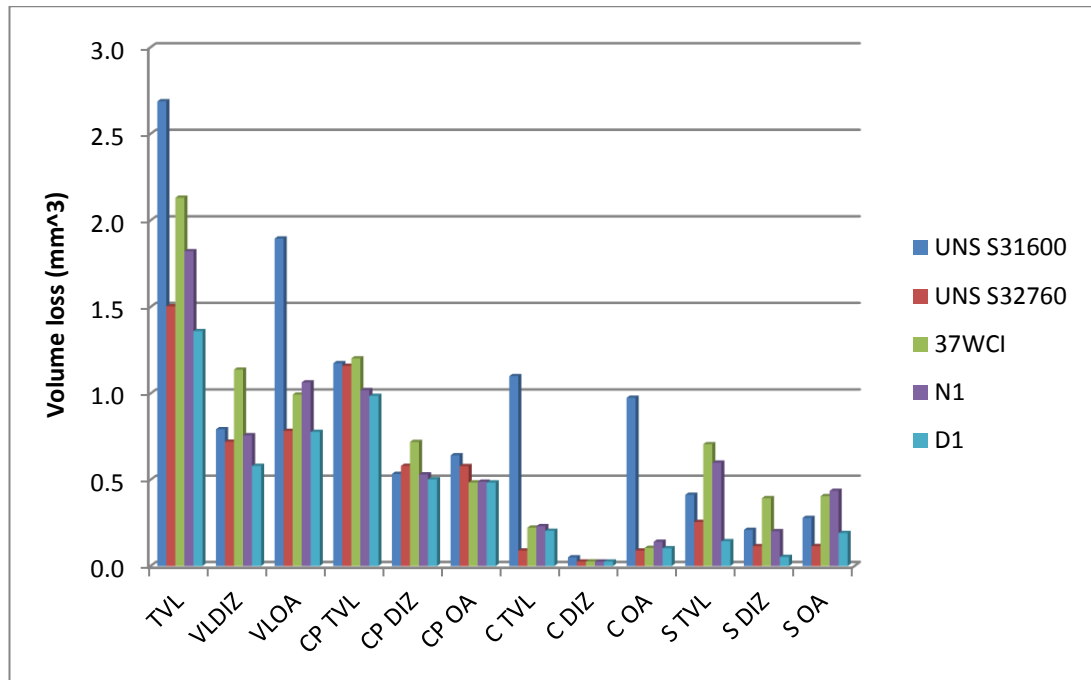
Figure 7.36: Summary of average volume loss breakdown of materials at pH 0.

Table 7.14: Summary of average volume loss at pH 0 (mm^3).

Material	TVL	VL DIZ	VL OA	**CP TVL	CP DIZ	CP OA	C TVL	C DIZ	C OA	*S TVL	S DIZ	S OA
UNS S31600	2.69	0.79	1.90	1.18	0.53	0.65	1.10	0.050	0.98	0.41	0.21	0.28
UNS S32760	1.50	0.72	0.78	1.16	0.58	0.58	0.09	0.025	0.09	0.25	0.11	0.11
37WCI	2.13	1.14	0.99	1.20	0.72	0.48	0.22	0.026	0.10	0.71	0.39	0.40
N1	1.82	0.76	1.06	1.02	0.53	0.49	0.23	0.025	0.14	0.6	0.20	0.44
D1	1.36	0.58	0.78	0.99	0.50	0.49	0.20	0.026	0.10	0.15	0.05	0.06

*Some negligible values are rounded up

** The CP results were obtained transferred from pH 7

7.5 Discussion

7.5.1 Neutral conditions

UNS S31600: As shown in chapter 5, UNS S31600 displayed moderate erosion-corrosion behaviour compared with the other tested alloys due to its low hardness whilst it possessed also the highest volume loss in either DIZ or OA (only in the DIZ its performance was similar with 37WCI). An interesting observation was that the average TVL of UNS S31600 in chapter 5 was 1.39 (velocity 21 m/s and sand concentration 0.5 g/l), whilst in the current chapter was higher due to higher sand concentration (0.8 g/l). On the other hand, the 37WCI alloy (also tested in chapter 5) showed no increase in these two testing regimes indicating that the difference in performance between a more erosion/abrasion resistant alloy and a less erosion/abrasion resistant material (corrosion is negligible for both UNS S31600-37WCI) increases in more aggressive erosive-corrosive conditions.

In terms of corrosion, it depicted the highest rate but in this environment, all tested alloys possess negligible corrosive attack due to mainly the relatively high Cr level.

UNS S32760: As expected, the UNS S32760 was better than UNS S31600 in overall erosion-corrosion performance since the ferrite/austenite microstructure offers enhanced erosion resistance than the fully austenite in conjunction with the higher hardness. The behaviour of UNS S32760 in the DIZ indicated good level of ductility and erosion resistance, whilst in the OA the relatively good corrosive sliding abrasion resistance contributed to lower volume loss than UNS S31600. Many past studies reported the superiority of UNS S32760 against UNS S31600 in erosion-corrosion at pH 7 [7.8–7.10].

In CP conditions, the overall volume loss of UNS S32760 was similar to UNS S31600. Thus, the benefits of higher hardness were more evident in erosion-corrosion conditions rather than in CP (in both DIZ/OA) since the UNS S32760 showed lower enhanced erosion due to corrosion (synergy) than UNS S31600. The correlation between high hardness and synergy was noticed in chapter 5 too.

37WCI: The overall performance of 37WCI was equal to UNS S32760, whilst the contributions of pure mechanical damage, corrosion and synergy were very similar for

both alloys. However, the volumetric analysis demonstrated its vulnerability in the DIZ due to brittleness and Cr carbides fracture in conjunction with the plastic deformation of austenitic matrix, trend that was demonstrated also in chapter 5 (supported by the relevant literature). In the OA, due to presence of small eutectic Cr carbides, the 37WCI alloy depicted the optimum abrasion-corrosion resistance, which was higher even than the corresponding of type N1/D1 alloys that possessed higher hardness. Thus, it was evident that the hardness is not always a predictive tool about the corrosive sliding abrasion behaviour of alloys that contain complex microstructures.

Type N1 and D1 alloys: Both alloys precipitated by σ-phase showed the lowest volume loss form all tested alloys at pH 7. Obviously, the increased hardness provided enhanced erosion resistance, whilst their corrosion performance was superior over 37WCI and UNS S31600 and similar to UNS S32760. It should be noted that, in the literature, the common hardness of the studied alloys with σ-phase was around 330-370 HV [7.11–7.16]. Only in two past studies, an aged duplex stainless steel (UNS S32750) reached the maximum hardness of 440 HV, whilst, in both studies, the detrimental effects on impact toughness and corrosion resistance were emphasised [7.17, 7.18]. An important feature was that the formation of σ-phase of N1 and D1 was not seemed to impair the good ductility, which in conjunction with the high hardness resulted in much lower wear scar depth/VL_{DIZ}, according to post-test analysis. As it is well known, the brittle materials possess lower erosion resistance in nominal incidence rather than in low angle of attack [7.19], which was not the case for the two alloys with the σ-phase. Moreover, in the OA zone, the type N1 and D1 alloys were similar to UNS S32760 but worse than 37WCI due to enhanced abrasion due to corrosion and this can be associated with the multi-phase microstructure and the presence of chlorides.

In terms of corrosion resistance, it has been emphasised in past studies that σ phase has catastrophic consequences for duplex stainless steels [7.4, 7.18, 7.20]. In general, the small particles of σ phase are formed at the grains that lead to cracking due to corrosive attack [7.21]. In case of type N1 and D1 alloys, however, the σ-phase is present as large ''islands'' (with high hardness) which apparently contributed to a high

resistance to erosion-corrosion damage. Ravindranath et al. showed that coarse σ-phase does not impair the corrosion resistance on the grain boundaries (intergranular corrosion) and hence the corrosion rates were almost equal to those in annealed condition according to the static corrosion tests in ferric sulphate-sulphuric acid solution [7.22]. Thus, the results from the latter cited work were in good agreement with the corrosion rates of both type N1 and D1 alloys, even under SLEC conditions, in which they were equal or better compared to UNS S32760. An important observation was the fact that no researcher has conducted corrosion measurements on alloys with σ-phase in SLEC conditions.

7.5.2 Acidic conditions

UNS S31600: Under very strong acidic conditions, the UNS S31600 displayed substantially high corrosion rates contributing to major increase in volume loss from pH 7 to pH 0, whilst the synergy was slightly higher. An important feature was that the increase of TVL from pH 7 to pH 0 was noticed in the OA region (VL_{OA}) where the corrosion is enhanced, since in the DIZ the dominant mechanism is the erosion. However, the corrosion rate in the DIZ was still 2 times higher than the other materials. Apparently, the nominal 17% Cr along with the 2.5% Mo and 12% Ni were inadequate to protect UNS S31600 from the severe corrosion attack, which confirms that this alloy is unsuitable for erosion-corrosion operations at pH 0.

UNS S32760: The erosion-corrosion resistance of UNS S32760 in strong acids was relatively excellent since minor increase in volume loss compared to neutral pH. Some past studies have shown the very good corrosion resistance of UNS S32760 in either H_2SO_4 or HCl [7.23,7.24]. The main reason of low TVL of UNS S32760 in strong acidic medium was the low synergy, which was a result of very good corrosion resistance considering that the erosion was the same as in neutral conditions.

In terms of corrosion resistance, its performance was superior over the other materials. However, according to the corrosion tests on segmented coupons, the corrosion rates in the DIZ were slightly higher than those of type N1, D1 alloys and 37WCI, whilst in the OA the corrosion performance was similar to D1 and 37WCI. This important

finding implies that the UNS S32760 can handle better intermediate angles (full specimen) from corrosion aspect, probably due to reduced galvanic phenomena between different angles (i.e DIZ/OA) which possess different E_{corr}. Moreover, it is possible that the galvanic phenomena between DIZ/OA regions were affected by micro-galvanic interactions in the microstructure of the tested alloys (37WCI, type N1 and D1 alloys). Thus, it was evident that the electrochemical tests on segmented samples is an important tool for materials in-depth investigation.

37WCI: Unlikely the UNS S32760, the 37WCI depicted significant increase in volume loss from pH 7 to pH 0 due to enhanced Cr carbides fracture in the DIZ region compared to the corresponding at pH 7. As shown in chapter 5, the 37WCI suffered high synergy in the DIZ even at pH 3, which could be associated with hydrogen embrittlement (HE). Thus, it is possible that HE affected significantly its performance in the DIZ in the current tests. Also, it is believed the corrosion rates in the DIZ (as measured – Table 7.9) cannot produce such a high synergy in such small surface area and this supports the assumption of HE involvement. In the OA region, 37WCI showed high synergy too, which was associated with the multi-stage microstructure and the no uniform Cr and Mo dispersion. The latter is a good example about the importance of the material's microstructure into aggressive acidic slurry.

The performance of 37WCI alloy at pH 0 is generally in good agreement with the expectations of the Weir Group PLC and it should be emphasised that the most acidic environment in which this material is used is equal to pH 1.

Type N1 alloy: The Ni-Cr alloy displayed moderate erosion-corrosion behaviour (but superior over 37WCI) due to mainly the high synergy, which was located in the OA, whilst in the DIZ its performance was similar to UNS S32760. As in case of 37WCI, the complex microstructure of this alloy and especially the no uniform Cr and Mo dispersion generated the high synergy, whilst the corrosion rates were similar with the 37WCI alloy in either full specimen or DIZ/OA regions.

Thus, it can be concluded that the microstructure can affect significantly the erosion-corrosion resistance of high alloyed materials such as type N1 alloy in HCl mediums. The general performance of type N1 alloy at pH 0 was generally in line with the Weir

Group PLC expectations considering that this alloy is not used in acidic environment with chlorides content.

Type D1 alloy: The type D1 alloy showed the lowest volume loss than all tested alloys. The excellent erosion-corrosion performance of type D1 alloy was associated with the uniform distribution of Cr and Mo into the multi-phase microstructure and hence, this alloy managed to withstand the enhanced erosion due to corrosion. In the DIZ area, it depicted again (as at pH 7) the optimum erosion-corrosion resistance indicating the benefits from σ-phase since a combination of high hardness and good ductility was achieved. In the OA it was equal to UNS S32760 demonstrating much lower synergy compared with the UNS S31600, 37WCI and type N1 alloy materials.

The results of type D1 alloy in acidic environment showed the same trend with two past studies (same authors), whereas a sigmatised Cr-Ni stainless steel was compared with UNS S31600 [7.12], AISI 321 and X60 steel [7.13]. In addition, Lu et al. demonstrated that the σ phase provided enhanced corrosive abrasion resistance on stainless steels under strong acidic conditions (H_2SO_4) [7.16]. It is worth mentioning that in the latter study, the maximum fraction area of σ phase was 10%, much lower than in case of type D1 alloy.

In terms of corrosion performance, the type D1 alloy depicted the same behaviour with 37WCI/type N1 alloy in either full specimen's tests or segmented for the same reasons. However, from ranking point of view, it might be slightly superior over 37WCI and type N1 alloy since the linear polarisation tests showed slightly higher R_p values for a given time (Table 7.10).

According to the Weir Group PLC, the behaviour of type D1 alloy, in particular in the DIZ, was as expected. Despite the fact that this material is not utilised in acidic water with chlorides, it is characterised as an alloy that can withstand the erosion-corrosion phenomenon when the operating and environmental conditions are varying.

7.6 Conclusions

1) At pH 7, the overall erosion-corrosion performance of the type N1 and D1 alloys was superior over the rest of materials demonstrating the benefits

from the controlled σ-phase in erosion-corrosion. The 37WCI and UNS S32760 had similar behaviour followed by UNS S31600. Also, the high hardness was beneficial in erosion-corrosion conditions and not under CP application on the UNS S32760 and 37WCI alloys. On the other hand, the high hardness of type N1 and D1 alloys was favourable even in CP conditions. Consideration of volume loss in the different hydrodynamic regions led to different ranking of materials, which was dependent on their microstructure and properties. For instance:

a) In the DIZ, the balance between erosion resistance and ductility was the key factor for optimum performance. Hence, the type N1 and D1 alloys demonstrated the lowest volume loss since the σ-phase did not impair their ductility.

b) In the OA, the 37WCI showed the lowest volume loss which is related to small eutectic Cr carbides (17% in volume fraction). The latter is an indication that hardness is not the predominant factor for abrasive corrosion behaviour in materials with complex microstructure, since the type N1 and D1 alloys were inferior to 37WCI despite their higher hardness.

2) At pH 0, synergy was a crucial factor for materials ranking and was directly correlated to alloys' microstructure and uniform dispersion of Cr and Mo. In terms of total volume loss, the type D1 showed the best performance indicating the benefits of σ-phase even in strong acidic slurries. The UNS S32760 inferior only to type D1 alloy since it exhibited very good overall corrosion performance. The type N1 alloy was the third ranked material followed by 37WCI, whilst UNS S31600 exhibited the highest volume loss due to extremely high corrosion rates. As at neutral pH, the breakdown of volume loss in DIZ/OA regions showed different ranking but the two duplex grades were again superior over the other alloys.

3) Apart from the importance of volumetric analysis in different hydrodynamic regions, the investigation of corrosion in these areas individually is a useful tool for materials evaluation with complex and unique microstructure. This was portrayed in the fact that 37WCI, type

N1/D1 alloys and UNS S32760 possessed similar corrosion rates in the DIZ and OA at pH 0 but the latter alloy was superior when DIZ and OA were enabled simultaneously (whole specimen corrosion tests).

7.7 References

[7.1]   J.M. Pardal, S.S.M. Tavares, M.D.P.C. Fonseca, J.A. De Souza, L.M. Vieira, H.F.G. De Abreu, Deleterious phases precipitation on superduplex stainless steel UNS S32750: characterization by light optical and scanning electron microscopy, Mater. Res. 13 (2010) 401–407.

[7.2]   I. Calliari, M. Breda, E. Ramous, K. Brunelli, M. Pizzo, C. Menapace, Impact Toughness of an Isothermally Treated Zeron®100 SDSS, J. Mater. Eng. Perform. 21 (2012) 2117–2123.

[7.3]   M. Rosso, I. Peter, D. Suani, About heat treatment and properties of Duplex Stainless Steels, J. Achiev. Mater. Manuf. Eng. 59 (2013) 26–36.

[7.4]   K.W. Chan, S.C. Tjong, Effect of secondary phase precipitation on the corrosion behavior of duplex stainless steels, Materials (Basel). 7 (2014) 5268–5304.

[7.5]   M. Pohl, O. Storz, T. Glogowski, Effect of intermetallic precipitations on the properties of duplex stainless steel, Mater. Charact. 58 (2007) 65–71.

[7.6]   R. Magnabosco, Kinetics of sigma phase formation in a Duplex Stainless Steel, Mater. Res. 12 (2009) 321–327.

[7.7]   P. Paulraj, R. Garg, Effect of Intermetallic Phases on Corrosion Behavior and Mechanical Properties of Duplex Stainless Steel and Super-Duplex Stainless Steel, Adv. Sci. Technol. Res. J. 9 (2015) 87–105.

[7.8]   V.A.D. Souza, A. Neville, Corrosion and synergy in a WC-Co-Cr HVOF thermal spray coating - Understanding their role in erosion-corrosion degradation, Wear. 259 (2005) 171–180.

[7.9]   U. Malayoglu, A. Neville, Mo and W as alloying elements in Co-based alloys - Their effects on erosion-corrosion resistance, Wear. 259 (2005) 219–229.

[7.10] H. Meng, X. Hu, A. Neville, A systematic erosion-corrosion study of two stainless steels in marine conditions via experimental design, Wear. 263 (2007) 355–362.

[7.11] S.S.M. Tavares, J.M. Pardal, J.L. Guerreiro, A.M. Gomes, M.R. da Silva, Magnetic detection of sigma phase in duplex stainless steel UNS S31803, J. Magn. Magn. Mater. 322 (2010) L29–L33.

[7.12] Y.G. Zheng, Z.M. Yao, W. Ke, Erosion – corrosion resistant alloy development for aggressive slurry flows, Mater. Lett. 46 (2000) 362–368.

[7.13] Y. Zheng, Z. Yao, X. Wei, W. Ke, The synergistic effect between erosion and corrosion in acidic slurry medium, Wear. 186-187 (1995) 555–561.

[7.14] D. Dyja, Z. Stradomski, A. Pirek, Microstructural and fracture analysis of aged cast duplex steel, Strength Mater. 40 (2008) 122–125.

[7.15] E. Analysis, Microstructure and phase analysis of duplex stainless steel after heat treatment, (2005) 34–37.

[7.16] X.-C. Lu, S. Li, X. Jiang, Effects of σ phase in stainless steels on corrosive wear behavior in sulfuric acid, Wear. 251 (2001) 1234–1238.

[7.17] S. Topolska, Effect of microstructure on impact\ntoughness of duplex and superduplex\nstainless steels, J. Achiev. Mater. Manuf. Enginering. 36 (2009) 143–149.

[7.18] D. Zou, Y. Han, W. Zhang, J. Yu, Sigma phase precipitation and properties of super-duplex stainless steel UNS S32750 aged at the nose temperature, J. Wuhan Univ. Technol. Mater. Sci. Ed. 26 (2011) 182–185.

[7.19] I. Finnie, Erosion of surfaces by solid particles, Wear. 3 (1960) 87–103.

[7.20] J. Saithala, J. Clapp, J.D. Atkinson, H. Ubhi, S. Mahajanam, Effect of sigma phase on the environment assisted cracking of super duplex stainless steel in oil field environments, NACE Int. (2012) 1–12.

[7.21] C.-C. Hsieh, W. Wu, Overview of Intermetallic Sigma Phase Precipitation in Stainless Steels, ISRN Metall. 2012 (2012) 1–16.

[7.22] K. Ravindranath, S.N. Malhotra, The Influence of Aging on the Intergranular Corrosion of 22-Chromium 5-Nickel Duplex Stainless-Steel, Corros. Sci. 37 (1995) 121.

[7.23] R. Francis, The performance of stainless steels in concentrated sulphuric acid, Stainless Steel World. (2009) 2–5. www.stainless-steel-world.net.

[7.24] A.R. Francis, G. Byrne, G.R.W.W. Materials, P. Works, N. Heath, Experiences with Zeron 100 ® superduplex stainless steel in the process industries, 40

(1999) 613–624.

7.8 Appendix
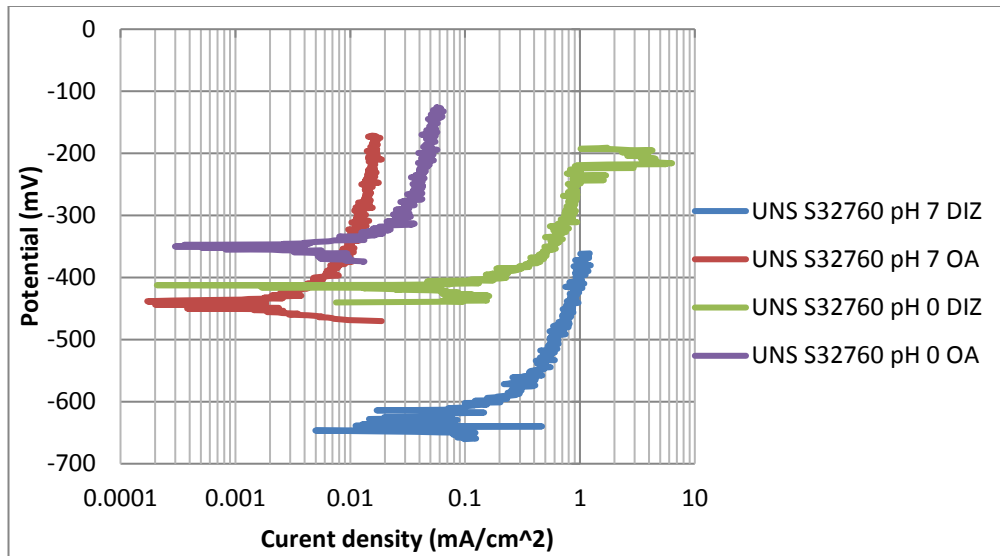
Figure 7.37: Anodic polarisation plots for UNS S32760 in the DIZ-OA regions at both pH levels.
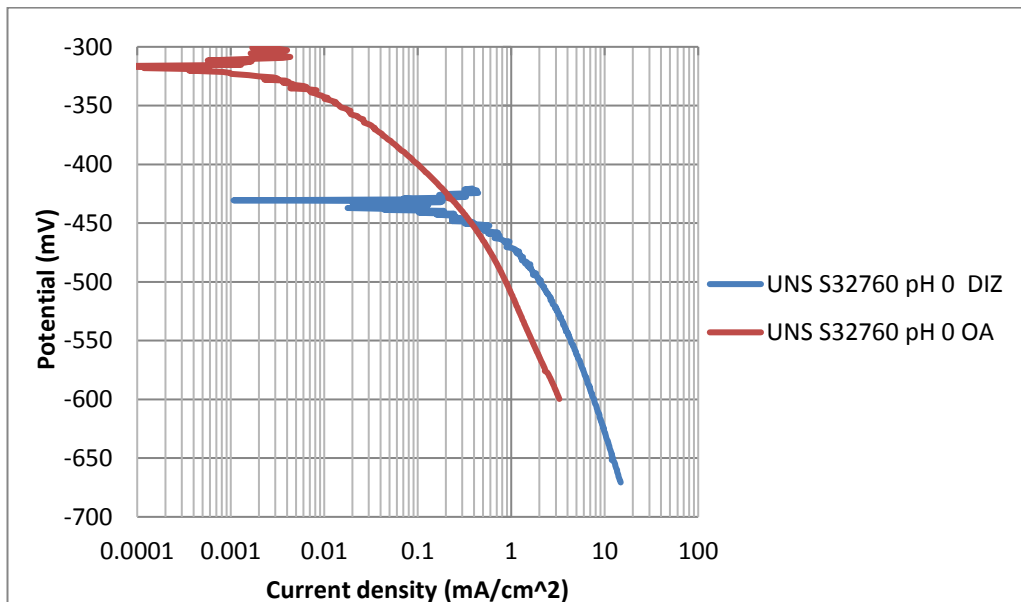
Figure 7.38: Cathodic polarisation plots for UNS S32760 in the DIZ-OA regions at pH 0.
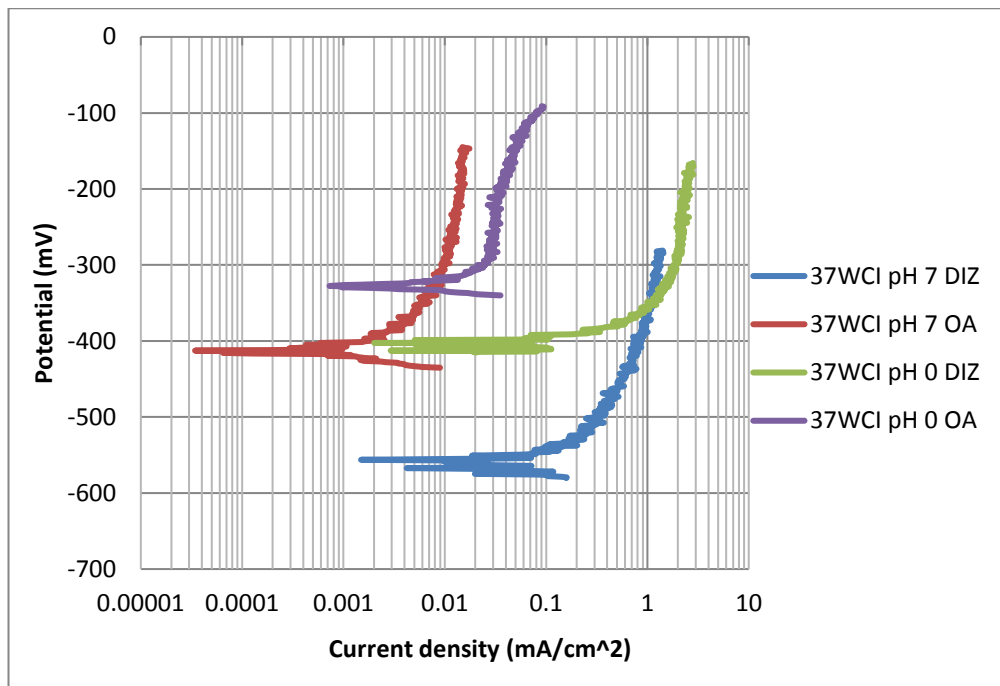
Figure 7.39: Anodic polarisation plots for 37WCI in the DIZ-OA regions at both pH levels.
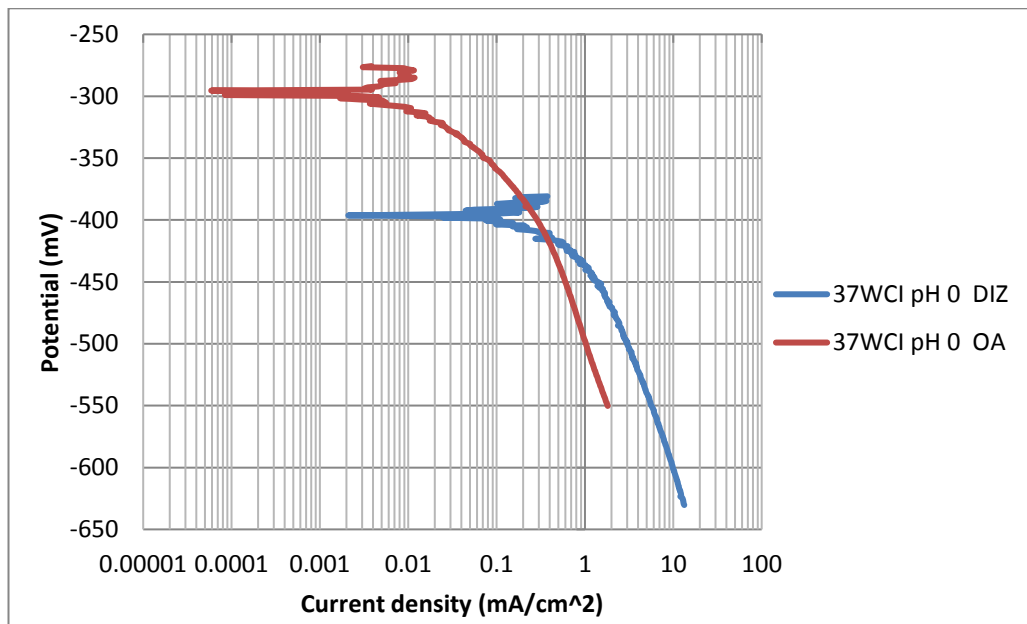
Figure 7.40: Cathodic polarisation plots for 37WCI in the DIZ-OA regions at pH 0
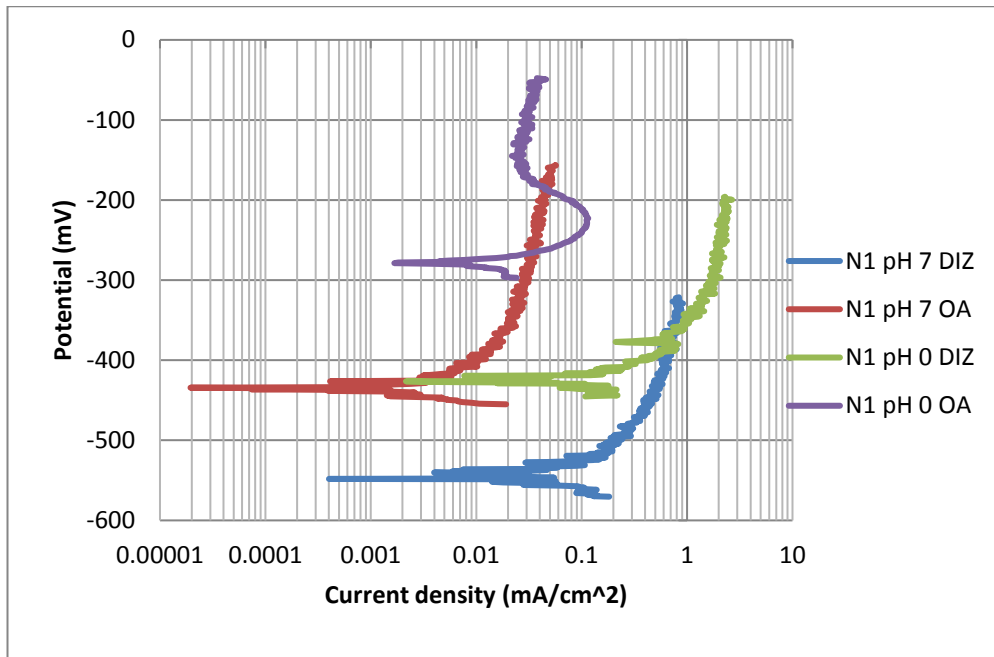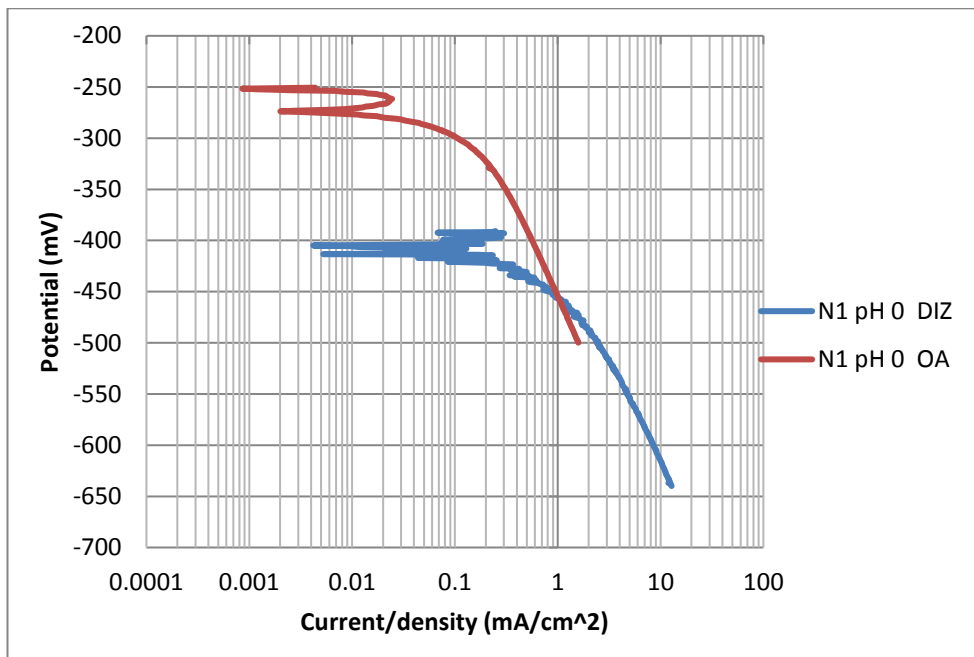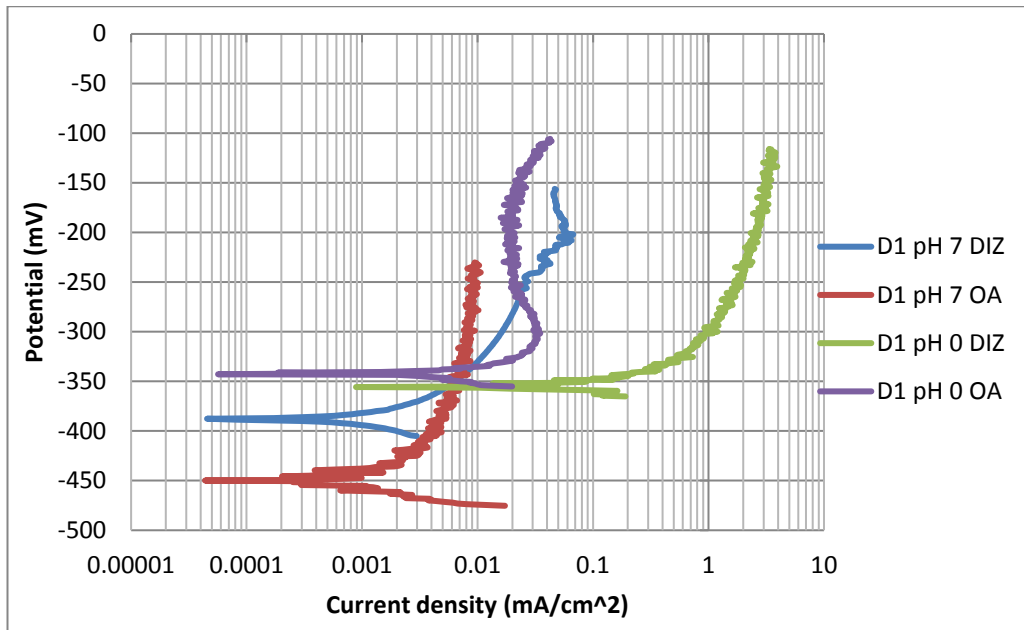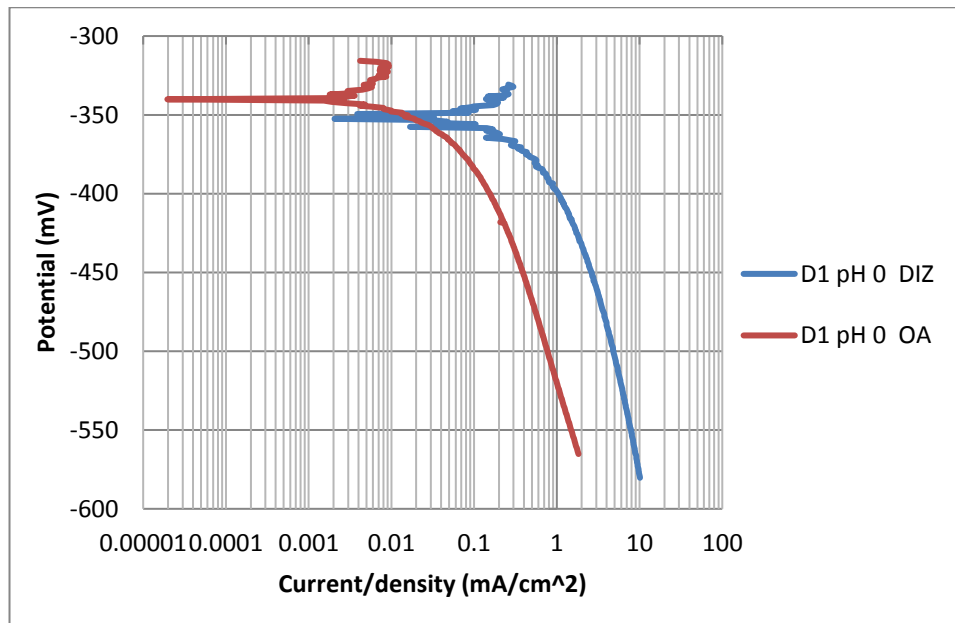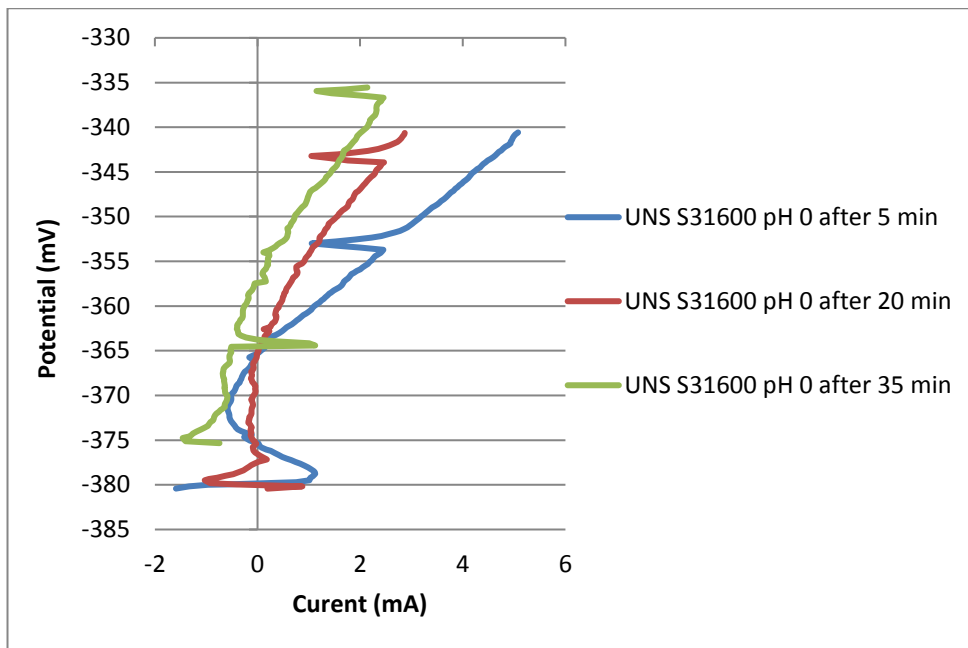
Figure 7.41: Anodic polarisation plots for N1 in the DIZ-OA regions at both pH levels.

Figure 7.42: Cathodic polarisation plots for N1 in the DIZ-OA regions at pH 0.

Figure 7.43: Anodic polarisation plots for D1 in the DIZ-OA regions at both pH levels.

Figure 7.44: Cathodic polarisation plots for D1 in the DIZ-OA regions at pH 0.

Figure 7.45: Linear polarisation plots for UNS S31600 in acidic conditions.
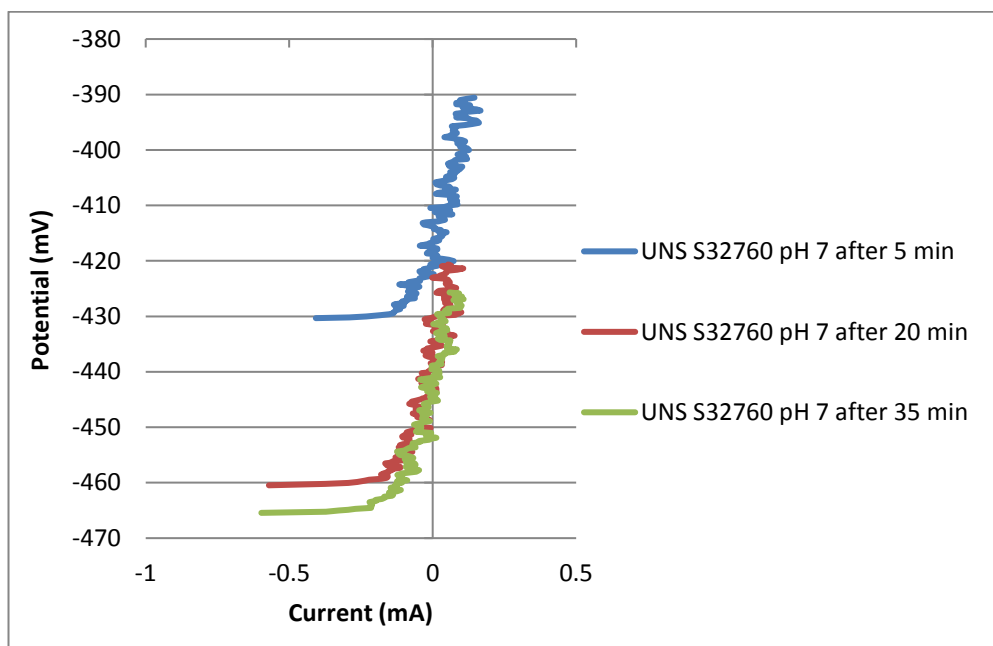
Figure 7.46: Linear polarisation plots for UNS S32760 in neutral conditions.
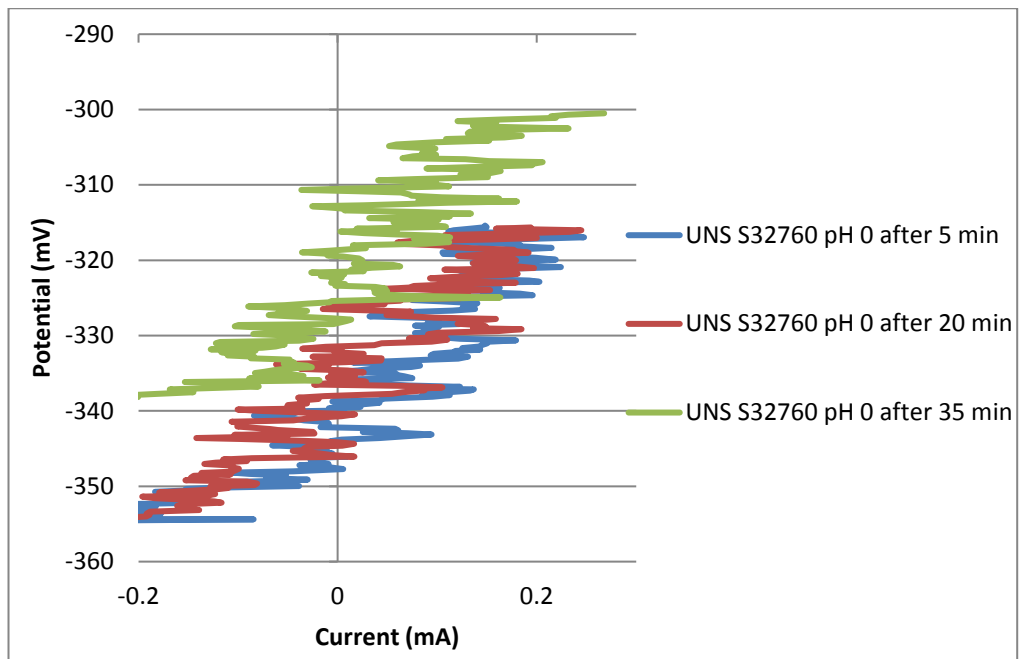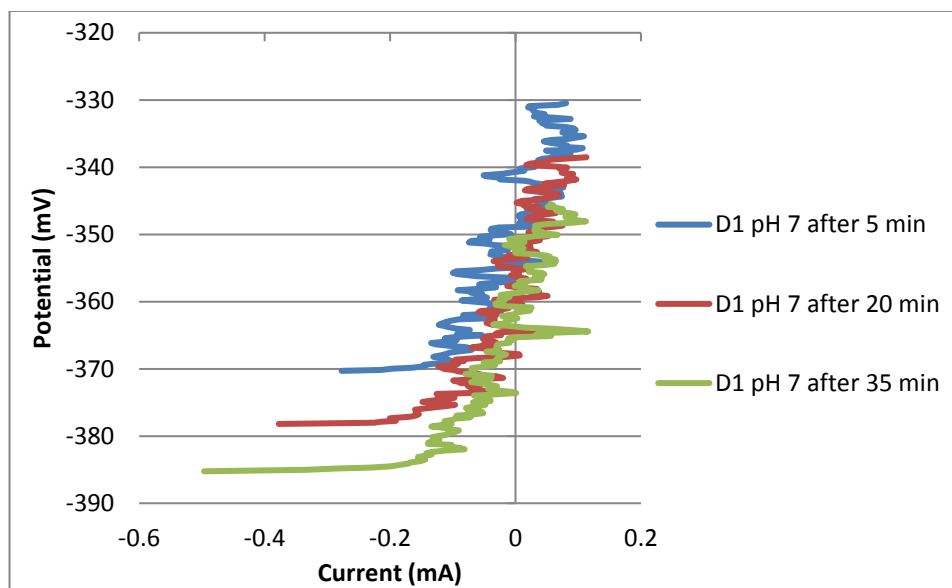
Figure 7.47: Linear polarisation plots for UNS S32760 in acidic conditions.
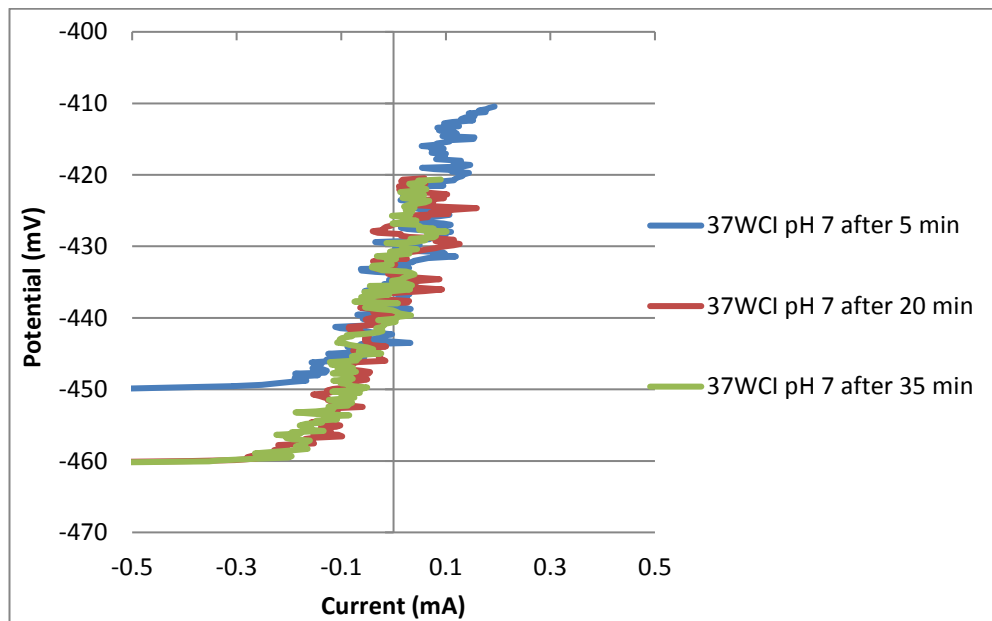
Figure 7.48: Linear polarisation plots for 37WCI in neutral conditions.
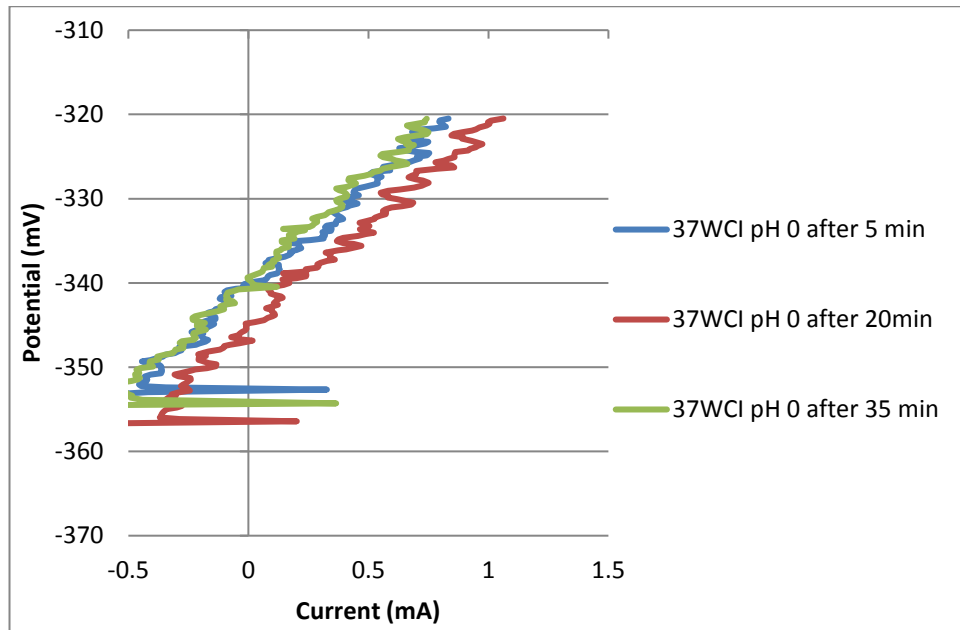
Figure 7.49: Linear polarisation plots for 37WCI in acidic conditions.
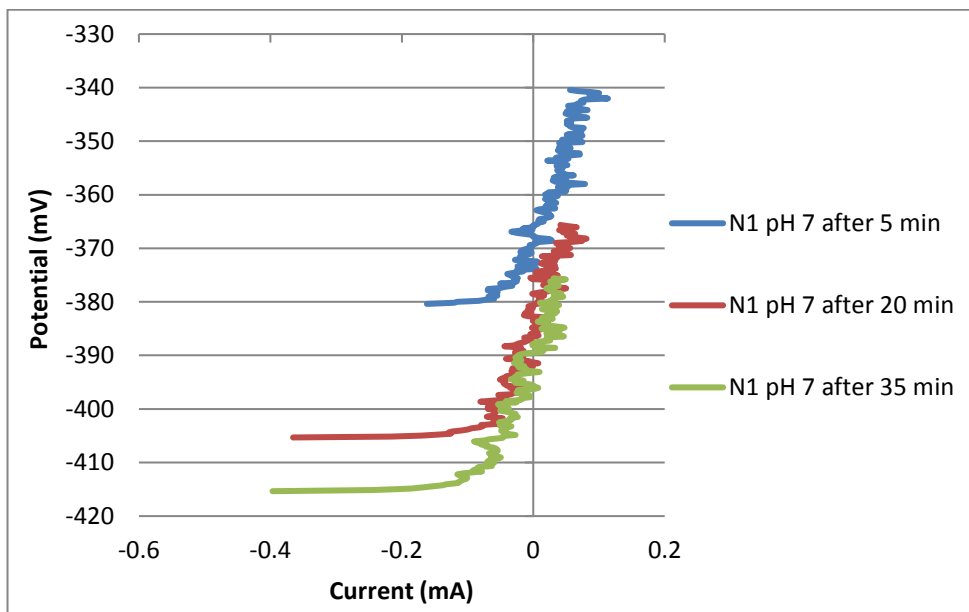
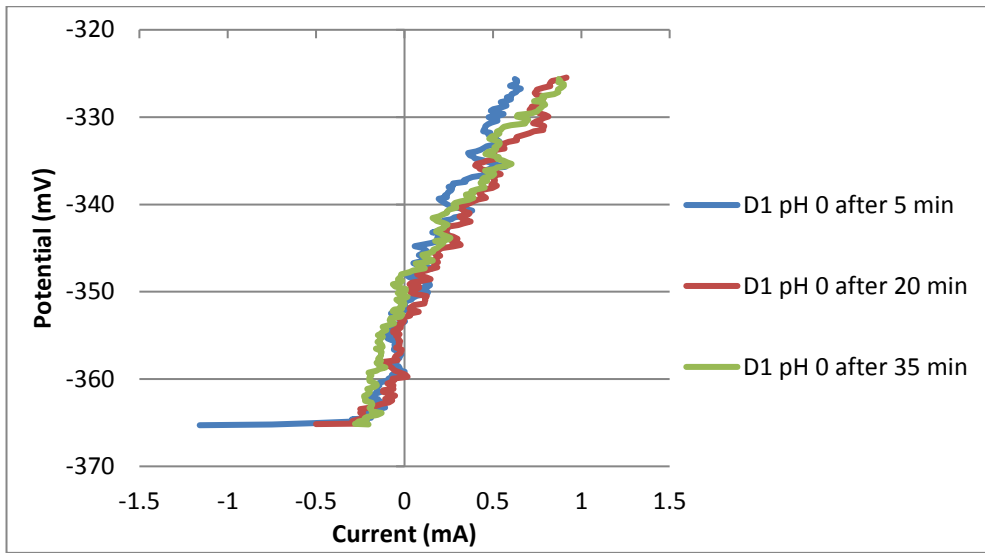Figure 7.50: Linear polarisation plots for N1 in neutral conditions.
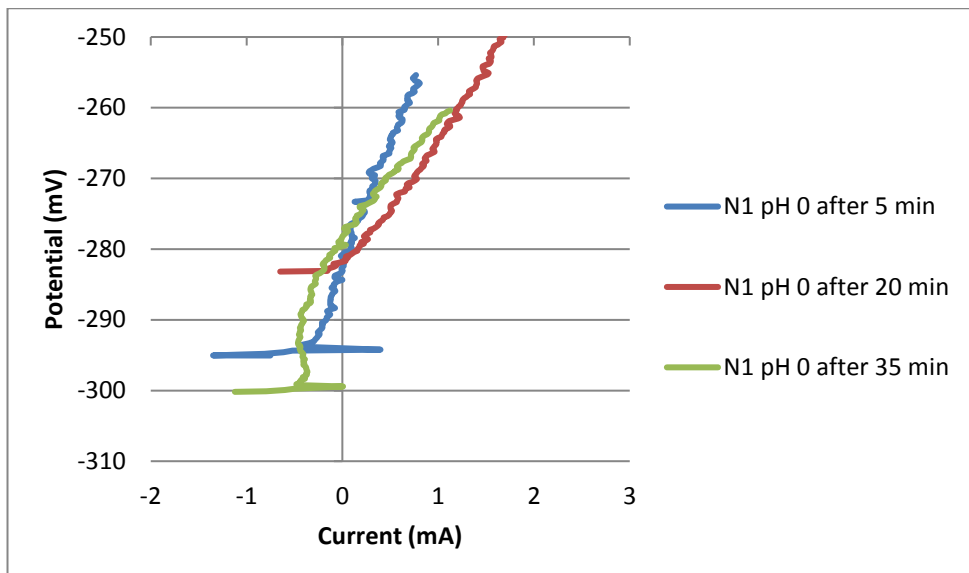
Figure 7.51: Linear polarisation plots for N1 in acidic conditions.

Figure 7.52: Linear polarisation plots for D1 in neutral conditions.

Figure 7.53: Linear polarisation plots for D1 in acidic conditions.

Chapter 8

The effect of salinity on erosion-corrosion performance of white cast irons and UNS S31600

8.1 Introduction

In this chapter, the effect of salinity on the erosion-corrosion performance of white cast irons (WCI) and UNS S31600 and has been investigated. A motivation for this study is based on the fact that very little work has been conducted by others on the effect of salinity on corrosion and much less with regards to the effect on erosion-corrosion. In addition, it is known that the mining industry extracts and processes a variety of ores containing various chloride contents so this creates a situation in which material selection becomes a major issue. From a materials perspective, a commercially available WCI with high volume fraction of carbides (CVF) and poor corrosion resistance that has not been tested in the previous chapters was added in the current experimental phase. The rationale for including this alloy was to complete the entire erosion-corrosion investigation on WCIs with respects to the CVF and the corresponding corrosion resistance.

8.2 Materials and methods

8.2.1 Materials

The materials investigated at different salinity levels under erosion-corrosion conditions are the same as presented in the chapter 6 apart from the 27WCINb (which includes niobium carbides) which was replaced with 30WCI. The 30WCI alloy is usually used in mining applications where abrasion occurs due to the presence of fine particles. However, due to its poor corrosion resistance, the use of 30WCI is largely dependent on the environmental/corrosive conditions that the material is exposed to.

The following materials were therefore evaluated:

- UNS S31600 (as the reference material)
- 27WCI
- 38WCI
- 30WCI

In terms of the microstructure, the UNS S31600, 27WCI and 38WCI were evaluated in previous chapters and hence, no further analysis was required in the current chapter. The 30WCI is a hypereutectic containing 30% Cr and 4.5% C supplied by the Weir Group PLC and is usually utilised in mining operations in which high abrasion rates in relatively non-corrosive environments (pH 6-14 and fresh water) occur. Figure 8.1 demonstrates its microstructure which consists of a fine distribution of hard primary Cr carbides (light colour), eutectic Cr carbides (light colour) and secondary carbides in a heat treated martensitic matrix (dark colour). The CVF is 50% whereas the remaining 25% is primary Carbides and the balance is 25% as eutectic Cr carbides, whilst the eutectic matrix is 50%. Table 8.1 demonstrates the bulk hardness and the hardness on the individual phases of the 30WCI alloy.
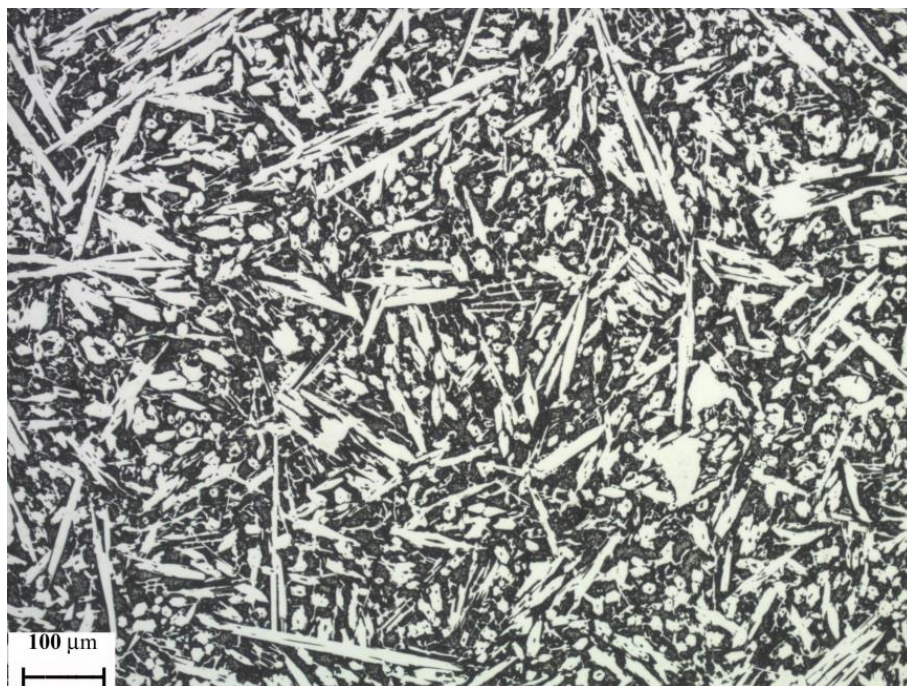

Figure 8.1: Microstructure of 30WCI [etched].

Table 8.1: Hardness values for 30WCI and constituent phases.

Bulk hardness HV$_{5kgf}$	Matrix hardness HV$_{200gf}$	Matrix hardness HV$_{200gf}$
900±10	670±40	1350±100

Figure 8.2 and Table 8.2 display the Cr content spot chemical analysis of a polished/etched 30WCI sample which involves Energy Dispersive Spectroscopy (EDS) determination on the Scanning Electron Microscope (SEM). Spectra 1 and 3 illustrate the Cr content in the eutectic matrix which had an average value around 11.5%. It should be noted that the Weir Group PLC quoted 8% Cr in the martensitic matrix. This implies that in chemical analysis presented in Figure 8.2 and Table 8.2, some secondary Cr carbides were included and hence explains why the Cr content was slightly higher. Spectrum 2 presents the Cr carbides which was enriched in Cr, as expected.
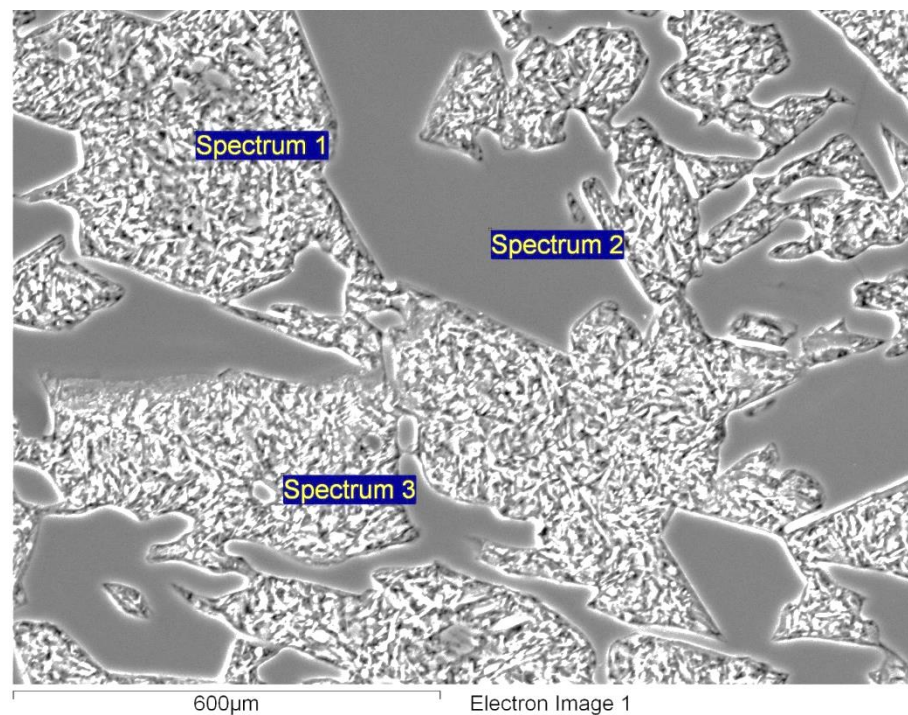

Figure 8.2: Spot chemical analysis on 30WCI [etched].

Table 8.2: Spot analysis of Figure 2.

Spectra	Cr %
Spectrum 1	12
Spectrum 2	62
Spectrum 3	11

8.2.2 Testing conditions - methods

The testing regimes in the current chapter were 0.05% NaCl and 10% NaCl at pH 7. The low salinity level ensured the simulation of the fresh water providing also adequate electrical conductivity for the electrochemical tests. Since the same testing conditions were implemented as in the chapter 6, the above NaCl concentrations are compared with the 3.5% NaCl (pH 7) results which, as a matter of completeness, are presented in this chapter. However, the 30WCI alloy was tested in seawater (3.5% NaCl) under erosion-corrosion and cathodic protection conditions (CP). It should be noted that the pure mechanical damage was considered the same in all different NaCl levels and hence, the CP results for UNS S31600, 27WCI and 38WCI alloys were obtained from chapter 6. Calibration tests at 3.5% NaCl of UNS S31600 were carried out periodically and the volume loss were the same as in previous chapter (1.49 mm^3 on average).

The erosion-corrosion assessment includes (as in previous chapter):

- Volume loss measurements after 1h solid-liquid erosion-corrosion (SLEC) tests.
- Electrochemical measurements on the whole and segmented tested samples via anodic polarisation and linear polarisation curves.
- Microscopic views of the tested specimens.
- Post-test analysis which includes surface profiling and volumetric analysis.

8.3 Results

8.3.1 Volume loss

Figure 8.3 presents the average volume loss of materials under study in different levels of salinity and under CP conditions. In fresh water, the 27WCI was the optimum material, followed by 38WCI and UNS S31600, whilst the 30WCI exhibited the highest volume loss. In the seawater environment, the 27WCI was slightly better than 38WCI and both alloys were superior over UNS S31600 and especially 30WCI. In 10% NaCl testing regime, there was a noticeable change in materials ranking; the 38WCI was superior over 27WCI followed by UNS S31600 and 30WCI. Finally, in CP conditions, 27WCI and 38WCI provided the best mechanical resistance, whilst UNS S31600 and 30WCI followed. An interesting observation was that all materials displayed lower volume loss in CP conditions than at 0.05% NaCl indicating the presence of corrosion plus synergistic effects, especially in the case of more corrosion resistant alloy such as UNS S31600 and 38WCI. Also, the two latter materials demonstrated minor changes in the overall volume loss but that was not the case for 27WCI and in particular, for the 30WCI.
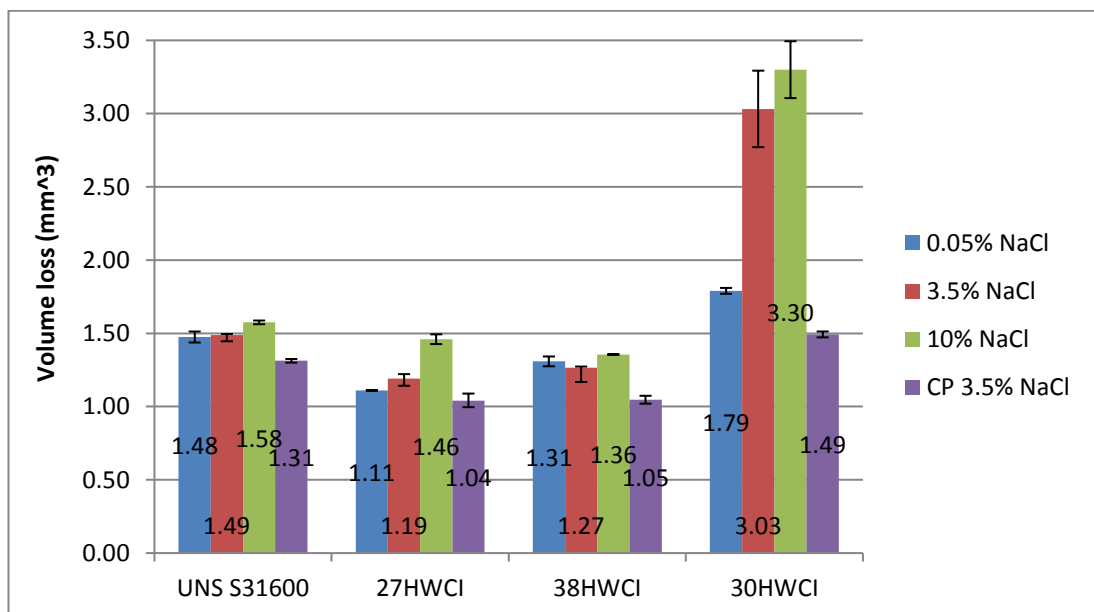

Figure 8.3: Average volume loss of materials under study in different NaCl solutions after 1h SLEC/CP tests.

8.3.2 Electrochemical tests

8.3.2.1 Anodic polarisation scans

The anodic polarisation curves for all materials/environments are shown below. As a matter of optimum presentation of the results, each alloy is presented in the three different conditions and therefore, all alloys are compared at each NaCl level.

Figures 8.4-8.7 demonstrate the anodic polarisation curves of individual materials in the three NaCl solutions. A common observation for all the tested alloys was that the corrosion rates increased with the increase of NaCl. UNS S31600 showed minor changes in all testing conditions but that was not the case for all WCIs.
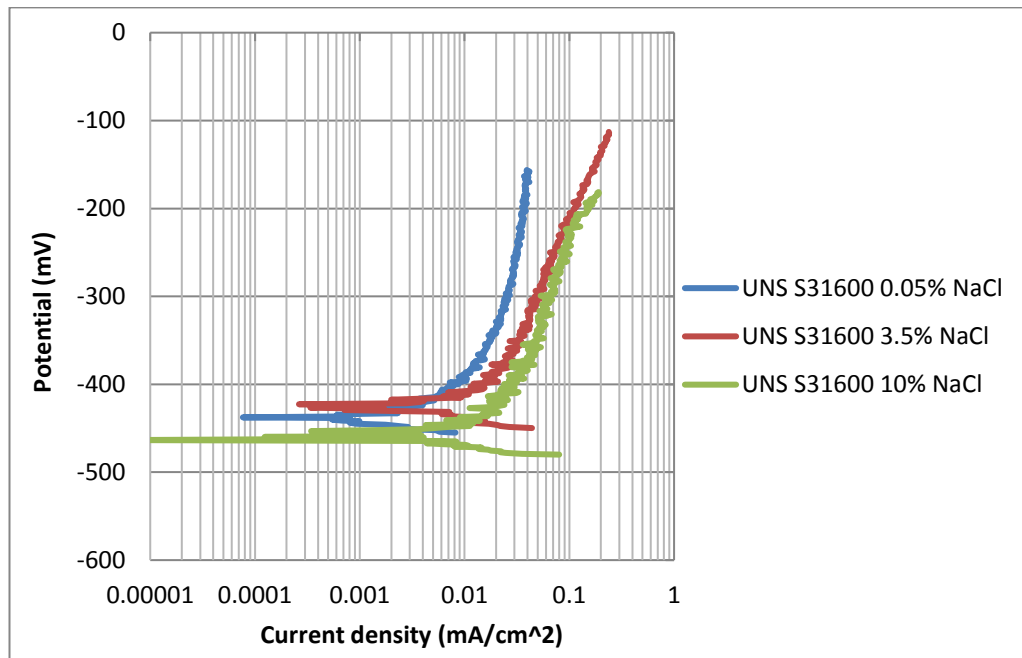
Figure 8.4: Anodic polarisation plots for UNS S31600 under SLEC conditions in three different salinity levels.
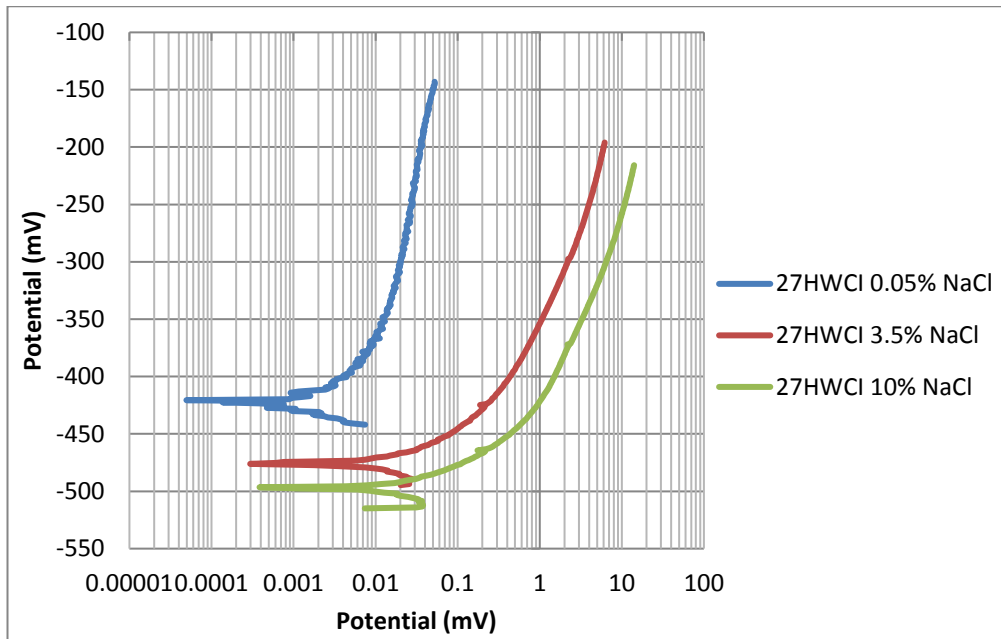
Figure 8.5: Anodic polarisation plots for 27WCI under SLEC conditions in three different salinity levels.
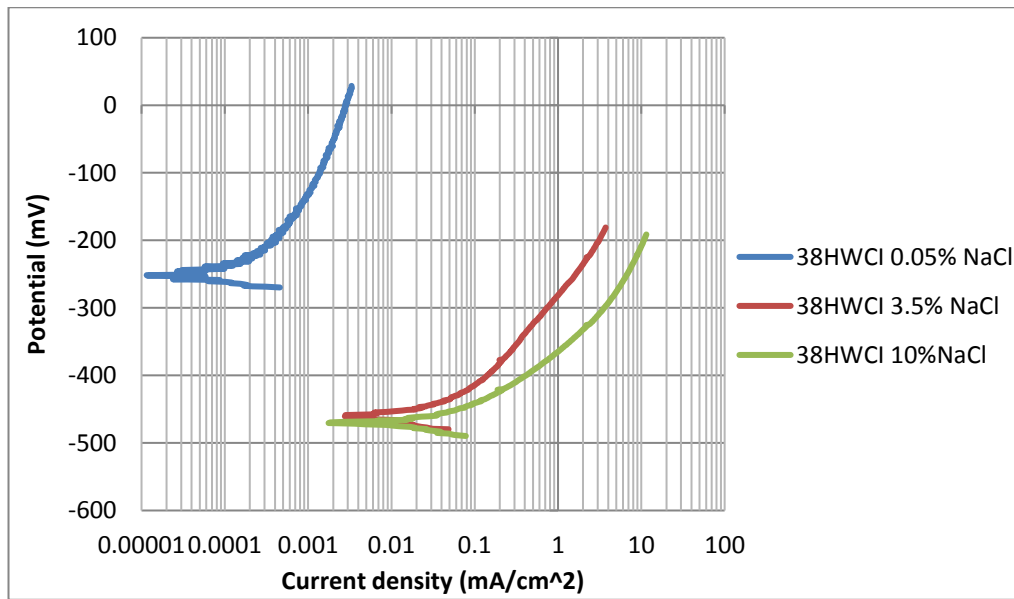

Figure 8.6: Anodic polarisation plots for 38WCI under SLEC in three different salinity levels.
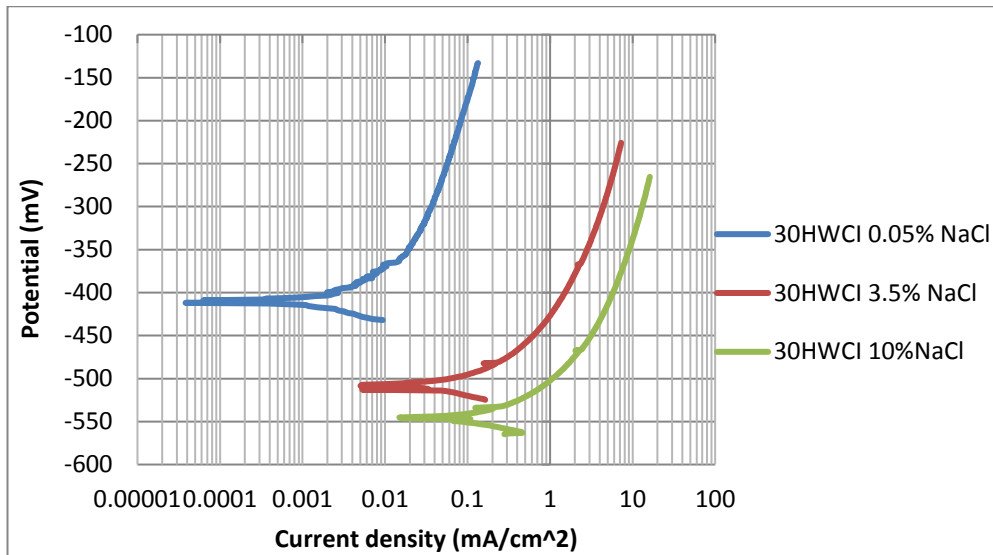
Figure 8.7: Anodic polarisation plots for 38WCI under SLEC conditions in three different salinity levels.

Furthermore, Figures 8.8-8.10 show the comparison of anodic polarisation curves of all materials in 0.05%, 3.5% and 10% NaCl, whilst in Table 8.3, the i_{corr} values and volume loss due to corrosion are presented. In fresh water, the WCIs, especially the 38WCI, were superior over UNS S31600, whilst by increasing the salinity, the UNS S31600 showed clear superiority. In all salinity levels, 38WCI showed the lowest corrosion rate compared to the other WCIs followed by 27WCI and 30WCI.
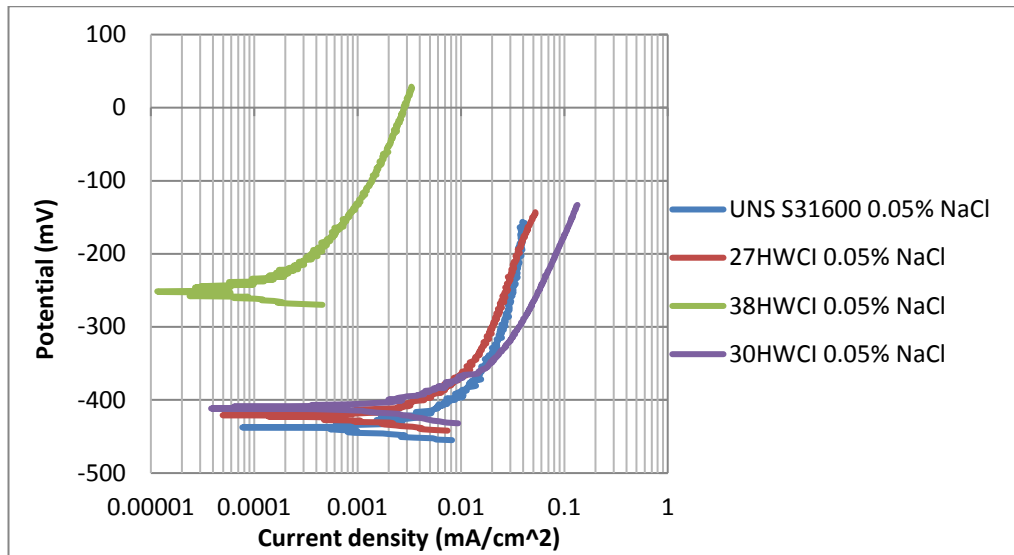
Figure 8.8: Anodic polarisation curves for materials under SLEC conditions at 0.05% NaCl.
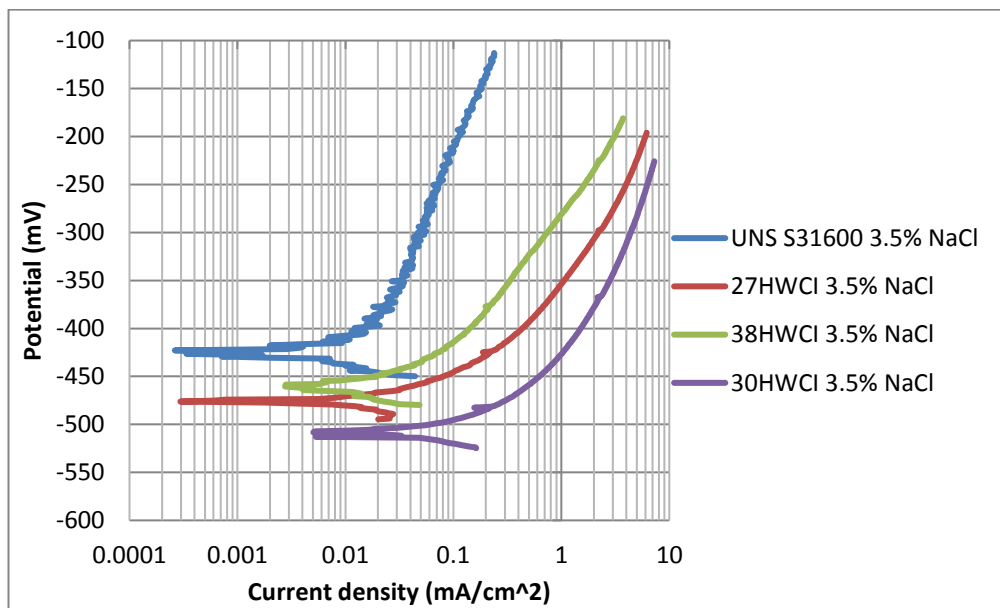

Figure 8.9: Anodic polarisation curves for materials under SLEC conditions at 3.5% NaCl.
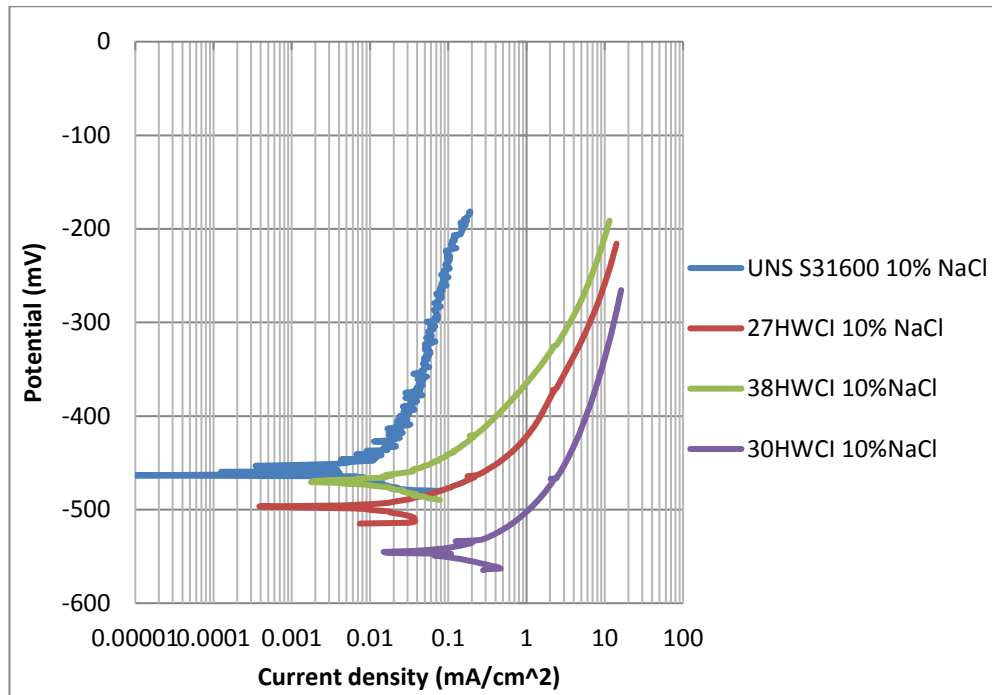
Figure 8.10: Anodic polarisation curves for materials under SLEC conditions at 10% NaCl.

Table 8.3: Electrochemical data for materials under study.

Material/%NaCl	i_{corr} (mA/cm^2)	Volume loss (mm^3)
UNS S31600/0.05	0.014	0.019
27WCI/0.05	0.008	0.012
38WCI/0.05	0.0002	0.000
30WCI/0.05	0.012	0.018
UNS S31600/3.5	0.017	0.02
27WCI/3.5	0.11	0.16
38WCI/3.5	0.05	0.08
30WCI/3.5	0.3	0.44
UNS S31600/10	0.025	0.035
27WCI/10	0.26	0.390
38WCI/10	0.13	0.200
30WCI/10	0.8	1.210

8.3.2.2 Segmented specimens - Anodic polarisation scans

Figures 8.11-8.14 display the anodic polarisation curves for materials under study in all salinity levels. A general observation was that all materials in all NaCl concentrations showed higher corrosion rates in the DIZ than in OA region due to impact erosion. However, the volume loss in the DIZ was lower than in the OA due to the fact that the OA was much greater area. It should be noted that the tests of 30WCI at 0.05% and 3.5% NaCl were unobtainable as a result of equipment limitations.

Tables 8.4-8.6 demonstrate the i_{corr} values and the corresponding volume loss in all NaCl solutions. It was noticed that the effect of NaCl concentration in the OA region resulted to the same materials ranking as in the total specimens, as presented in the previous section. However, this was not the case for the DIZ which is discussed in further below.
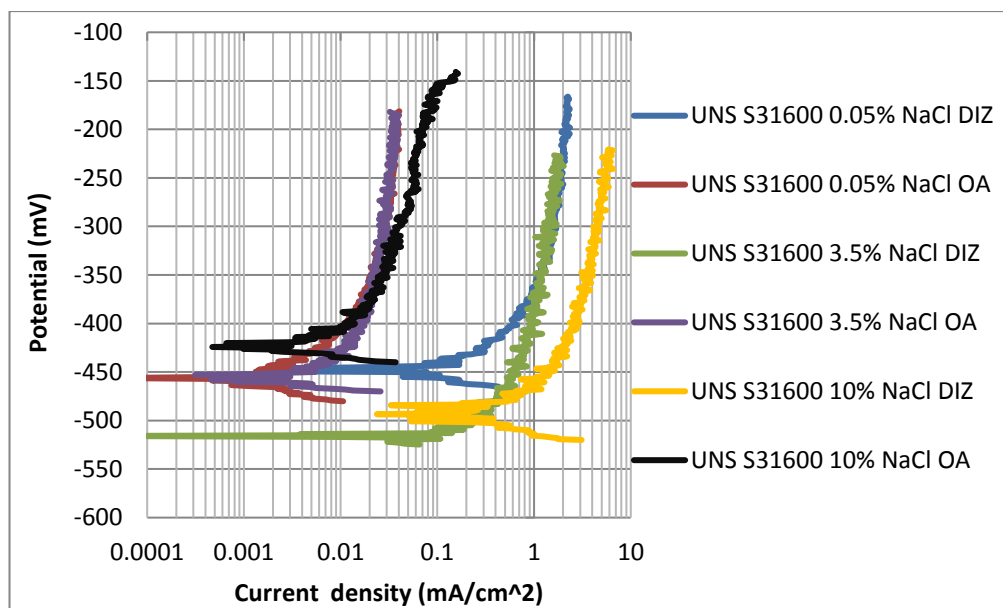

Figure 8.11: Anodic polarisation scans of UNS S31600 at DIZ-OA regions under different salinity levels.
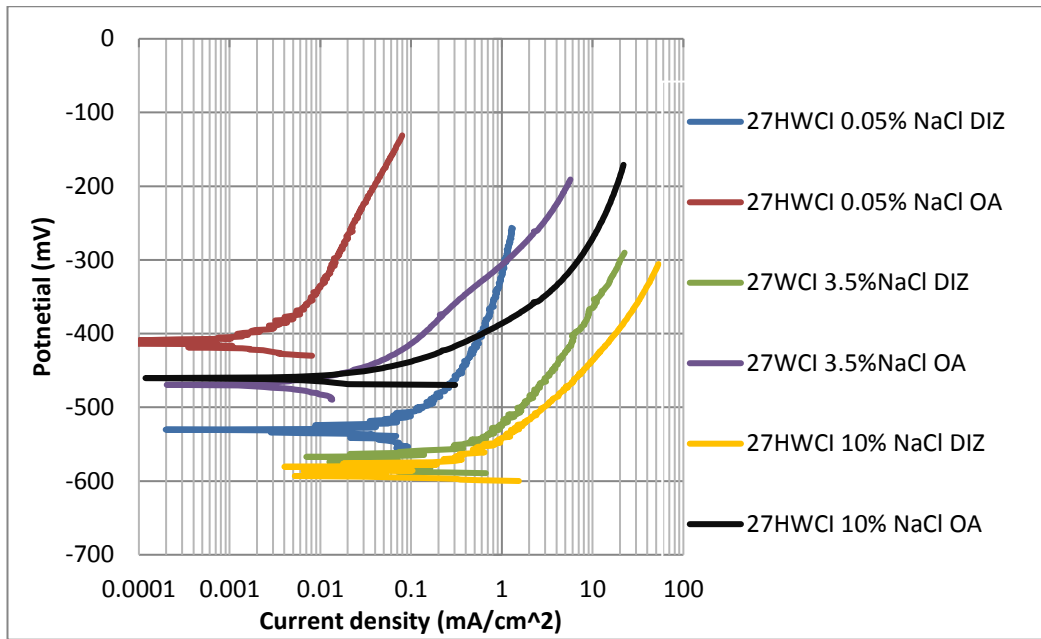
Figure 8.12: Anodic polarisation scans of 27WCI at DIZ-OA regions in different salinity levels.
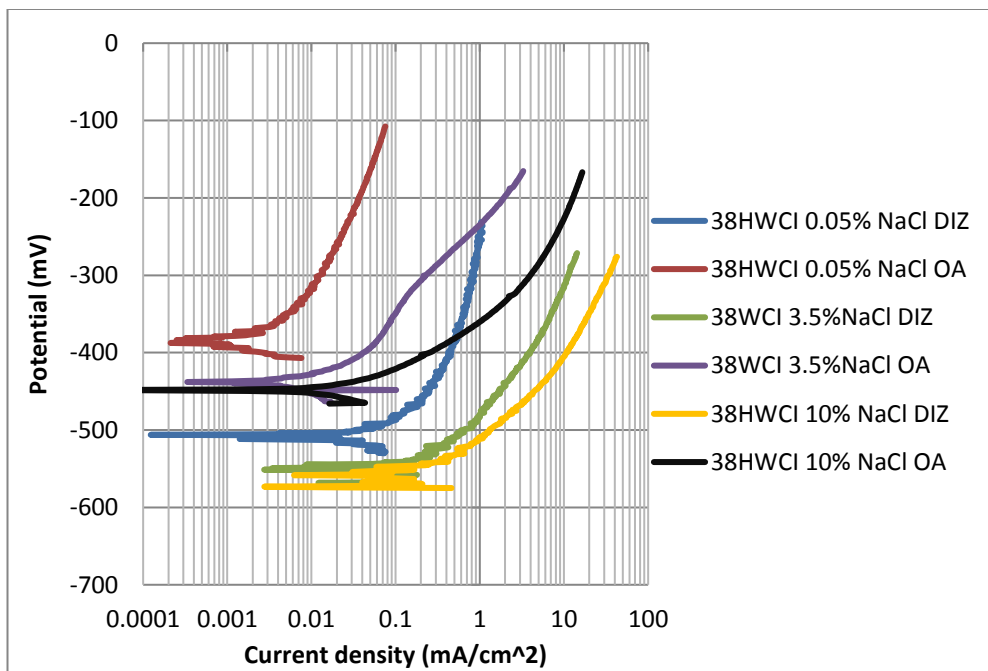

Figure 8.13: Anodic polarisation scans of 38WCI at DIZ-OA regions in different salinity levels.
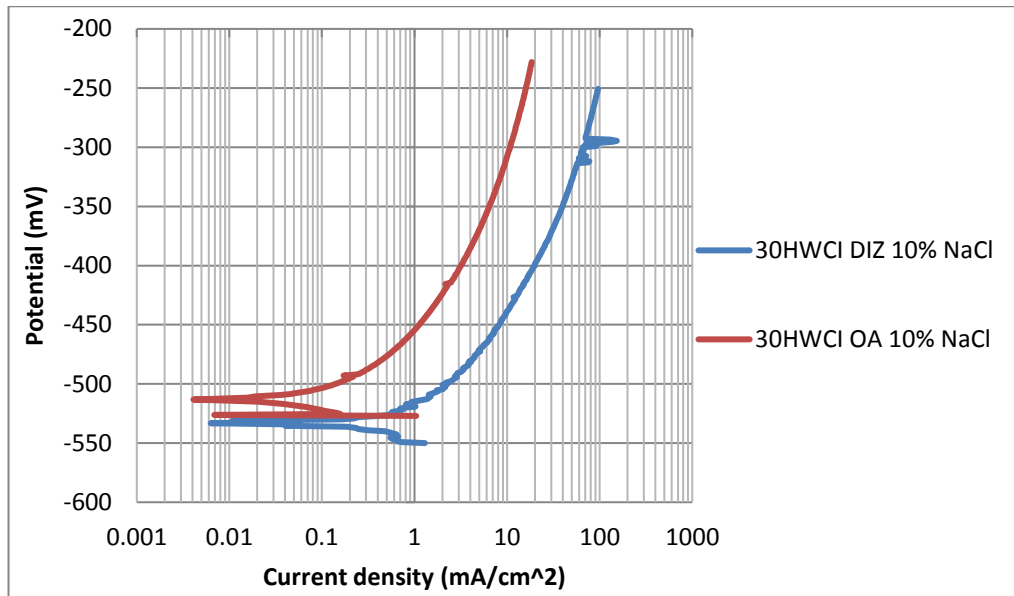
Figure 8.14: Anodic polarisation scans of 30WCI at DIZ-OA regions in 10%NaCl.

Table 8.4: Electrochemical data for materials under study in 0.05% NaCl.

Material/region	i_{corr} (mA/cm^2)	Volume loss (mm^3)
UNS S31600 DIZ	0.6	0.01
UNS S31600 OA	0.01	0.01
27WCI DIZ	0.13	0.003
27WCI OA	0.05	0.007
38WCI DIZ	0.18	0.004
38WCI OA	0.004	0.005
30WCI DIZ/OA	N/A	N/A

Table 8.5: Electrochemical data for materials under study in 3.5% NaCl.

Material/region	i_{corr} (mA/cm^2)	Volume loss (mm^3)
UNS S31600 DIZ	0.55	0.01
UNS S31600 OA	0.01	0.01
27WCI DIZ	0.65	0.01
27WCI OA	0.03	0.04
38WCI DIZ	0.40	0.01
38WCI OA	0.02	0.03
30WCI DIZ/OA	N/A	N/A

Table 8.6: Electrochemical data for materials under study in 10% NaCl.

Material/region	i_{corr} (mA/cm^2)	Volume loss (mm^3)
UNS S31600 DIZ	1.2	0.03
UNS S31600 OA	0.01	0.02
27WCI DIZ	0.70	0.02
27WCI OA	0.11	0.16
38WCI DIZ	0.45	0.01
38WCI OA	0.10	0.15
30WCI DIZ	2.00	0.05
30 WCI OA	0.55	0.81

8.3.2.3 Linear polarisation scans

Further consideration about the corrosion rates of materials under study was carried out through linear polarisation scans. A typical representation is displayed in Figure 8.15 which shows UNS S31600 linear polarisation curves at 0.05% NaCl, whilst the rest of alloys are shown as an Appendix to this chapter (Figures 8.31-8.41). Table 8.7 shows the R_p values from which the following features were observed:

- Lower Rp values (high corrosion rates) with increasing the NaCl concentration.
- Generally similar materials ranking as from the i_{corr} values from the full anodic polarisation curves.
- For a given material/pH value, R_p values are generally similar over the experimental exposure time. This is indicative of a broadly constant corrosion rate with time.
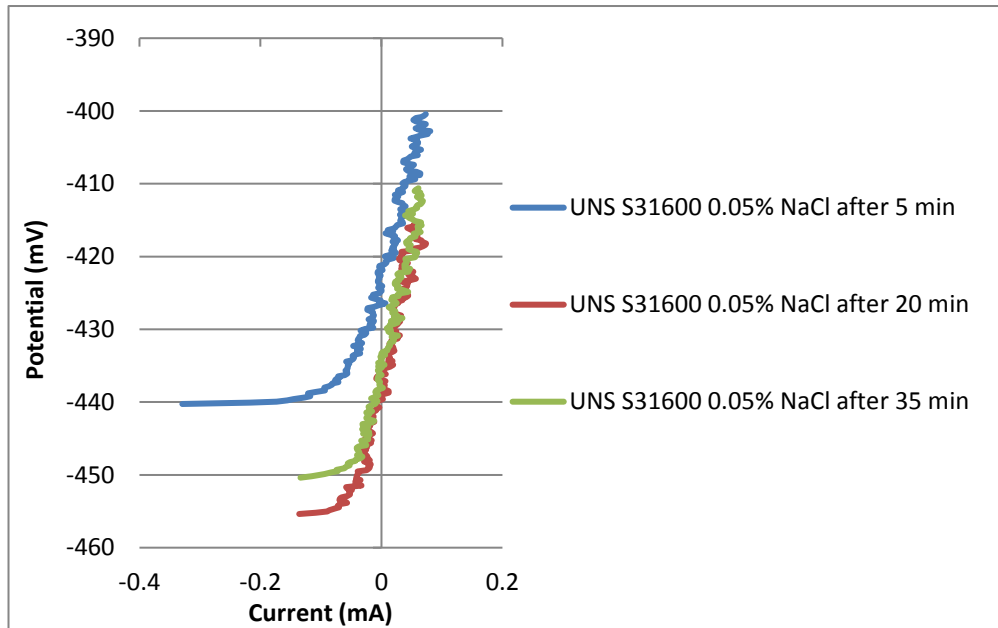

Figure 8.15: Linear polarisation curves for UNS S31600 at 0.05% NaCl.

Table 8.7: Linear polarisation data for materials under study in all NaCl solutions.

Material/%NaCl	R_p (Ohm) after 5 min	R_p (Ohm) after 20 min	R_p (Ohm) after 35 min
UNS S31600/0.05	400	400	400
UNS S31600/3.5	120	120	120
UNS S31600/10	100	100	90
27WCI/0.05	371	400	400
27WCI/3.5	38	36	37
27WCI/10	24	18	18
38WCI/0.05	6000	6000	5600
38WCI/3.5	71	69	60
38WCI/10	33	25	20
30WCI/0.05	360	333	333
30WCI/3.5	20	16	16
30WCI/10	10	8	5

8.3.3 Post-test analysis

8.3.3.1 Surface profiling

Figure 8.16 demonstrates the wear scar depths for materials under study in all testing environments. At 0.05% NaCl, the 27WCI alloy depicted the lowest wear scar, followed by UNS S31600, 38WCI and 30WCI. In seawater, again 27WCI was the best material, whilst UNS S31600 and 38WCI displayed similar wear scar depths, followed by 30WCI. On the other hand, at 10% NaCl, the 38WCI alloy experienced slightly the lowest wear scar depth, followed by 27WCI, UNS S31600 and 30WCI. In CP conditions, the UNS S31600 and 27WCI/38WCI illustrated similar wear scars, whilst 30WCI showed again the deepest damage.
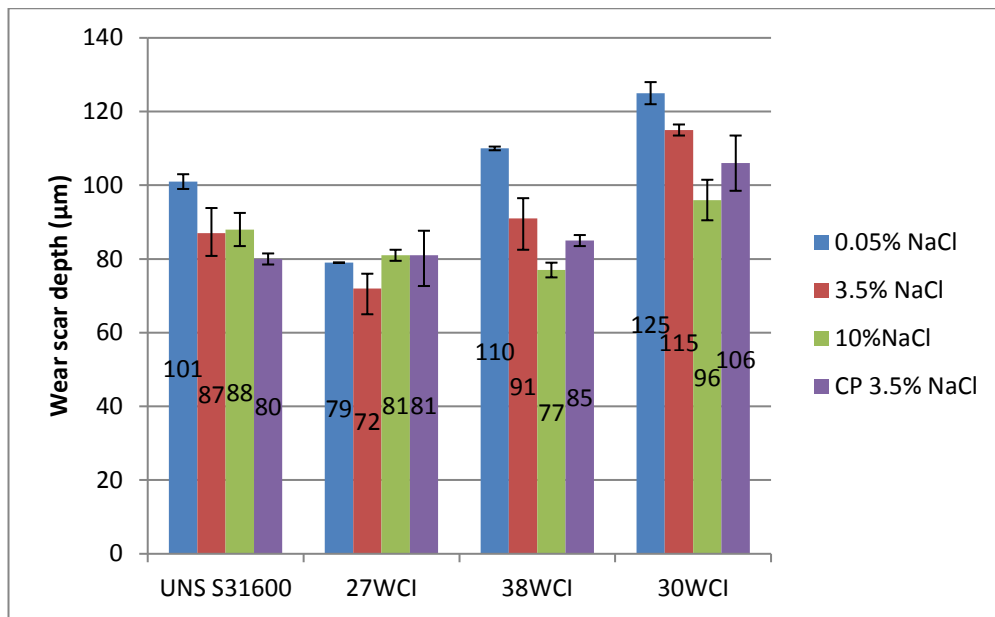
Figure 8.16: Average wear scar depths for materials under study in all testing environments.

8.3.3.2 Volumetric analysis

Figures 8.17-8.20 present the volume loss in the different hydrodynamic zones (DIZ-OA) for tested materials. In fresh water, the 27WCI alloy was slightly better than UNS S31600 in the DIZ, whilst 38WCI and 30WCI displayed higher volume loss. In the OA, 27WCI and 38WCI showed the lowest volume loss, whilst UNS S31600 and 30WCI experienced similar performance. In seawater, the performance of 30WCI was inferior to the rest of materials in both hydrodynamic zones. The comparison of UNS S31600-37WCI-38WCI had been presented in the previous chapter. At 10% NaCl, UNS S31600 was superior over the WCIs in the DIZ, followed by 38WCI/27WCI and finally 30WCI. In the OA, the 38WCI was the optimum alloy, followed by 27WCI, UNS S31600 and finally 30WCI which displayed substantial difference compared to the other materials. In CP conditions, the 30WCI showed better sliding abrasion only compared to UNS S31600, whilst in the DIZ displayed the highest volume loss.
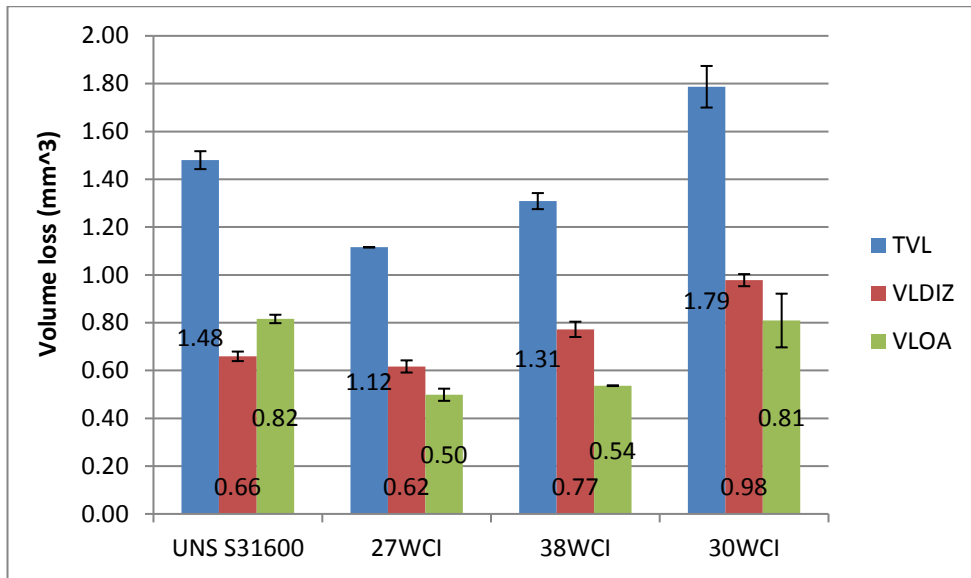
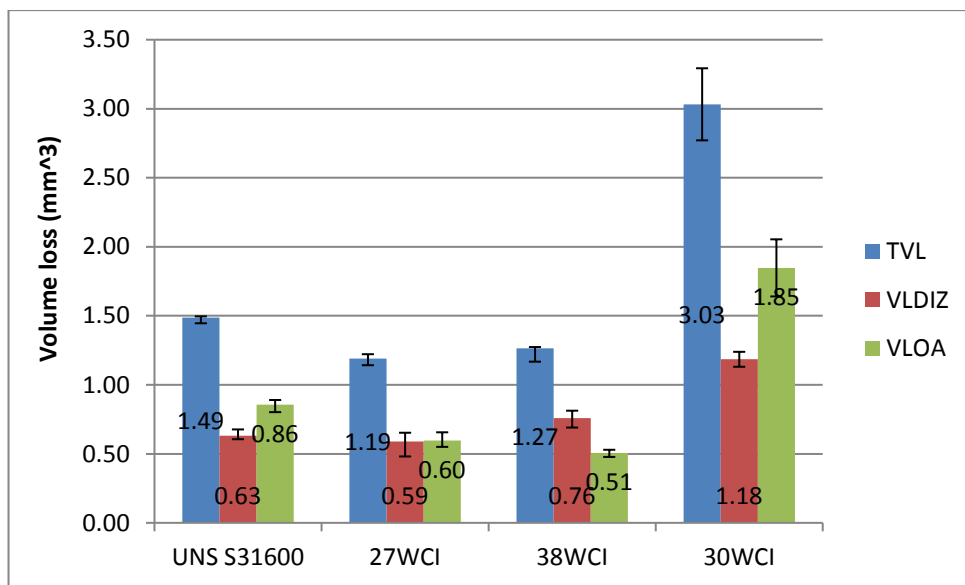Figure 8.17: Breakdown of average volume loss at 0.05% NaCl.

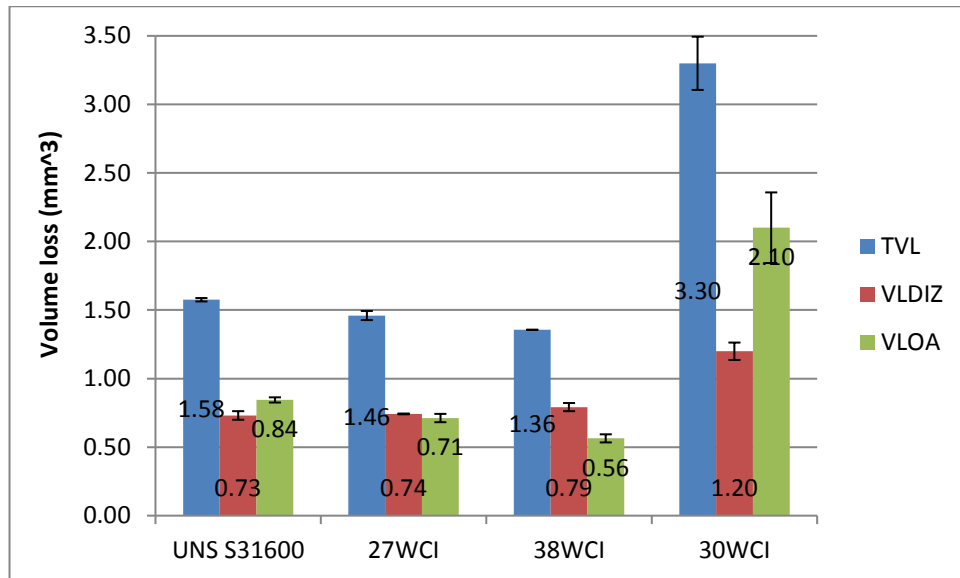Figure 8.18: Breakdown of average volume loss at 3.5% NaCl.

Figure 8.19: Breakdown of average volume loss at 10% NaCl.

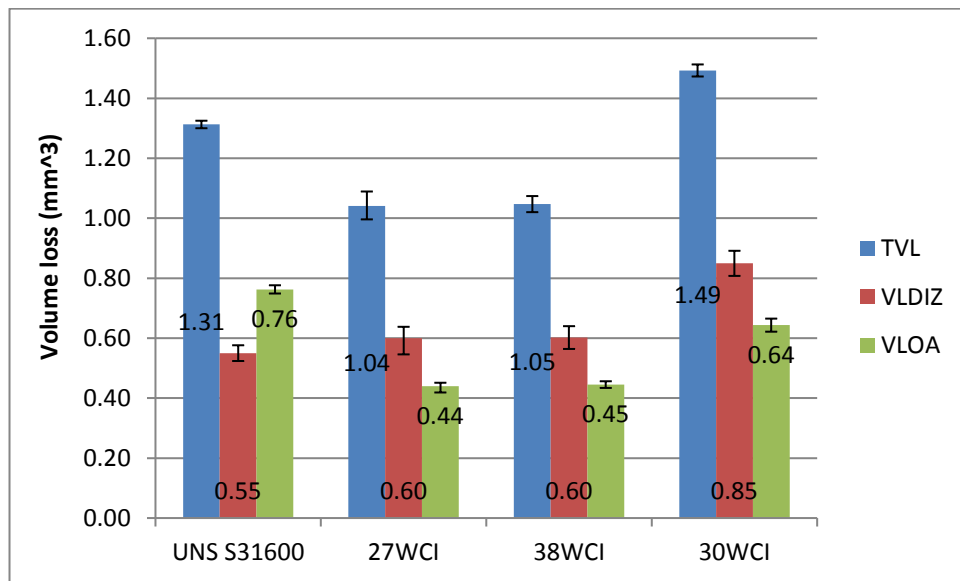Figure 8.20: Breakdown of average volume loss in CP conditions.

As it has been shown in chapter 5, that the deeper wear scars are not associated necessarily with higher VL_{DIZ} and this was noticed in the current experimental phase. As shown in Figures 8.21-8.22, the deepest regions in the wear scar of UNS S31600 and 30WCI at 10% NaCl are maintained in relatively high values for longer distance

than in case of 0.05% NaCl conditions and hence it is possibly to be the reason for the highest VL_{DIZ} in the brine water compared to the fresh solution.
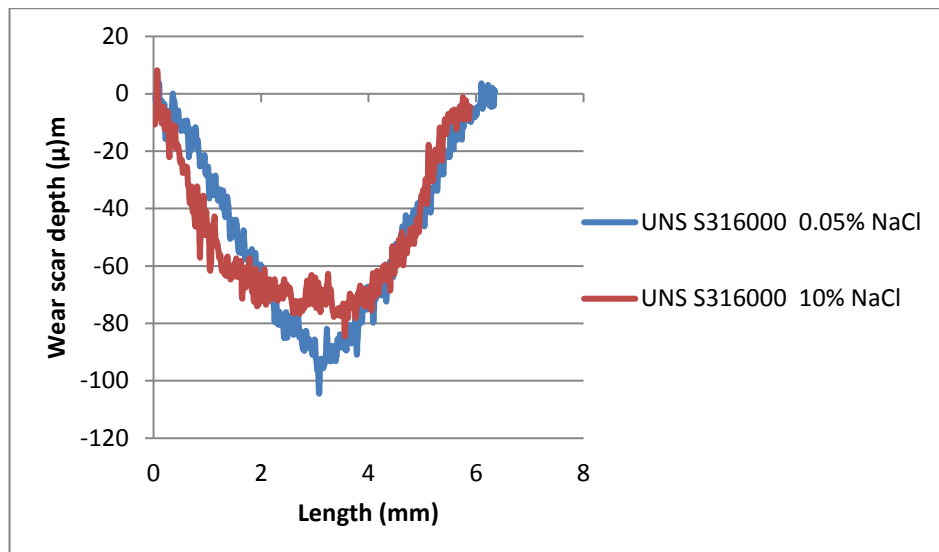

Figure 8.21: Wear scar profile of UNS S31600 at 0.05% and 10% NaCl.
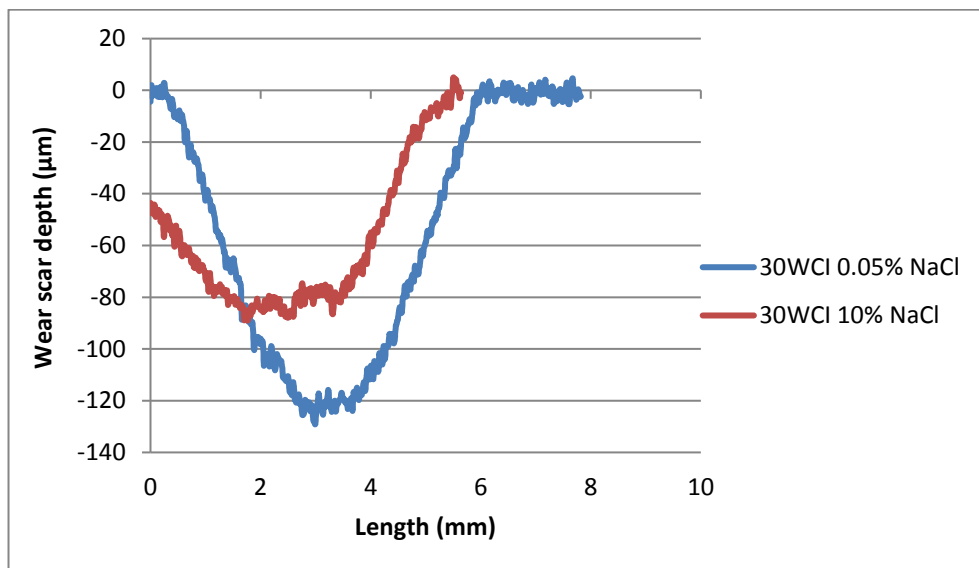

Figure 8.22: Wear scar profile of 30WCI at 0.05% and 10% NaCl

8.3.3.3 Microscopic post-test evaluation

Figure 8.23 demonstrates the microscopic view of 27WCI in the OA at 0.05% NaCl in which no corrosion attack was evident - common characteristic for all WCIs. In the Appendix of this chapter, Figures 8.42-8.43 show the OA of 27WCI and 38WCI at 10% NaCl respectively, in which very little corrosion was observed. On the contrary, as shown in Figures 8.44-8.45, the corrosive attack was obvious on 30WCI at 3.5% and 10% NaCl respectively. Also, in Figure 8.46, the "comets" pitting corrosion further on the OA region is presented.
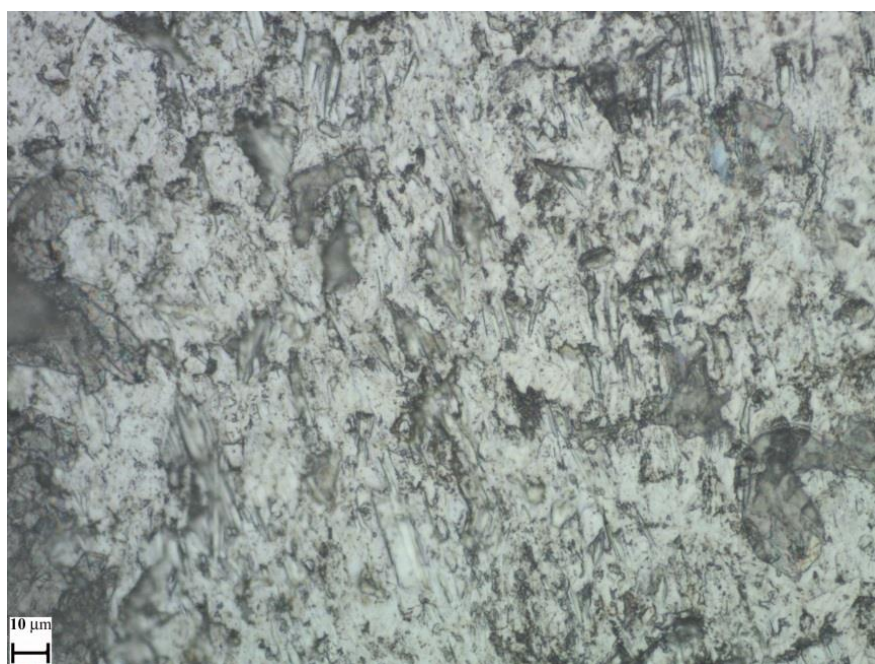
Figure 8.23: Microscopic view of 27WCI OA at 0.05% NaCl.

8.3.3.4 Crack investigation on 30WCI

The crack investigation method, which was demonstrated in previous chapters, was implemented on 30WCI to investigate further the poor erosion-corrosion performance in the DIZ. As a matter of consistency, a tested coupon in seawater was cross sectioned and polished as was presented in all WCIs earlier in this thesis. Figure 8.24 shows the DIZ area of 30WCI in which a significant crack was observed. The same crack is displayed in Figures 8.25-8.26 at higher magnifications indicating the crack initiation

from the primary Cr carbides which eventually is occurring in the eutectic matrix too. Additionally, cracks were found even in the OA which is the explanation for the poor sliding abrasion resistance of 30WCI (Figure 8.27).
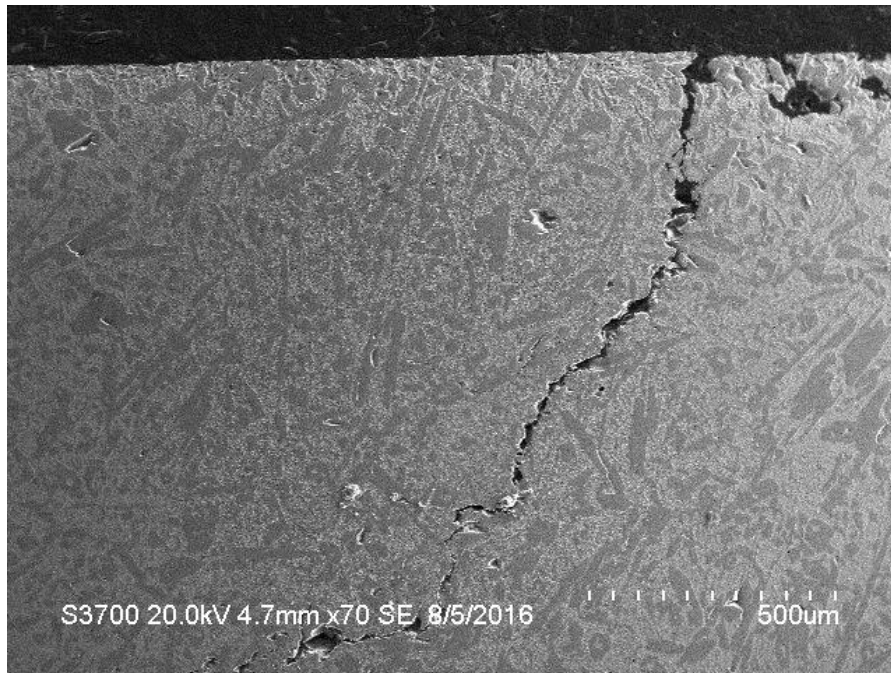

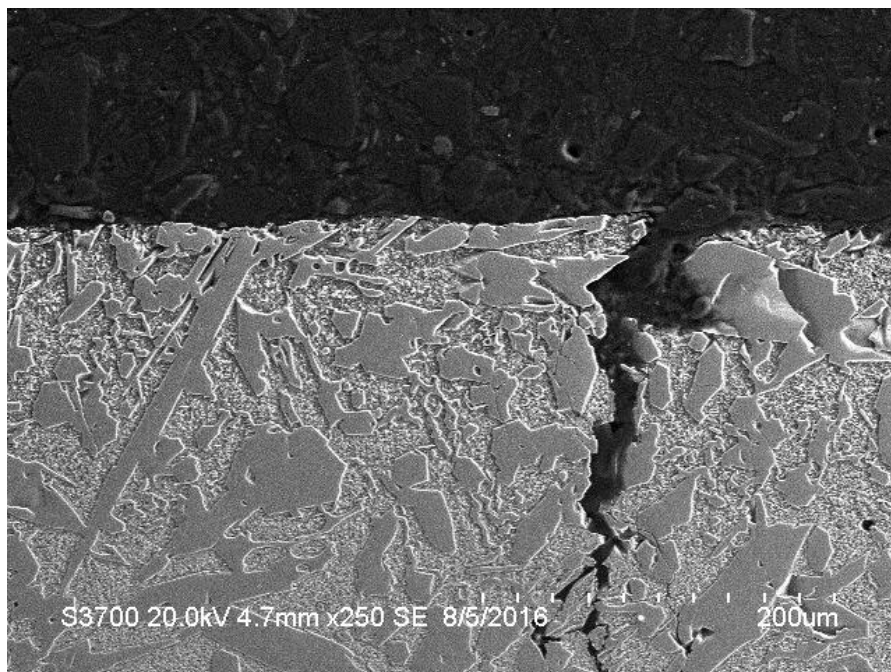Figure 8.24: Crack on 30WCI in the DIZ at 3.5% NaCl [etched].

Figure 8.25: Crack on 30WCI (same as in Figures 8.40) in the DIZ at 3.5% NaCl in high magnification [etched].
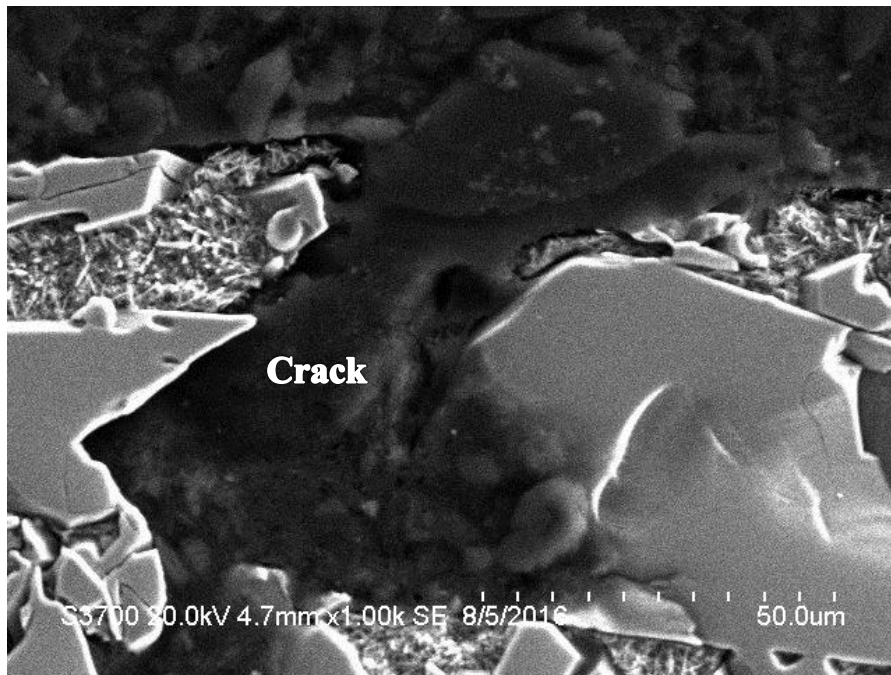
Figure 8.26: Mouth of Crack on 30WCI (same as in Figures 8.40-8.41) in the DIZ at 3.5% NaCl in high magnification [etched].
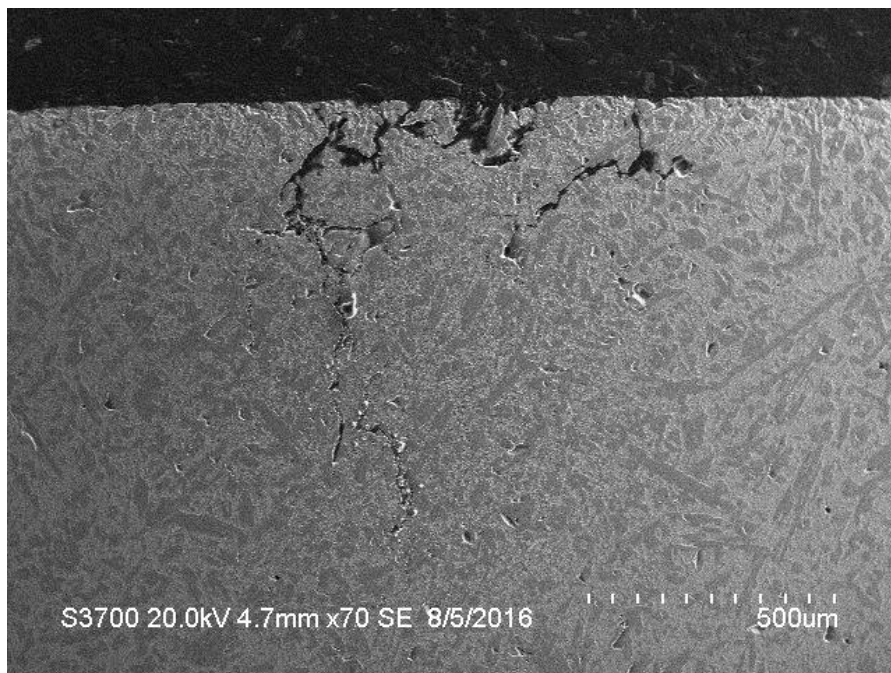
Figure 8.27: Cracks on 30WCI in the OA at 3.5% NaCl [etched].

8.3.4 Summary of results

The proportion of each deterioration mechanism to the total volume loss for a given material/environment is demonstrated in Table 8.8. Also, the average volume loss of due to different degradation mechanisms in the DIZ/OA for materials under study are summarised. Figures 8.28-8.30 present the summary of all results for fresh, seawater and brine (10% NaCl), whilst the same results are shown in Tables 8.9-8.11 as a more detailed demonstration. The terms CP, C and S refer to Cathodic Protection, Corrosion and Synergy respectively, whilst the S_{OA} was obtained by subtraction of S_{DIZ} from S_{TVL}.

Table 8.8: Proportion of each mechanism for materials under study in all testing regimes.

Material	Mechanical damage 0.05%/3.5%/10% NaCl	Corrosion 0.05%/3.5%/10% NaCl	Synergy 0.05%/3.5%/10% NaCl
UNS S31600	88/88/83	1/1/2	11/11/15
27WCI	94/87/71	1/13/29	5/0/0
38WCI	80/83/77	0/6/15	20/11/8
30WCI	83/49/45	1/14/37	14/37/18

Figure 8.28: Summary of average volume loss breakdown of materials under study at 0.05% NaCl.

Table 8.9: Summary of average volume loss for materials under study at 0.05% NaCl (mm^3).

Material	TVL	VL DIZ	VL OA	CP TVL	CP DIZ	CP OA	C TVL	C DIZ	C OA	S TVL	S DIZ	S OA
UNS S31600	1.48	0.66	0.82	1.31	0.55	0.76	0.019	0.015	0.013	0.14	0.09	0.05
27WCI	1.11	0.62	0.50	1.04	0.60	0.44	0.012	0.003	0.007	0.06	0.01	0.05
38WCI	1.31	0.77	0.54	1.05	0.60	0.45	0.000	0.004	0.005	0.26	0.17	0.09
30WCI	1.79	0.98	0.81	1.49	0.85	0.64	0.018	-	-	0.28	0.13	0.15

Figure 8.29: Summary of average volume loss breakdown of materials under study at 3.5% NaCl.

Table 8.10: Summary of average volume loss for materials under study at 3.5% NaCl (mm^3).

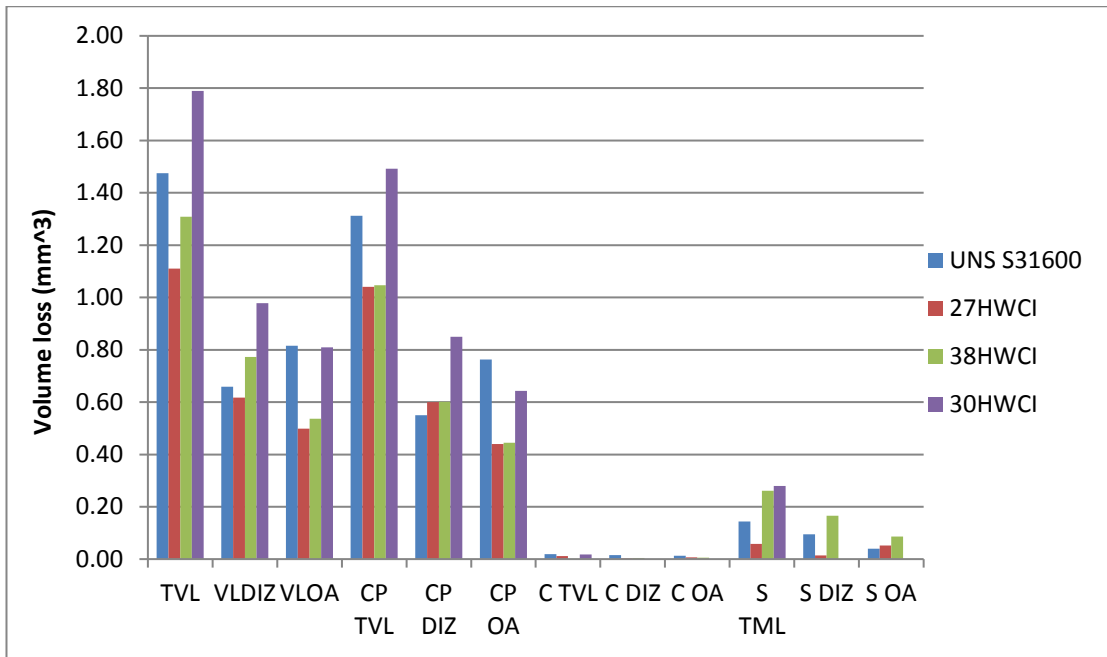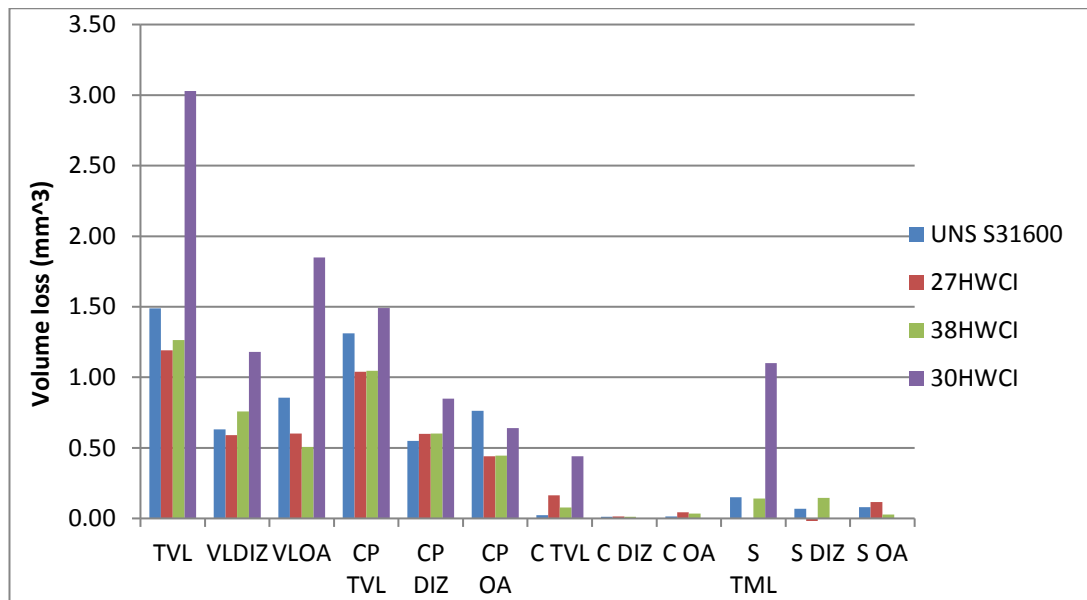| Material	TVL	VL DIZ	VL OA	CP TVL	CP DIZ	CP OA	C TVL	C DIZ	C OA	S TVL	S DIZ	S OA
UNS S31600	1.49	0.63	0.86	1.31	0.55	0.76	0.02	0.01	0.02	0.15	0.07	0.08
27WCI	1.19	0.59	0.60	1.04	0.60	0.44	0.17	0.01	0.04	0.00	0.02	0.00
38WCI	1.27	0.76	0.51	1.05	0.60	0.45	0.08	0.01	0.03	0.14	0.15	0.03
30WCI	3.03	1.18	1.85	1.49	0.85	0.64	0.44	-	-	1.10	-	-
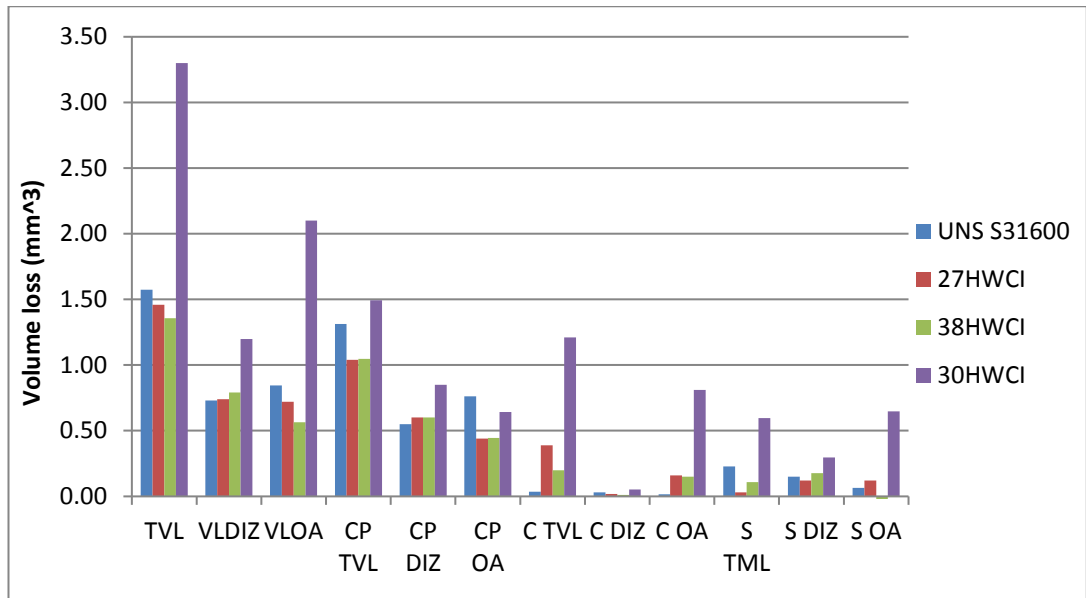
Figure 8.30: Summary of average volume loss breakdown of materials under study at 10% NaCl.

Table 8.11: Summary of average volume loss for materials under study at 10% NaCl (mm^3).

Material	TVL	VL DIZ	VL OA	CP TVL	CP DIZ	CP OA	C TVL	C DIZ	C OA	S TVL	S DIZ	S OA
UNS S31600	1.58	0.73	0.84	1.31	0.55	0.76	0.03	0.03	0.01	0.23	0.15	0.08
27WCI	1.46	0.74	0.72	1.04	0.60	0.44	0.390	0.018	0.16	0.03	0.12	0.09
38WCI	1.36	0.79	0.56	1.05	0.60	0.45	0.20	0.01	0.15	0.11	0.18	0.07
30WCI	3.30	1.20	2.10	1.49	0.85	0.64	1.21	0.05	0.81	0.60	0.30	0.30

8.4 Discussion

The data presented in the previous section revealed important information about the effect of salinity on erosion-corrosion. For better presentation of the findings, each material/environment is analysed separately in the current section.

8.4.1 UNS S31600

The erosion-corrosion performance of UNS S31600 at all salinity levels was unaffected from 0.05% to 3.5% NaCl and marginally affected from 3.5% to 10% NaCl. The corrosion rates were negligible in all testing regimes with a minor increase as the NaCl concentration was increased. However, in the case of seawater to brine, the increase of corrosion rate was higher compared to the increase from fresh to seawater and this trend was enhanced in WCIs since they possess poorer corrosion resistance than UNS S31600. Thus, it can be concluded that the brine can be considered as more corrosive environment than the seawater when erosion with suspended sand particles are present. An important observation was the fact that despite UNS S31600 showed much lower corrosion rates than WCIs at corrosive mediums (3.5 and 10% NaCl) it depicted worse corrosion performance than WCIs (almost equal to 30WCI though) in fresh water. This is an indication that when the environment is not corrosive, the erosion/abrasion resistance of the target material affects its corrosion resistance. Similar trend was reported in a past study in which an austenitic stainless steel was compared in corrosive abrasive tests with WCIs [8.1].

In terms of enhanced erosion due to corrosion (synergy), the UNS S31600 displayed relatively high rates in all NaCl concentrations and this contributed to higher volume loss than 27WCI and 38WCI - but lower than 30WCI (in all testing environments). Subsequently, in can be concluded that the synergistic effects are enhanced when the erosion/abrasion and/or corrosion resistance is not relatively high. In case of UNS S31600, the poor erosion/abrasion resistance led to enhanced erosion due to corrosion. An important feature, *which was common to all tested materials in this chapter*, was the higher volume loss in fresh water than in CP conditions, indicating that the synergy is an important factor for materials *ranking, even in fresh water*. Similar trend was observed in a past study where WCIs were tested in Na_2SO_4 [8.2]. The post-test analysis showed that the minor increase of volume loss from 3.5% to 10% NaCl occurred in the DIZ area, possibly because the high synergistic effects had more significant effect in the zone where the erosive rates are higher.

8.4.2 27WCI

The 27WCI alloy demonstrated the optimum erosion-corrosion performance at 0.05% and 3.5% NaCl environment. As has been shown in previous chapters (at in 3.5% NaCl aqueous solution), this alloy possesses very good abrasion resistance as a result of high hardness/eutectic Cr carbides and simultaneously, good balance between erosion and impact which contributed to relatively good performance in the DIZ. Thus, the moderate corrosion resistance was masked from the good erosion/abrasion behaviour in fresh and seawater solution. The effect of salinity on 27WCI was the minor increase of volume loss from fresh to seawater, whilst (relatively) major increase was observed from seawater to brine. In fact, the increase of volume loss in all three testing regimes was directly linked to the increase of corrosion rates. In 10% NaCl conditions, the 27WCI was inferior to 38WCI as a result of higher corrosion rates indicating that in more corrosive environments the corrosion resistance is a crucial factor for optimum erosion-corrosion performance. In a past study, the same trend was noticed in terms of erosion-corrosion performance; the volume loss of a 16% Cr hypoeutectic WCI was increased in 3% NaCl compared to 0.02% NaCl [8.3]. It is worth mentioning that the results in the current study in terms of increased corrosion rates with increasing NaCl content above 3.5% NaCl were in good agreement with some past studies in either tests under flowing conditions without sand particles [8.4], or in static conditions [8.5]. On the other hand, some other researchers showed that in static conditions, increasing the salt above a certain level (usually above 3% NaCl) decreases the corrosive attack [8.6–8.9]. Thus, it can be concluded that the correlation between corrosion and salinity level is dependent on the specific operating conditions (i.e flowing conditions with or without particles) and material's corrosion resistance. However, the results from the current work can be considered unique since (by the time that the current thesis was in progress) no published work was identified referring to corrosion evaluation in different salinity levels under flowing conditions with sand particles in suspension. The post-test analysis demonstrated that the minor increase of volume loss from fresh to seawater medium was in the OA, whilst from seawater to brine medium the increase was noticed in both regions.

8.4.3 38WCI

The 38WCI is the most corrosion resistant WCI with martensitic matrix that has been tested in the current PhD thesis due to its high Cr in the matrix (20%) and this contributed to minor increase of total volume loss in the most corrosive environment, at 10 %NaCl. A noticeable finding for this alloy was the substantially low corrosion rate at 0.05% NaCl as a result of balance between erosion and corrosion resistance in no corrosive medium. However, despite the corrosion rate of 38WCI were much lower than in both saline mediums its synergy masked the benefits from corrosion resistance (at 0.05% NaCl) and hence, the total volume loss maintained in similar levels with the most corrosive testing conditions. The high synergy in fresh water might be attributed to the complex microstructure of this alloy (i.e containing primary and eutectic Cr carbides). The superior corrosion resistance of 38WCI over 27WCI led to lower total volume loss (than 27WCI) in 10% NaCl and the rest of tested materials. Thus, it was evident that a meticulous materials selection should be conducted in mining operations when the level of chlorides is varying.

The clear superiority of 38WCI over the rest of alloys in brine solution was portrayed in the OA where the corrosion is more prominent than in the erosion dominant DIZ region.

8.4.4 30WCI

The 30WCI was the poorest corrosion resistant alloy since it contained the lowest dissolved Cr in the matrix and this contributed to significantly high corrosion rates at 3.5% and 10% NaCl. On the other hand, its corrosion rate in fresh water was similar with the UNS S31600 indicating that in non-corrosive mediums, materials with the general corrosion resistance of 30WCI (at least 8% Cr in the matrix) are not attacked by corrosion. In addition, the corrosive attack was located only in the OA and not in the DIZ since in the latter zone the erosion is the dominant mechanism, as it has been reported in the entire thesis. In terms of total volume loss, this alloy was significantly worse than the other materials at 0.05% NaCl and 10% NaCl testing conditions due to high corrosion rates which resulted in enhanced erosion due to corrosion. On the other hand, despite the corrosion and synergy rates were much lower in fresh water than in both saline environments, the 30WCI displayed higher total volume loss than the other

alloys. The reason for that was the poor resistance in mechanical damage which was associated with the high brittleness produced by the 50% CVF from which the 25% was primary Cr carbides. In addition, the poor erosion/abrasion resistance of 30WCI was clearly demonstrated through CP results. In several past studies it has been displayed the vulnerability of hypereutectic WCIs in terms of toughness and eventually in erosion/abrasion resistance [8.10–8.12]. As expected, the brittleness of 30WCI was portrayed mainly in the DIZ region producing substantially higher volume loss that the rest of tested materials which was increased in seawater and brine as a result of enhanced corrosion and, in particular, synergy. As shown in Figures 8.24-8.26, extensive cracks on primary Cr carbides of this alloy were present in 3.5% NaCl medium. As has been demonstrated so far in this thesis, the severity of cracks on WCIs in the DIZ dictates their volume loss in this region and hence, it can be reasonably assumed that the 30WCI possess less cracks in fresh water and CP conditions since the VL_{DIZ} was lower than in both saline environments. In the OA, cracks were observed in 3.5% NaCl medium (Figure 8.27) too, which can be related to the high corrosion rate or just in abrasive attack. The performance of 30WCI in the OA in fresh water was similar to UNS S31600, whilst in CP tests it depicted lower volume loss than the austenitic stainless steel. However, 30WCI was still inferior to 27WCI and 38WCI in all conditions (in the OA) indicating that the high CVF was detrimental from abrasion point of view [8.10].

It is believed that the fracture behaviour and the relatively poor abrasion resistance of 30WCI was due to the size of the erodent particles (500 μm) and this was extensively explained through the findings in the literature review in chapter 6 on the analysis of 38WCI cracks. Also, it was validated via personal communication with material's supplier [8.13].

8.5 Conclusions

1) Increasing the salinity, the erosion-corrosion attack is increased mostly for the tested alloy with poor corrosion resistance and less for alloys with good corrosion resistance. However, the increase of corrosion rates was identified

only in the OA in which the erosion mechanism is less prominent compared with the DIZ where the erosion is dominant the mechanism.

2) The corrosion rates were increased with the increase of NaCl concentration under erosive conditions with solid particles for all tested alloys, trend which is opposed with past studies with different experimental conditions (i.e corrosion measurements with no solid particles contained or even in static water). To the best of the author's knowledge, the present study is unique in that it presents corrosion measurements in different salinity levels under erosion-corrosion conditions with solid particles.

3) High synergistic effects were observed for all tested materials even in fresh water. For WCIs, the synergy was replaced partially by pure corrosion with increase of chlorides content.

4) In fresh water, there was no electrochemical attack on WCIs, which possess generally poorer corrosion resistance than UNS S31600 austenitic stainless steel, since the abrasion mechanism in the OA seemed to control materials corrosion resistance.

5) In terms of material ranking, the 27WCI was the optimum alloy in fresh and seawater, followed by 38WCI, UNS S31600 and 30WCI. At 10% NaCl, the 38WCI was superior over 27WCI due to its corrosion resistance, followed again by UNS S31600 and 30WCI.

6) The post-test analysis provided important information about materials performance in different hydrodynamic regions and comprised a validation of mechanisms identification that occur in DIZ-OA zones (i.e impact/erosion, abrasion).

8.6 References

[8.1]   V. Rajagopal, I. Iwasaki, Corrosion properties of cast iron ball materials in wet grinding, Corrosion. 48 (1992) 124–131.

[8.2]   S.W. Watson, B.W. Madsen, S.D. Cramer, Wear-corrosion study of white cast irons, Wear. 181-183 (1995) 469–475.

[8.3] W.J. Tomlinson, M.G. Talks, Erosion and corrosion of pure iron under cavitating conditions, Ultrasonics. 29 (1991) 171–175.

[8.4] K.S.E. Al-Malahy, T. Hodgkiess, Comparative studies of the seawater corrosion behaviour of a range of materials, Desalination. 158 (2003) 35–42.

[8.5] M.D. Asaduzzaman, C. Mohammad, I. Mayeedul, Effects of concentration of sodium chloride solution on the pitting corrosion behavior of AISI 304L austenitic stainless steel, Chem. Ind. Chem. Eng. Q. 17 (2011) 477–483.

[8.6] E.A.H. Al Zubaidy, F.S. Mohammad, G. Bassioni, Effect of pH, salinity and temperature on aluminum cookware leaching during food preparation, Int. J. Electrochem. Sci. 6 (2011) 6424–6441.

[8.7] H. Silman, Corrosion and Corrosion Control: An introduction to corrosion science and engineering, 2008.

[8.8] S.H. Mameng, A. Bergquist, E. Johansson, Corrosion of Stainless Steel in Sodium Chloride Brine Solutions, Corros. 2014. (2014) 1–12.

[8.9] K. Zakowski, M. Narozny, M. Szocinski, K. Darowicki, Influence of water salinity on corrosion risk - The case of the southern Baltic Sea coast, Environ. Monit. Assess. 186 (2014) 4871–4879.

[8.10] R.J. Chung, X. Tang, D.Y. Li, B. Hinckley, K. Dolman, Abnormal erosion-slurry velocity relationship of high chromium cast iron with high carbon concentrations, Wear. 271 (2011) 1454–1461.

[8.11] Y.P. Wang, D.Y. Li, L. Parent, H. Tian, Improving the wear resistance of white cast iron using a new concept - High-entropy microstructure, Wear. 271 (2011) 1623–1628.

[8.12] Y.P. Wang, D.Y. Li, L. Parent, H. Tian, Performances of hybrid high-entropy high-Cr cast irons during sliding wear and air-jet solid-particle erosion, Wear. 301 (2013) 390–397.

[8.13] An internal communication with Edward Humphries, Director of R&D, Weir

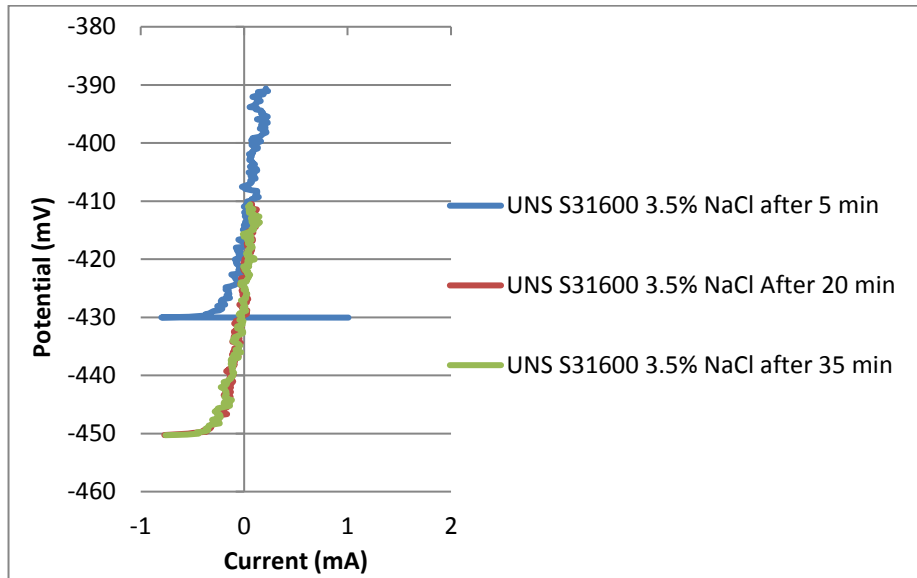Minerals Sydney, Australia, (2016).

8.7 Appendix

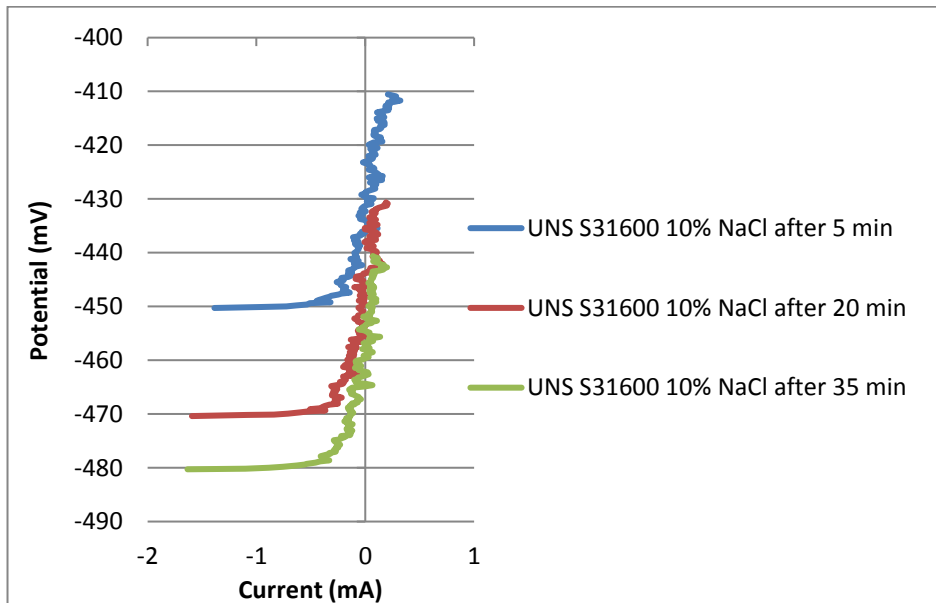Figure 8.31: Linear polarisation curves for UNS S31600 at 3.5% NaCl.

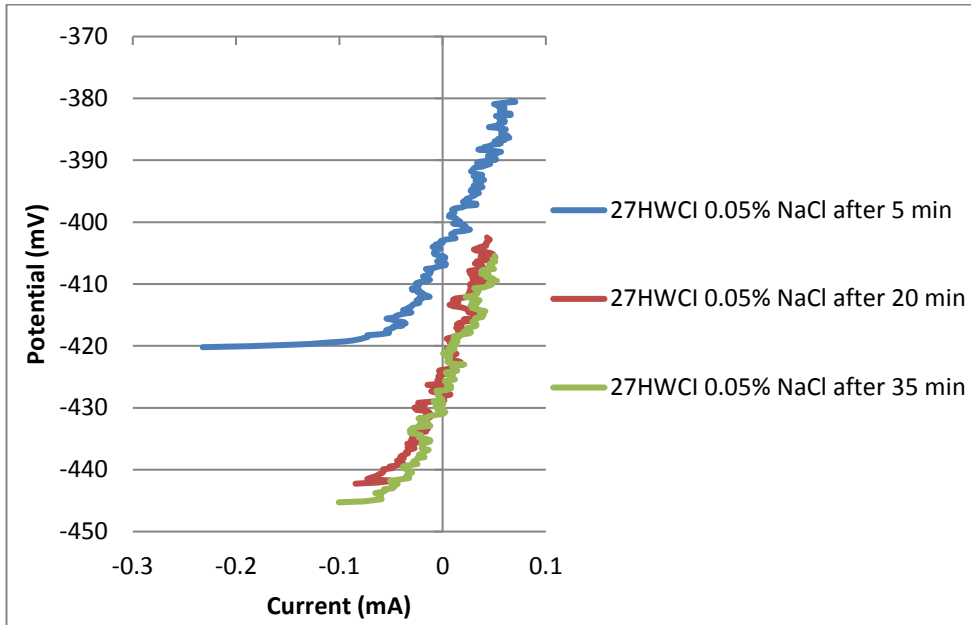Figure 8.32: Linear polarisation curves for UNS S31600 at 10% NaCl.

Figure 8.33: Linear polarisation curves for 27WCI at 0.05% NaCl.
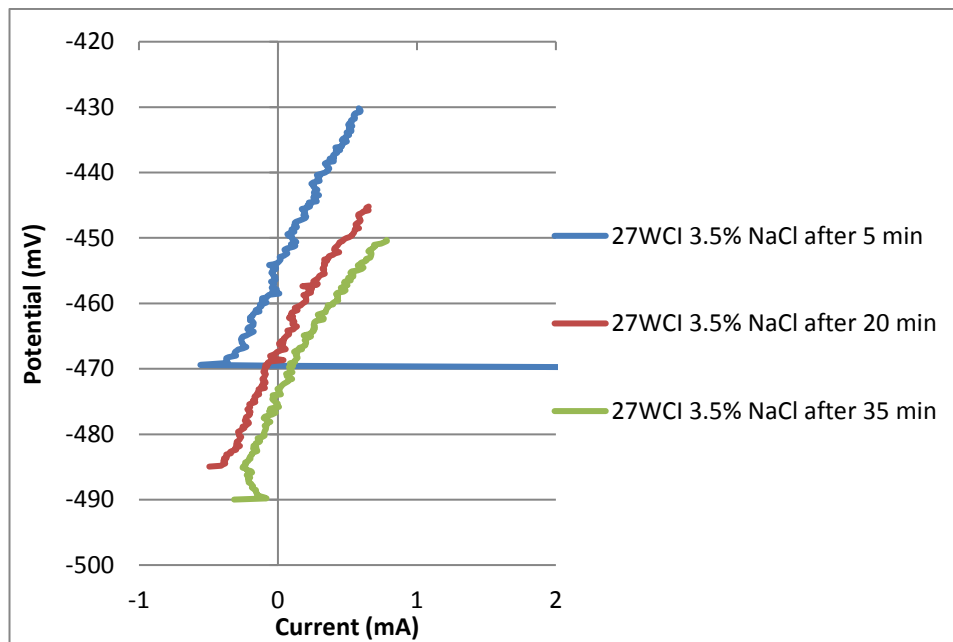

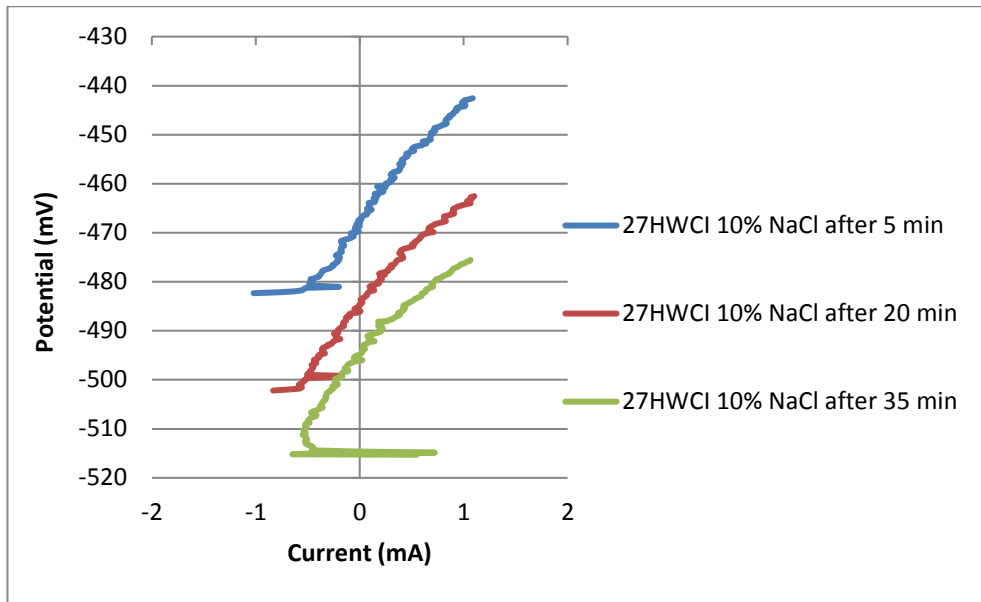Figure 8.34: Linear polarisation curves for 27WCI at 3.5% NaCl.

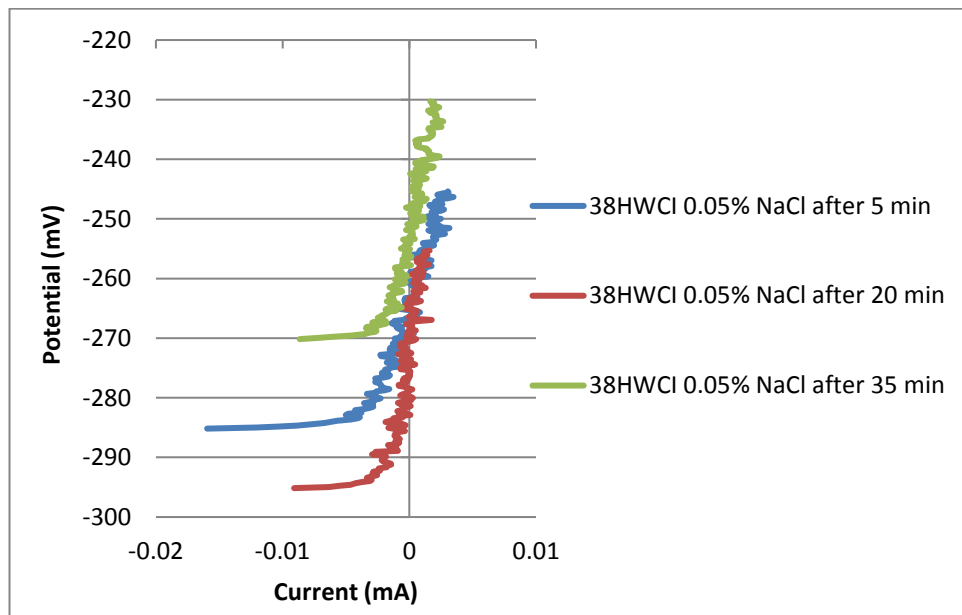Figure 8.35: Linear polarisation curves for 27WCI at 10% NaCl.

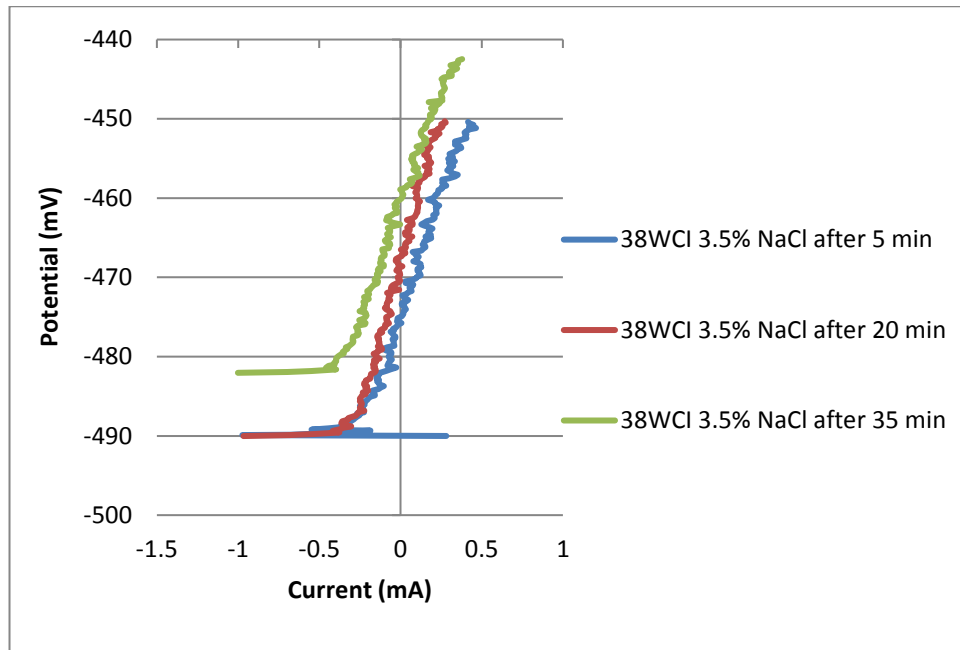Figure 8.36: Linear polarisation curves for 38WCI at 0.05% NaCl.

Figure 8.37: Linear polarisation curves for 38WCI at 3.5% NaCl.

Figure 8.38: Linear polarisation curves for 38WCI in 10% NaCl.

Figure 8.39: Linear polarisation curves for 30WCI at 0.05% NaCl.

Figure 8.40: Linear polarisation curves for 30WCI in 3.5% NaCl.

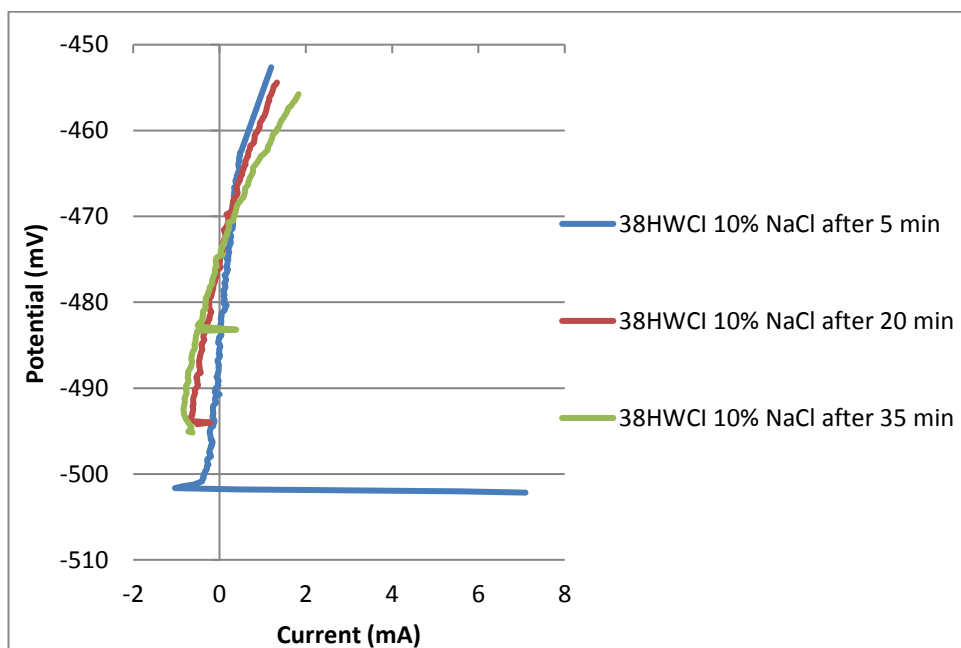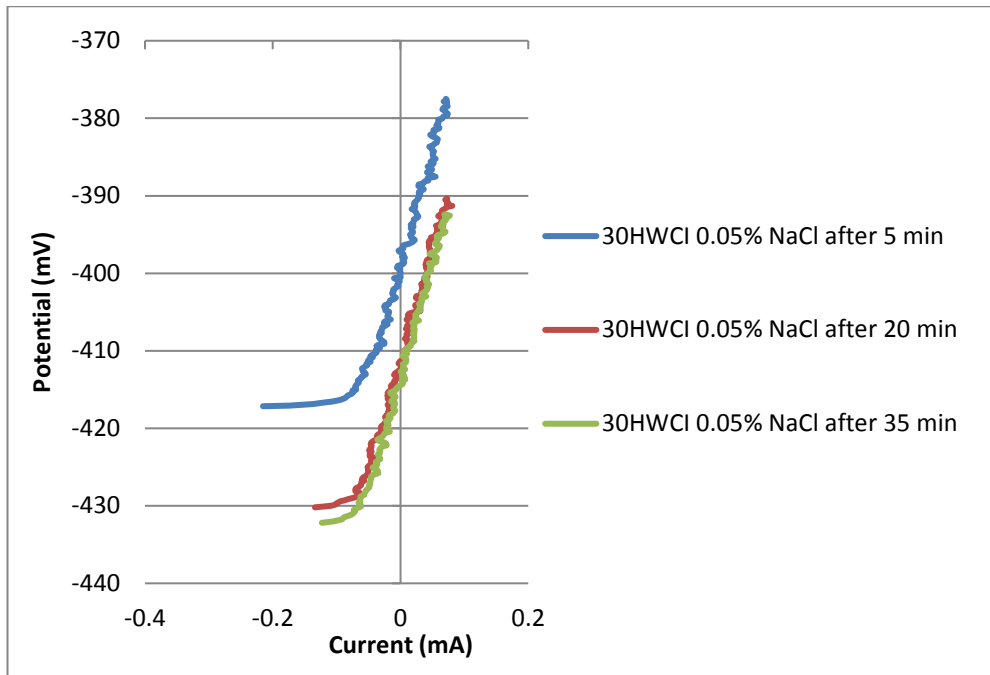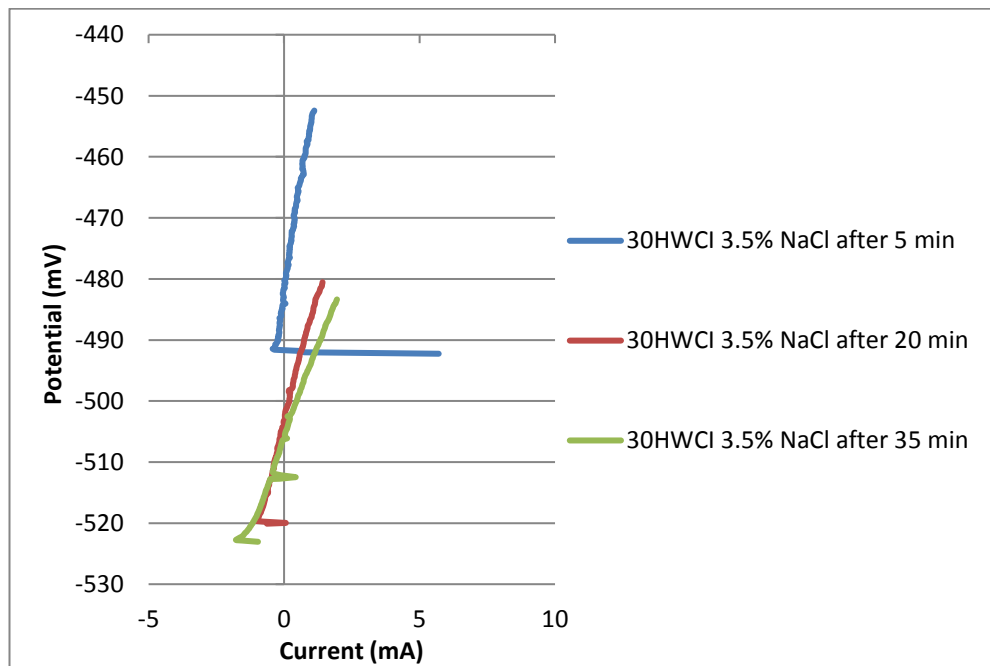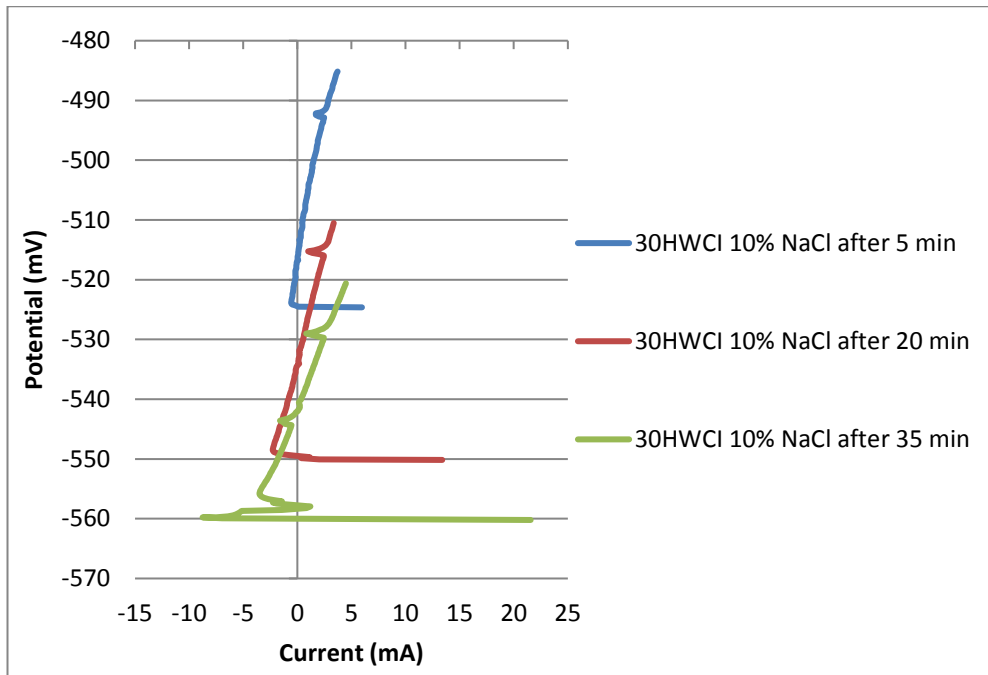Figure 8.41: Linear polarisation curves for 30WCI in 10% NaCl.

Figure 8.42: Microscopic view of 27WCI OA at 10% NaCl.

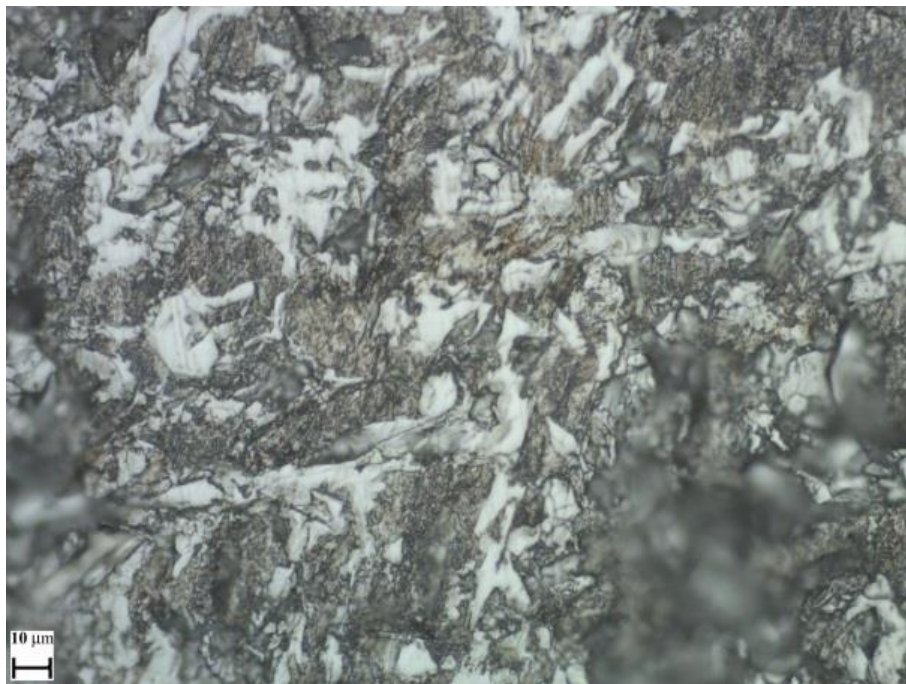Figure 8.43: Microscopic view of 38WCI OA at 10% NaCl.

Figure 8.44: Microscopic view of 30WCI OA at 3.5% NaCl.

Figure 8.45: Microscopic view of 30WCI OA at 10% NaCl.

Figure 8.46: Pitting corrosion on 30WCI at 10% NaCl.

Chapter 9

Concluding remarks and recommendations for future work

9.1 Introduction

This final chapter presents a guide for industry, with respects to the evaluated materials, highlighting the conclusions that contribute to development of new alloys followed by materials ranking. Moreover, this chapter can be considered as a valuable database for industrial purposes due to the close qualitative correlation between the laboratory results and the data obtained in the field service [6.2]. The material ranking refers to 3.5% NaCl/pH 7 and 3.5% NaCl/pH 3 environments since, in these two testing mediums, various alloys were evaluated and reported in the preceding chapters. The results presented in chapters 7-8 comprise an individual materials ranking for pH 7/pH 0 conditions and various salinity levels. Furthermore, the overall conclusions obtained by the scientific approach that has been implemented in the current study is shown. Finally, several recommendations about future work based on the current project are presented.

9.2 General conclusions

The current study shows that increasing the carbide volume fraction (CVF) on white cast irons (WCI), in applications where coarse sand particles with average 500 μm diameter are present, is beneficial only when eutectic carbides are formed. The increase of CVF leads to large primary carbides formation which enhances the brittleness of WCIs, and hence, these alloys become vulnerable to cracking under erosive-corrosive conditions (especially at high angles erosion). Considering the various corrosive environments, the high Cr dissolved in the metallic matrix is vital in saline water, whilst at low pH values the austenitic matrix that combines elements such as Ni, Mo and Cu (apart from high Cr) is essential. However, alloys that are precipitated by σ-phase (sigma) can be beneficial in corrosive wear only when the

formation of σ-phase is controlled in terms of materials composition and heat treatment's conditions.

9.3 Material Ranking

The term "Relative erosion-corrosion resistance" (RECR) is introduced in order to compare the tested alloys with the reference material studied in this work - UNS S31600 in solid liquid erosion-corrosion (SLEC) conditions, whilst the error bars are also taken into consideration. The RECR is the ratio between the volume loss of UNS S31600 and the volume loss of the individual alloys and thus, the RECR of UNS S31600 is 1 (optimum RECR is >1). It is worth mentioning that cathodic protection (CP) results are not included in the ranking since the pure mechanical damage does not provide any industrial value (unless CP is used in the field service) due to the presence of synergy (even in fresh water in which corrosion is very low/chapter 8) in erosion-corrosion conditions. In addition, the materials ranking is based on total volume loss (TVL), volume loss in the direct impinged zone (VL_{DIZ}) and volume loss in the outer area (VL_{OA}) enhancing the data provided through the current programme and emphasising the importance of examining the materials in different hydrodynamic regions individually.

Figure 9.1 presents the overall RECR of all the alloys tested in 3.5% NaCl at pH 7. In terms of TVL, the type N1 and D1 alloys exhibited the highest RECR, whilst they were only slightly superior to the 27WCI alloy. The 37WCI, 38WCI and UNS S32760 displayed marginally lower RECR than 27WCI. The UNS S42000 was just superior over UNS S31600, whilst 27WCINb and especially the 30WCI depicted significantly lower RECR than UNS S31600. Both 27WCINb and 30WCI had two common characteristics; they possess the most brittle microstructure and the poorest corrosion resistance, in particular the 30WCI.

In the DIZ, the RECR of the tested materials was different to that of the TVL; the type N1 and D1 alloys were again the highest ranked materials since they combined the optimum balance between erosion resistance and ductility withstanding the impact loads efficiently. The UNS S32760 and 27WCI depicted better RECR than the UNS

S31600 which was followed by 37WCI and 38WCI. The most brittle WCIs (27WCINb and 30WCI) showed substantially inferior performance to the 38WCI.
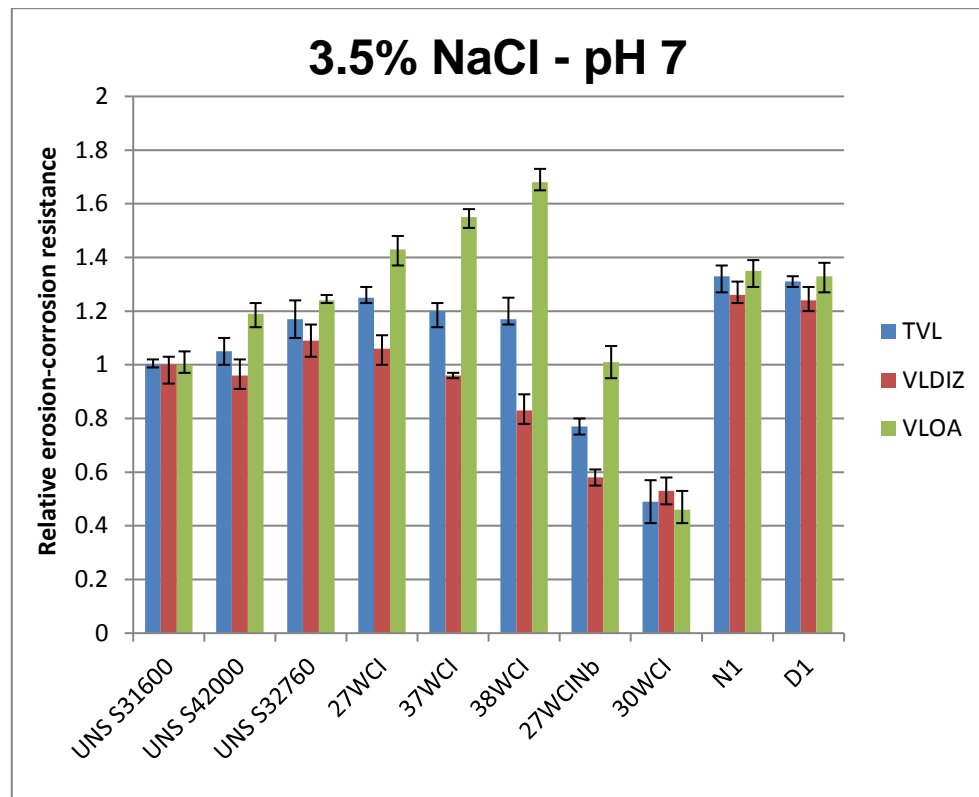

Figure 9.1: Materials ranking at 3.5% NaCl and pH 7 in terms of relative TVL, VL_{DIZ} and VL_{OA}.

Figure 9.2 demonstrates the RECR of the tested alloys at pH 3 and 3.5% NaCl. The TVL was greatly affected by the metallic structure of the tested alloys; the austenitic structure was significantly superior over the martensitic structure due to higher corrosion resistance, but only in the OA. Thus, the lowest TVL was observed in the cases of UNS S31600 and 37WCI, followed by 38WCI and 27WCI. The UNS S42000 was slightly inferior to the latter alloys, whilst the 30WCI exhibited the highest TVL.

In the DIZ, corrosion was suppressed since the erosion was the dominant mechanism, and hence different ranking occurred; the UNS S31600 was superior over all tested materials followed by the UNS S42000. The RECR of the WCIs was affected by enhanced erosion due to corrosion resulting in inferior performance compared with the

stainless steels. The 27WCI was superior over 37WCI, whilst the 38WCI and especially the 27WCINb exhibited the lowest RECR.

In the OA, the comparison of the austenitic alloys compared with the martensitic showed the same trend as the TVL (austenitic superior over martensitic). The 37WCI was the optimum alloy due to its better abrasion resistance in comparison with the UNS S31600. In terms of the martensitic alloys, the 38WCI illustrated the best RECR as a combination of the higher Cr in the metallic matrix – better corrosion resistance and the good abrasion resistance. The abrasion resistance of the 27WCI masked its higher corrosion rates compared to UNS S42000 providing better RECR than the martensitic stainless steel. Finally, the 27WCINb alloy showed similar RECR with the UNS S42000.
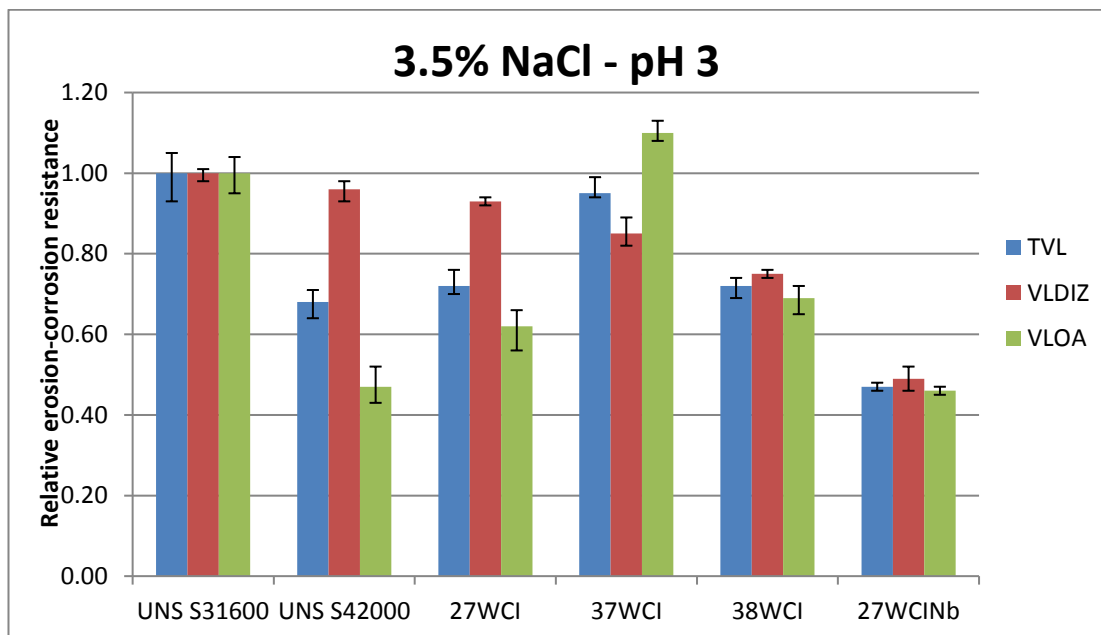

Figure 9.2: Materials ranking at 3.5% NaCl and pH 3 in terms of TVL, VL_{DIZ} and VL_{OA}.

9.4 Detailed conclusions

The overall concluding remarks and significant outcomes from the erosion-corrosion experiments, regardless of the testing environment, are summarised as follows:

1. The implemented scientific approach enabled the entire evaluation of materials erosion-corrosion performance, which includes metallurgical analysis and investigation of erosion, corrosion and synergy individually.

2. The post-test analysis (a typical example is Figure 9.1) indicates the importance of evaluating the performance of materials in different hydrodynamic regions in which the proportions of erosion, corrosion and synergy are varying. To the extent of post-test analysis, it was evident that the corrosion investigation in both DIZ and OA was a valuable tool.

3. The microstructure and the chemical composition of an individual alloy dictates its erosion-corrosion performance for a given environment.

4. The hardness cannot necessarily be considered as an assessment tool to predict the corrosive wear behaviour of alloys with complex microstructures in both DIZ and OA regions, even at pH 7 in which the erosion is the dominant mechanism. As shown in Figure 9.1, the RECR of 27WCINb (690 HV hardness) and 30WCI (900 HV hardness) was inferior to UNS S31600 (175 HV hardness) in terms of TVL, VL_{DIZ} and VL_{OA} (only in the OA the 27WCINb had similar volume loss compared to UNS S31600). However, comparing alloys that possess hard phases with stainless steels, the hardness was beneficial in terms of synergy and contributed to lower volume loss (in neutral conditions pH).

5. The optimum erosion-corrosion performance in the DIZ is achieved by a combination of erosion resistance and ductility.

6. In the OA zone, the optimum performance is accomplished by abrasion resistance (hard phases in the microstructure, carbides etc.) and corrosion resistance.

7. In terms of corrosion, enhanced rates were noticed in high velocity regions (i.e DIZ compared to OA).

8. The enhanced erosion due to corrosion is a key factor in materials performance, whilst combined corrosion and erosion/abrasion resistance individually provides minimal synergy.

9. As exhibited in chapter 6 and chapter 8, the primary Cr carbides in WCIs were deleterious in terms of mechanical damage, especially in the DIZ region in

which more cracks were observed compared with the OA zone. This was portrayed in comparison between 27WCI (possess only eutectic carbides) and 38WCI/30WCI (possess eutectic and primary carbides).

10. The Nb carbides were more vulnerable than Cr carbides (with the same volume fraction – 27WCI) in terms of mechanical damage and hence more cracks were generated in both DIZ and OA regions.

11. The corrosion performance under SLEC conditions can be affected by the erosion/abrasion resistance, as shown in the case of 27WCINb alloy.

12. The controlled formation of σ-phase was beneficial, as demonstrated in cases of type N1 and D1 alloys, and this consists of one of the most important findings of the current project since it is opposed to the general notion about the catastrophic consequences of σ-phase.

13. The austenitic UNS S31600 showed superior corrosion resistance over the martensitic 38WCI despite the latter alloy possessing slightly higher Cr content in the metallic matrix compared with the nominal Cr content on UNS S31600 (20% against 17%). This was attributed to the benefits of Ni and Mo additions on the UNS S31600 (chapter 6).

The effect of low pH can be summarised as follows:

1. The corrosion resistance and the synergy under SLEC conditions dictate the RECR since both mechanisms are enhanced in low pH conditions compared to the neutral pH.

2. The austenitic alloys were superior over the martensitic alloys in erosion-corrosion.

3. The corrosive attack on all materials was prominent only in the OA region, whilst in the DIZ no significant effect of acidic water was observed.

4. The low pH can impair significantly the erosion-corrosion performance of white cast irons in the DIZ due to high synergy, which led to enhanced cracking (chapters 5-7 and Figures 9.1-9.2).

5. In strong acidic slurries, the low synergy was related to the uniform dispersion of Cr and Mo elements in materials with complex microstructure, as shown in

the comparison of type D1 alloy with the 37WCI and type N1 alloy in chapter 7.

In different salinity levels (Chapter 8), the following can be summarised:

1. To the best of the author's knowledge, the entire investigation of erosion-corrosion phenomena under the presence of sand particles is unique and has not been reported elsewhere.

2. The corrosion resistance in low salinity was clearly affected by the erosion/abrasion resistance.

3. Higher corrosion rates were measured with increase of salinity under SLEC conditions, especially for the martensitic alloys.

4. The TVL for materials with relatively good corrosion resistance (UNS S31600/38WCI) was slightly increased with the increase of NaCl content from 3.5% to 10%.

5. Despite the low corrosion rates in fresh water, the synergy mechanism was maintained on the same level (or even higher) as in seawater and hence, this led to higher volume loss than in CP conditions where only mechanical damage occurs.

9.5 Recommendations for future work

Considering the information obtained from the present work, further topics (as shown below) could be investigated which are correlated with the mining industry or in oil & gas applications.

1. Research on the effect of angle of attack in the erosion-corrosion resistance of various alloys taking into consideration that the engineering components are exposed to various angles in the field service.

2. Investigation on the effect of different type of sand particles (size/shape) in erosion-corrosion resistance of WCIs. These alloys are considered sensitive in applications with different sand particles in mining industry due to their complex microstructure, especially when large primary Cr carbides are present. Thus, research on this topic will be valuable from both industrial and scientific perspectives.

3. The current work investigated the erosion-corrosion behaviour of WCIs with Nb carbides. Despite the fact that the Nb carbides were not beneficial in terms of erosion-corrosion due to their extensive fracture, it was evident that the corrosion rates, which were affected by the poor erosion resistance regardless the environment, remained the same at pH 7 and pH 3 despite the martensitic metallic structure. Hence, it is suggested that more research could be carried out in the role of Nb carbides volume fraction in erosion-corrosion under both neutral and acidic conditions. In addition, an interesting topic would be the investigation of a WCI that contains some Nb traces dissolved into the metallic matrix, apart from the Nb carbides presence.

4. The effect of salinity on erosion-corrosion is definitely a topic that needs to be investigated. Various materials that are used in many industries can be evaluated, whilst the real value of this topic is the direct correlation with the field service.